NTNU – Trondheim
Norwegian University of
Science and Technology

Comparing alternative flexible pipe fatigue stress models with focus on the Bflex helix models

Lidong Wang

Marine Technology
Submission date: June 2014
Supervisor: Svein Sævik, IMT
Co-supervisor: Naiquan Ye, Marintek

Norwegian University of Science and Technology
Department of Marine Technology

NTNU – Trondheim
Norwegian University of
Science and Technology

Comparing alternative flexible pipe fatigue stress models with focus on the Bflex helix models

Lidong Wang

10 June 2014

MASTER THESIS

Marine Structural Engineering

Department of Marine Technology

Faculty of Engineer Science and Technology

Norwegian University of Science and Technology

Supervisor 1: Professor Svein Sævik

Supervisor 2: Doctor Naiquan Ye

Preface

This master thesis has been carried out during the spring semester of 2014 at the Department of Marine Technology, NTNU.

This thesis is an important part of the two years master study program, the work includes software study, literature study and analysis work in Bflex2010 for stress comparisons based on different models with different types of helix element.

The idea of this master thesis is to compare the recently developed model with the previous models, so that we can give out more details of the new model, and get some calibrations to more precise results. It is a pleasure that I have been given this opportunity to do the comparison work, this is a great way of increasing my knowledge during the analysis work.

I assume that those who read this thesis are familiar with mathematics, structural mechanics and flexible pipe technology.

Trondheim, June 2014

....

Lidong Wang

Acknowledgement

I would like to extend my gratitude to the Master Program at the Marine Technology Department, NTNU, from which I have learned not only the advanced knowledge, but also the aspiring learning attitudes.

I would like to thank Professor Svein Sævik from NTNU and senior scientific researcher Naiquan Ye from Marintek for their great help during the master thesis work, their guidances during the course of the semester have been very constructive guiding my thesis in the right direction and getting the right results as discussed in the thesis, and our discussions have been both rewarding and encouraging.

I also would like to thank my classmates who during their thesis work have been using Bflex2010. Our discussions about Bflex2010 and the theory behind have been so helpful, meaning that I can learn the software quickly, and also solidify my knowledge about non-linear finite element method, which helps my study and research to a great extent.

At last, I would like to thank the Faculty of Marine Technology Department, who have helped me to install Bflex2010 in the computer lab, so that I can finish the analysis work as quickly as possible, and through the poster program, we have shown our own work to the others, thus learning from each other.

Trondheim, June 2014

Lidong Wang

Summary

The fast development of the offshore oil & gas industry towards deep and complicated sea fields come along with some problems and challenges both for design and operation. A flexible riser operating in deep water will have to withstand large environmental forces, such as the large internal hydrostatic pressure and the cyclic movement of the riser due to wave and current, which differs from the shallow water domain. In addition, it is also vital to evaluate the effect on the riser from complex reservoirs with high temperatures and pressures.

Most pipes are designed for a service life of 20-25 years, yet at the Norwegian Continental Shelf Offshore Sector, the average service life of flexible riser is roughly 50% of the planned target. Among the influencing factors, stress is an important evaluation parameter for assessing the service life.

In connection with these challenges, this thesis deals with the stress and slip behaviour for non-bonded flexible pipe of three different models (itcode0, itcode1 and fullfe), comparisons are made among these three models. Besides, pipes with different cross sections are analysed, namely 4 inch, 6 inch, 7.5 inch, 8 inch, and 16 inch pipe cases. In addition to the two tensile layers pipe construction for all the pipe size cases, the 7.5 inch pipe with four tensile layers case is also included.

The main advantage of this thesis is the application of the new developed beam elements in Bflex2010, namely HSHEAR353, HSHEAR363 and HCONT463, implemented in the new model FullFE. For HSHEAR353 element, the transverse degrees of freedom of the helix are included, while for HSHEAR363 element, the radial degree of freedom of the plastic layer is introduced, which means that the new model FullFE simulates the most realistic situation for design and operation.

Two main parts are carried out in the thesis work. The first part, consisting of chapter 2 and 3, is the results of a literature study with regard to flexible pipe technology and methodologies which are involved in this thesis. The second part, chapter 4, 5, 6 and 7 are the results of modelling, post-processing, stress analysis and fatigue analysis. In this part, the basic idea of modelling is to simplify the flexible pipe as a simple cantilever beam, and apply the prescribed displacement at the free end in order to solve the static problem.

For comparison of stress components, the procedures are first to get the local stress components of the tensile armour layer and the corresponding global normal curvature through

the Bflex2010post module. Secondly, to extract the stress of the third element of each tendon in order to eliminate the effect of boundary condition, then finally, plot the same stress components of the three models in the same figure for comparison.

As mentioned in the scope of work, the assumption of plane surfaces remain plane until slip versus including the effect of shear deformations in the plastic layers is carried out by comparing the stress components of fullfe model as well as the itcode0 and itcode1 models under the loxodromic assumption. In order to verify whether the wire slips along the geodesic curve or the longitudinal curve, stress components comparisons of fullfe model as well as the itcode0 and itcode1 under the loxodromic and geodesic assumptions are studied.

In the main text, the 4 inch pipe case is specialized as an example to analyse in more detail, the analyses of the 6 inch pipe, 7.5 inch pipe, 8 inch pipe and the 16 inch pipe cases are summarised in chapter 7.

For comparison of fatigue analyses, the maximum fatigue damage of each tensile layer of all the pipe cases are extracted, through the values, we can understand which model sustain the most damage under the same bending load condition.

Scope of work

Due to the important role of the flexible pipe to both the floating production system and the oilfield profit, the service life and sustainability of the flexible pipe become a pivotal research topic. Among the factors which affect the service life, stress in the tensile armour layer is one key factor. Therefore, precise calculations of stress are becoming much more vital, different helix elements in Bflex2010 software related to the tensile layer governed by the slip behaviour are compared in different models based on the following assumptions:

- **The assumption of plane surfaces remaining plane until slip** *versus* **including the effect of shear deformations in the plastic layers.**
- **Whether the wires slips against the Geodesic** *or* **it remains at the initial curve path (Loxodromic)due to friction effects.**

In order to guide the thesis in the right direction, in agreement with the supervisors, it is carried out as the following procedures:

1. Literature study related to flexible pipes, methods for global and local response analysis focusing on the issue of calculating the fatigue stress in flexible pipes.
2. Establish necessary input for flexible riser local stress analyses. Different pipe cross-sections are to be evaluated covering different relevant dimensions/applications, and a full and detailed overview of the cross-section input and load case analysis shall be included in the report.
3. Establish local Bflex models for the flexible pipe cross-section using ITCODE0, ITCODE1 and the new FullFE (element type HSHEAR353, HSHEAR363 and HCONT463) assumptions.
4. Perform the fatigue stress analysis in Bflex using the models above and compare the results in terms of stress history plots showing the results from the different models in the same plot. The plots should include the axial stress σ_{xx-ax}, normal curvature stress σ_{xx-my} and transverse curvature stress σ_{xx-mz} as well as the total longitudinal stress σ_{xx}, and the fatigue damage for a typical SN curve.
5. Conclusions and recommendations for the further work

Nomenclature

Abbreviations

API	American Petroleum Institute
CARC	Carcass Layer
DNV	Det Norske Veritas
DOF	Degree of Freedom
FAT	Factory Acceptance Test
FEA	Finite Element Analysis
FEM	Finite Element Method
FIP	Final Internal Pressure
FLS	Fatigue Limit State
FullFE,fullfe	Model Name 1
geo	Geodesic Curve
HCF	High Cycle Fatigue
HCONT	Helix Contact Element
HDPE	High Density Polyethylene
HSHEAR	Helix Shear Element
ITCODE0,itcode0	Model Name 2
ITCODE1,itcode1	Model Name 3
LCF	Low Cycle Fatigue
LM	Lagrange Multiplier Method
lox	Loxodromic Curve

MBR	Minimum Bending Radius
MM	Mixed Method
NFEM	Non-linear Finite Element Method
NOV	National Oilwell Varco
PLF	Pressure Load Factor
PM	Penalty Method
PVD	Principle of Virtual Displacements
PVDF	Poly Vinylidene Fluoride
RP	Recommended Practice
SBM	Sandwich Beam Model
SCF	Stress Concentration Factor
SCR	Steel Catenary Riser
TDP	Touch Down Point
TENS	Tensile Armour Layer
THER	Thermoplastic Layer
TTR	Top Tensioned Riser
ULS	Ultimate Limit State
ZETA	Zeta Type Pressure Spiral

Greek Letters

α	Lay angle of the tensile armour wires
β, γ	Relative displacement between tendon and core
β_2	Global curvature quantities at the cross section centre
β_{2c}	Critical global curvature

$\Delta\pi$	Incremental potential
$\Delta\sigma, \Delta\sigma_0, \Delta\sigma^*$	Stress range
γ_i	Decomposition of the u_3
κ_i	Initial accumulated curvature
κ_t	Transverse curvature
κ_y	Global normal curvature
μ	Friction coefficient
ω_i	Torsion and curvature deformation components
$\prod$	Potential energy of tendon
ψ	Angular coordinate starting from the lower side of the pipe cross section(if not specified)
ψ_0	Transition angle between two regions
ρ	Steel material density
ρ_i	Internal fluid density
σ_a	Alternative stress
σ_m	Mean stress
σ_y	Material yield stress
σ_{fat}	Fatigue limit for completely reversed loading
σ_{max}	Maximum stress
σ_{min}	Minimum stress
σ_{ut}	Ultimate tensile stress of the material
σ_{xx-ax}	Axial stress of tendon
σ_{xx-my}	Normal curvature stress of tendon

σ_{xx-mz}	Transverse curvature stress of tendon
σ_{xx}	Total longitudinal stress of tendon
θ_1	Torsion rotation
ε_{ii}	Strain quantities about the X^i axis
ε_i	Strain and rotation quantities about the X^i axis
$\bar{\alpha}$	Mean absolute angle of the tensile armour layer.
$\bar{\sigma}_{xx-ax}$	Average axial stress of all the tensile layers
u_3	Radial displacement of the specified HSHEAR363 element node

Roman Letters

$\boldsymbol{G_I}$	Base vectors directed along the local curvilinear coordinate in undeformed configurations.
$\boldsymbol{I_i}$	Global coordinate base vectors
$\boldsymbol{I_j}$	Local coordinate base vectors
$\boldsymbol{n}$	Outward surface normal vector
$\boldsymbol{t}$	Tangent vector
θ_j^{iA}	i=1,2;j=1,2,3; rotation degree of freedom at the i end of element A
$\bar{R}, R$	Mean radius of the corresponding pipe layer
c, k	Non-linear shear stiffness parameter
c_n	Penalty stiffness parameter
D_p	Inner diameter of the layer where internal pressure applied
E_{xx}	Longitudinal Green strain
EI_i	Bending stiffness of the tensile armour wire
f_i	Filter coefficient

g_0	Initial gap
M_c	Start slip bending moment
M_f	Full slip bending moment
n_{tot}	Total number of the wires
p	Pitch
P_e, P_i	External/Internal pressure
q^I	Contact force per unit length along the inner side of helix element
q^{I+1}	Contact force per unit length along the outer side of helix element
Q_1	Axial force of the tendon before slip
q_3	Contact force
q_t	Shear force
q_{1c}	Maximum shear stress
S^{11}	Stress of the tendon
S_f^{11}	Full slip stress value
u_j^{iA}	i=1,2;j=1,2,3; translation degree of freedom at the i end of element A
u_x, u_y, u_z	Displacements of an arbitrary point P
u_{1p}	Wire displacement under plane surface remain plane after bending assumption
u_1	Longitudinal displacement along tendon
$u_{i,j}$	Differentiation of the displacement components u_i along axis X^i with respect to the curvilinear coordinate X^j
v_p	Tendon displacement under plane remain plane assumption
v_s	Actual longitudinal displacement along the tendon

W_i	Internal work
w_{ip}	Prescribed torsion and curvature quantities
X^i	Local coordinates
Z^i	Global coordinates
A	Cross section area
b,h	Width/Height of the cross section
D	Diameter of the layer where internal pressure is applied, not the Carcass layer
e	Gap between two adjacent tendons at the same layer
E,C_σ	Elastic modulus of material
EA	Axial stiffness of the tensile armour wire
G	Determinant of the metric tensor
g	Current gap
I.D	Inner diameter
m	Negative inverse slope of the S-N Curve
N	Number of cycles to failure
O.D	Outer diameter
t	Friction force per unit length

Contents

List of Figures

List of Tables

Chapter 1 Introduction

With the increasing consumption and high demand for transportation of subsea oil & gas, flexible pipe technology has successfully been applied during the recent years in connection with offshore production systems.

However, during the operation of the riser system, uncertainties such as riser section failure and harsh environment which will not only influence the flexible riser, but also threaten the environment and field economy, and should therefore be taken care of. In brief, the study of flexible pipe technology is becoming more and more important to the oil & gas companies and to the marine engineering companies.

A brief overview of the flexible riser system (http://imageshack.com/a/img834/3474/y5e7.jpg) is shown below:

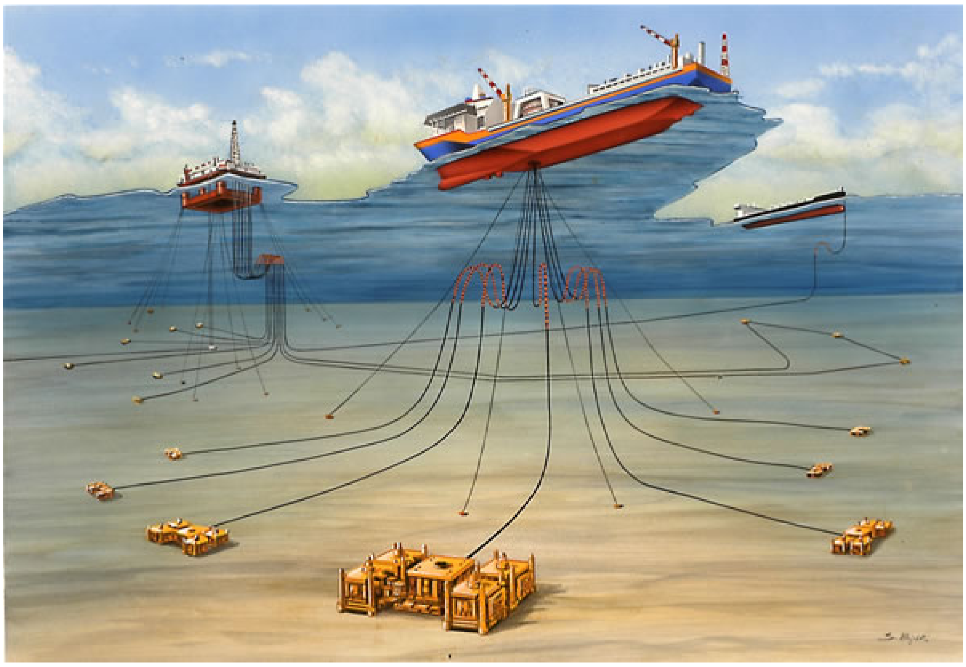

Figure 1.1: Brief overview of the flexible riser system.

1.1 Motivation

To warrant the safe operation of the flexible pipes in an intricate sea state, we have to be clear about the failure modes, among which, stress in the tensile layer is a pivotal factor. It is therefore necessary to have an insight in how the stress components behave during a load history such as cyclical bending, and a better understanding of how to predict accurate values, which in turn will lead to improved secure operation and profit maximization.

Due to the intricate structure of the flexible pipe and application, the tensile layers in flexible pipe play an important role with respect to the pipe's service life. This is because these layers are responsible for carrying the longitudinal loading. A contact layer is added up between 2 tensile layers in order to avoid direct steel contact and to increase the friction force, but due to the lay angle of the tensile layer relative to the supporting pipe, the flexible pipe will withstand a severe twisting during bending, which will lead to many other failure modes. If the tensile layers lose their capacity, the pipe will lose their function, or even disastrous events affecting people and the environment.

In order to make sure that the stress in the tensile layer is within the safe stress capacity range, it is quite necessary to give much accurate stress value of the tensile layers.

1.2 Main Contributions

This master thesis is mainly focusing on studying the behaviour between the stress components in the tensile armour layer and the global normal curvature of the pipe, including establishing different pipe models.

In the former tensile layer analysis, only the longitudinal slip is considered, which may result in inaccurate stress value, so in this thesis, we compare the results between the models(ITCODE0, ITCODE1) which only considering the longitudinal slip and the model(FullFE) which considering both the longitudinal and transverse slip.

From the results, we can conclude that the ITCODE0 and ITCODE1 models show high coincidence, while the FullFE model shows much more conservative, but due to the friction values are the same for the models, the slope of the curve in each domain should be the same, which is against the observation. More research about the new FullFE model should be examined with respect to the elements used.

As agreed with Professor Svein Sævik, short introduction about the fatigue analysis is included in Chapter 7.

At last, I hope the work done in this thesis will provide both valuable information and better recommendation in practical domain.

1.3 Structure of the Report

The structure of this thesis report is shown below:

Chapter 2: short review of the flexible pipe technology, including the common flexible riser configurations, the structure of bonded and unbonded pipe, and the function of each pipe layer.

Chapter 3: theories and methodologies related to this thesis are presented, including the brief outline of the non-linear finite element analysis, the introduction of the software Bflex2010, the Geodesic and Loxodromic assumptions, detail introductions of the elements used in this thesis, the analytical stress and the brief introduction of failure modes and design criteria.

Chapter 4: the procedure of modelling is given, more details of the parameters can be referred to Appendix A, more details of the cross section calculation can be referred to Appendix B.

Chapter 5: the main stress analyses results are shown in this chapter, different stress components of different pipe dimensions for 3 models are analysed, including the comparison between the loxodromic and geodesic assumptions, the influence of the friction, and the explanations. Due to the large amount of figures outputted in this thesis, these figures are referred to Appendix C and Appendix D.

Chapter 6: summaries of the stress analysis related to the pipe cases in appendices are given.

Chapter 7: the fatigue analysis is shown in this chapter, including the fatigue theory part and the maximum fatigue damage for all the pipe cases for the 3 models.

Chapter 8: main findings and conclusions related to this thesis topic are specified.

Chapter 9: suggestions about the improvements of the analysis work and the further recommendation work related to this thesis topic are specified.

Chapter 2 Flexible Pipe Technology

The riser system is an essential conductor connecting floaters on the sea surface and the wellheads at the seabed, basically, including two types, rigid riser and flexible riser, while for the latter type, bonded and unbonded types are involved. Besides, a hybrid riser is the combination of the rigid and flexible risers. With regard to the cost of material and installation, the riser should be as short as possible, but it must have sufficient flexibility to allow for large excursions of the floater.

In this chapter, a brief introduction of the common flexible riser configurations as well as flexible bonded and unbonded pipe are presented, for more information, see[4].

2.1 Common Flexible Riser Configurations

The common flexible riser configurations are listed below:

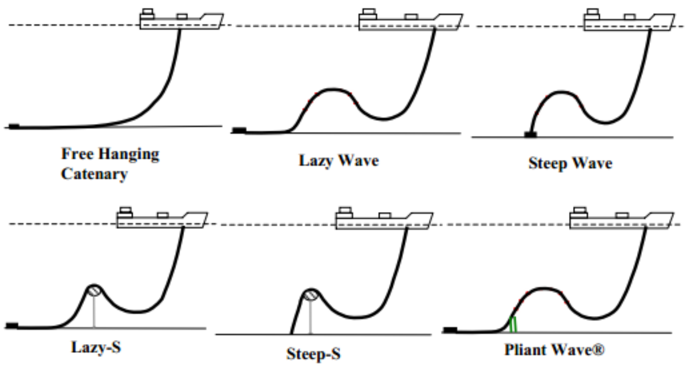

Figure 2.1: Common flexible riser configurations.

- *Free Hanging Catenary*

  Due to the minimal requirements of subsea infrastructure and ease of installation, this is the simplest and also the cheapest configuration, which is only simply lifted off or lowers down on the seabed. When exposing to the high vessel motions, however, it is likely to suffer from the compression buckling at the riser touch down area and "birdcaging" phenomenon on tensile armour wires and large top tension due to the long riser length supported when applied in deep water, also called Steel Catenary Riser (SCR).

- *Lazy Wave and Steep Wave*

  Lazy Wave Configuration is suitable for steep waves due to the minimum requirements of the subsea infrastructure. But this is easy to change the configuration when the internal fluid density changes.

  Steep Wave Configuration, on the other hand, can maintain the configuration even though the internal fluid density changes. But it needs a subsea base and subsea bend stiffener, which is high technology demanded and very costly.

  Both configurations need buoyancy modules, which are clamped tightly to the riser in order to avoid any slippage, and also the clamping process should not cause any damage to the outer sheath of the riser, or it will cause water injection into the annulus.

- *Lazy S and Steep S*

  Two kinds of subsea buoy are applied in the 'S' Riser Configuration:

  a) Buoyant buoy: positioned through chains to seabed.

  b) Fixed buoy: fixed to a structure at the seabed.

  The advantage is that the buoy removes the Touch Down Point (TDP) problem, at the same time, the buoy can also absorb the tension variation induced by the floater.

  Because of the complex installation requirements, Lazy-S configuration needs a mid-water arch, tether and tether base. Steep-S needs a buoy and subsea bend stiffener, 'S' Riser configurations are only considered while the Free Hanging Catenary and the Wave configurations are not suitable for a special work field.

  By the comparison of these two 'S' configurations, as the Lazy-S might result in compression problems at the riser TDP, the Steep-S is much more popular.

- *Plaint Wave Configuration*

  Similar to the Steep Wave configuration, the tension can be transferred to the anchor rather than the TDP. The benefit is that it is tied back to the well located beneath the floater, which makes the well intervention becoming possible without an additional vessel, besides, it is suitable for a wide range of bore fluid densities and vessel motions while keeping the configuration stable, including high stress in the riser structure.

  Because of the complicated subsea installation, it is only used when the Free Hanging Catenary, Lazy Wave or Steep Wave configurations are not applicable.

2.2 Flexible Bonded and Unbonded Pipe

According to the cross section properties, i.e. principles of providing flexibility, the flexible pipe[1] can be divided into bonded and unbonded pipes. More details about the bonded pipe can be referred to Reference[2], unbonded pipe can be referred to Reference[3].

Bonded Pipe (Figure 2.2): flexible pipe in which the steel reinforcement is integrated and bonded to a vulcanized elastomeric material where textile material is included in the structure to obtain additional structural reinforcement or to separate elastomeric layers. No relative slip since the layers are bonded with each other, the theory of this type is that there exists a low shear modulus rubber which can control and restrict the stresses induced by bending and hence provide flexibility, it is often used in short length required field.

Unbonded Pipe (Figure 2.3): multiple layers are free to move between each other, the flexibility is supplied by the relative slip of armouring tendons, it is often used as risers, in long length required field.

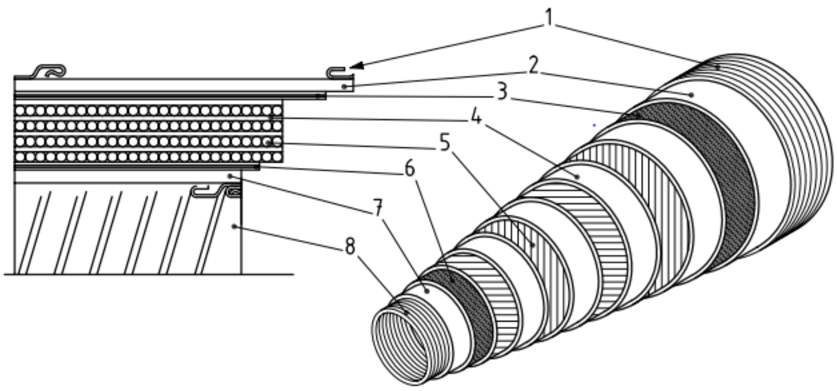

Figure 2.2: Cross-section of bonded flexible pipe.

Where:

1. Outer Warp	5.Reinforcement Layer
2. Cover	6.Breaker Layer
3. Break Layer	7.Liner
4. Cushion Layer	8.Carcass

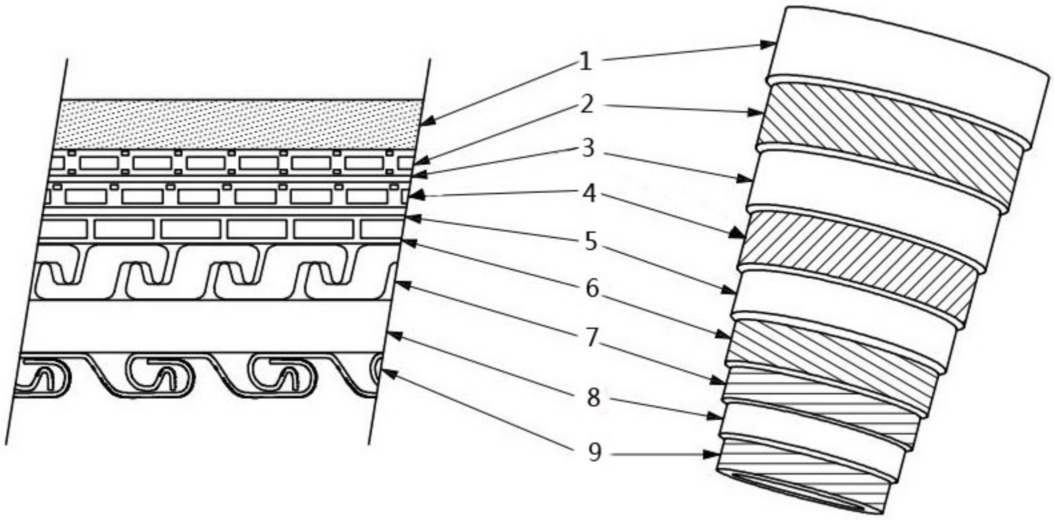

Figure 2.3: Cross-section of unbonded flexible pipe.

Where:

1. Outer Sheath
2. Outer Layer of Tensile Armour
3. Anti-wear Layer
4. Inner Layer of Tensile Armour
5. Anti-wear Layer

6.Back-up Pressure Armour
7.Interlocked Pressure Armour
8.Internal Pressure Sheath
9.Carcass

Layers from inner to outer of the unbounded flexible pipe are illustrated as follows:

- Interlocked stainless steel carcass:

  The carcass layer is made from a flat steel strip, formed into corrugated profile, which can resist external hydrodynamic pressure and prevent collapse induced by external pressure, installation loads and gases in the annulus, which is termed as the space between internal polymer sheath and the external polymer sheath. Due to the function as the innermost layer, which will contact the internal fluid directly, the material should be anti-corrosion, the common interlocked carcass profile is shown below:

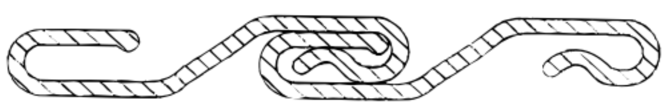

Figure 2.4: Interlocked carcass profile.

- Internal Pressure Sheath:

  The motivation of this layer is to provide a pressure tight barrier for internal content and external fluid as a sealing component, which is always made from a thermoplastic by extrusion over the carcass. Three popular materials are widely used:

  1) Polyamide(Nylon), PA11 or PA22
  2) Poly Vinylidene Fluoride (PVDF)
  3) High Density Polyethylene (HDPE) and Cross Linked Polyethylene(XLPE)

- Pressure Armour Layer (Zeta Spiral/Flat Spiral/C-Shape/T-Shape):

  The function of this layer is to provide support of pressure barrier, resist internal pressure, and also resist external pressure in order to provide capacity of loading in hoop direction. The pressure spiral wire is made of interlocked profile, using low-alloyed carbon steel grades with typically high yield strength.

  The pressure armour may consists of 1-2 wires in a layer with lay angle α close to 90°. The common configurations of the pressure armour profiles are shown below:

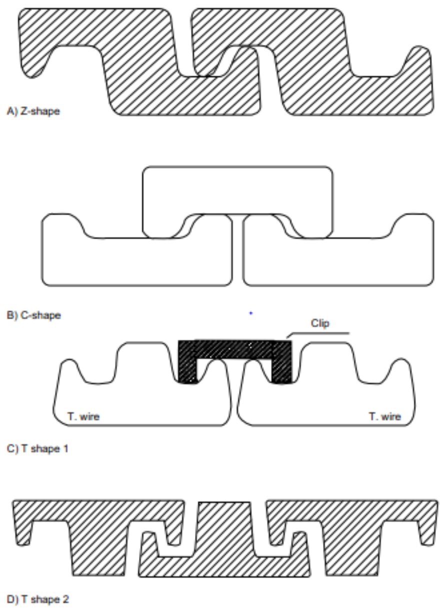

Figure 2.5: Different types of pressure armour profiles.

- Tensile Armour Layer:

  The Tensile Layer is usually made of 30~80 rectangular (other type such as rods) steel tendons helically with a lay angle α between $\pm 29° \sim \pm 55°$. The design purpose is to sustain axial (end-cap force) and torsional loading, in order to balance torsion, however normally, there are two cross-wound layers, which are separated by the anti-wear layer to avoid metal contact, on the other hand, the slip between the tendons and inner layers will provide the flexibility.

- External Sheath:

  This layer which can be seen from outside, is designed to keep the inner layers from contacting sea water and so is anti-corrosion, the material is always thermoplastic non-metallic.

  For example, the flexible pipe supplier, NOV Flexible company, the manufacturing technique of the inner sheath and the outer sheath is heating the raw PVDF material and using the water cooling system, usually the colour of the inner sheath is white, while the outer sheath yellow.

Chapter 3 Methodology

The common feature of the rigid pipe and the flexible pipe lies in the global response, and the main difference between the rigid pipe and the flexible pipe is at the local response, which means for the former one, it can be solved analytically by establishing several equilibriums, on the contrary, for the latter one, we can also establish equilibriums, but it can only be solved numerically, which means applying the Finite Element Method(FEM).

3.1 Non-linear finite element analysis

Generally, 3 main non-linear effects during the structural analysis should be taken care of, termed as: Geometry Non-linearity, Material Non-linearity and Boundary Non-linearity.

- Geometry Non-linearity(Large displacement)

  In the geometry non-linearity problems, the deflections of the structure are large compared with the original dimensions of the structure, so the stiffness and loads will change as the structure deforms.

  Steps to perform a geometry non-linearity analysis:

  1. Create a finite element model-avoid curved beam elements
  2. Define time-varying loads or restraints, and boundary condition for non-linear statics, constant loads can also be included.
  3. Create a solution set and define time increments for the solution

- Material Non-linearity

  Material behaviour is based on the current deformation state and possibly the past history deformation, and other constitutive variables (pre-stress, temperature, time, moisture, electromagnetic fields, etc.) may also have some influences.

  This property is mainly shown in the structures which undergo non-linear elasticity, plasticity, viscoelasticity, creep or inelastic rate effects, and is usually related to the Young's Modulus.

- Boundary Non-linearity

  During the analysis of the structure, the boundary conditions may change in the contact area. These nonlinearities include force boundary condition and displacement boundary condition nonlinearities.

Pressure loads of fluid are the most important engineering application concern, including hydrostatic loads on submerged or container structures, aerodynamic and hydrodynamic loads caused by the motion of hydro form fluids (wind loads, wave loads and drag forces).

In addition to the non-linear sources illustrated above, other sources such as non-linear pipe-soil interaction force and non-linear hydrodynamic loading, as well as transient temperature and pressure loads due to variable fluid flow conditions are also related to the flexible pipe analysis.

3.2 Bflex2010 program system

BFLEX2010 is tailored for global non-linear static and dynamic analysis of the flexible pipes. The program is based on the principle of virtual displacement and the Co-rotational Total Lagrangian formulation is implemented to model the non-linear effect, while Newton-Raphson Iteration procedure is applied to carry out the non-linear FEA. The program takes the effect of multi-directional slip of the tensile armour into account, and the bending moment induced by each armour layer's response to the external curvature and the effect on pipe curvature along the riser is also taken into account [6].

PFLEX is designed to perform stress analysis of pressure armour caused by ovalisation of the pipe. Only the hoop direction stress components of the pipe are calculated.

BOUNDARY module is to calculate transverse stress in pressure armour, i.e. stress induced by contact forces acting on individual armour wires.

LIFETIME module is to calculate fatigue life for armour components, which is based on S-N curve from small scale tests.

XPOST is a graphical user interface for 3-dimensional results visualization.

BPOST carries out the post processing of local results data in Prefix.raf.

3.3 Geodesic and Loxodromic Curve Assumptions

Bending behaviour of a flexible pipe is much more complicated than the axisymmetric load cases, which is due to the existence of the helical reinforcing layers that will tend to slip relative to the surrounding layers, and also the bending moment is much larger than M_f (Friction Moment).

In order to find the stresses in the tendons during the slip phase, a constant curvature along the Loxodromic curve or Geodesic curve slippage path is assumed along the pipe, which results in different tendon stress components.

3.3.1 Geodesic Curve

The Geodesic Curve is termed as the minimum curve between two sufficiently close points on the surface and has no transverse curvature. Therefore, there only exists one geodesic curve between two close points, and the curve normal vector is parallel to the surface normal vector on this curve.

3.3.2 Loxodromic Curve

This elastic bending theory is to neglect the transverse slip based on the work by sævik[21].

The Loxodromic Curve is termed as that tendon is attached to the supporting core with infinite friction coefficient, and then the tendon along the curve hence has no transverse and longitudinal slip behaviour. But when there is a bending on the riser, however large the friction coefficient, the axial strain from the compression side to the tension side is too large and should be eliminated by a longitudinal slip along the loxodromic curve path.

3.3.3 Stress components calculation under two assumptions

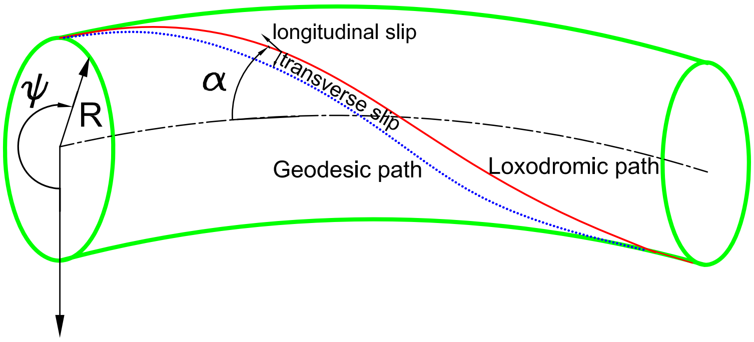

Figure 3.1: Geodesic and Loxodromic curves.

Stress under geodesic assumption

Reference to [24], the dynamic bending stress components under geodesic assumption can be listed as below:

- Axial stress

$$\sigma_{xx-ax} = min(ERcos^2\alpha\kappa_y cos\psi, 2[\frac{\pi R}{2sin\alpha A}(P_0 + P_i)b(1+e)\mu cos\psi]) \tag{3.1}$$

- Normal curvature stress

$$\sigma_{xx-my} = \frac{3}{2}cos^2\alpha\kappa_y hEcos\psi \tag{3.2}$$

- Transverse curvature stress

$$\sigma_{xx-mz} = 0 \tag{3.3}$$

Stress under loxodromic assumption

The dynamic bending stress components under loxodromic assumption can be listed as below:

- Axial stress

$$\sigma_{xx-ax} = min(ERcos^2\alpha\kappa_y cos\psi, 2[\frac{\pi R}{2sin\alpha A}(P_0 + P_i)b(1+e)\mu cos\psi]) \tag{3.4}$$

- Normal curvature stress

$$\sigma_{xx-my} = \frac{1}{2}cos^4\alpha\kappa_y hEcos\psi \tag{3.5}$$

- Transverse curvature stress

$$\sigma_{xx-mz} = \frac{1}{2} cos\alpha(1 + sin^2\alpha)\kappa_y bEsin\psi \tag{3.6}$$

3.4 Analytical stress theory

3.4.1 Stick and slip stress of cross section

Initially, the pipe behaves like a rigid beam according to Navier's hypothesis with bending increasing [20].With reference to Figure 3.6, and only considering the plane surfaces remaining plane assumption i.e. $\beta_2 \neq 0$, the derivation of axial force Q_1 in the tendon before slip is formulated as below:

$$\left.\begin{aligned} Q_1 &= EA\varepsilon \\ \varepsilon &= \frac{dz'}{dz} = \frac{du \cdot cosa}{dz} = \frac{du \cdot cosa}{\frac{dx}{cosa}} = \frac{du}{dx} \cdot cos^2\alpha \end{aligned}\right\} \Rightarrow \quad Q_1 = EA\frac{du}{dx} \cdot cos^2\alpha \tag{3.7}$$

$$\left.\begin{aligned} \Delta L &= [\rho + (-Rcos\psi)] \cdot d\varphi \\ L &= dx \\ \rho \cdot d\varphi &= ds \\ ds &\approx dx \\ \rho &= \frac{1}{\beta_2} \\ \beta_2 &= \frac{d\varphi}{ds} \approx \frac{d\varphi}{dx} \end{aligned}\right\} \Rightarrow \quad \frac{du}{dx} = \frac{\Delta L}{L} = -R \cdot cos\psi \cdot \beta_2 \tag{3.8}$$

By combining Eq.3.7 and Eq.3.8, the axial force Q_1 is:

$$Q_1 = -EAcos^2\alpha Rcos\psi\beta_2 \tag{3.9}$$

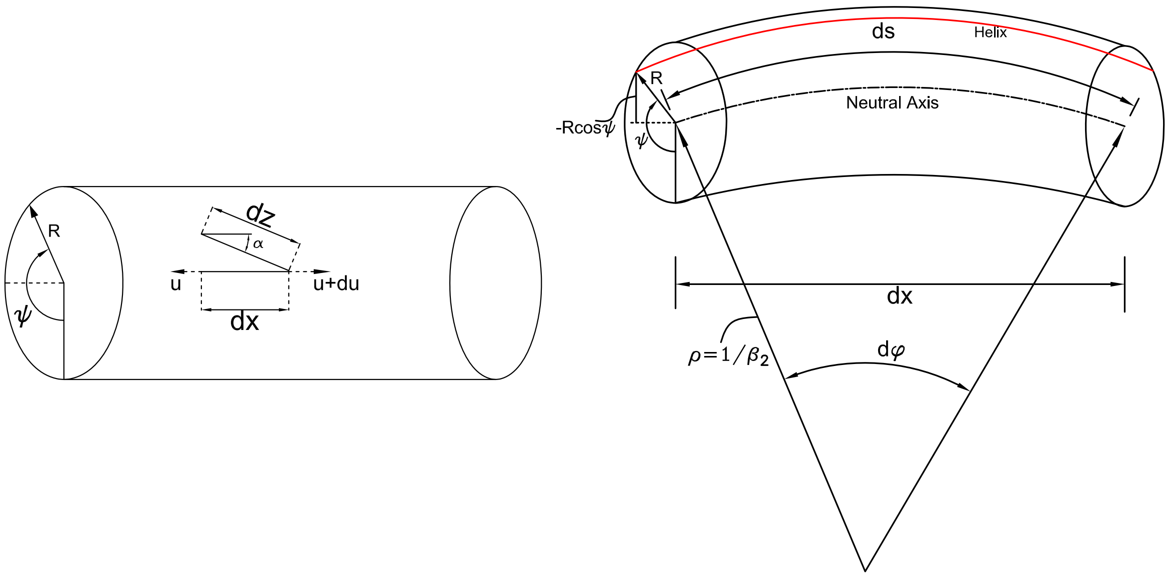

(a) Helix axial strain. (b) Plane remain plane assumption.

Figure 3.2: Derivations of the tendon axial force.

The associated shear force q_1 per unit length along the helix wire which have to fulfil the plane surfaces remaining plane assumption can be derived by differentiating the axial force with respect to the local length coordinate X^1 and applying the relation $\psi = \frac{sin\alpha}{R}X^1$:

$$q_1 = EAcos^2\alpha sin\alpha sin\psi\beta_2 \tag{3.10}$$

The maximum shear stress q_{1c} is found at the pipe neutral axis of bending as for standard beam theory in terms of contact force q_3^I, q_3^{I+1}:

$$q_{1c} = \mu(q_3^I + q_3^{I+1}) \tag{3.11}$$

where μ is the friction coefficient and the index I refers to the inner and outer surfaces of the wire.

The critical curvature is then found as:

$$\beta_{2c} = \frac{\mu(q_3^I + q_3^{I+1})}{EAcos^2\alpha sin\alpha} \tag{3.12}$$

The stress at the topside outer fibre of the pipe at this stage is:

$$S^{11}(\psi = \pi) = \frac{Q_1}{A} = Ecos^2\alpha R\beta_{2c} = \frac{\mu(q_3^I + q_3^{I+1})R}{Asin\alpha} \tag{3.13}$$

It should be noted that this value is a factor $\frac{\pi}{2}$ less than the value found by Eq.3.17 assuming full slip along the quarter pitch helical path.

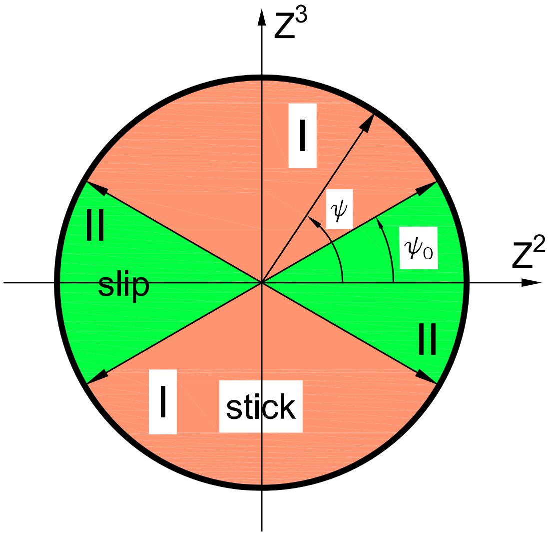

Figure 3.3: The stick-slip domain of cross section.

Figure 3.3 shows one part of the cross-section will be in the slip domain (Region II), another domain will be in the stick-domain (Region I) when considering an arbitrary cross-section exposed to plane bending about axis Z^2. Considering one quarter (so the angle ψ starts from the neutral axis, which is different from the angle defined starting from the lower side of the cross section in the other parts) of the cross-section and at the tensile side(we say the upper right part of Figure 3.3), the transitions between these two regions [13] can be expressed by the angle ψ_0:

$$\psi_0 = cos^{-1}(\frac{\beta_{2c}}{\beta_2}) \tag{3.14}$$

where β_2 are the global curvature quantities at the cross-section centre, and β_{2c} are the critical global curvature.

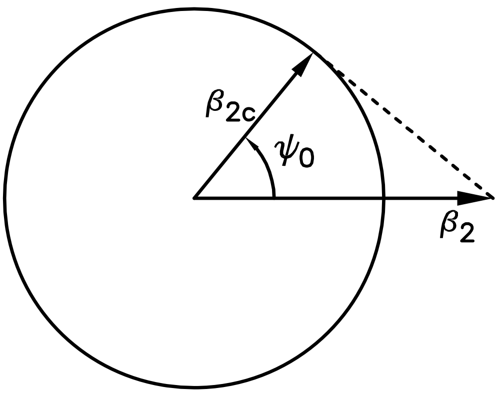

Figure 3.4: The translation angle ψ_0.

With reference to Figure5.3, the slip behaviour happens at the neutral axis first according to the standard beam theory, and the slip length of the helix is $\frac{R\psi}{sin\alpha}$, the stress distribution in Region II of the specified quarter is:

$$S^{11}(\psi) = \frac{\mu(q_3^I + q_3^{I+1})R}{sin\alpha A}\psi \tag{3.15}$$

Stress distribution in Region I, formulated by differentiation of the shear force, the second part is the boundary condition of the stick-slip domain:

$$S^{11}(\psi) = C_\sigma cos^2\alpha R\beta_2(sin\psi - sin\psi_0) + \frac{\mu(q_3^I + q_3^{I+1})R}{sin\alpha A}\psi_0 \tag{3.16}$$

where

C_σ: Young's Modulus

α :lay angle

R :mean layer radius

ψ: the angular coordinate starting from the neutral axis of the pipe

A:tendon cross section area

q_3^I: contact force from the inner layer

q_3^{I+1}: contact force from the outer layer.

Full slip is under the condition that $\psi = \psi_0 = \frac{\pi}{2}$, the stress full value[See reference 21, Eq.(62)] is give by:

$$S_f^{11} = \frac{\pi}{2}\frac{\mu(q_3^I + q_3^{I+1})R}{sin\alpha A} \tag{3.17}$$

The associated bending moment can be derived by integration of the stress. The start slip bending moment contribution from layer I is formulated as:

$$M_c = \frac{R^2\mu(q_3^I + q_3^{I+1})n}{2tan\alpha} \tag{3.18}$$

The full slip bending moment from the same layer is determined to be:

$$M_f = \frac{R^2\mu(q_3^I + q_3^{I+1})n}{\pi tan\alpha} \tag{3.19}$$

The difference between these two moment values is a factor $\frac{\pi}{4}$, and it is in agreement with the value obtained when comparing the initial and full yield bending moment.

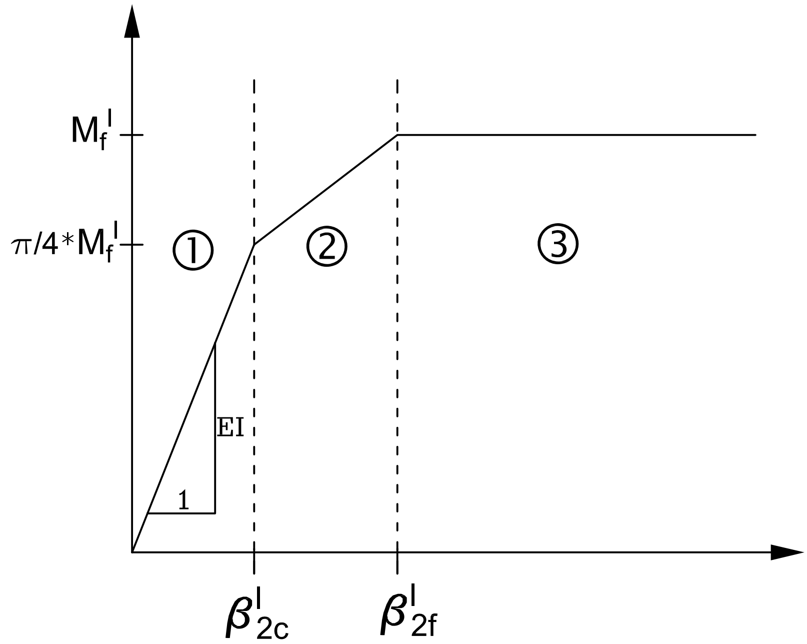

Figure 3.5: Moment curvature diagram.

3.4.2 Kinematics of Helix Element

By neglecting shear deformation and end section warping and only considering the motion of the helix centre line, the kinematic quantities which governs the longitudinal strain can be derived, the work was done by Svein Sævik in 1993 [11], 1999 [12] and 2011 [21].

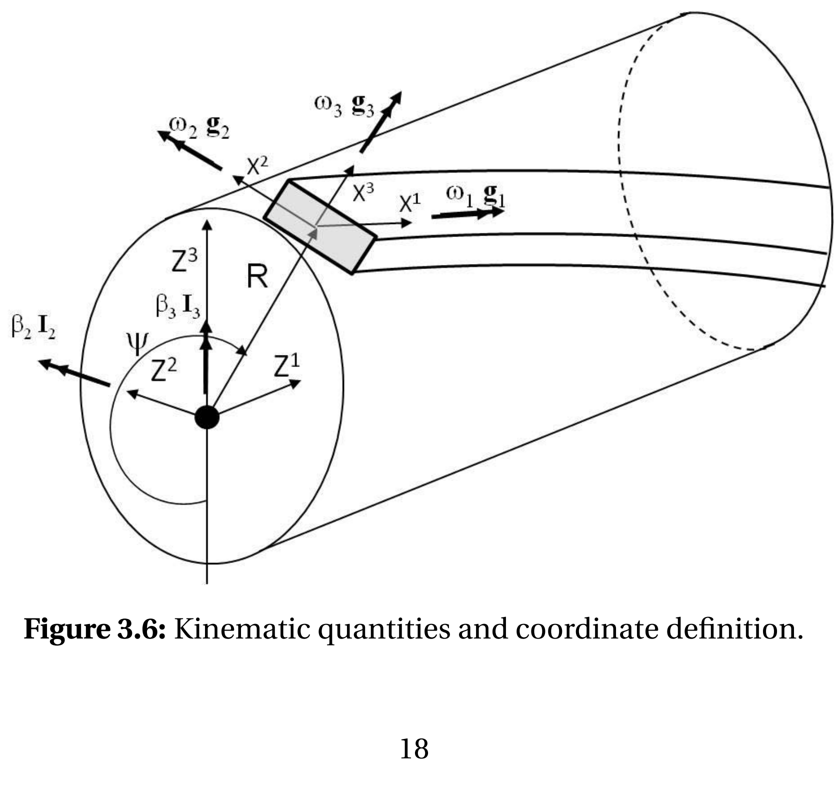

Figure 3.6: Kinematic quantities and coordinate definition.

With reference to Figure 3.6, the following terms are obtained for the Green strain tensor in the Cartesian coordinate system [See reference 16, Eq.(1-7)]:

$$GE_{11} = \varepsilon_1 + X^3\omega_2 - X^2\omega_3 + \frac{1}{2}\varepsilon_1^2 + \frac{1}{2}\varepsilon_2^2 + \frac{1}{2}\varepsilon_3^2 \tag{3.20}$$

where:

$$\varepsilon_1 = u_{1,1} - \kappa_3 u_2 + \kappa_2 u_3 \tag{3.21}$$

$$\varepsilon_2 = u_{2,1} + \kappa_3 u_1 - \kappa_1 u_3 \tag{3.22}$$

$$\varepsilon_3 = u_{3,1} - \kappa_2 u_1 + \kappa_1 u_2 \tag{3.23}$$

$$\omega_1 = \kappa_1 u_{1,1} - \kappa_t u_{2,1} + \kappa_3(u_{3,1} + \kappa_1 u_2) + \kappa_2(u_{2,1} - \kappa_1 u_3) + \omega_{1p} \tag{3.24}$$

$$\omega_2 = -u_{3,11} + \kappa_2 u_{1,1} - 2\kappa_1 u_{2,1} - \kappa_3\kappa_t u_2 + \kappa_1\kappa_1 u_3 + \omega_{2p} \tag{3.25}$$

$$\omega_3 = u_{2,11} + \kappa_3 u_{1,1} - 2\kappa_1 u_{3,1} + \kappa_2\kappa_t u_2 - \kappa_1\kappa_1 u_2 + \omega_{3p} \tag{3.26}$$

Statements:

G: the determinant of the metric tensor given as:

$$G = (1 + X^3\kappa_2 - X^2\kappa_3)^2 \tag{3.27}$$

E_{11}: the Green strain tensor i curve linear coordinates

ε_1: the 1^{st} order axial strain

ε_2: the centre line rotation about the X^3 axis

ε_3: the centre line rotation about the X^2 axis

ω_1: the effective torsion increment corrected for the effect of curvature along a distance dX^1

ω_2: the associated effective normal curvature increment about the X^2 axis

ω_1: the associated transverse curvature increment about the X^3 axis

ω_{ip}: the components of any prescribed torsion and curvature values from bending

$u_{i,j}$:the differentiation of the displacement components u_i along axis X^i with respect to the curvilinear coordinate X^j

κ_1: the initial total accumulated torsion of the cross-section centreline

κ_2: the initial accumulated curvature in the (X^1, X^3) plane

κ_3: the initial accumulated curvature in the (X^1, X^2) plane

The rule of the sign convention in these expressions is such that positive torsion and curvature are based on obtaining positive rotation when applying the right hand rule and moving an unit distance along the X^1 axis, and in the initial helix state, we can also obtain ω_i, ε_i, $\kappa_1 = \frac{sin\alpha cos\alpha}{R}$, $\kappa_2 = \frac{sin^2\alpha}{R}$ and $\kappa_3 = 0$.

Under the assumption that the wire is forced to follow the supporting surface, the kinematic constraint describing the torsion rotation θ_1 can be expressed as:

$$\theta_1 = \kappa_1 u_1 - \kappa_t u_2 \tag{3.28}$$

The transverse curvature κ_t is given by:

$$\kappa_t = \frac{cos^2\alpha}{R} + sin^2\alpha\left(\frac{-w_{2,11}sin\psi}{1 - Rw_{2,11}sin\psi} + \frac{w_{3,11}cos\psi}{1 + Rw_{3,11}cos\psi}\right) \tag{3.29}$$

where w_i is the global displacement along the global axis Z^i.

3.4.3 Sandwich beam model for HSHEAR352

The sandwich beam model(SBM) for HSHEAR353 is shown below:

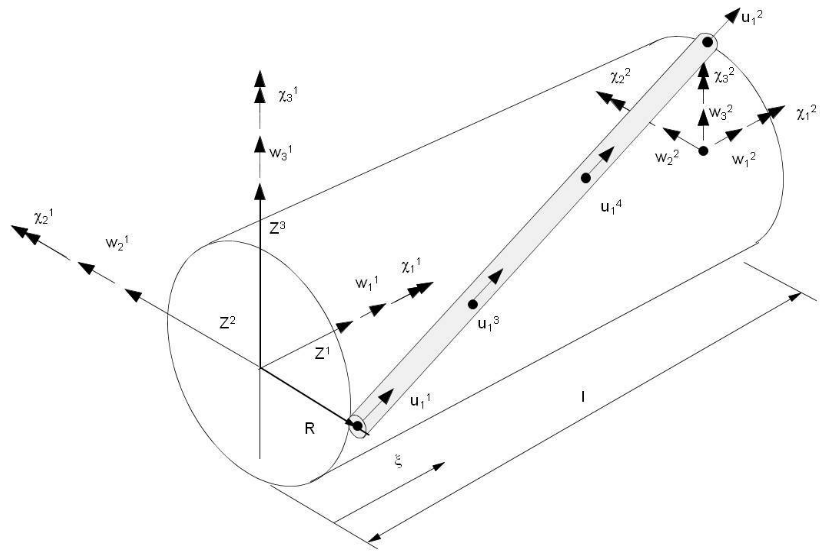

Figure 3.7: Sandwich beam model for HSHEAR352.

Reference to proceeding [19], the shear interaction model is shown below:

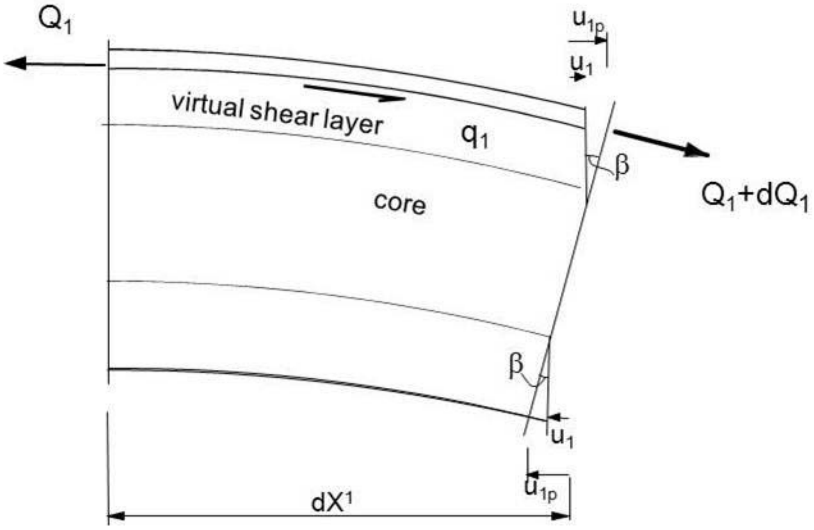

Figure 3.8: Shear interaction model.

In this thesis work, loxodromic curve assumption is applied for itcode0 and itcode1 models, and only considering axial displacements between the core and each wire, the internal work contribution from each tendon can be written as:

$$W_i = \int_0^l EA(\beta_{,1} + u_{1p,1})\delta\beta_{,1} + c\beta\delta\beta + GI_1\omega_{1p}\delta\omega_1 + EI_2\omega_{2p}\delta\omega_2 + EI_3\omega_{3p}\delta\omega_3 dX^1 \tag{3.30}$$

where:
$\beta = u_1 - u_{1p}$: the relative displacement between tendon and core along the helical path, see Figure 3.8
ω_{ip}: the prescribed torsion and curvature quantities if plane surfaces remained plane and the wire strain, torsion and curvature being described by the loxodromic curve quantities.
c: the non-linear shear stiffness parameter determined by the stick-slip behaviour between layers, value is 0 in the slip domain.

Reference to [21], the sandwich beam model is briefly introduced. In this model, the method taken with respect to the stick-slip behaviour in bending is by considering each individual tendon sliding relative to the supporting core layer and study the contribution to the internal work applying the Principle of Virtual Displacements (PVD) weak form as, [See reference 21, Eq.(75)]:

$$W_i = \int_0^l C_\sigma A(\gamma_{,1} + u_{1p,1})\delta(\gamma_{,1} + u_{1p,1}) + k\gamma\delta\gamma dX^1 \tag{3.31}$$

where:

$\gamma = u_1 - u_{1p}$: the relative displacement between tendon and core along the helical path, same as β mentioned above

u_1: represents the longitudinal displacement along the tendon

u_{1p}: the tendon displacement that would occur if plane surfaces remain plane after bending

The plane surface remaining plane after deformation can be expressed in terms of the transverse displacement quantities:

$$u_{1p} = Rcos\alpha cos\psi w_{3,1} - Rcos\alpha sin\psi w_{2,1} \tag{3.32}$$

where w_i are the transverse displacement components at the cross-section centre.

Reference to [13], the potential energy of the tendon sliding on the supporting core layer is:

$$\prod = \frac{1}{2}\int_0^l EA(\frac{dv_s}{ds})^2 + \frac{1}{2}k(v_s - v_p)^2 ds \tag{3.33}$$

where:

EA: the axial stiffness of the tendon

v_s: the actual longitudinal displacement along the tendon

v_p: the tendon displacement that would occur if plane surfaces remain plane after bending

k: the non-linear shear stiffness parameter describing the friction stick-slip behaviour.

3.4.4 Torsion and curvature due to axisymmetric loads and bending

Generally, we can divide the loads applied to the flexible pipe into 2 parts: axisymmetric loads and asymmetric loads. The axisymmetric loads are defined as loads which can keep the cylindrical shape of the overall pipe. Reference to Figure 3.9, the torsion and curvature due to overall pipe axial, torsion and radial motions are defined as:

$$\omega_1 = \frac{sin^3\alpha cos\alpha}{R} w_{1,1} - \frac{sin^3\alpha cos\alpha}{R^2} u_3 + cos^4\alpha \chi_{1,1} \tag{3.34}$$

$$\omega_2 = -\frac{sin^2\alpha cos^2\alpha}{R} w_{1,1} + \frac{sin^2\alpha cos^2\alpha}{R^2} u_3 + (2sin\alpha cos^3\alpha + sin^3\alpha cos\alpha)\chi_{1,1} \tag{3.35}$$

where χ_i is the prescribed rotation quantities at the pipe centreline.

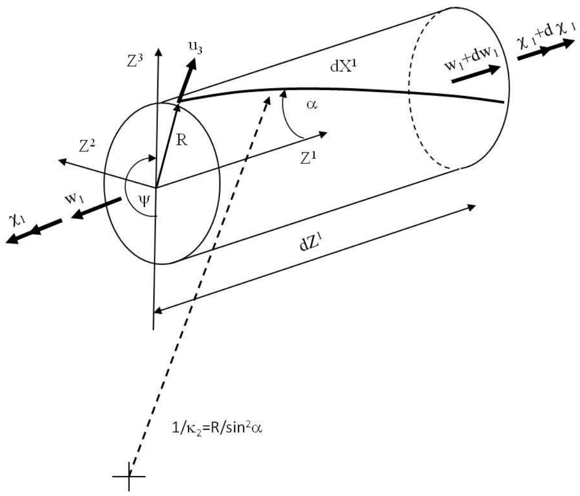

Figure 3.9: Axisymmetric deformation quantities.

The prescribed torsion and bending quantities [10] ω_{ip} are:

$$\omega_{1p} = sin\alpha cos^3\alpha(cos\psi\beta_2 + sin\psi\beta_3) \tag{3.36}$$

$$\omega_{2p} = -cos^4\alpha(cos\psi\beta_2 + sin\psi\beta_3) \tag{3.37}$$

$$\omega_{3p} = (1 + sin^2\alpha)cos\alpha(sin\psi\beta_2 - cos\psi\beta_3) \tag{3.38}$$

The expressions related to torsion and curvature ω_i along the modified loxodromic curve are:

$$\omega_1 = 2sin\alpha cos^3\alpha cos\psi\beta_2 \tag{3.39}$$

$$\omega_2 = -cos^2\alpha cos2\alpha cos\psi\beta_2 \tag{3.40}$$

$$\omega_3 = (1 + sin^2\alpha)cos\alpha cos\psi\beta_2 \tag{3.41}$$

3.5 Pipe elements

In this thesis work, modelling is based on using the pipe elements, i.e. core layer is established by elements PIPE52 and HSHEAR363, tensile layers are built by elements HSHEAR352 and HSHEAR353, contact layers are using element HCONT463.

Brief introduction of pipe element theory and the details of pipe elements mentioned above will be introduced in this section.

3.5.1 Pipe element theory

Tensor and vector theories are of the main mathematical applications in this software. For more details, referring to bflex theory manual [14]. Furthermore, for the tensile layer, due to the shape of the cross section, curved beam theory is also applied, the derivation of the equations are shown in the master thesis written by Mats.Jorgen.Thorsen[24].

The pipe element is the finite element model which includes six beam degrees of freedom (DOFs) per node, the orientation and motion of the beam node is referred to a global coordinate system with base vectors $\mathbf{I}_i$, but the element deformation is measured relative to a local beam element system $\mathbf{I}_j$ attached to each element, and the rigid body deformations are neglected during deformation. Figure 3.10 gives the definition of beam nodes motion.

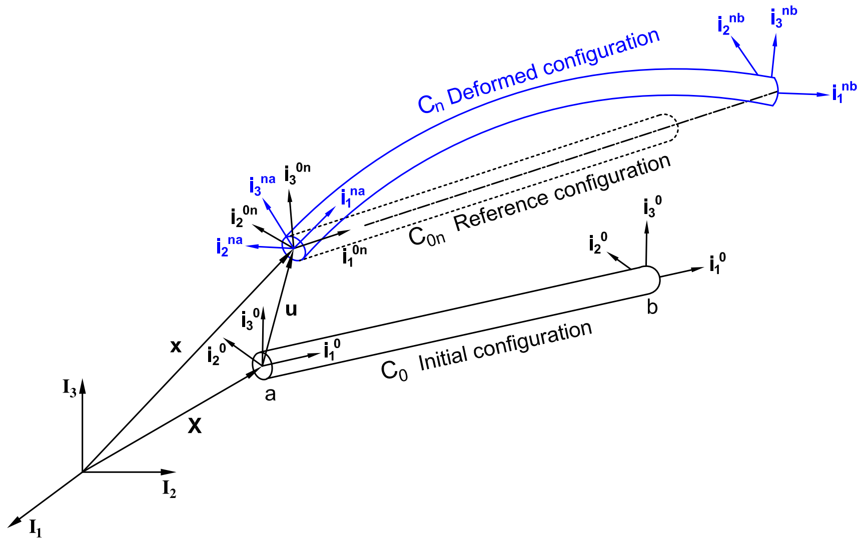

Figure 3.10: Motion of beam nodes[9].

The position of nodal base vector system is defined in terms of the transformation matrices, these matrices values can be found in the Prefix.bof file. In the material section, linear elastic material is applied for all layers, and under the assumption of plane surface remaining plane, then kinematic related to elastic beam element can be applied in the theory.

Under the conditions mentioned above, Bernoulli-Euler and Navier hypothesis are applied in the beam equilibrium equation. Green strain tensor is used as strain measure when formulating the incremental equilibrium equations, which means that the second order longitudinal strain term in the Green strain is neglected, so are for coupling terms between longitudinal strain and torsion and for shear deformations.

The displacements of an arbitrary point P, defined by local coordinates x, y, z in the cross section may be expressed as follows:

$$\begin{cases} u_x(x,y,z) = u_{x_0} - y u_{y_0,x} - z u_{z_0,x} \\ u_y(x,y,z) = u_{y_0} - z\theta_x \\ u_z(x,y,z) = u_{z_0} - y\theta_x \end{cases} \tag{3.42}$$

Then the longitudinal Green strain is found to be:

$$E_{xx} = u_{x_0,x} - y u_{y_0,xx} - z u_{z_0,xx} + \frac{1}{2}(u^2_{y_0,x} + u^2_{z_0,x}) \tag{3.43}$$

On the process of tension value in Bflex2010, the value varies from positive to negative, which is contrary to the definition that tension value is positive. In the Bflex theory, all the sign of values are defined by the base vector shown as below:

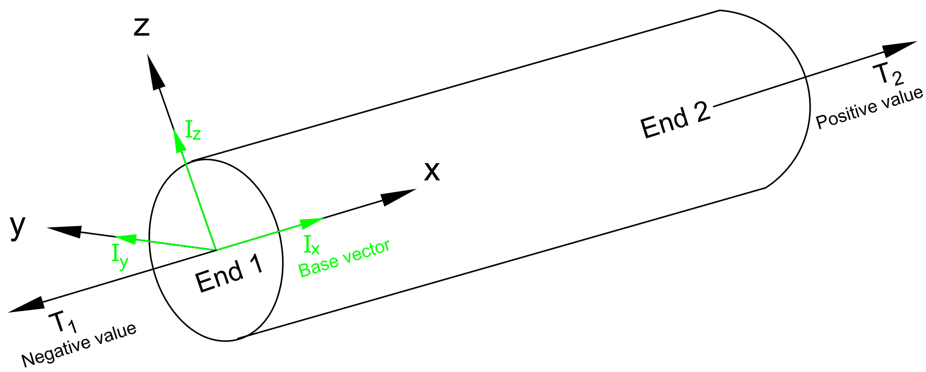

Figure 3.11: Tension definition.

3.5.2 Element PIPE52

The PIPE52 element is the elastic / elastoplastic pipe element, which handles the core and resultant moment based model for the armour layers. This element can also model the bending stiffener, the axisymmetric and bending contributions from a flexible pipe.

3.5.3 Element HSHEAR352

The HSHEAR352 element (referred to Figure 3.7) is the elastic helix tensile armour element, this element is composed of 6 nodes with 2 centroid nodes and 4 helix nodes. For each centroid node, existing 6 DOFs, while for each helix node, existing only the local axial DOF along the helix, so totally 16 DOFs to describe the element. However, for the system point of view, the 2 internal nodes (the friction force is applied on these 2 internal nodes, which enable the cubic interpolation) of the helix are dummy, only the 2 end nodes of the helix and the 2 centroid nodes are used to establish the element, which is defined in polar coordinate system, enabling the helix longitudinal slip behaviour.

3.5.4 Element HSHEAR353

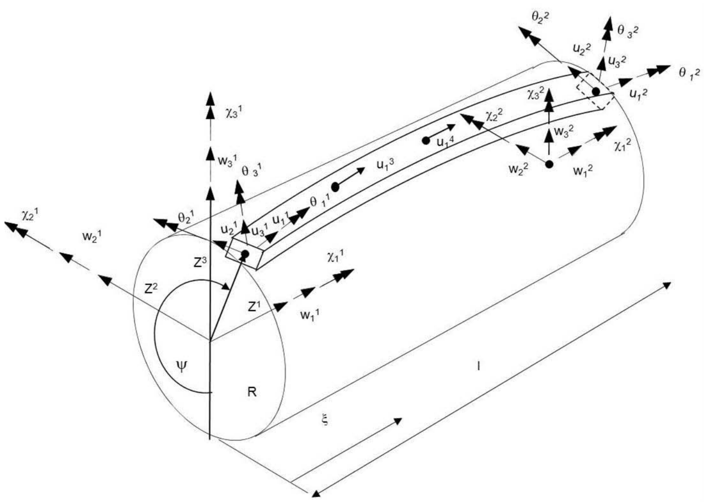

Figure 3.12: DOFs of HSHEAR353 element.

The HSHEAR353 element (referred to Figure 3.12) is an elastic helix tensile armour element which is in the same number of nodes as HSHEAR352 element. But for the 2 end nodes of the helix, existing 6 DOFs, so totally 26 DOFs to describe the element, 12 of them are associated to the standard beam DOFs at the centreline used to describe the prescribed global strain quantities, 14 of them are used to describe the local displacement of the wire relative to the core. Using these DOFs can allow cubic interpolation in all directions in order to eliminate the membrane locking phenomenon due to the curvature coupling terms, see [19].

For torsion DOF of the two end nodes of the helix, however, can be described through [Equation 3.28], so actually 24 DOFs to describe the element, but still 6 DOFs are attached to the 2 end helix nodes so as to match the standard beam DOFs. This element is also defined in polar coordinate system, which enables bi-directional slip and the damping model only includes global Rayleigh damping.

The internal virtual work contribution from the HSHAEAR353 element is:

$$W_i = \int_0^l \left[EA(\beta_{1,1} + u_{1p,1})\delta\beta_{,1} + GI_1(w_1 + w_{1p})\delta(w_1 + w_{1p}) + EI_2(w_2 + w_{2p})\delta(w_2 + w_{2p}) + EI_3(w_3 + w_{3p})\delta(w_3 + w_{3p})\right] dX^1 \tag{3.44}$$

The main difference between HSHEAR352 and HSHEAR353 is the for the former element, the friction force is applied on the two internal nodes, whereas for the latter element, friction force is applied in a separated contact element (HCONT453 or HCONT463).

3.5.5 Element HSHEAR363

The purpose of developing this element is to allow radial motion which is described by local radial and ovalization motions in addition to the standard beam quantities, this shell element can model the core layer approximately. One additional node is introduced, 3 DOFs of this node are to deal with the circumferential strain and the associated ovalization. The HSHEAR363 element is shown below as Figure 3.13:

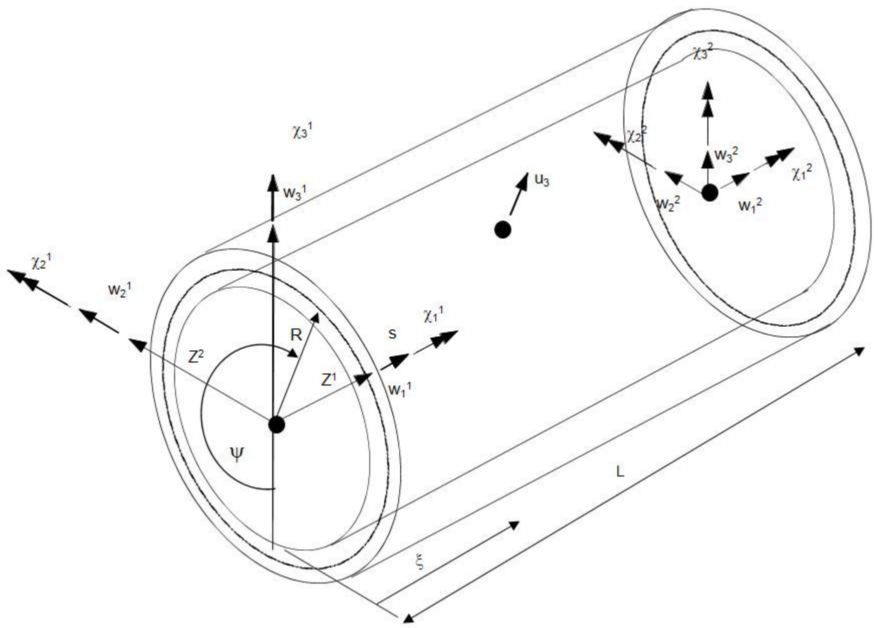

Figure 3.13: DOFs of HSHEAR363 element.

The radial displacement u_3 (Figure 3.14)is assumed to be formulated as:

$$u_3 = \gamma_1 + \gamma_2 cos2\psi + \gamma_3 sin2\psi \tag{3.45}$$

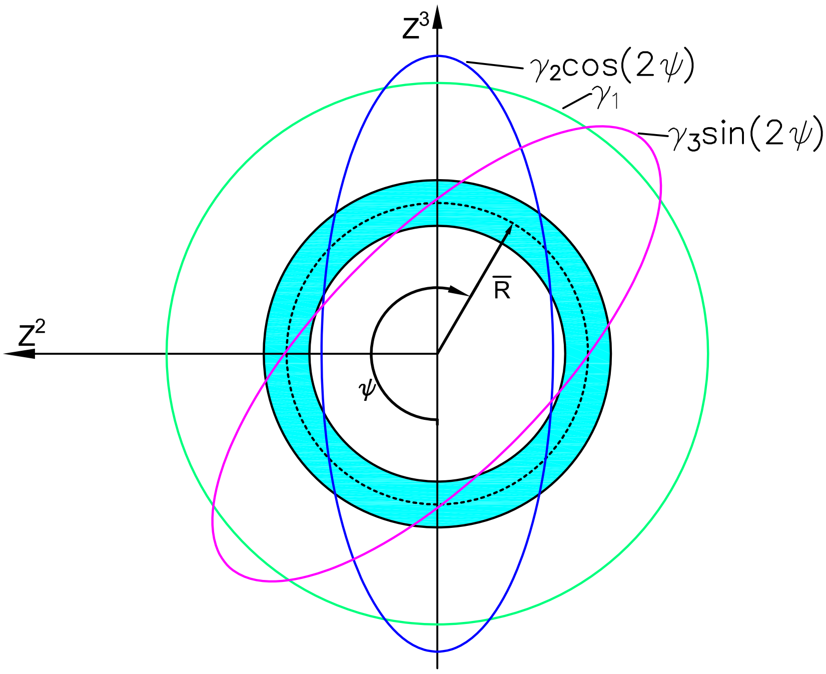

Figure 3.14: The additional DOFs of the HSHEAR363 element.

This element can deal with the plastic layers, the pressure armour layers and the tape layers, which is shown in Chapter 4.

For the pressure armour layers and the tape layers, the longitudinal strain can be expressed as:

$$\varepsilon_{11} = cos^2\alpha w_{1,1} + \frac{sin^2\alpha}{R}u_3 + Rsin\alpha cos\alpha\chi_{1,1} - u_{3,22}sin^2\alpha X^3 \tag{3.46}$$

For the plastic layers, the strain quantities are formulated as:

$$\begin{aligned} \varepsilon_{11} &= w_{1,1} + w_{3,11}Rcos\psi - w_{2,11}Rsin\psi \\ \varepsilon_{22} &= \frac{u_3}{R} - u_{3,22}X^3 \\ \varepsilon_{33} &= R\chi_{1,1} \end{aligned} \tag{3.47}$$

Helix contact element overview

Contact elements are non-structural elements, however, artificial lumped mass and lumped damping are allowed for numerical purposes, considering 2 elements (element A and B) which came into contact, after a time Δt, two situations may occur:

1. Gap opening

$$g = (\Delta\mathbf{u}_B - \Delta\mathbf{u}_A)\cdot\mathbf{n} + g_0 \geqslant 0 \tag{3.48}$$

2. Contact

$$g = (\Delta \mathbf{u}_B - \Delta \mathbf{u}_A) \cdot \mathbf{n} + g_0 < 0 \tag{3.49}$$

where:

g_0: initial gap.

g: the current gap at time $t + \Delta t$ in the direction of $\mathbf{n}$.

$\mathbf{n}$: the outward surface normal vector of body A.

Further, if contact has been established, relative slippage including friction work will occur when:

$$\gamma = (\Delta \mathbf{u}_B - \Delta \mathbf{u}_A) \cdot \mathbf{t} + \gamma_0 \neq 0 \tag{3.50}$$

where:

$\mathbf{t}$: the tangent vector pointing towards Body B.

There are three commonly used principles when dealing with contact problems see [15], these are

1) Lagrange multiplier method(LM),

2) Penalty method(PM),

3) Mixed Method(MM).

In LM, the constraint conditions for a contact problem are satisfied by introducing Lagrange parameters in the variation statement.

In PM, the contact pressure is assumed proportional to the amount of penetration by introducing a pointwise penalty parameter, the final stiffness matrix does not contain additional terms.

In MM, it is highly dependent on the selected order of the contact pressure.

The constitutive relation used to model friction in the contact elements consists of two major ingredients:

1) A friction surface,

2) A slip rule.

3.5.6 Element HCONT453

The HCONT453 element is a contact element between two HSHEAR353 element, which describes the interlayer contact forces and the friction with regard to the relative displacement.

The element is composed of 4 nodes, which are both the end nodes of the 2 HSHEAR353 helix element, if we neglect the torsion of both the helix elements, this contact element contains 20 DOFs, but totally 24 DOFs are set up in order to match the standard beam DOFs, the DOFs of HCONT453 model is referred to Figure 3.15.

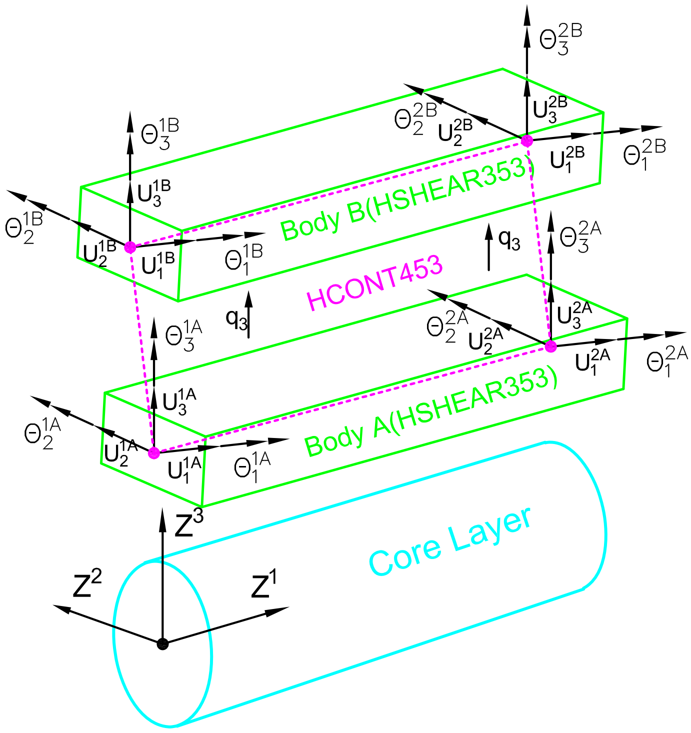

Figure 3.15: DOFs of HCONT453 element.

The internal work related to the HCONT453 element is formulated as:

$$\begin{aligned}\Delta\pi = &-\int\limits_{S_c}(q_3+\Delta q_3)\bullet u_3 ds - \frac{1}{2c_n}\int\limits_{S_c}\Delta q_3^2 ds \\ &-\int\limits_{S_c} q_t \bullet \Delta\beta ds - \frac{1}{2}\int\limits_{S_c}\Delta q_t \bullet \Delta\beta ds\end{aligned} \tag{3.51}$$

where c_n is a penalty stiffness parameter.

3.5.7 Element HCONT463

This contact element is to fit the quantities as defined for the HSHEAR353 and HSHEAR363 elements, for the HSHEAR353 element, both the longitudinal and transverse directions are included at one end, whereas for the HSHEAR363 element, radial displacement is introduced only. If we neglect the torsion DOFs in both the end nodes of the helix, then the contact element includes 13 (5+5+3) DOFs. To match the standard 6 DOFs in each node of the helix, the element is implemented with 15 (6+6+3) DOFs, the DOFs of HCONT463 model is referred to Figure 3.16.

Only in the radial motion, considering the helix beam element HSHEAR353 named B, comes into contact with HSHEAR363, named A, then the displacements includes the radial displacement along B side is described by 4 DOFs, while in the A side, 3 DOFs are included, so totally 7 DOFs in the radial direction.

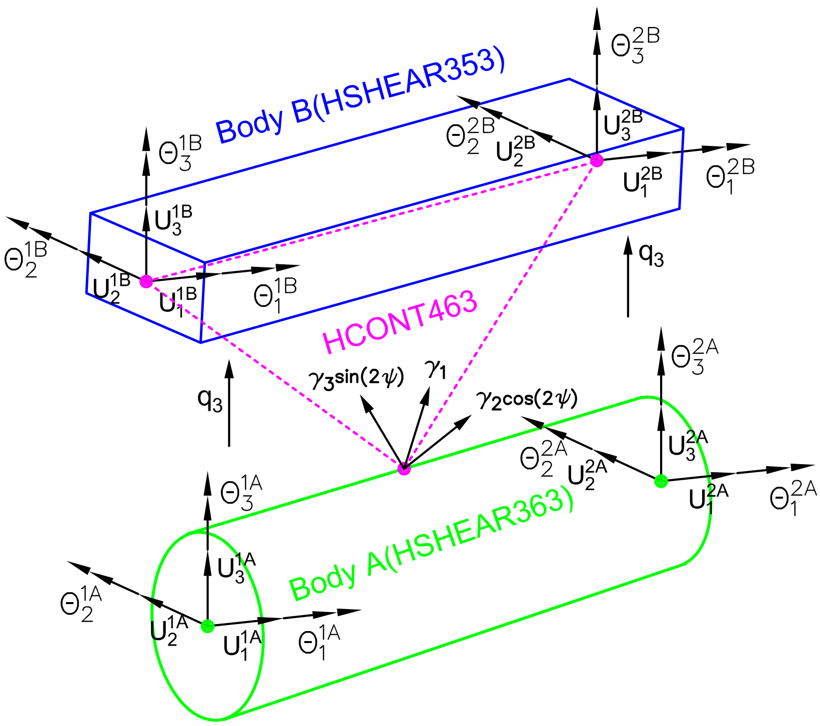

Figure 3.16: DOFs of HCONT463 element.

3.6 Brief Introduction of Failure Modes and Design Criteria

Due to the complicated structure of the flexible pipe, it is essential to have a comprehensive understanding of the flexible pipe performance and failure modes both in the design phase and the operational phase, which means that the flexible pipe should satisfy the functional requirements under the actual loading conditions.

3.6.1 Failure Modes

Referenced to the handbook[5], two failure modes are caused by the transportation of fluid:

- *Leakage*
- *Reduction of the internal cross section*

More details are illustrated in the flow chart below:

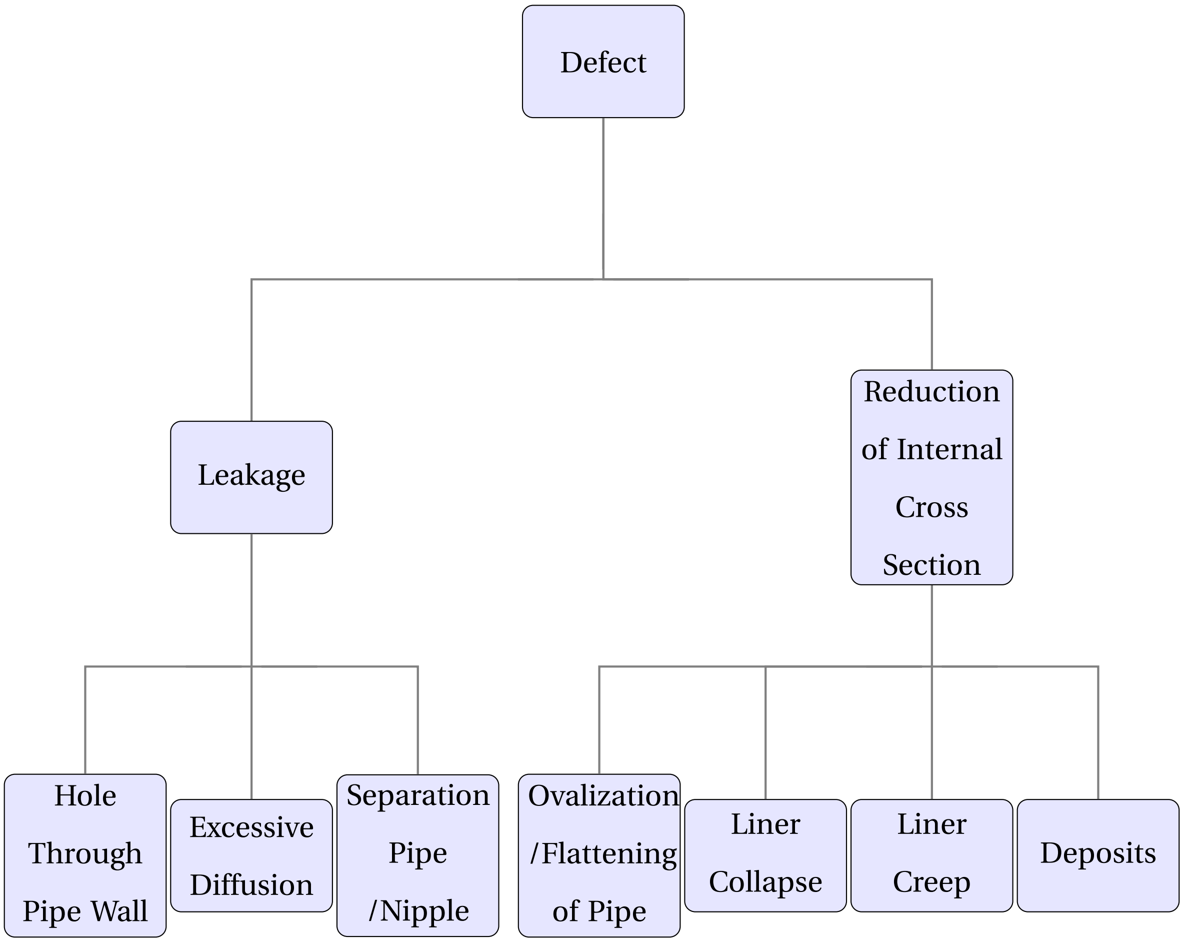

Due to over load tension, compression, bending, torsion, fatigue as well as erosion and diffused fluid, there will be some failures in the tensile and pressure armours, the checklist for design can be found in API Recommended Practice 17B[1].

Pipe Global Failure Modes	Potential Failure Mechanisms	Design Solution/Variables [Ref.API Spec 17J [3] Design Criteria]

Collapse	1.Collapse of Carcass and/or pressure armour due to excessive tension	1.Increase thickness of carcass strip, pressure armour or internal pressure sheath(smooth bore collapse)
	2.Collapse of Carcass and/or pressure armour due to excessive pressure	2.Modify configuration or installation Design to reduce loads
	3.Collapse of carcass and/or pressure armour due to installation loads or ovalization due to installation loads	3.Add intermediate leak-proof sheath (smooth bore pipes)
	4.Collapse of internal pressure sheath in smooth bore pipe	4.Increase the area moment of inertia of carcass or pressure armour
Burst	1.Rupture of pressure armours due to excess internal pressure	1.Modify design,e.g.,change lay angle,wire shape,etc.
	2.Rupture of tensile armours due to excess internal pressure	2.Increase wire thickness or select higher strength material if feasible
		3.Add additional pressure or tensile armour layers
Tensile Failure	1.Rupture of tensile armors due to armour due to excessive tension	1.Increase wire thickness or select higher strength material if feasible.
	2.Collapse of Carcass and/or pressure armors and/or internal pressure sheath due to excessive tension	2.Modify configuration designs to reduce loads.
	3.Snagging by fishing trawl board or anchor, causing over bending or tensile failure	3.Add two more armor layers.
		4.Bury pipe.
Compressive Failure	1.Bird-caging of tensile armor wires.	1.Avoid riser configuration that cause excessive pipe compression
	2.Compression leading to upheaval buckling and excess bending.	2.Provide additional support /restraint for tensile armors, such as tape and/or additional

		or thicker outer sheath.
Over bending	1.Collapse of carcass and/or pressure armor or internal pressure sheath. 2.Rupture of internal pressure sheath. 3.Unlocking of interlocked pressure or tensile armor layer. 4.Crack in outer sheath.	1.Modify configuration designs to reduce
Torsional Failure	1.Failure of tensile armor wires. 2.Collapse of carcass and/or internal pressure sheath. 3.Birdcaging of tensile armor wires.	1.Modify system design to reduce torsional 2.Modify cross-section design(e.g. change lay angle of wires,and extra layer outside armor wires, etc.)to increase torsional
Fatigue Failure	1.Tensile armor wire fatigue. 2.Pressure armor wire fatigue.	1.Increase wire thickness or select alternative material,so that fatigue stresses are compatible with service life requirements. 2.Reduce fatigue loads
Erosion	1.Of internal carcass	1.Material selection. 2.Increase thickness of carcass. 3.Reduce sand content. 4.Increase min bending radius(MBR)
Corrosion	1.Of internal carcass. 2.Of pressure of tensile armor exposed to seawater,if applicable. 3.Of pressure of tensile armor exposed to diffused product.	1.Material selection. 2.Cathodic protection system design. 3.Increase layer thickness. 4.Add coating or lubricants

Table 3.1: Checklist of Failure Modes for Structural Design of Unbonded Flexible Pipe.

Some failure modes configurations are shown below:

Figure 3.18: Bird-caging failure.

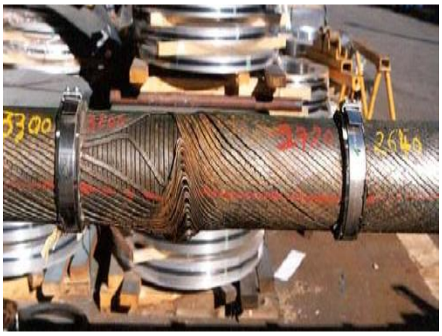

Figure 3.19: Lateral buckling failure.

Figure 3.17: Rupture failure of flexible pipe.

3.6.2 Design Criteria

A design criterion is designed to prevent the failure, which is reflected in the form of utilization factor, ratio of structural capacity and applied load, by consideration of many uncertainties, the allowable utilization factor in rules is much lower than 1.

According to API 17B [1], the design criteria can be determined by the following parameters:

- Strain: critical parameter for internal pressure and outer sheaths(polymer sheath).
- Creep: happened in the internal pressure sheath.
- Stress: use the utilization factor to define the safety of the steel material, allowance of residual wire stress.
- Hydrostatic Collapse: related to the buckling load of the internal carcass.

- Mechanical Collapse: related to internal carcass due to excessive tension, take all supporting layers into account.
- Torsion: during installation and service conditions, flexible pipe should have torsional strength sufficient to withstand torsional loads.
- Crushing Collapse and Ovalization: happened during conventional laying operations.
- Compression: including effective compression(negative effective tension)and axial(true wall)compression
- Service-life Factor: permissible levels of degradation should be defined.

Chapter 4 Modelling and Post Processing

In this chapter, we mainly describe the procedure of modelling for the 4 inch pipe models, more details about the explanation of the parameters of input file, refer to Appendix A.

In the following sections, only simple commands are given, more details can be found in the Bflex2010 Usermanual[18].

4.1 Pipe coordinate and element explanation

The length of the 4 inch pipe is 1196.0 mm for itcode0, itcode1 and fullfe models. Unit: MPa, N, mm.

For itcode0 and itcode1 models, three layers are defined, named: core layer, tensile1 layer (tenslayer1) and tensile2 layer(tenslayer2). For the core layer, 21 nodes are defined in the global coordinate system, 20 elements are established, while 16 tendons are simulated for the tensile1 layer and tensile2 layer. The tensile layers are defined in the polar coordinate system, with each tendon 21 nodes, 20 elements.

PIPE52 element (Refer to 3.5.2) is applied to core layer, for two tensile layers, element type HSHEAR352 element (Refer to 3.5.3) is applied to two tensile layers.

For fullfe model, 21 nodes are defined for core layer first, then define 7 structural layers, named (from inner to outer): carcass layer, seal layer, zeta layer, (seal and zeta layer are defined by the same way), tensile1 layer, strutape layer, tensile2 layer, outersheath layer. While 4 contact layers are defined, named: contactseal layer (between seal layer and tensile1 layer), tapeoutwardcontact layer (between tensile1 layer and strutape layer), tapeinwardcontact layer (between strutape layer and tensile2 layer), sheathcontact layer (between tensile2 layer and outsheath layer).

All structural layers elements are established by connecting the core nodes and the layer nodes.

For structural layer tensile1 and tensile2, element type HSHEAR353 (Refer to 3.5.4) is used, nodes and elements are defined in the same way as itcode0 and itcode1 cases, while for the other structural layers, element type HSHEAR363 (Refer to 3.5.5) is used, 20 nodes are defined for each layer, these are 3 nodes element.

For the contact layer, using element HCONT463 (Refer to 3.5.7).

4.2 Cross section definition

4.2.1 4 inch pipe model input data

No	Layer	Material	I.D [mm]	Thick [mm]	O.D [mm]
1	CARC	Steel_316	101.6	5.0	111.6
2	THER	Plast_PVDF	111.6	5.1	121.8
3	ZETA	Steel_110	121.8	6.4	134.6
4	THER	Plast_PA11	134.6	2.0	138.6
5	TENS	Steel_190	138.6	2.0	142.6
6	THER	Plast_PA11	142.6	2.0	146.6
7	TENS	Steel_190	146.6	2.0	150.6
8	THER	Rubber	150.6	6.0	162.6
Carcass Layer / Pressure Armour Layer / Tensile Armour Layer details					
Layer	Metric $[mm] \times [mm]$	Mfg Pitch [mm]	Wires	Angle deg[°]	Area $[mm^2]$
1-CARC	–	12.7014	1	87.828	36.0
3-ZETA	–	15.3807	1	87.813	79.23
5-TENS	5×2	565.3604	61	-38.0	10
7-TENS	5×2	597.5288	65	38.0	10

Table 4.1: The 4 inch pipe original data.

4.2.2 4 inch cross-section parameters calculation

1. **Carcass Layer**:

   - Mean Radius: $\overline{R}=\frac{I.D}{2}+\frac{h}{2}=\frac{101.6}{2}+\frac{5}{2}=53.3mm$
   - Area: Given $A = 36mm^2$
   - Lay Angle: Given $\alpha = 87.828°$
   - Pitch: $p = 2 \times \pi \times \overline{R}/tan(\alpha) = 2 \times \pi \times 53.3/tan(87.828°) = 12.7014mm$

2. **Pressure layer**:

   - Mean Radius:$\overline{R}=\frac{I.D}{2}+\frac{h}{2}=\frac{121.8}{2}+\frac{6.4}{2}=64.1mm$

- Area: Given $A = 79.23mm^2$
- Lay Angle: Given $\alpha = 87.813°$
- Pitch: $p = 2 \times \pi \times \overline{R}/tan(\alpha) = 2 \times \pi \times 64.1/tan(87.813°) = 15.3807mm$

3. **Tensile layer1**:
   - Mean Radius:$\overline{R}$=$\frac{I.D}{2} + \frac{h}{2} = \frac{138.6}{2} + \frac{2}{2} = 70.3mm$
   - Area: $A = b \times h = 5 \times 2 = 10mm^2$
   - Lay Angle: Given $\alpha = -38°$
   - Pitch:Given $p = 2 \times \pi \times \overline{R}/tan(\alpha) = 2 \times \pi \times 70.3/tan(|-38°|) = 565.3604mm$

4. **Tensile layer2**:
   - Mean Radius:$\overline{R}$=$\frac{I.D}{2} + \frac{h}{2} = \frac{146.6}{2} + \frac{2}{2} = 74.3mm$
   - Area: $A = b \times h = 5 \times 2 = 10mm^2$
   - Lay Angle: Given $\alpha = 38°$
   - Pitch:$p = 2 \times \pi \times \overline{R}/tan(\alpha) = 2 \times \pi \times 74.3/tan(38°) = 597.5288mm$

The material property can be referred to Appendix A.1.2.

4.3 Boundary Condition

According to different methods used in this thesis, explanations of the boundaries are described as below:

4.3.1 Itcode0 and Itcode1 Boundary Condition

For the core layer, node number 1 at the left hand is fixed in all the six directions, node number 21 at the right hand is fixed in the y direction, which means the y-direction.

For the first and second tensile layers, due to the property of the element used for tensile armour, HSHEAR352, all the nodes at both ends of all the tendons are fixed in the first direction, which means the x-direction.

4.3.2 Fullfe Boundary condition

For the core layer, node number 1 at the left hand is fixed in all six directions, the all nodes are fixed in the second, forth and sixth directions, which means no translation in the y direction, no rotation about the x axis and z axis.

For the first and second tensile layers, due to the property of the element used for tensile armour, HSHEAR353, all the nodes at both ends of all the tendons are fixed in the first and second directions, which means no translation in the x and y directions, then all the nodes of all the tendons are fixed in the 4 and 5 directions, which means no rotation about the x and y axis.

For the carcass layer, all the nodes are fixed in the 1, 2, 3 directions, which means no translation in the x, y and z directions.

For the seal, zeta, tape and outersheath layers, all the nodes are fixed in the 2, 3 directions, which means no translation in the y and z directions.

4.4 Load history

In this thesis, constant internal pressure load is applied only, then prescribed displacement is applied at the right hand of the pipe, which makes it like a cantilever beam to move up and down in the x-z plane.

For internal pressure, factor 1.0 is applied for the itcode0 and itcode1 cases, while for the fullfe case, factor 1.112 is applied in order to tune the mean stress at timeini time 2s, the pressure load factor can be referred to table 4.2.

In BFLEX2010, load factor is linearly interpolated between two points. In this thesis, the prescribed displacement factor and the internal pressure factor are shown in the table next:

Time(s)	Load factor
0	0.0
2	0.0
25	-1.0
50	1.0
75	-1.0
100	0.0

(a)Prescribed displacement factor.

Time(s)	Load factor
0	0.0
0.5	1.0
100	1.0

(b)Internal pressure factor.

Table 4.2: Load history.

4.5 Model Simplification

Based on the boundary condition and the load history mentioned above, this model can be simplified to a cantilever beam with constant internal pressure and cyclic displacement, shown in the figures below:

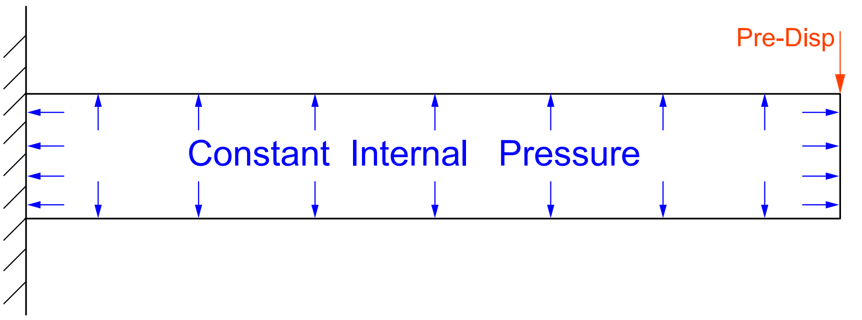

Figure 4.1: Configuration before bending.

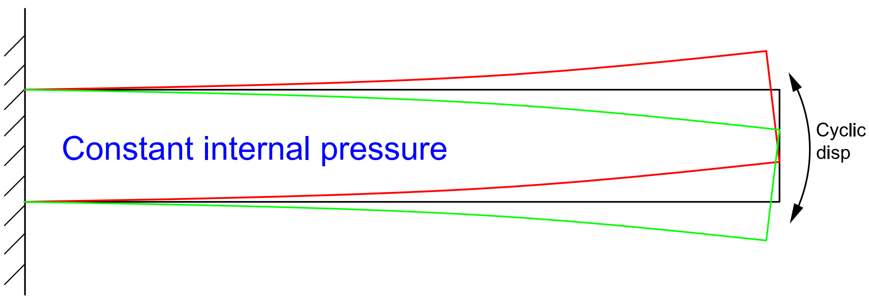

Figure 4.2: Configuration after bending.

4.6 Post Processing

According to the analysis demands, Bflex2010post input file with suffix (.2bpi) is applied. In Bflex2010 Software, for the rectangular cross section tendon, each element is divided into 3 sections (2 end sections and 1 mid section) along the element length, with 4 corners on each section, stress components are integrated in each corner of the 3 sections , curvature is integrated in the 2 end sections, the general tendon element section and corner distribution at the pipe topside location are shown in Figure 4.3.

For the core layer curvature, the first end section is applied by using command card ELPLOT, while for the armour tendon, the first corner of the first end section is applied by using the command card IPPLOT. For more details, see Section[A.2]. Figures 4.4 are used to show the stress components distribution around the cross section, and from the value, the local coordinate system can be decided.

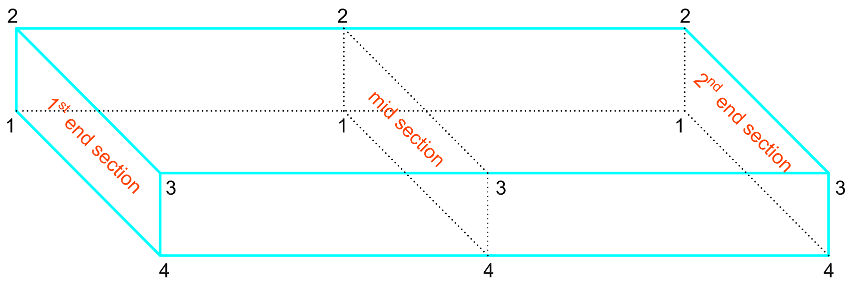

Figure 4.3: Tendon element section and corner location.

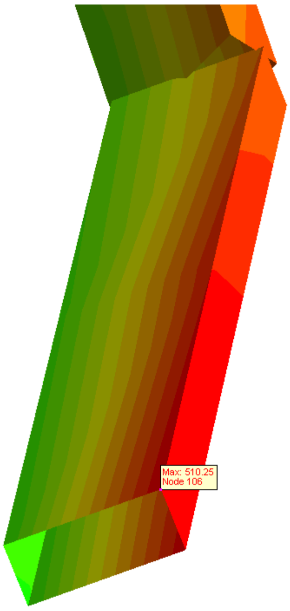

(a)σ_{xx} distribution.

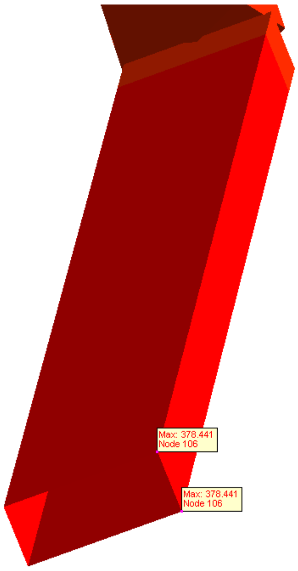

(b)σ_{xx-ax} distribution.

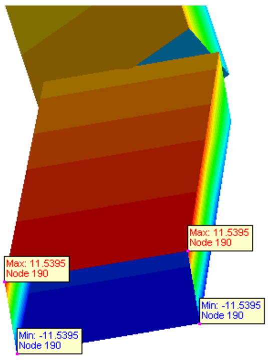

(c)σ_{xx-my} distribution.

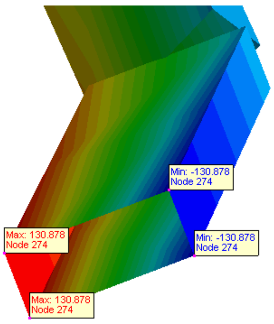

(d)σ_{xx-mz} distribution.

Figure 4.4: Stress components distribution.

Chapter 5 Stress Analysis

5.1 Pipe length definition

In order to eliminate the effect of pipe length (if too short, the stress shows high value), the pitch of the first tensile layer of each pipe is defined as the same value, 2.115.

The length of each pipe is calculated by the following equation, listed in the Table 5.1:

$$L = \frac{2\pi \bar{R}}{tan\alpha} \times p \tag{5.1}$$

where:

$\bar{R}$: the mean radius of the corresponding layer(the first tensile layer, defined in Section 4.2.2).

α: the lay angle of the corresponding layer(the first tensile layer).

p: the pitch value of the first tensile layer, 2.115.

Pipe(inch)	4	6	7.5	8	16
Length(mm)	1196.0	1349.0	2347.0	3118.0	3866.0

Table 5.1: Pipe length.

5.2 Local stress components of the tensile armour

In this section, the local stress components of the tensile armour, analysed in this thesis, are shown in the configuration below:

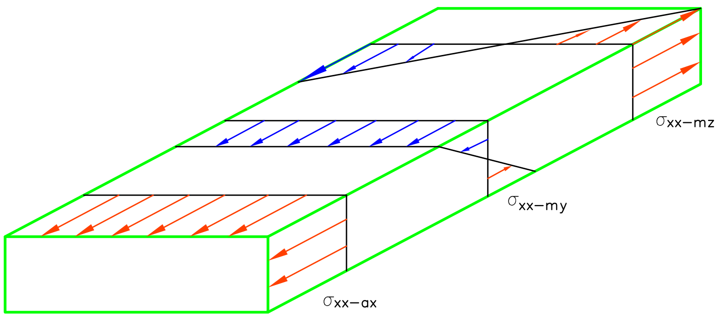

Figure 5.1: Local stress components of the tendon.

- σ_{xx} : local longitudinal stress of the tendon, can be composited by the three stress components below:

$$\sigma_{xx} = \sigma_{xx-ax} + \sigma_{xx-my} + \sigma_{xx-mz}$$

- σ_{xx-ax}: local axial stress over the wire cross-section due to axial force caused by pressure, tension, torsion, moment and friction.
- σ_{xx-my}: local normal curvature stress due to bending about the weak axis, max value at the inner and outer surface of the tendon.
- σ_{xx-mz}: local transverse curvature stress due to bending about the strong axis, max value at both sides of the tendon.

5.3 Estimated tensile layer axial stress

All the cases analysed in this thesis are only under the internal pressure load with the same bending load. Before bending load applied, the tensile layer shows tension behaviour due to internal pressure, and the total longitudinal stress is the same as the axial stress. The estimated average axial stress of all the tensile layers can be estimated through equation:

$$\bar{\sigma}_{xx-ax} = \frac{\frac{\pi}{4} \times {D_p}^2 \times P_i}{n_{tot} \times b \times h \times cos\bar{\alpha}} \tag{5.2}$$

where:

$\bar{\sigma}_{xx-ax}$: average total longitudinal stress of all the tensile layers. Unit:(MPa).

D_p: inner diameter of the layer (not the Carcass layer) where internal pressure applied. Unit:(mm).

P_i: internal pressure. (Before tune by the load history factor: 20 MPa).

n_{tot}: total tendons of all the pipe tensile layers. Unit:–.

b: width of the tendon cross section. Unit:(mm).

h: height of the tendon cross section. Unit:(mm).

$\bar{\alpha}$: average absolute lay angle of all the tensile layers. Unit:deg[°].

The estimated average axial stress for all cases are listed in the table below:

Parameters \ Cases	4 inch	6 inch	8 inch	16 inch	7.5 inch:No carcass	
	2 tensile layer				2 tens	4 tens
D_p	111.6	166.4	227.2	427.1	190.5	190.5
n_{tot}	126	86	110	183	86	182
b	5	10	12.5	12	15	15
h	2	4	5	4	5	5
$\bar{\alpha}$	38	45	30.24	39	37.5	37.25
$\bar{\sigma}_{xx-ax}$	197.04	178.81	136.52	419.74	111.40	52.46

Table 5.2: Estimated average axial stress.

Comments: $\bar{\sigma}_{xx-ax}$ varies for different pipe cases, and the value is mainly decided by the inner diameter D_p, total tendons of the pipe n_{tot} and the geometry of the tendon cross section b and h.

5.4 Pressure load factor calculation

Initially, the internal pressure is $20MPa$, and the pressure load factor (PLF) is 1 for all cases, which results in different mean stress value. In order to make all the cases to be comparable, pressure load factor need to be rectified. The method is carried out by the following procedures:

1) Read the original axial stress σ_{xx-ax} at the tune time (timeini=2s) for all the cases;

2) Set the same axial stress for all the cases, using the value of the 4 inch itcode0 case, $\sigma_{xx-ax} = 223.56(MPa)$ as standard;

3) Calculate the pressure load factor by using the following equation:

$$\text{PLF} = \frac{\text{Standard value}}{\text{Original value}}$$

4) Get the final internal pressure (FIP) by using the following equation:

$$\text{FIP} = 20 \times \text{PLF}(MPa)$$

The original axial stress and the pressure load factor for all the cases are listed in Table 5.3, which are used in the input file.

Comments of the pressure load factor:

1) For all the cases, the pressure load factors are the same for itcode0 and itcode1 models.

2) For all the cases, the pressure load factor of the fullfe model is larger than itcode0 and itcode1 models.

3) For different pipe sizes, no comparisons of the pressure load factors.

4 inch	σ_{xx-ax}	PLF
ITCODE0	223.56	1.00
ITCODE1	223.56	1.00
FullFE	201.07	1.11

(a) 4 inch case.

6 inch	σ_{xx-ax}	PLF
ITCODE0	208.19	1.07
ITCODE1	208.19	1.07
FullFE	173.48	1.29

(b) 6 inch case.

8 inch	σ_{xx-ax}	PLF
ITCODE0	146.45	1.53
ITCODE1	146.45	1.53
FullFE	127.71	1.75

(c) 8 inch case.

16 inch	σ_{xx-ax}	PLF
ITCODE0	436.05	0.51
ITCODE1	436.05	0.51
FullFE	381.78	0.59

(d) 16 inch case.

7.5 inch -2	σ_{xx-ax}	PLF
ITCODE0	131.91	1.70
ITCODE1	131.91	1.70
FullFE	111.20	2.01

(e) 7.5 inch two tenslayer case.

7.5 inch -4	σ_{xx-ax}	PLF
ITCODE0	69.39	3.22
ITCODE1	69.39	3.22
FullFE	67.71	3.30

(f) 7.5 inch four tenslayer case.

Table 5.3: Pressrue load factor for all the cases.

5.5 Stress analysis statements

Element number statement

Due to the effect of the boundary, the third element of each tendon of all the tensile layers is specialized to be analysed. The method to read the third element is either by reading the XPOST file or calculated through the parameters in the input file.

Position statement

In this thesis, for all the stress analysis of the tensile layers, four positions are specialized to perform, which means the top side, front side, bottom side and back side shown as below:

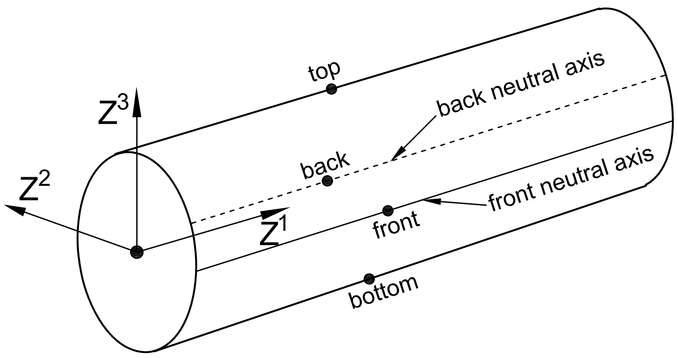

Figure 5.2: The four position of the tensile layer to analyse.

Stress component location statement

Stress component analysis is specified to different location element:

a) σ_{xx} and σ_{xx-ax}, specified to the top side element;

b) σ_{xx-my}, specified to the top side element;

c) σ_{xx-mz}, specified to the front element.

Model assumption statement

a) FullFE model: considering every slip behaviour influence;

b) ITCODE0 and ITCODE1 models: in Section 5.7, both the loxodromic and geodesic slip assumptions are studied.

c) ITCODE0 and ITCODE1 models: in Section 5.8, only considering the loxodromic assumption.

Pipe cases layout statement

In the main text, only the 4 inch pipe case is quoted, the other pipe cases are listed in Appendix B, Appendix C and Appendix D.

Stress analysis statement in Section 5.7 and Section 5.8

In this thesis, the relationship between the global normal curvature and the stress components is studied, the area in the hysteresis loop is the work done by the friction force after slip.

In Section 5.7, stress components σ_{xx-my} and σ_{xx-mz} of both tensile layers are analysed.

In Section 5.8, stress components σ_{xx-ax}, σ_{xx-my} and σ_{xx-mz} and the total longitudinal stress σ_{xx} are analysed.

Figure layout statement

Due to the figure size and the artistic of compose type, figures come after the explanation, and for each page 2 figures are set up.

5.6 Friction sensitivity study

As mentioned in Section 3.3, when the pipe is subjected to bending, the helix will slip on the support pipe as shown below:

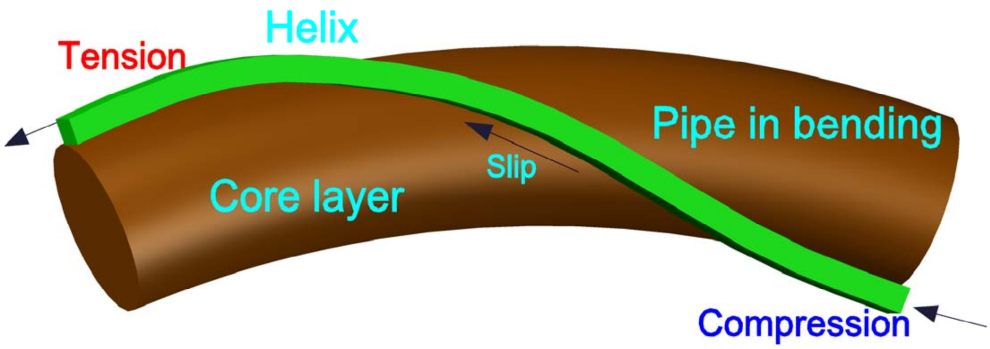

Figure 5.3: Slip behaviour of helix in bending.

The top side of the helix shows tension behaviour while the bottom tends to be compressed under bending load, but due to the effect of the internal pressure before slip, the axial stress σ_{xx-ax} of the compressed side is still positive.

Friction between the adjacent layers will dominate the slip behaviour, so the sensitivity study of friction will help to explain the stress curvature plots. The friction data are obtained from the prefix.blf file, tabulated in the Table 5.4, and the corresponding plots are shown.

In Bflex2010, the friction force per length (stiffness) is defined by equation:

$$\text{Friction Force} = \frac{\text{Unit Force}}{\text{Relative Displacement}}$$

Four points are specified for the friction behaviour, where the first three points are used for plotting.

The friction in the stick domain is defined by the first and second points, while in the slip domain, the second and third points are specified.

The fourth point is relatively large than other point values in order to avoid rigid stiffness and assure convergence.

5.6.1 The friction data and friction plot

4 inch pipe model friction data								
Layer	tensile layer 1				tensile layer 2			
models	Point	Relative Disp (–)	Unit Force (–)	Applied fric-force per-length	Point	Relative Disp (–)	Unit Force (–)	Applied fric-force per-length
itcode0-loxodromic	1	0	0	3.173651	1	0	0	0.988989
	2	0.29985E-02	0.9		2	0.29985E-02	0.9	
	3	0.59970E-02	1		3	0.59970E-02	1	
	4	0.10000E+05	10		4	0.10000E+05	10	
itcode0-geodesic	1	0	0	3.173651	1	0	0	0.988989
	2	0.29985E-02	0.9		2	0.29985E-02	0.9	
	3	0.59970E-02	1		3	0.59970E-02	1	
	4	0.10000E+05	10		4	0.10000E+05	10	
itcode1-loxodromic	1	0	0	3.173651	1	0	0	0.988989
	2	0.29985E-02	0.9		2	0.10438E-02	0.9	
	3	0.59970E-02	1		3	0.20875E-02	1	
	4	0.10000E+05	10		4	0.10000E+05	10	
itcode1-geodesic	1	0	0	3.173651	1	0	0	0.988989
	2	0.29985E-02	0.9		2	0.10438E-02	0.9	
	3	0.59970E-02	1		3	0.20875E-02	1	
	4	0.10000E+05	10		4	0.10000E+05	10	
fullfe	1	0	0	3.008309	1	0	0	0.955223
	2	0.28423E-02	0.9		2	0.10081E-02	0.9	
	3	0.56846E-02	1		3	0.20163E-02	1	
	4	0.74300E+05	10		4	0.74300E+05	10	

Table 5.4: The 4 inch pipe model friction data.

5.6.2 Explanation of the 4 inch case friction plots

In the following analysis, higher/larger stiffness means rigid behaviour, on the contrary, softer behaviour.

Figure 5.4 shows that for the itcode0 model, all the layers of both geodesic and loxodromic cases present the same friction behaviour, while for the fullfe model, the outer layer shows higher stiffness than the inner layer. When comparing itcode0 and fulfe models, the inner layer (black line) of the fullfe model shows larger stiffness in the stick domain, similar stiffness in the slip domain, and the outer layer (blue line) of the fullfe model shows high stiffness than itcode0 model both in the stick and slip domain.

Figure 5.5 shows that for the itcode1 model, same layer of both geodesic and loxodromic cases present the same friction behaviour, and the outer tensile layer appears larger stiffness than the inner layer in the stick and slip domain. When comparing itcode1 and fulfe models, the inner layer (black line) of the fullfe model shows larger stiffness than the inner layer of itcode1 model under both the loxodromic and geodesic assumptions, in the stick domain, similar stiffness in the slip domain. The outer layer (blue line) of the fullfe model shows similar stiffness to the itcode1 model under two assumptions in both the stick and slip domain.

Figure 5.6 shows that for itcode0 and itcode1 models under loxodromic assumption, all layers of itcode0 model and the inner layer of the itcode1 model follow the same friction trend, while the outer layer of itcode1 model appears higher stiffness and similar to the outer layer of the fullfe model in both the two domains.

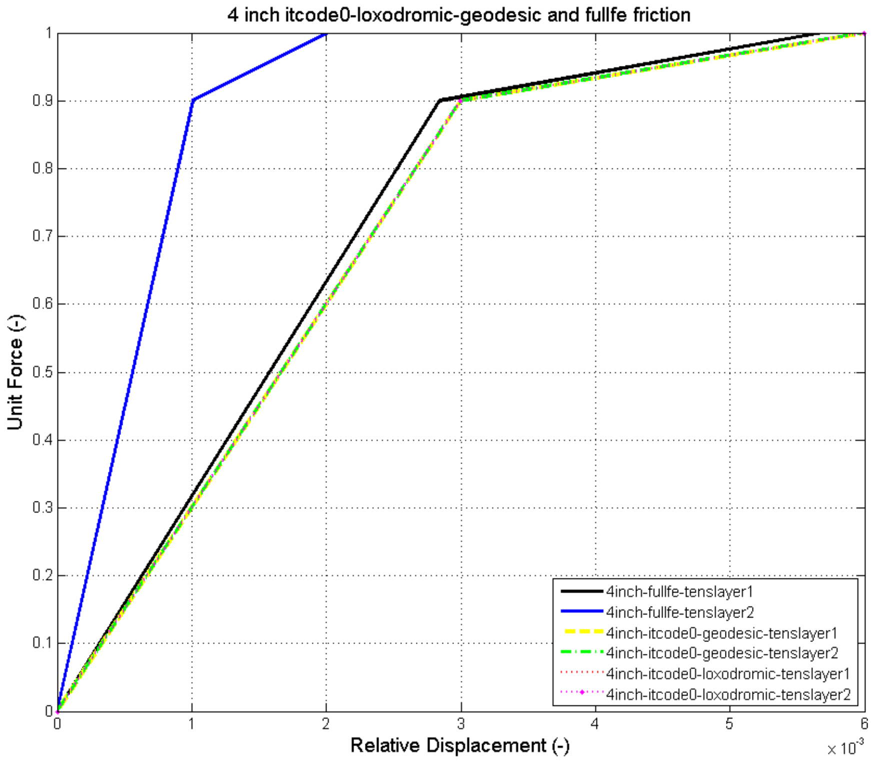

Figure 5.4: The 4 inch lox-geo friction for itcode0 and fullfe.

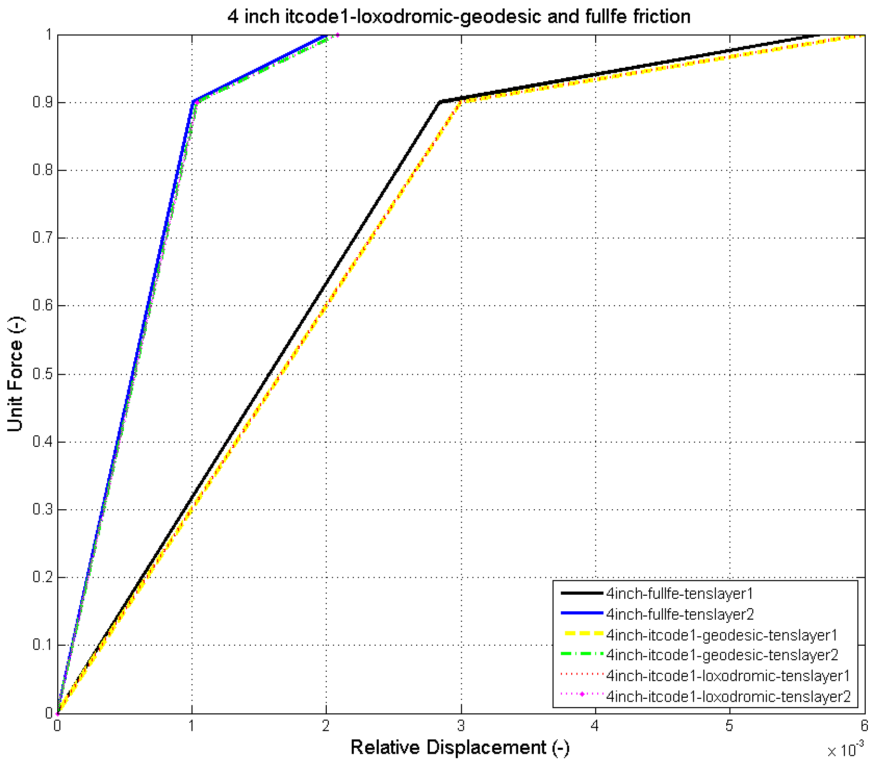

Figure 5.5: The 4 inch lox-geo friction for itcode1 and fullfe.

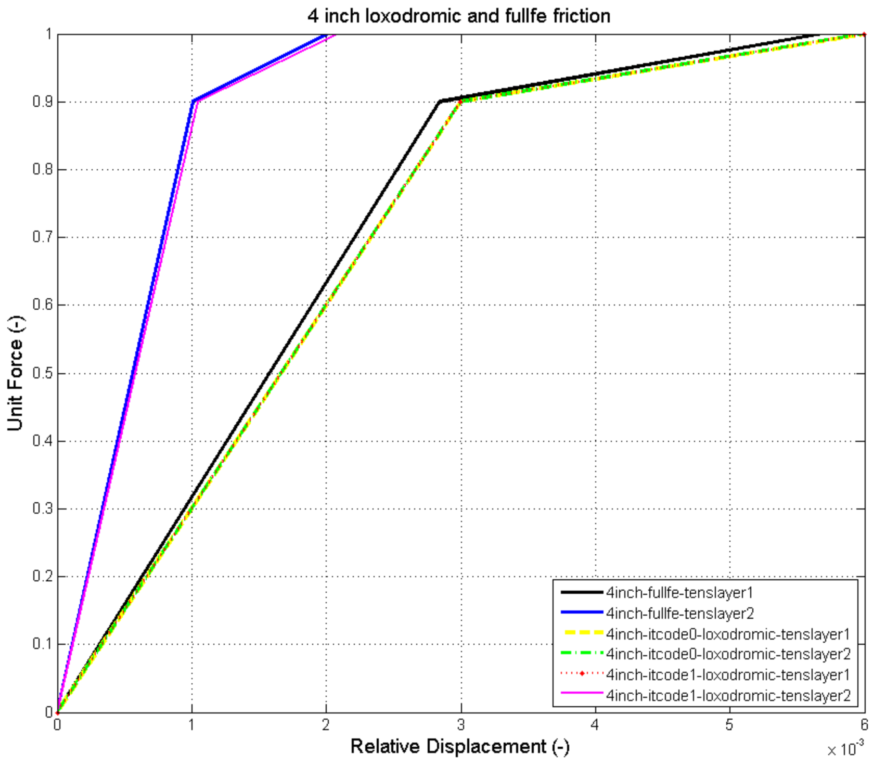

Figure 5.6: The 4 inch lox friction for itcode0-itcode1 and fullfe.

5.7 Stress study for loxodromic and geodesic assumptions

5.7.1 Explanation of the 4 inch models under two assumptions

In this section, the sensitivity studies of the stress components σ_{xx-my} and σ_{xx-mz} under the loxodromic and geodesic assumptions are presented.

Figure 5.7 –Figure 5.10 show the stress sensitivity between ITCODE0 models with two assumptions and FullFE model.

Figure 5.11–Figure 5.14 show the stress sensitivity between ITCODE1 models with two assumptions and FullFE model.

From all the figures listed below, the stress component σ_{xx-mz} is 0 for the geodesic method which is according with Eq. 3.3.

The stress components σ_{xx-my} and σ_{xx-mz} for fullfe model are more similar to the loxodromic method of itcode0 and itcode1 cases than the geodesic method.

Comparing the two tensile layers, σ_{xx-my} and σ_{xx-mz} shows the same trend.

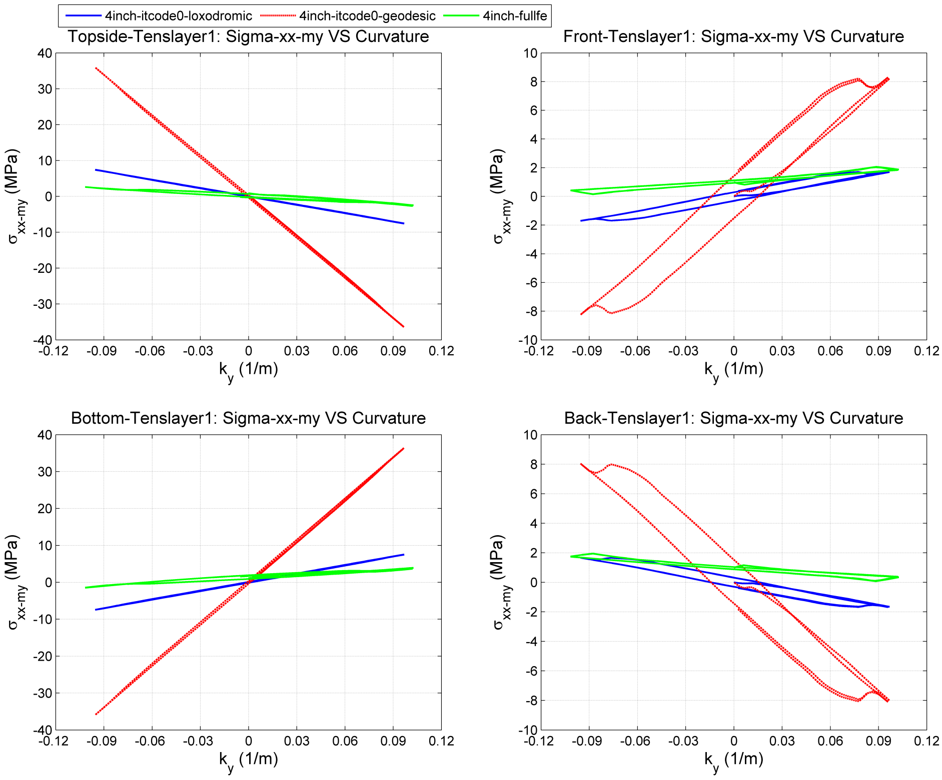

Figure 5.7: The 4 inch tenslayer1 σ_{xx-my} lox-geo for itcode0 and fullfe.

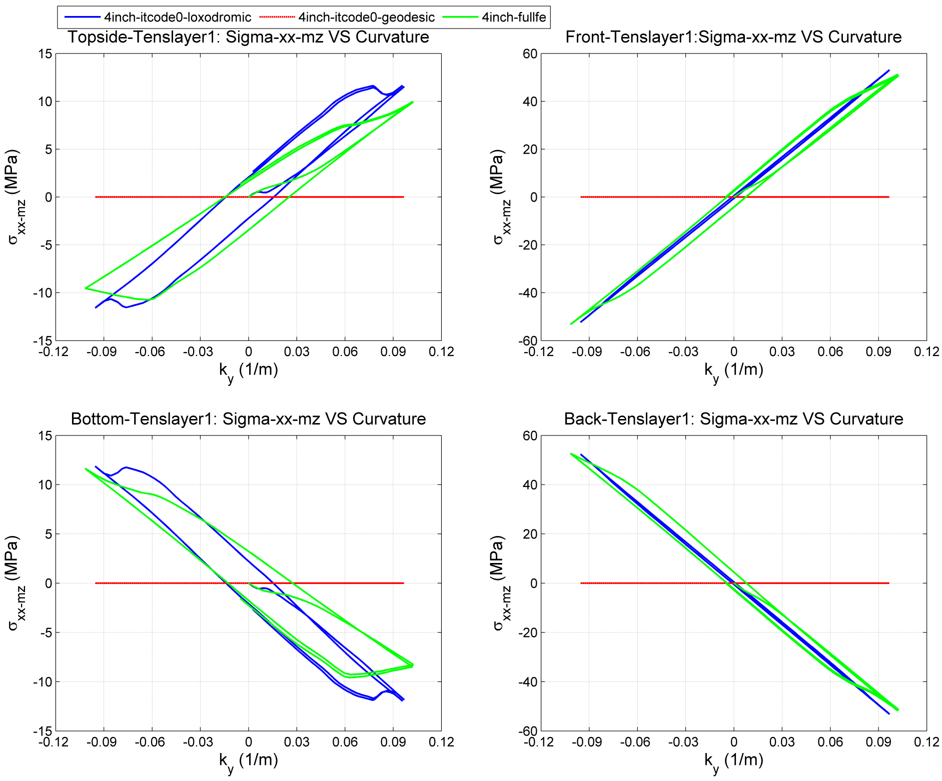

Figure 5.8: The 4 inch tenslayer1 σ_{xx-mz} lox-geo for itcode0 and fullfe.

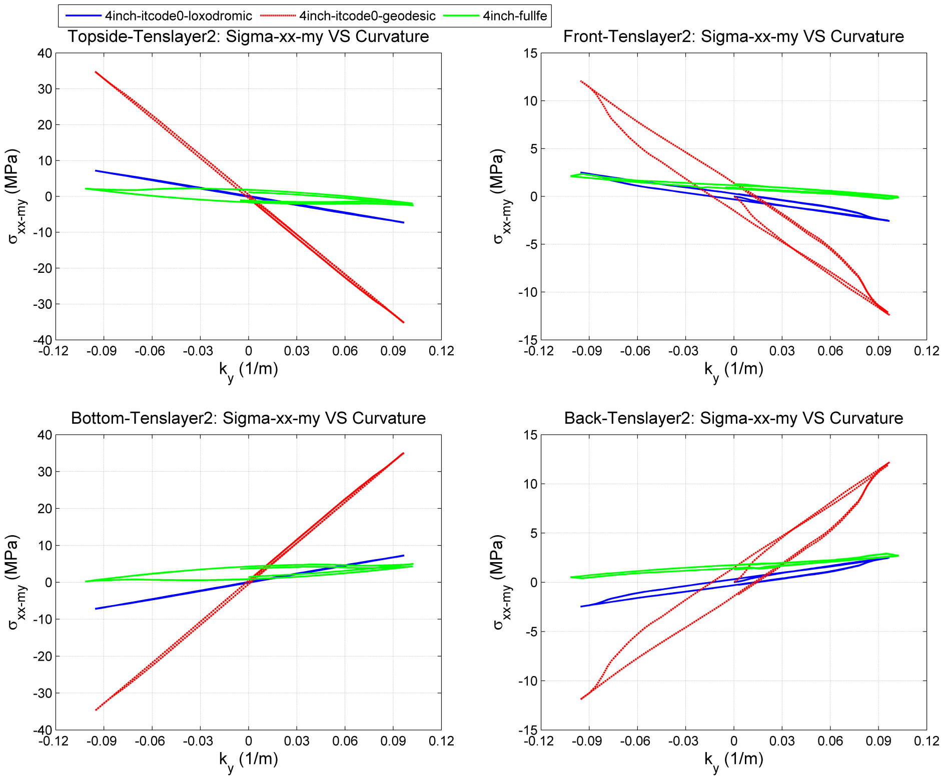

Figure 5.9: The 4 inch tenslayer2 σ_{xx-my} lox-geo for itcode0 and fullfe.

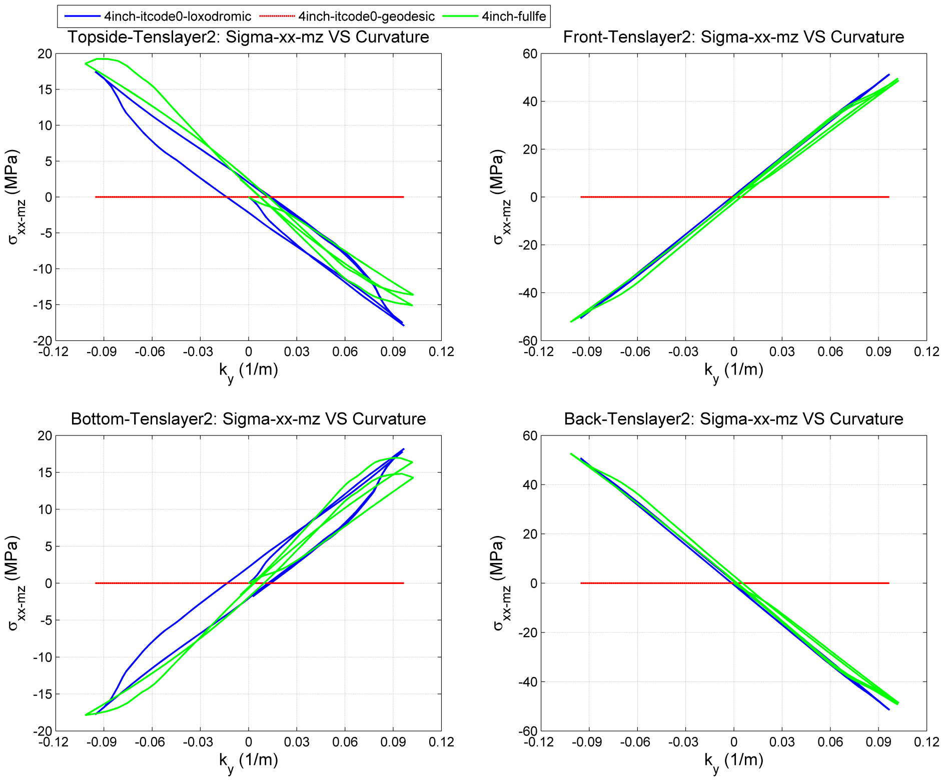

Figure 5.10: The 4 inch tenslayer2 σ_{xx-mz} lox-geo for itcode0 and fullfe.

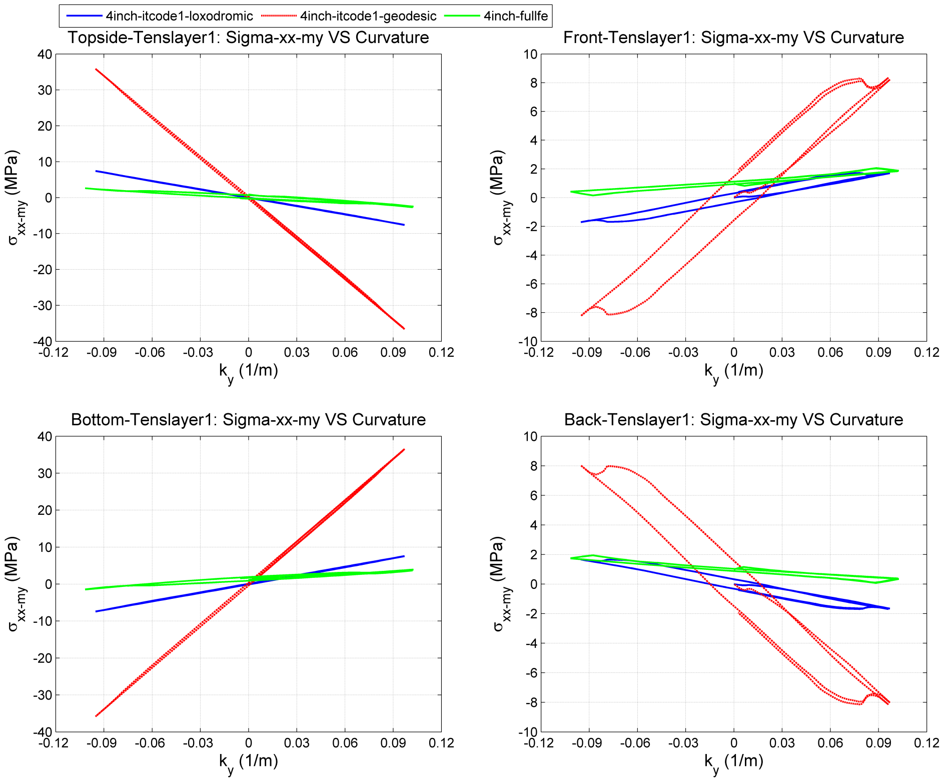

Figure 5.11: The 4 inch tenslayer1 σ_{xx-my} lox-geo for itcode1 and fullfe.

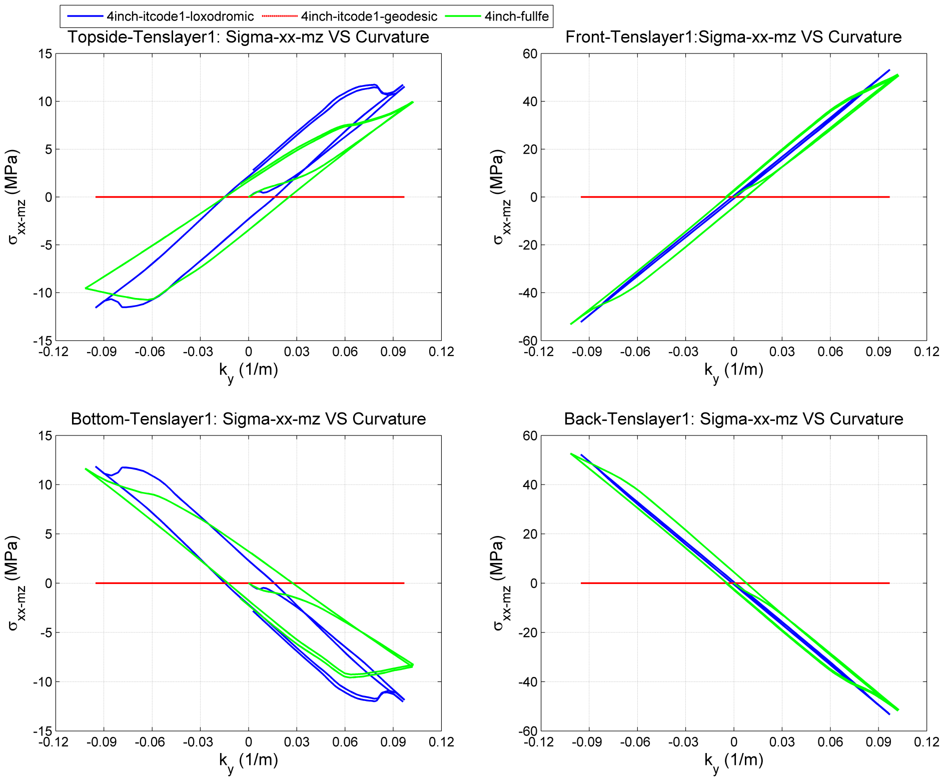

Figure 5.12: The 4 inch tenslayer1 σ_{xx-mz} lox-geo for itcode1 and fullfe.

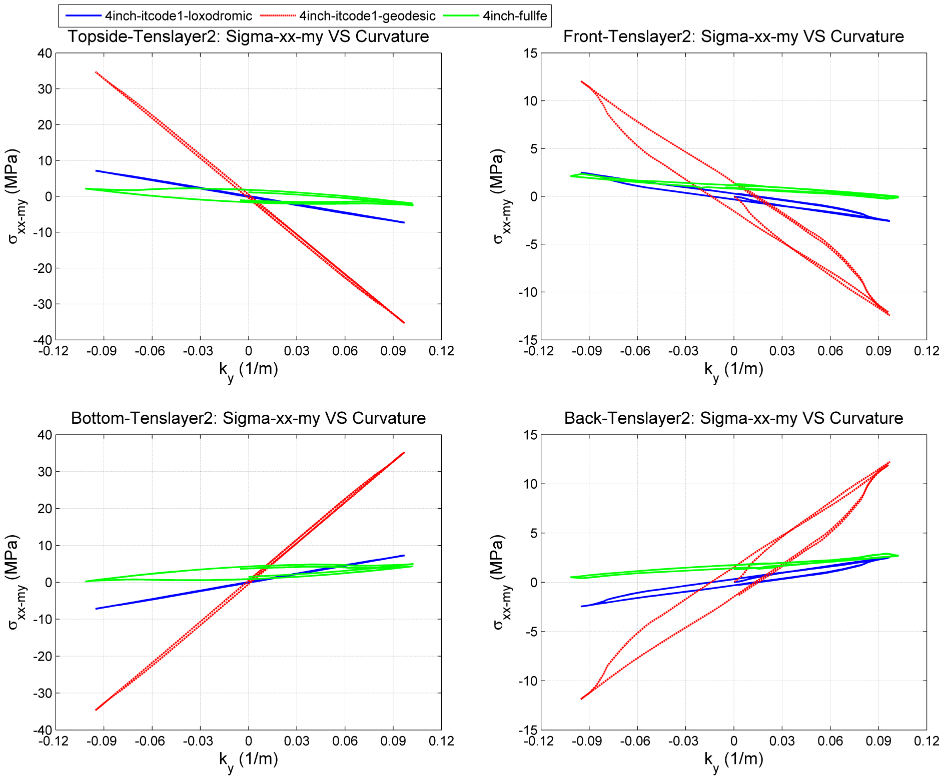

Figure 5.13: The 4 inch tenslayer2 σ_{xx-my} lox-geo for itcode1 and fullfe.

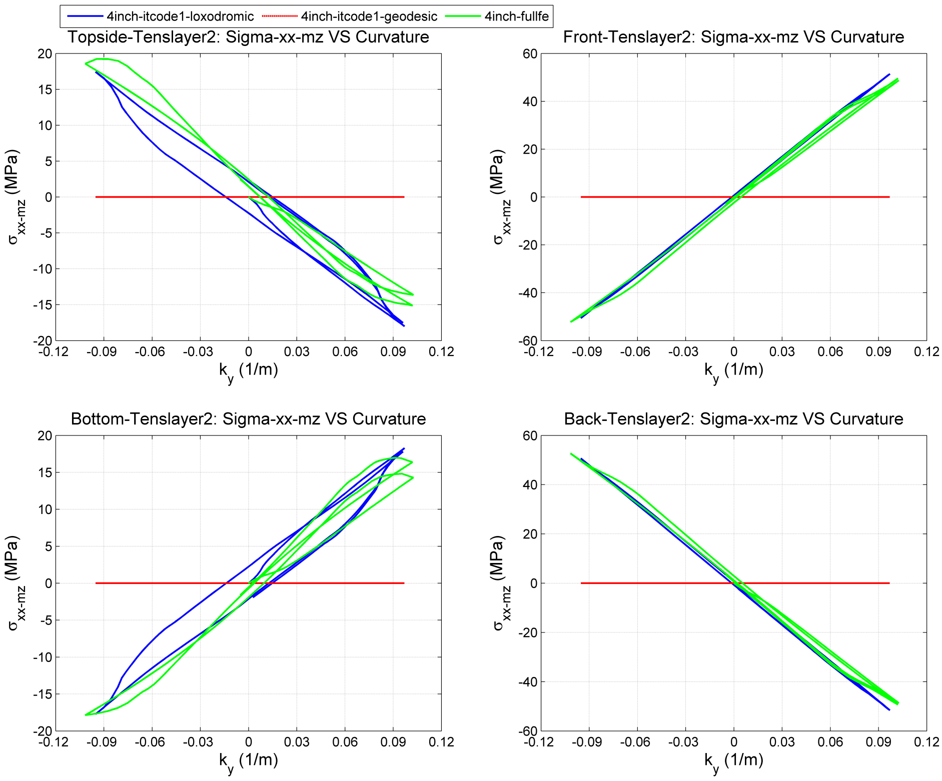

Figure 5.14: The 4 inch tenslayer2 σ_{xx-mz} lox-geo for itcode1 and fullfe.

5.8 Stress study for loxodromic assumption and fullfe model

5.8.1 Explanation of the tensile layer stress for three models

Figure 5.15 and Figure 5.16 show the relationship between global normal curvature κ_y and the total longitudinal stress σ_{xx} and the axial stress σ_{xx-ax} of the first tensile layer, respectively.

Referring to the top side element, itcode 0 and itcode1 models show high similarity, while for the fullfe model, the stiffness in the stick domain is lower than other models, which is against the phenomenon of Figure 5.6, the stiffness is higher than itcode0 and itcode1 models. In the slip domain, the stiffness shows almost the same, which accords with the friction plots. Based on the loxodromic assumption, when subjected to bending, the bending stress is mainly taken by the axial stress, so the hysteresis loop is larger than the other stress components σ_{xx-my} and σ_{xx-mz}.

Figure 5.17 and Figure 5.18 show the relationship between global normal curvature κ_y and the normal curvature stress σ_{xx-my} and the transverse curvature stress σ_{xx-mz} of the first tensile layer, respectively.

Referring to the top side element of Figure 5.17, σ_{xx-my} and κ_y shows linear relationship for itcode0 and itcode1 models, the slop is estimated from the figure is -78.5 $(MPa \cdot m)$, by applying Eq. 3.5, the theoretical slop is:

$$\begin{aligned}
\text{Analytical slop} &= \frac{1}{2} \times cos^4\alpha \times h \times E \times cos\psi \\
&= \frac{1}{2} cos^4(-38°) \times 0.002 \times 2.07E5 \times cos\pi \\
&= -79.82(MPa \cdot m)
\end{aligned}$$

which verify that the normal curvature stress calculated by Bflex2010 is in accord with the theoretical value. While for the fullfe model, hysteresis loop is occurring, which means σ_{xx-my} and κ_y shows no linear relationship, and this also verifies that the fullfe model considers all the influence, due to the stress value is relatively small, the fullfe model is applicative.

Referring to the front side element of Figure 5.18, σ_{xx-mz} and κ_y also shows linear relationship for itcode0 and itcode1 models, which is also according with Eq. 3.6. While for the fullfe model, hysteresis loop is also occurring, which means σ_{xx-mz} and κ_y shows no linear relationship.

Comparing to the first tensile layer, σ_{xx-ax} at the second tensile layer also shows the same trend. The hysteresis loop area, however, is smaller than for the first tensile layer, which means that the work done by the friction force is smaller, and this can also explain that the inner tensile layer undertakes the most stress and force. Stress components σ_{xx-my} and σ_{xx-mz} of the two tensile layers shows high similarity for three models. From Figure 5.6, for the second tensile layer, itcode1 model shows higher stiffness than itcode0 model, and this is different from the Figure 5.20, which shows itcode0 and itcode1 models highly coincide, the code should be checked.

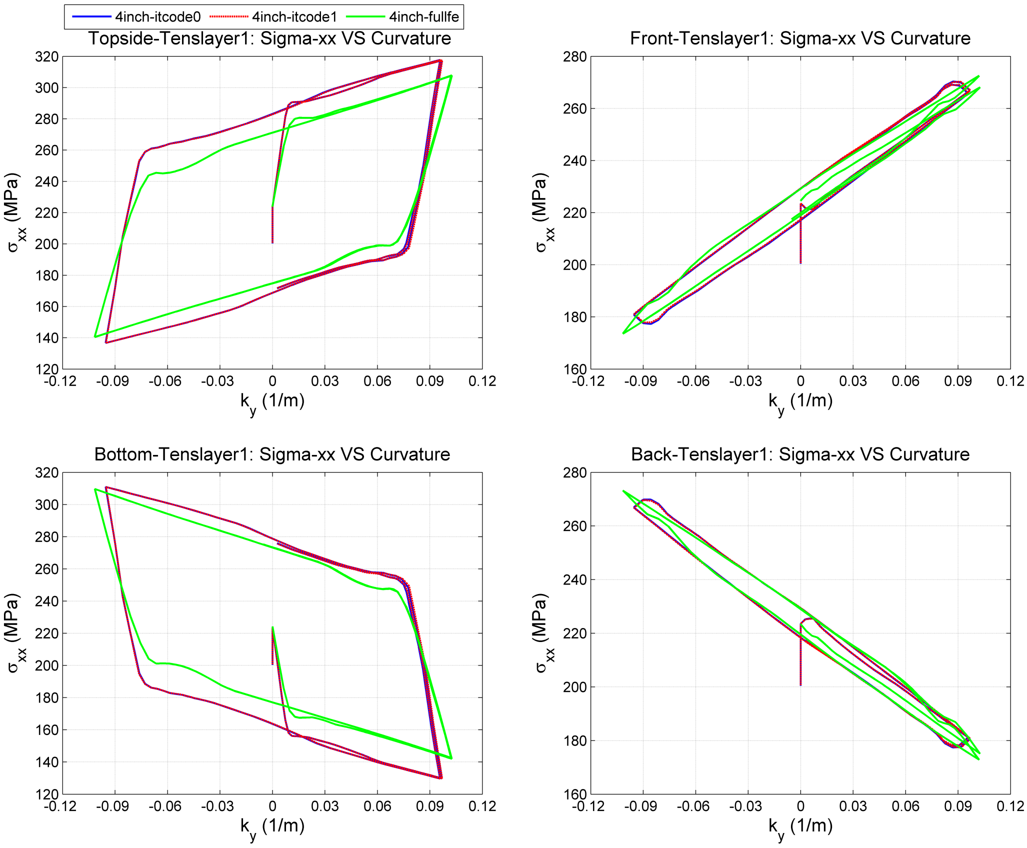

Figure 5.15: The 4 inch tenslayer1 σ_{xx} for three models.

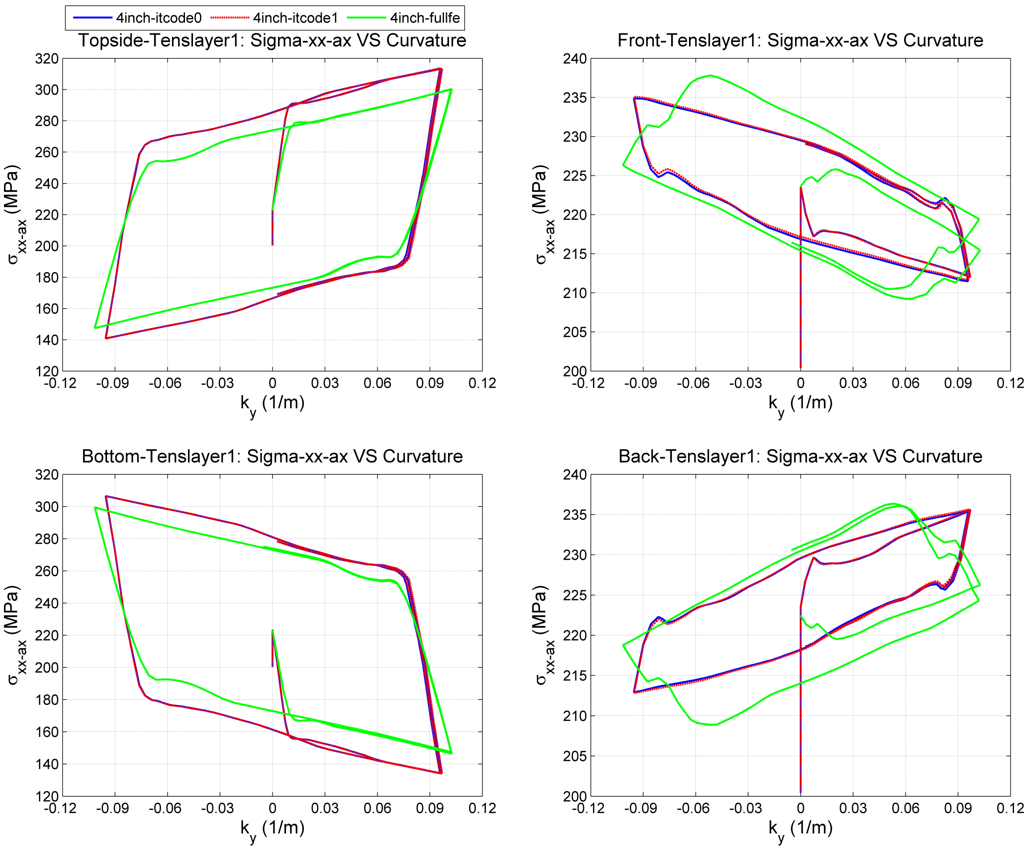

Figure 5.16: The 4 inch tenslayer1 σ_{xx-ax} for three models.

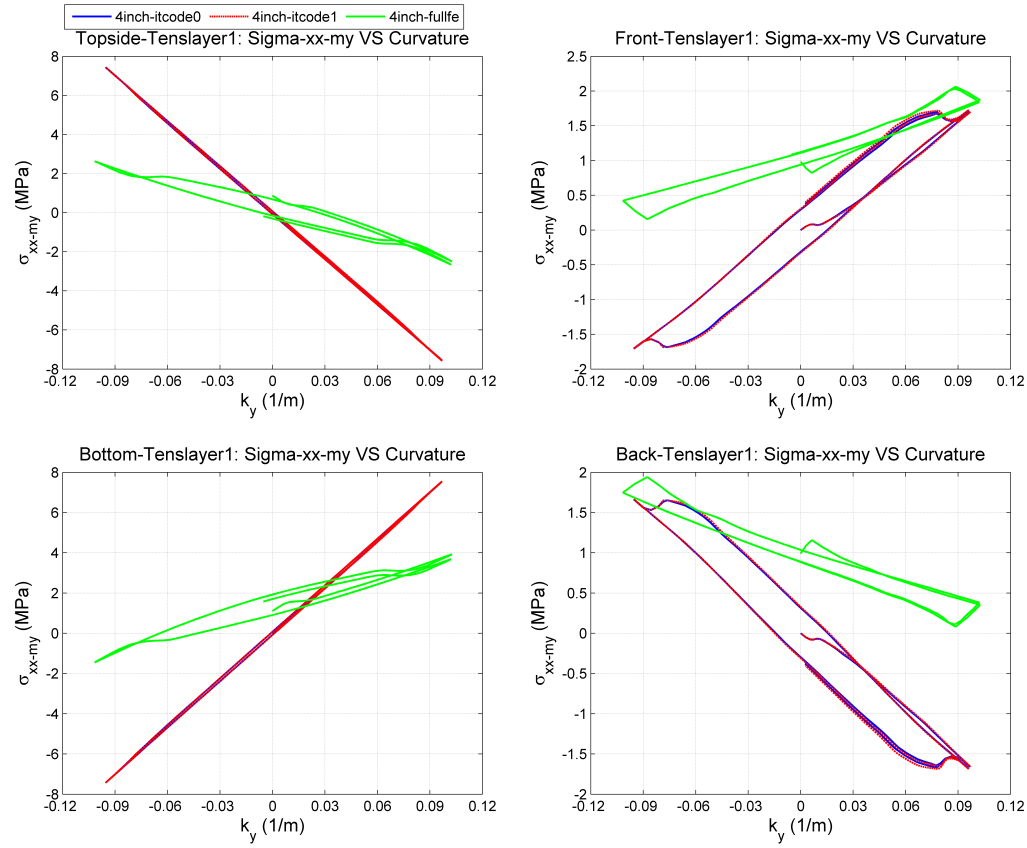

Figure 5.17: The 4 inch tenslayer1 σ_{xx-my} for three models.

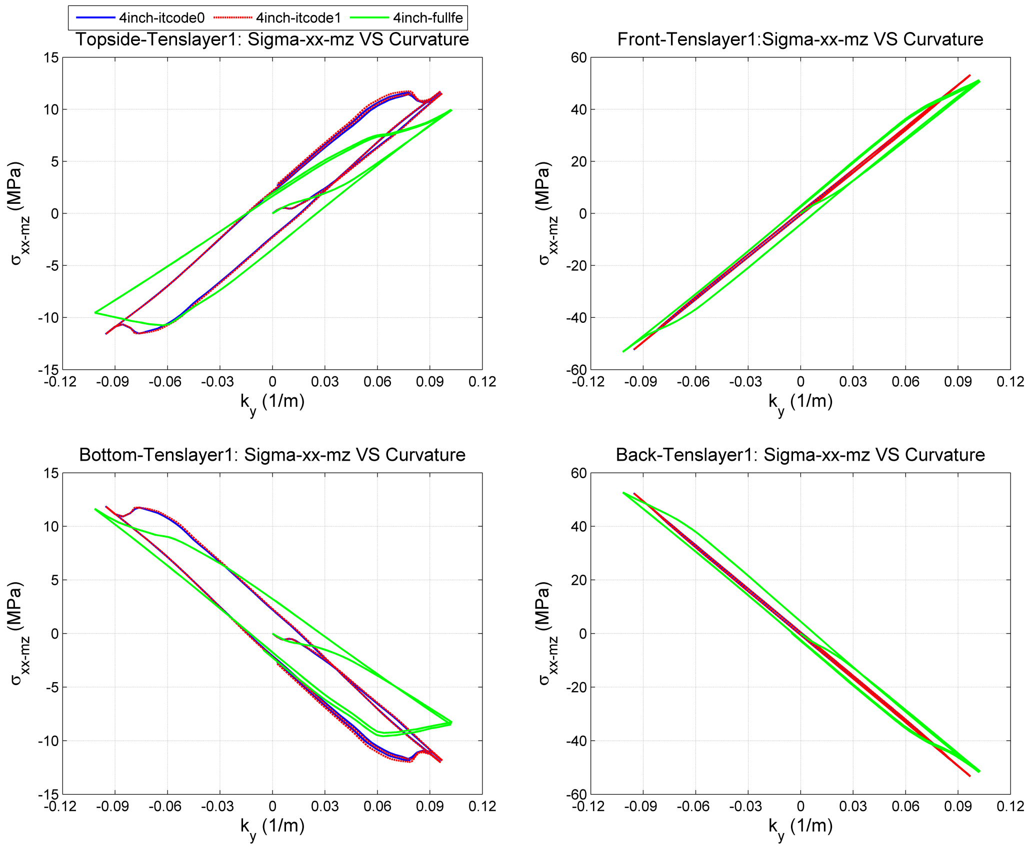

Figure 5.18: The 4 inch tenslayer1 σ_{xx-mz} for three models.

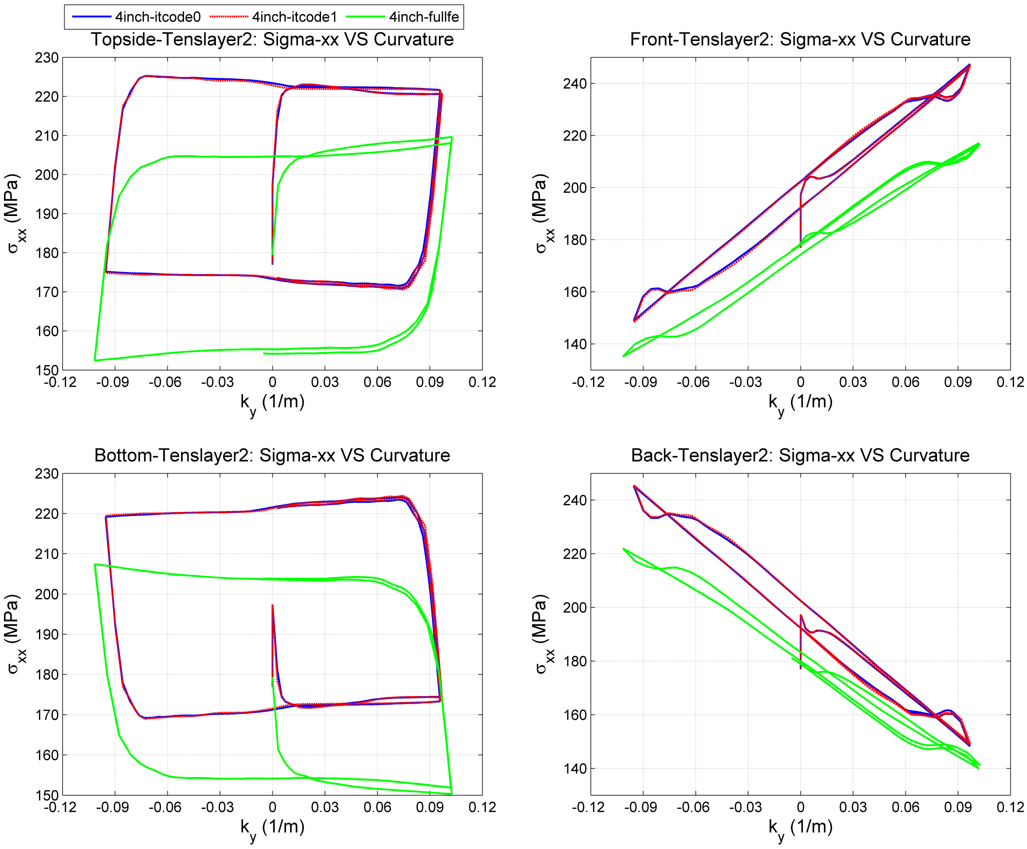

Figure 5.19: The 4 inch tenslayer2 σ_{xx} for three models.

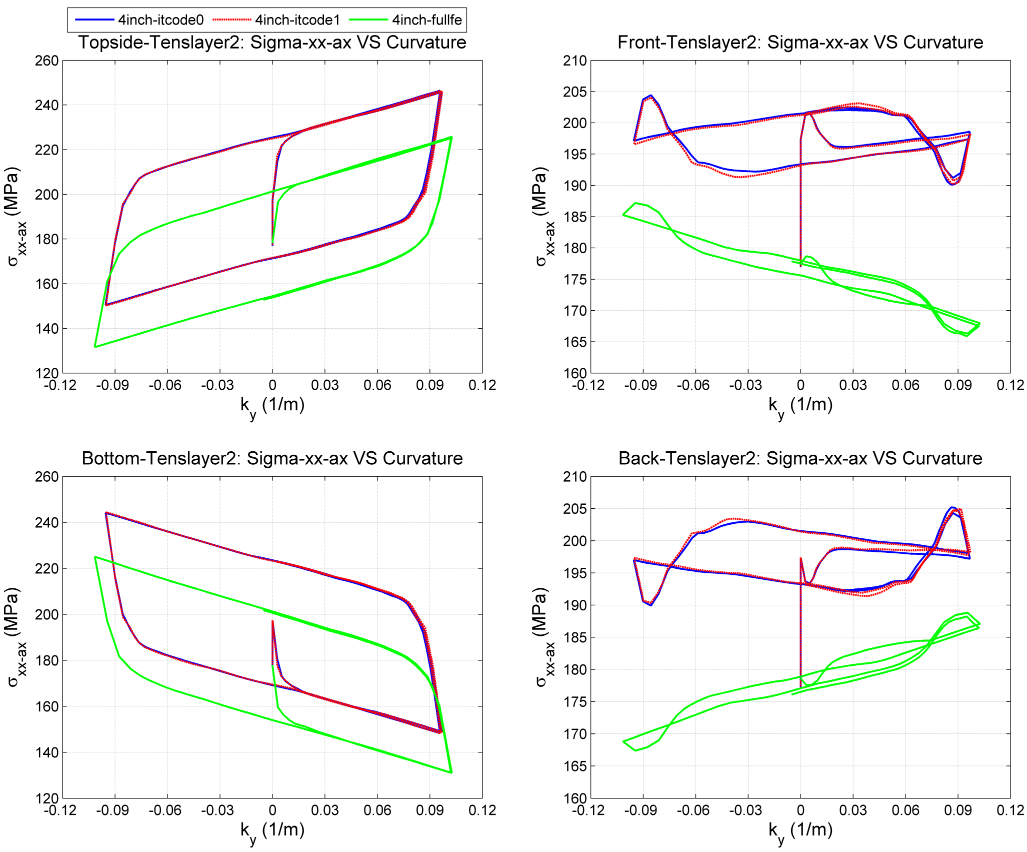

Figure 5.20: The 4 inch tenslayer2 σ_{xx-ax} for three models.

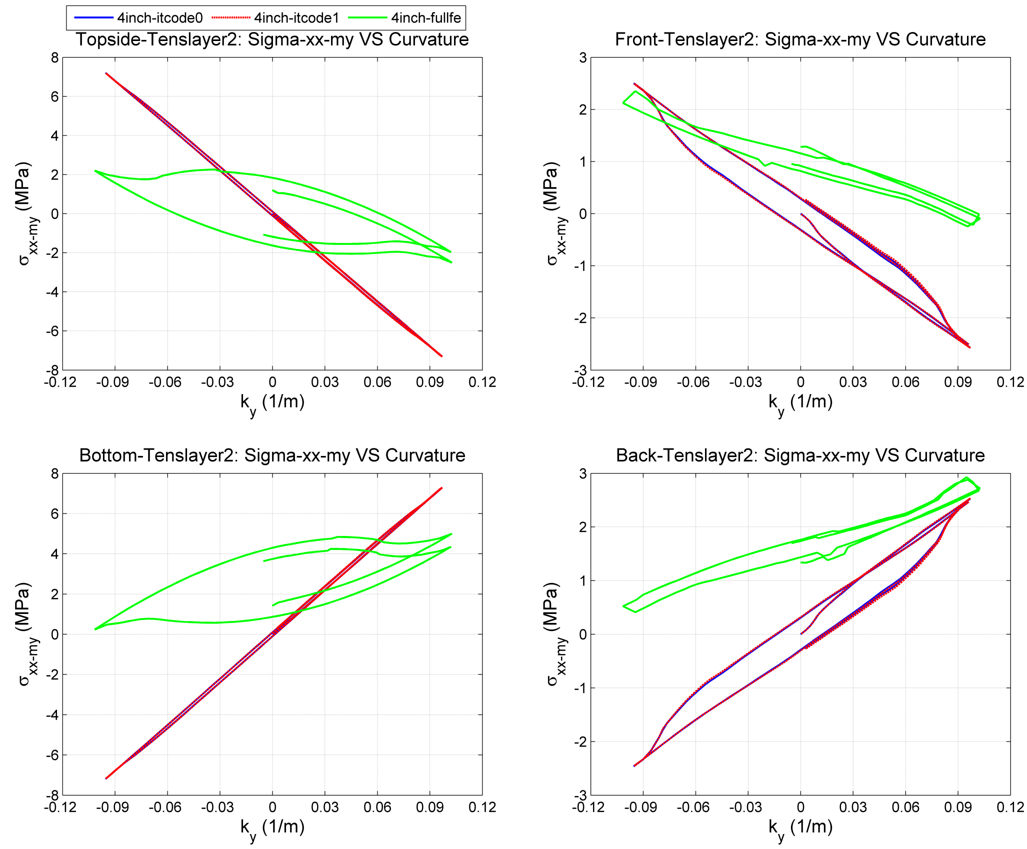

Figure 5.21: The 4 inch tenslayer2 σ_{xx-my} for three models.

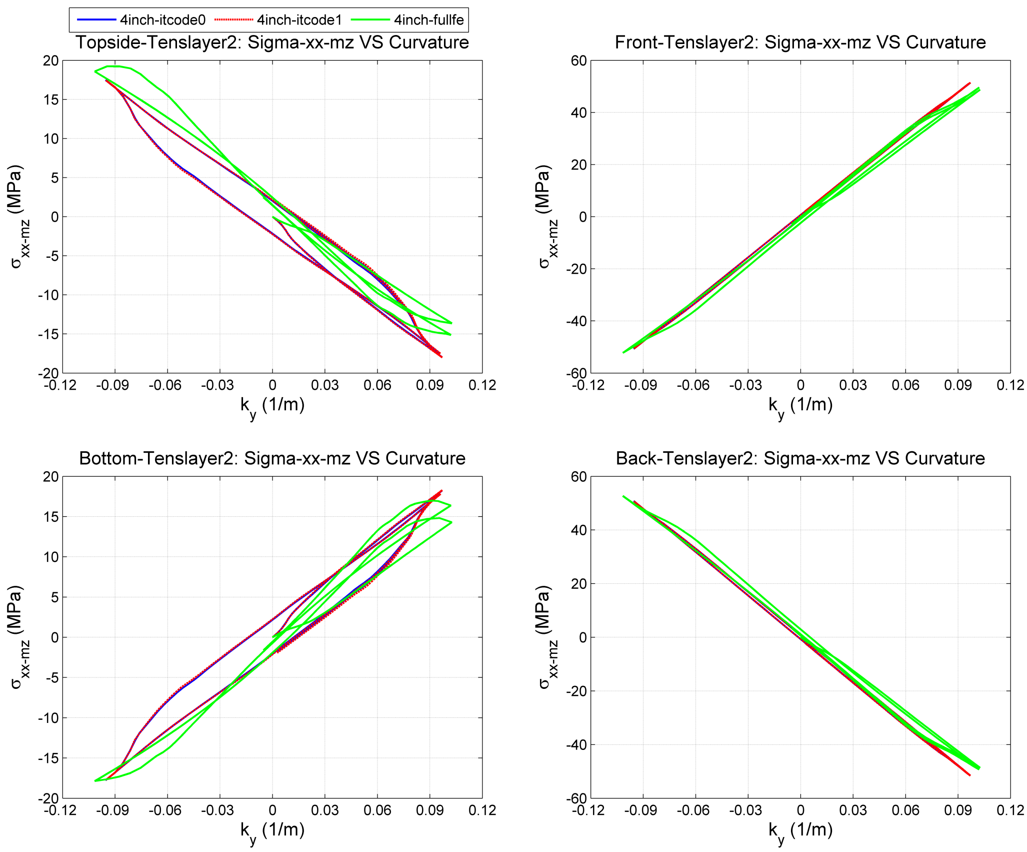

Figure 5.22: The 4 inch tenslayer2 σ_{xx-mz} for three models.

5.8.2 Explanation of the difference for axial stress behaviour

The contact pressure configuration for two tensile layers is shown below: The shear force

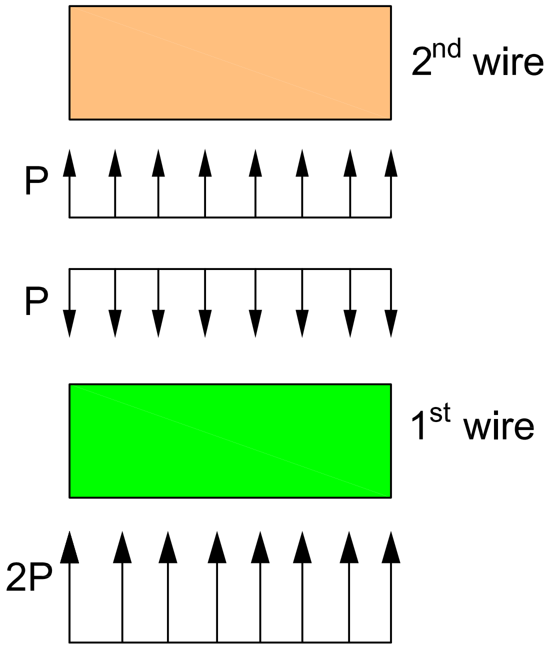

Figure 5.23: Contact pressure for two tensile armour layers.

based on contact pressure is:

$$q_z^{I+1} + q_z^I = \frac{t}{\mu} \tag{5.3}$$

where: q_z^{I+1} is the outside contact force, q_z^I is the inside contact force, t is the shear force per unit length, μ is the friction coefficient, for all layers of all cases: 0.1.

According to Table 5.4 and Figure 5.6, the stiffness of the hysteresis can be calculated by using the equation below:

$$k = \frac{dt}{du} \cdot t \tag{5.4}$$

where:

t:the friction force per-length.

$\frac{dt}{du}$: the slope of Figure 5.6.

Considering the stick phase of Figure 5.6, for the first tensile layer, the stiffness of the three models are:

$$\text{itcode0 and itcode1:} k = (0.9/0.29985E-02) \times 3.173651 = 952.572$$

$$\text{fullfe:} k = (0.9/0.28423E-02) \times 3.008309 = 952.566$$

which means the stiffness is the same in the stick domain, but referring to Figure 5.16, the slope is not the same, the fullfe model shows softer than itcode0 and itcode1 models.

The following reasons are checked:

1) the number of element for mesh;

2) the transverse motion of the fullfe model

For the first reason, 3 cases of the fullfe model are carried out: 20 elements size, 40 elements size and 80 elements size, the sensitivity table is shown below:

$\Delta\sigma = 100MPa$					
Model	itcode0	itcode1	fullfe		
Ele#	20	20	20	40	80
$\Delta\kappa(1/\mathrm{m})$	0.016	0.016	0.0288	0.0291	0.0253
$\frac{\Delta\sigma}{\Delta\kappa}(MPa \cdot m)$	6250.00	6250.00	3478.26	3442.34	3951.00

Table 5.5: Element number sensitivity for fullfe model.

From the table we can see that with the increasing element number, the stiffness of the stick domain for fullfe model changes little, so the element mesh might not be the factor to the phenomenon that the fullfe model is softer than the itcode0 and itcode1 models.

For the second reason, the transverse curvature for fullfe model is checked in Bflex2010, the value is 0, which means no transverse motion of the pipe under bending load.

The only possible reason is that for the fullfe model, the fullfe model takes all the factors into account, such as the loacl warp of the helix,the transverse degree of freedom of element HSHEAR353, and this should be checked further.

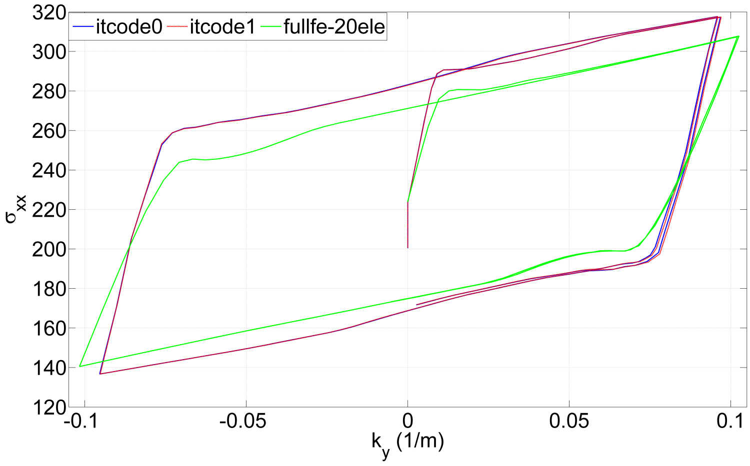

(a) FullFE 20 element.

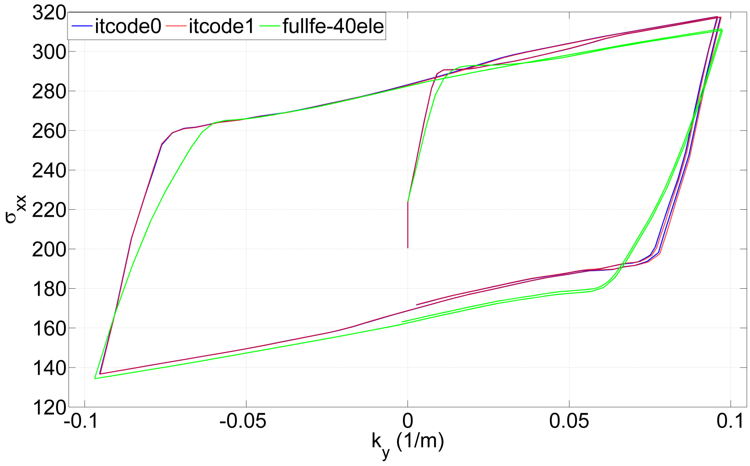

(b) FullFE 40 element.

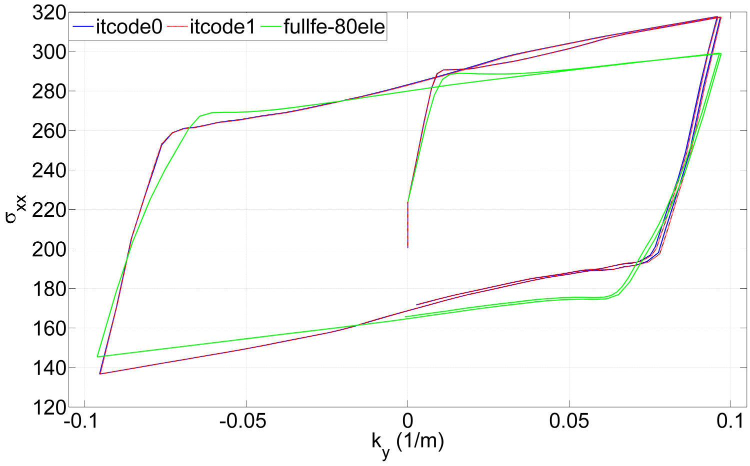

(c) FullFE 80 element.

Figure 5.24: FullFE model with different mesh size.

Chapter 6 Stress analysis of pipe in Appendix

6.1 Pipe cases in Appendix C

Friction explanation

The friction data and friction plots in this section can be referred to Appendix C.1, C.2.1, C.3.1.

- The 6 inch pipe friction explanation

Figure C.1, Figure C.2 and Figure C.3 shows the same behaviour as the 4 inch pipe case.

- The 8 inch pipe friction explanation

Figure C.20 shows that for itcode0 and fulfe models, the inner layer (black line) of the fullfe model shows slightly small stiffness in both the stick domain and the slip domain, and the outer layer (blue line) of the fullfe model shows high stiffness than itcode0 model.

Figure C.21 shows that for itcode1 and fulfe models, the inner layer (black line) of the fullfe model shows slightly small stiffness than the inner layer of itcode1 model under both the loxodromic and geodesic assumptions in two domains. The outer layer (blue line) of the fullfe model shows slightly small stiffness to the outer layer of itcode1 model under two assumptions in both the stick and slip domains.

Figure C.22 shows that for itcode0 and itcode1 models under loxodromic assumption, the stiffness of all layers of itcode0 model and the inner layer of the itcode1 model is sightly larger than the inner layer of fullfe model, while the outer layer of itcode1 model appears slightly larger stiffness than the outer layer of the fullfe model in both two domains.

- The 16 inch pipe friction explanation

Figure C.39 shows that the inner layer (black line) of the fullfe model shows small stiffness than all the layer of itcode0 model under two assumptions in both the stick domain and the slip domain, and the outer layer (blue line) of the fullfe model shows high stiffness than itcode0 model.

Figure C.40 shows that for itcode1 and fulfe models, the inner layer (black line) of the fullfe model shows small stiffness than the inner layer of itcode1 model under both the loxodromic and geodesic assumptions in two domains. The outer layer (blue line) of the fullfe model shows small stiffness to the outer layer of itcode1 model under two assumptions in both the stick and slip domains.

Figure C.41 shows that for itcode0 and itcode1 models under loxodromic assumption, the stiffness of all layers of itcode0 model and the inner layer of the itcode1 model is larger than the inner layer of fullfe model, while the outer layer of itcode1 model appears larger stiffness than the outer layer of the fullfe model in both two domains.

Stress explanation under two assumptions

- The 6 inch pipe case

The stress comparisons under two assumptions relevant to the 6 inch pipe show the same conclusions as the 4 inch pipe cases.

- The 8 inch pipe case

The stress comparisons under two assumptions relevant to the 8 inch pipe show the same conclusions as the 4 inch pipe cases.

- The 16 inch pipe case

The stress comparisons under two assumptions relevant to the 16 inch pipe show the same conclusions as the 4 inch pipe cases.

Stress explanation under loxodromic assumption and fullfe model

- The 6 inch pipe case

The stress comparisons of two tensile layers of itcode0 and itcode1 models and fullfe model relevant to the 6 inch pipe show the same conclusions as the 4 inch pipe cases. For axial stress σ_{xx-ax} of the fullfe model in the stick domain, the stiffness is inconsistent with the friction plots.

- The 8 inch pipe case

The stress comparisons of the first tensile layer of itcode0 and itcode1 models and fullfe model relevant to the 8 inch pipe show the same conclusions as the 4 inch pipe cases. For axial stress σ_{xx-ax} of the fullfe model in the stick domain, the stiffness is inconsistent with the friction plots. While for the second tensile layer, consistent.

- The 16 inch pipe case

The stress comparisons of the first tensile layer of itcode0 and itcode1 models and fullfe model relevant to the 16 inch pipe show the same conclusions as the 4 inch pipe cases. For axial stress σ_{xx-ax} of the fullfe model in the stick domain, the stiffness is consistent with the friction plots. While for the second tensile layer, inconsistent.

6.2 Pipe cases in Appendix D

Friction explanation

The friction data and friction plots in this section can be referred to AppendixD.1.1 and D.1.3.

- The 7.5 inch two tensile layer pipe friction explanation

Figure D.1, comparison between the itcode0 model under two assumptions and the fullfe model, shows the same behaviour as the 4 inch pipe case.

Figure D.2, comparison between the itcode1 models under two assumptions and the fullfe model, shows that for itcode1 and fulfe models, the inner layer (black line) of the fullfe model shows slightly larger stiffness than the inner layer of itcode1 model under both the loxodromic and geodesic assumptions in two domains. The outer layer (blue line) of the fullfe model shows slightly smaller stiffness than the outer layer of itcode1 model under two assumptions in both the stick and slip domains.

Figure D.3, comparison between the itcode0 and itcode1 models under loxodromic assumption and the fullfe model, shows that for itcode0 and itcode1 models under loxodromic assumption, the stiffness of all layers of itcode0 model and the inner layer of the itcode1 model is sightly smaller than the inner layer of fullfe model, while the outer layer of itcode1 model appears slightly larger stiffness than the outer layer of the fullfe model in both two domains.

- The 7.5 inch four tensile layer pipe friction explanation

Figure D.20, comparison between the itcode0 model under two assumptions and the fullfe model, shows the same behaviour as the 4 inch pipe case, and all the four layers of itcode0 model under two assumptions shows the same friction plot.

Figure D.21 and Figure D.22, shows the general trend is the same as the 8 inch pipe case.

Stress explanation of the 7.5 inch pipe cases

The general trend of the stress components σ_{xx-my} and σ_{xx-mz} are the same as the 4 inch pipe case, the slightly difference may be due to the lack of the carcass layer.

Chapter 7 Fatigue Analysis

7.1 Fatigue Theory

A material may lose the integrity when exposed to cyclic loading, even the value is small, the fatigue analysis, however, is not an exact science because of the imperial testing results and many assumptions made during the calculation.

During the period of analysis, the stress-life (S-N) approach is widely used to perform the fatigue limit state(FLS) analysis, which is based on experimental data from fatigue tests. We can find the introduction about the S-N Curve theory in many manuals such as DNV-RP-C203[8] and DNV-RP-F204[7]. The Bflex2010 Lifetime module is also based on the S-N diagram for longitudinal failure mode, the methods for taking the mean stress into account for longitudinal failure mode such as the Goodman and Gerber interpolation will be introduced.

7.1.1 S-N Curve

The S-N Curve is the relationship between the stress range and the cycle limits, the basic design S-N Curve equation[22] is given as:

$$\log N = \log \overline{a} - m \log \Delta\sigma \tag{7.1}$$

N: the predicted number of cycles to failure for stress range $\Delta\sigma$
$\Delta\sigma$: stress range
m:negative inverse slope of the S-N Curve
$log\overline{a}$:the intercept of the $logN$ axis of the S-N Curve, formulated as:

$$\log \overline{a} = \log a - 2 s_{\log N} \tag{7.2}$$

$loga$: the intercept of mean S-N Curve with $\log N$ axis
$s_{\log N}$: the standard of $\log N$.
m and $\overline{a}$ can be found in the RP for different cases, and also $\Delta\sigma$ should be established from the analysis, one typical diagram is shown below:

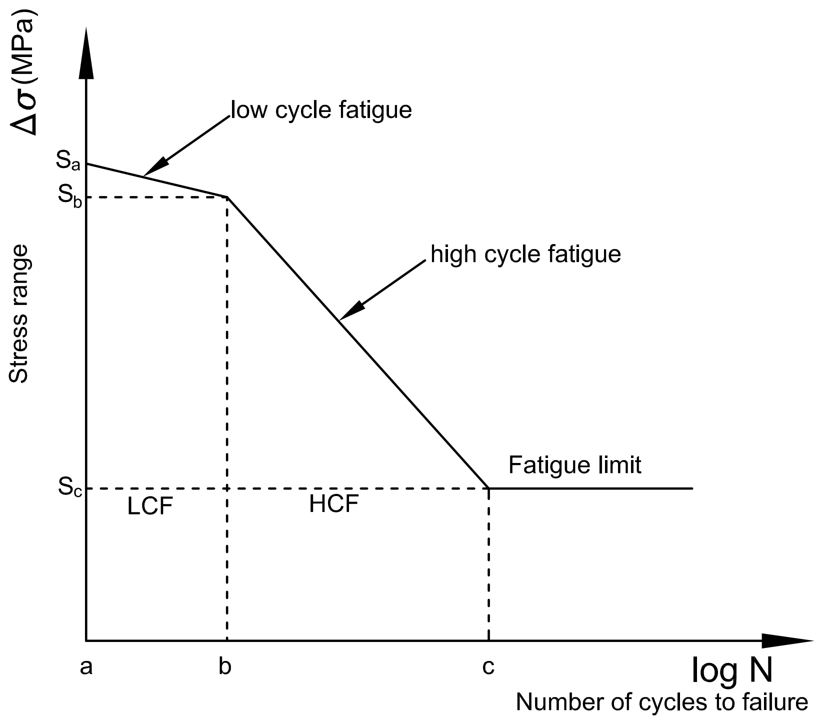

Figure 7.1: One typical S-N curve.

7.1.2 Goodman Relation

The Goodman relation(http://en.wikipedia.org/wiki/Goodman_relation) is an equation which is used to quantify the interaction of the mean stress and alternative stress on the fatigue life of a material in the material science and fatigue domain. The Goodman diagram, also called a Haigh diagram or a Haigh-Soderberg diagram, shows the relationship between(liner) mean stress and (linear) alternative stress, indicating when the material fails at some given number of cycles.

A scatter plot of experimental data shown on such a plot can often be approximated by a parabola known as the Gerber line, which can in turn be (conservatively) approximated by a straight line called the Goodman line.

The Goodman equation and figure are shown below:

$$\sigma_a = \sigma_{fat} \times (1 - \frac{\sigma_m}{\sigma_{ut}}) \tag{7.3}$$

where,

σ_a:the alternative stress;

σ_m:the mean stress;

σ_{fat}:the fatigue limit for completely reversed loading;

σ_{ut}:the ultimate tensile stress of the material;

The area below the curve indicates that the material should not fail at the given stress, while the area above the curve represents likely failure fo the material.

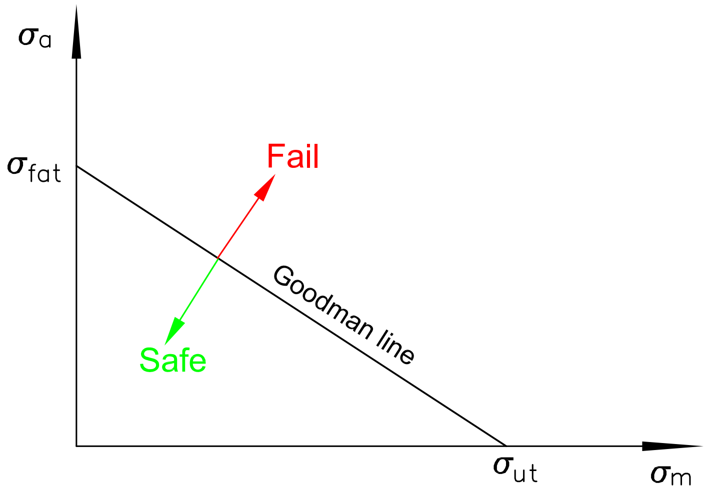

Figure 7.2: The Goodman diagram.

7.1.3 Mean Stress Correction

The criteria for a multi-axial fatigue failure can be shown in terms of the Von Mises equivalent stress range $\Delta\sigma$, which is based on the principles stated in [23].

Two methods are specified to test fatigue life by uni-axial testing: the mean stress σ_m and the R ratio constant, shown as $R = \frac{\sigma_{min}}{\sigma_{max}}$.

For tension-tension test, the range of R ratio is 0.1~0.5 in order to avoid compression, and the stress range at a given R ratio can be expressed in terms of the mean stress σ_m:

$$\Delta\sigma = 2\sigma_m \frac{1-R}{1+R} \tag{7.4}$$

which means that at a given stress range with a fixed R-ratio, each fatigue test represent a linear line in the Haig Diagram shown below:

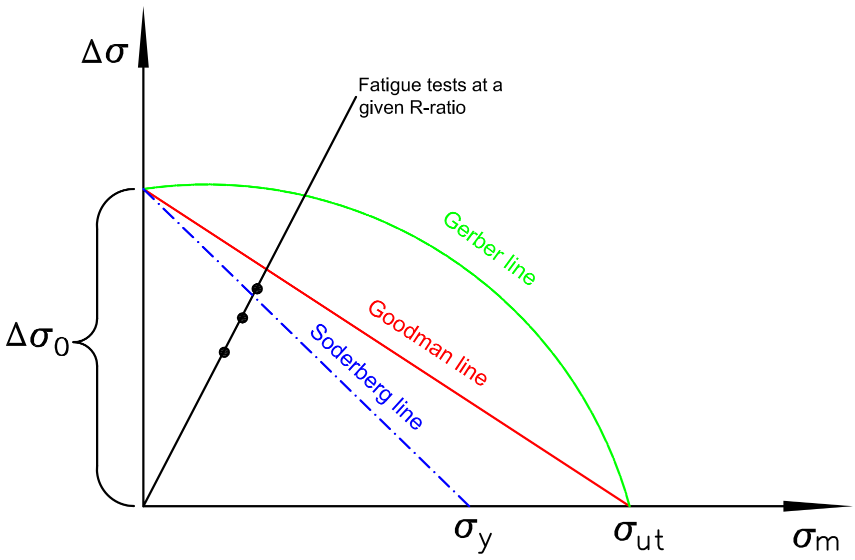

Figure 7.3: The Haig diagram.

For many cases, however, there exists only one R-ratio, it is common to use Goodman or Gerber assumptions to transform between different mean stress levels ($R = -1$) and the calculated mean stress.

- The transformation based on the Goodman assumption is:

$$\Delta\sigma_0 = \frac{\Delta\sigma}{1 - \frac{\sigma_m}{\sigma_{ut}}} \tag{7.5}$$

- The transformation based on the Gerber assumption is:

$$\Delta\sigma_0 = \frac{\Delta\sigma}{1 - (\frac{\sigma_m}{\sigma_{ut}})^2} \tag{7.6}$$

For a given S-N Curve at $R = -1$ under the two assumptions:

- Under Goodman assumption:

$$\Delta\sigma_0 = \frac{\Delta\sigma^*}{1 - \frac{(1+R)\Delta\sigma^*}{2(1-R)\sigma_{ut}}} \tag{7.7}$$

- Under Gerber assumption:

$$\Delta\sigma_0 = \frac{\Delta\sigma^*}{1 - (\frac{(1+R)\Delta\sigma^*}{2(1-R)\sigma_{ut}})^2} \tag{7.8}$$

where:

$\Delta\sigma^*$: stress range to be used in the S-N Curve to find the number of cycles until failure for each load case, it can be solved by equating the above two equations under the same assumption. For the Goodman assumption, it is a liner relation, while for Gerber assumption, it is a quadratic relation in terms of $\Delta\sigma^*$.

Three types of the fluctuating stresses can affect the fatigue failure, for Figure 7.4(b) and 7.4(c), the mean stress is not zero.

where,

Alternative stress:$\sigma_a = \frac{\sigma_{max} - \sigma_{min}}{2}$

Mean stress:$\sigma_m = \frac{\sigma_{max} + \sigma_{min}}{2}$

Figure7.4(a):$\sigma_m = 0, \sigma_a = \sigma_{max}, \sigma_{max} = -\sigma_{min}$

Figure7.4(b):$\sigma_{min} = 0, \sigma_a = \sigma_m = \sigma_{max}/2$

7.1.4 Residual longitudinal stress

The residual longitudinal stress for assessing the profiled pressure armour and tensile armour will be affected by the FAT, and in order to obtain the exact fatigue damage, the entire stress history from manufacturing throughout FAT procedure and dynamic loading should be simulated [17].

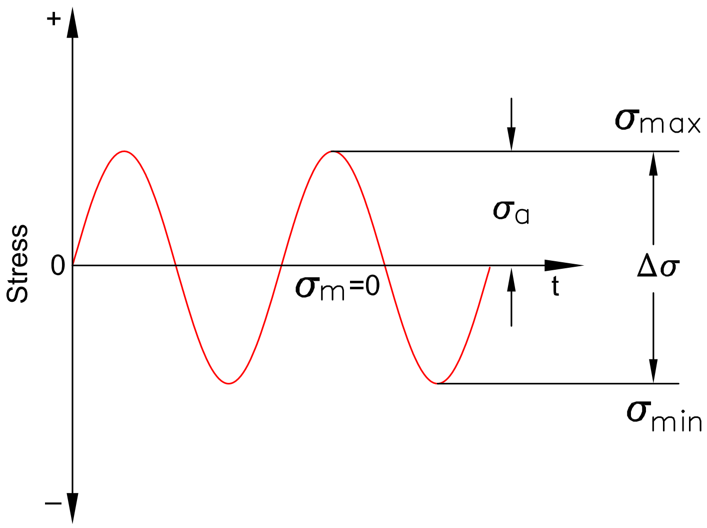

(a) Fully reversed.

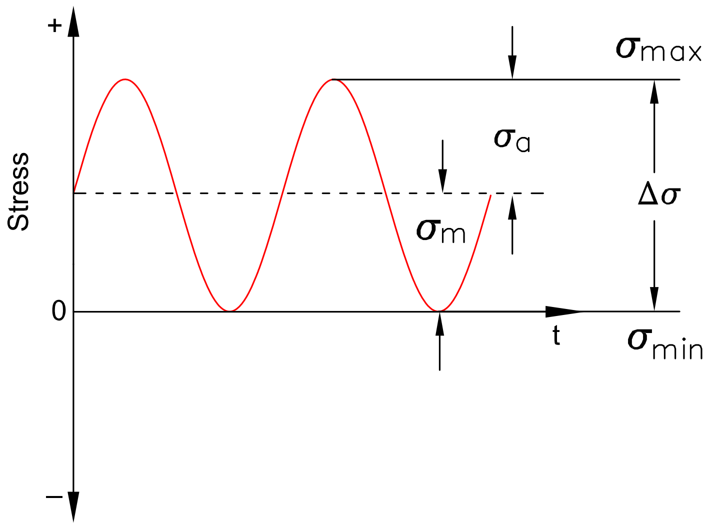

(b) Repeated.

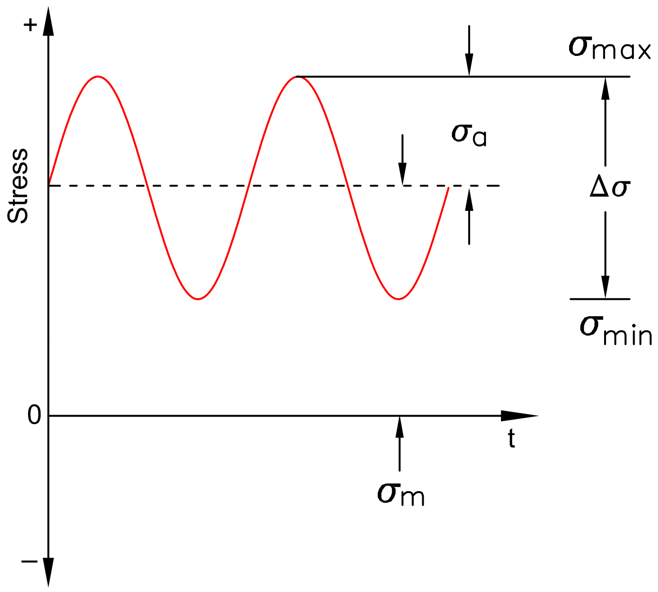

(c) Fluctuating.

Figure 7.4: Fluctuating stress types.

7.2 Fatigue Results Analysis

7.2.1 Sensitivity of fatigue methods

The applied fatigue data and the corresponding S-N curve in this thesis are shown below:

Applied Fatigue Data Parameters									
NUSMOD	NFDPO1	R1	IGERB1	INTCO1	SCF1	SIGUTS	POINT	SRANGE	NCYFAL
2	2	0.1	1	1	1	1250	1	10	1E10
							2	1000	3.5E3

Table 7.1: The applied fatigue data in the testing cases.

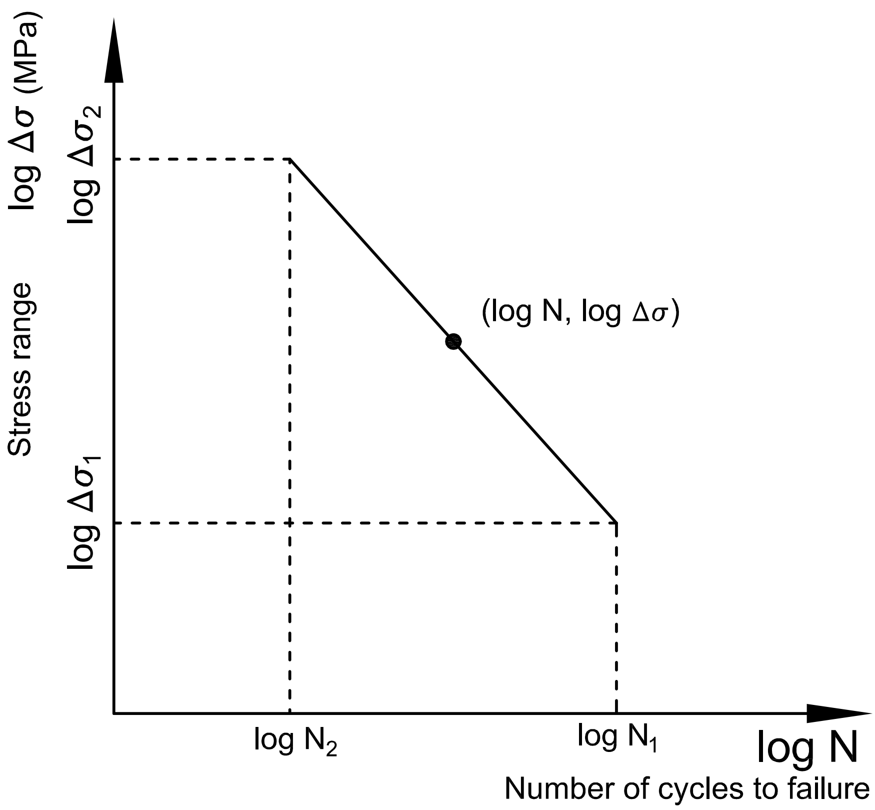

Figure 7.5: Applied S-N curve.

The theoretical S-N curve by applying two defined points is:

$$\log \Delta\sigma = \frac{\log \Delta\sigma_2 - \log \Delta\sigma_1}{\log N_2 - \log N_1}(\log N - \log N_1) + \log \Delta\sigma_1 \tag{7.9}$$

The sensitivity study of the fatigue methods is processed by checking the IGERB1 parameter in the table below(take the same line in the file randomly):

IGERB1	$\Delta\sigma(MPa)$	Mod.$\Delta\sigma(MPa)$	$\Delta\sigma_m(MPa)$	Damage	Acc.Damage
0	289	289	219	Infinity	Infinity
1	289	289	219	5.2e-6	5.2e-6
2	289	289	219	6.6e-9	6.6e-9
3	289	289	219	Infinity	Infinity
4	289	289	219	Infinity	Infinity

Table 7.2: Sensitivity of fatigue methods by changing parameter IGERB1.

By applying equation 7.9, the number of cycles to failure corresponding to $\Delta\sigma = 289(MPa)$ is:

$$
\begin{aligned}
N &= 10^{(\log N_1 + \frac{\log\Delta\sigma - \log\Delta\sigma_1}{\log\Delta\sigma_2 - \log\Delta\sigma_1}\cdot(\log N_2 - \log N_1))} \\
&= 10^{(10+\frac{\log 289 - \log 10}{\log 1000 - \log 10}\cdot(\log 3500 - \log 10))} \\
&= 192429
\end{aligned}
$$

While in the Bflex2010post file, 1 load cycle is applied, so the fatigue damage is:

$$
Damage = \frac{1}{N} = \frac{1}{192429} = 5.2e-6
$$

From the theoretical fatigue damage value, we can see that by using IGERB1=1 is correct, and the calculation in the next section is based on applying IGERB1=1. However, for IGERB=0, 3 and 4, the damage shows infinity, which is unreasonable, and the code should be checked.

7.3 Maximum Damage of All Pipe Cases

Pipe \ Model	FullFE		ITCODE0		ITCODE1	
	TENS1	TENS2	TENS1	TENS2	TENS1	TENS2
4"	1.43e-5	4.90e-6	1.96e-5	4.93e-6	1.95e-5	4.80e-6
6"	3.51e-5	1.68e-5	4.57e-5	1.61e-5	4.56e-5	1.62e-5
7.5"	2.17e-6	1.10e-7	2.72e-6	8.29e-7	2.72e-6	8.29e-7
8"	3.64e-6	6.94e-7	6.37e-6	1.82e-6	6.36e-6	1.82e-6
16"	5.15e-6	8.65e-7	4.16e-6	6.48e-7	4.18e-6	6.50e-7

Table 7.3: Maximum fatigue damage of two tensile layer cases.

Tensile layer No.	7.5"-4 tensile layer Model		
	FullFE	ITCODE0	ITCODE1
1	1.04e-5	1.92e-5	1.94e-5
2	2.80e-6	1.18e-5	1.20e-5
3	9.33e-7	2.65e-6	2.67e-6
4	1.29e-7	1.07e-6	1.25e-6

Table 7.4: Maximum fatigue damage of four tensile layer cases.

Comments about the maximum fatigue damage:

- The fatigue data for these cases are not suited to the input files, which means that the fatigue damage is not the designed damage.
- For the 6 inch pipe, the maximum fatigue damage is 1 for the two layers of all the models, which means that, under this load history, this pipe will damage and can not sustain more load.

- For the 3 models of all the pipe cases (except the 6 inch pipe), the maximum fatigue damage of the inner tensile layer is larger than the outer tensile layer, which indicates that the inner tensile layer should be taker much care of during the operation.
- For ITCODE0 and ITCODE1 models, the maximum fatigue damage is the almost the same for the corresponding layer.
- For the FullFE model, the maximum fatigue damage of each layer is smaller than the corresponding layer of ITCODE0 and ITCODE1 models, (except the 6 inch and the 16 inch pipe.)

Chapter 8 Conclusions

This thesis has concentrated on the problems relevant with stress analysis of flexible risers. Two main issues have been investigated, the first is to study the assumption of plane surface remaining plane until slip versus including the effect of shear deformations in the plastic layers, and the second is to verify whether the wire slips against the geodesic curve or it remains at the initial curve path (loxodromic) due to friction effects.

For the first issue, stress components comparisons of fullfe model as well as the itcode0 and itcode1 models under the loxodromic assumption are carried out, the conclusions from this issue are:

1. For all the stress components, the itcode0 and itcode1 models show same behaviours.

2. The hysteresis loop of the fullfe model is smaller than the other two models for stress σ_{xx} and σ_{xx-ax}.

3. For itcode0 and itcode1 models, the normal curvature stress σ_{xx-my} and the transverse curvature stress σ_{xx-mz} linearly dependent on the global normal curvature at the top side and the front side elements, respectively. While for the fullfe model, small hysteresis loop occurs, but due to the area of the loop is not relatively large, the fullfe model is acceptable.

4. For total longitudinal stress σ_{xx} and axial stress σ_{xx-ax} at the top side element, at slip domain, the stiffness of the fullfe model is the same as the itcode0 and itcode1 models, but at the stick domain, the stiffness of the fullfe model is smaller than the other models, this phenomenon is inconsistent with the stiffness of the friction plot. Several reasons have been checked such as:

   - mesh size
   - contact force
   - transverse curvature

   From the checking, the mesh size of the fullfe model dose not change the stiffness at stick domain much, and the transverse curvature is zero for fullfe model.The contact force calculated from BFLEX2010POST is the same with the value calculated from friction table. Therefore, these three reasons do not affect the stiffness of fullfe model at the stick domain, and the possible reasons maybe due to the new developed elements, HSHEAR353, the transverse degree of freedom is introduced; HSHEAR363, radial degree of freedom is introduced and the contact element HCONT463 which connects the elements above. These elements should be checked in Bflex2010 code in detail.

5. For 6 inch pipe case, the stress components of the two tensile layers show similar behaviour to the 4 inch pipe case. But for the axial stress σ_{xx-ax} of the fullfe model at the stick domain, the stiffness is inconsistent with the friction plot.

6. For 7.5 inch pipe case, similar to the 4 inch pipe case, but the stress components of the fullfe model show slightly unregular, which possibly be due to the lack of the carcass layer.

7. For 8 inch pipe case, the stress components show the same conclusions with the 4 inch pipe case. The axial stress σ_{xx-ax} of the fullfe model at the stick domain, the stiffness is inconsistent with the friction plots, while for the second tensile layer the stiffness is consistent.

8. For 16 inch pipe case, same conclusions as the 4 inch pipe case. For axial stress σ_{xx-ax} of the fullfe model at the stick domain, the stiffness is consistent with the friction plots, while for the second tensile layer, the stiffness is inconsistent.

For the second issue, stress components comparisons of fullfe model as well as the itcode0 and itcode1 models under the loxodromic and geodesic assumptions are carried out, the conclusions from the this issue are:

1. For normal curvature stress σ_{xx-my} at the top side element, the geodesic assumption shows high stress value than the loxodromic assumption and the fullfe model. The behaviour of the fullfe model is much similar to the loxodromic assumption. Local stress component σ_{xx-my} and the global normal curvature κ_y shows linear property both for itcod0 and itcode1 models. While for the fullfe model, small hysteresis loop occurs.

2. For transverse curvature stress σ_{xx-mz}, no value shown in the tensile layer under the geodesic assumption for all four locations. At the front side element, the fullfe model

shows similar behaviour to itcode0 and itcode1 models under the loxodromic assumptions, also σ_{xx-mz} and κ_y shows linear property both for itcodeo and itcode1 models. While for the fullfe model, small hysteresis loop occurs.

3. For 6 inch pipe, 7.5 inch pipe, 8 inch pipe and 16 inch pipe cases, the comparisons of the stress components show the same trend as for the 4 inch pipe cases, while for the 7.5 inch pipe, the stress components show slightly unregular behaviour, this maybe due to the lack of the carcass layer.

From the results mentioned above, the theories in chapter 3 can be verified.

From the fatigue analysis chapter, generally, maximum fatigue damage of inner tensile armour layer is larger than outer layer, and for the corresponding layer, the value of FullFE model is smaller than itcode0 and itcode1 models.

It is important to keep in mind that the riser configuration assessed in this thesis is a simplified model(short cantilever beam model), many simplifications such as the cross section input data have been made during modelling and analysis. Hence, uncertainties in the analysis results should be taken into account.

Chapter 9 Furture Work

The main purpose of this thesis work is to study the stress curvature behaviour between the new developed model FullFE with the previous models ITCODE0 and ITCODE1.

From the main results, we can see that in the slip domain, the stress-curvature behaviour is the same for the three models, in the stick domain, however, the FullFE model shows softer than ITCODE0 and ITCODE1 models, this seems not right. So the suggestion about the improvements of this thesis will be introduced.

9.1 Modelling Improvements

Model simplification: the model used in this thesis behaves like a cantilever beam, which is part of the whole flexible pipe system, so the length of the model will influence the results, the suggestion is to model longer pipe.

Mesh and Integration points: 20 element mesh size is applied in the pipe length direction, 16 integration points around the cross section are used to integrate the tendons, as Bfelx2010 software is tailored for flexible pipe, the suggestion is that the mesh size and the integration points should be selected reasonably, otherwise, time consuming and convergence error.

Boundary condition: considering the model simplification, the core layer of the model is clamped at one end, and at the free end, the translation in the y direction is restricted, which makes sure that the pipe moves in the X-Z plane, and according to the elements used for the tensile armour layer, different degrees of freedom are restricted for the 3 models. In reality, the flexible pipe move not only in one plane, due to the wave, wind and current loads, the movement of the flexible pipe is complicated, suggestion is to optimize the boundary condition to the realistic situation.

Cross section input data: in order to simplify the model, the cross section input data are simplified from the original pipe data. For example, 2 PVDF Solef60512 Copolymer layers are integrated into one THER layer, and the friction coefficient values are the same for different layers, the suggestion is to model the pipe according to the original data.

Load condition: only the internal water pressure is applied, in reality, the flexible pipe withstand not only the internal pressure, but also the external pressure, and due to the function of the pipe, the density of the fluid for transportation is different from sea water, usually the internal and external fluid of the flexible pipe are different from each other. Cyclic bending is carried out by the prescribed displacement value, suggestion is to apply not only the internal pressure, but also the external pressure, also with different fluid, carry out more comparisons with different prescribed displacement values.

Material selection:linear material properties are applied for all the layers, so for the material card in Bflex2010, the task is to verify that the properties are exact and reasonable. Besides, it is also of importance to get good knowledge on how linear material of tensile armour layer affects stress of flexible pipe.

9.2 Stress analysis Improvements

Due to the boundary condition effect, the 3rd element of each tendon of the tensile armour layer is analysed, for stress σ_{xx}, the top side location is of interest, however, when selecting the element, the element is not at the top side location exactly, and the 4th element should also be studied.

According to the element properties, using different end and corner may have some influence, which should also be studied.Further, for the model contains two tensile armour layers, the influence from the outer layer on several results can be carried out: the influence on curvature, the influence on the relative displacement of the contact element, the influence on local bending stress and so on.

9.3 Recommendations for further work

In order to be truly confident in the results, further studies taking the actual geometry and material properties of the tensile layers into account should be performed. In this thesis, the torsion of tendons and the effects between tendons are neglected, which will affect the results. Lateral buckling behaviour may also affects the results. Therefore, there is undoubtfully more work relevant with these factors should be carried out in the further study.

For the stress components study carried out by the itcode0, itcode1 and fullfe models, the way to increase the accuracy of the calculation is to select small convergence rate and small step load. Besides, there is a large number of wires in the tensile layers, forces may be transferred from one layer to the adjacent layer as both the contact force and the friction force, so the interaction effects maybe alter the behaviour.

Further, in this thesis, the material of all the layers has been assumed to behave linearly elastic at the load history. When subjected to bending, large stresses may occur, which means that the material behaviour may in reality to be elasticity.

In conclusion, in addition to the improvements mention in the two sections above, the true material behaviour should be included. As suggested in the conclusion chapter, the new developed elements HSHEAR353, HSHEAR363 and HCONT463 should be checked in Bflex2010 codes.

References

[1] American Petroleum Institute. API RECOMMENDED PRACTICE 17B-*Recommended Practice for Flexible Pipe*, 2002.

[2] American Petroleum Institute. ANSI/API SPECIFICATION 17K-*Specification for Bonded Flexible Pipe*, 2005. ISO 13628-10.

[3] American Petroleum Institute. ANSI/API SPECIFICATION 17J-*API 17J: Specification for Unbonded Flexible Pipe*, 2008.

[4] Yong Bai and Qiang Bai. *Subsea Pipelines and Risers.* Elsevier Science Ltd, 2005.

[5] S. Berge, A. Engseth, I. Fylling, C.M. Larsen, B.J. Leira, I. Nygaard, and A. Olufsen. Handbook on design and operation of flexible pipes. Technical report, The Foundation for Scientific and Industrial Reasearch at the Norwegian Institute of Technology.

[6] S. Berge, S. Sævik, N. Langhelle, Holmås.T, and O.I. Eide.

[7] DET NORSKE VERITAS. RECOMMENDED PRACTICE DNV-RP-F204-*RISER FATIGUE*, OCTOBER 2010.

[8] DET NORSKE VERITAS. RECOMMENDED PRACTICE DNV-RP-C203 -*Fatigue Design of Offshore Steel Structures*, OCTOBER 2011.

[9] Mathisen K.M. *Large Displacement Analysis of Flexible and Rigid Systems Considering Displacement-Dependent Loads and Non-Linear Constraints.* PhD thesis, Norwegian Institute of Technology, Trondheim, Norway, 1990.

[10] S. Sævik. *On Stresses and Fatigue in Flexible Pipes.* PhD thesis, NTH, Trondheim, Norway, 1992.

[11] S. Sævik. A finite element model for predicting stresses and slip in flexible pipe armouring tendons. *Computers and Structures*, 46(2):219 – 230, 1993.

[12] S. Sævik. A finite element model for predicting longitudinal stresses in nonbonded pipe pressure armours. In *Proc. of MARINFLEX ISBN 1-87461-229-3, London, UK*, 1999.

[13] S. Sævik. Comparison between theoretical and experimental flexible pipe bending stresses. In *Proc. of OMAE 2010, ISBN: 978-0-7918-3873-0, Shanghai, China*, 2010.

[14] S. Sævik. BFLEX2010 - *Theory Manual.* MARINTEK, Trondheim, Norway, 2010.

[15] S. Sævik and J. K. Ø. Gjøsteen. Strength analysis modelling of flexible umbilical members for marine structures. *Journal of Applied Mathematics*, 2012(1):18, 2012.

[16] S. Sævik and H. Li. Shear interaction and transverse buckling of tensile armours in flexible pipes. In *Proc. of the 32nd International Conference on Ocean, Offshore and Arctic Engineering, International Conference on Offshore Mechanics and Arctic Engineering, ISBN: 978-0-7918-5536-2, Nantes, France*, 2013.

[17] S. Sævik and N.Ye. Armour layer fatigue design challenges for flexible risers in ultra-deep water depth. In *Proc. of the 28th International Conference on Ocean, Offshore and Arctic Engineering, ISBN: 978-0-7918-4343-7, Honolulu, Hawaii, USA*, 2009.

[18] S. Sævik, O. D. Økland, G. S. Baarholm, and J. Gjøsteen. BFLEX2010 - *Users Manual.* MARINTEK, Trondheim, Norway, 2009. Marintek Document.

[19] S. Sævik and M. J. Thorsen. Techniques for predicting tensile armour buckling and fatigue in deep water flexible risers. In *Proc. of the 31nd International Conference on Ocean, Offshore and Arctic Engineering, International Conference on Offshore Mechanics and Arctic Engineering, Rio de Janeiro, Brazil*, 2012.

[20] Svein Sævik. Lecture notes in offshore pipeline technology. Part of Lectures Pipeline Technology in NTNU.

[21] Svein Sævik. Theoretical and experimental studies of stresses in flexible pipes. *Computers and Structures*, 89(23):2273 – 2291, 2011.

[22] S.Berge. Fatigue design of welded structures. Department of Marine Technology,NTNU,2004.

[23] G. Sines and J. Waisman. *Metal Fatigue.* McGraw-Hill Book Company,Inc., 1959.

[24] M. J. Thorsen. Capacity of deep water flexible risers., 2011.

Appendix A Explanations of Modelling and Post Processing

For more details of the parameter explanations can be referred to *Bflex2010 Usermanual* [18], here only use the 4" pipe as an explanation.

A.1 Commands interpretations in 3 testing cases

Statement: all the commands interpretations below are according to the 3 models which are studied in the master thesis. Other commands refer to *bflex2010_usermanual*.

For the coordinate degree of freedom definition:

1: translation in the x direction,

2: translation in the y direction,

3: translation in the z derection,

4: rotation about the x axis,

5: rotation about the y axis,

6: rotation about the z axis.

A.1.1 Analysis Control Step Command

HEAD:Among 3 models, the 4", 1.196 m, wellstream pipe is studied.

CONTROL:Defining the 8 governing parameters for the simulation analysis, which contains:

- MAXIT: maximum number of iterations, value:500
- NDIM: dimension of analysis, value:3
- ISOLVR:equation solver parameter,use the most efficient sparse solver, value:2
- NPOINT:number of integration points around the cross section, which will be used in defining pipe non-linear elements (in theELPROP:SCALEFACT=61/16)and visual model meshing (helix number) in XPOST, value:16
- IPRINT:print control parameter,options are:

0 and 00:deactivate print to both .bof and .blf file,

01:activate print to .blf file,

10:activate print to .bof file,

11:activate print to both .bof and .blf file.

- CONR:convergence radius, value:1.E9 (sometimes the dot is very important)
- GAC:acceleration of gravity
- ISTRES:start procedure,useSTRESSFREE, which means the initial configuration is stress free.

TIMECO: defines the analysis as a function of time, which contains:

- T:total time to simulate to, value:200
- DT:time increment to be used to reach the required time, value: 0.5, which means 1 step is 0.5s.
- DTVI:time increment between each restart/visual storage to the .raf file, value:0.5, which means storage the data every 0.5s
- DT0:time increment between each zero setting of the accumulated convergence control vectors, value:10.0(sometime .0 is very important), which means set the accumulated convergence error to be 0 every 10s.
- TYPE:analysis type is STATIC
- STEPTYPE:type of step control, value AUTO,if STEPTYPE is given, then the parameters below will overrule the CONTROL MAXIT and CONR
- ITERCO:iteration control parameter, value NONE,do not use GO-ON
- ITCRIT:iteration criterion parameter,options

DISP:displacement norm is used

FORC:force norm is used

ENER:energy norm is used

ALL:all norms are used

- MAXIT:maximum number of iterations,value,150
- MAXDIV:maximum number of sub-divisions, value,50
- CONR:convergence radius, if you use ALL at ITCRIT, then all three convergence radius must satisfy the convergence radius at the same time, otherwise it will not be converged.

In the TIMECO command, when the STEPTYPE parameter is given, then the TIMECO command will overrule the CONTROL command in terms of the Maximum Iteration Number(MAXIT) and the Convergence (CONR), in these cases the value is AUTO, the only value in Iteration Control Parameter (ITERCO) is NONE, using two examples to explain the MAXIT (Maximum number of iterations) and the MAXDIV (Maximum number of sub-divisions) in the TIMECO if STEPTYPE is given:

Example 1: The first step is not converged												
In STEPTYPE: MAXIT=2,MAXDIV=7												
Load Step Length=1, the green color number is the converged step												
1 $(\frac{1}{1})$	0.5 $(\frac{1}{2})$	0.25 $(\frac{1}{4})$	0.167 $(\frac{1}{6})$	0.333 $(\frac{2}{6})$	0.125 $(\frac{1}{8})$	0.25 $(\frac{2}{8})$	0.1 $(\frac{1}{10})$	0.2 $(\frac{2}{10})$	0.083 $(\frac{1}{12})$	0.167 $(\frac{2}{12})$	0.071 $(\frac{1}{14})$	0.143 $(\frac{2}{14})$
Statements:												
①:the 7 small steps are steps 0.5,0.25 and the GREEN number.												
②: between two consecutive GREEN number,it is converged												

Table A.1: Example to show calculation process for MAXIT=2, MAXDIV=7.

<table>
<tr><td colspan="9">Example 2: The second step is not converged</td></tr>
<tr><td colspan="9">In STEPTYPE: MAXIT=3,MAXDIV=7</td></tr>
<tr><td colspan="9">Load Step Length=0.5, the green color number is the converged step</td></tr>
<tr><td>0.5
(0.5)</td><td>1.0
(1)</td><td>0.75
$(0.5+\frac{0.5}{2})$</td><td>0.625
$(0.5+\frac{0.5}{4})$</td><td>0.5833
$(0.5+\frac{0.5}{6})$</td><td>0.5625
$(0.5+\frac{0.5}{8})$</td><td>0.55
$(0.5+\frac{0.5}{10})$</td><td>0.54167
$(0.5+\frac{0.5}{12})$</td><td>0.53571
$(0.5+\frac{0.5}{14})$</td></tr>
<tr><td colspan="9">Statements:
①:the 7 small steps are steps exclude 0.5 and 1.
②: equation:$(0.5+\frac{0.5}{2})$,the first term is the converged step (in this case:0.5)
just before the none-converged step(in this case:1),
the numerator is the load step length,
the denominator is $i \times 2$,where i=1,2 ...,MAXDIV</td></tr>
</table>

Table A.2: Example to show calculation process for MAXIT=3, MAXDIV=7.

A.1.2 Establish Material Property Command

In the 3 testing cases, all materials are linear type, including 3 steel types: steel_316,steel_110, steel_190, 2 plastic types:plast_PVDF,plast_PA11, 1 glass type:glass_fil and 1 rubber type:rubber. The properties of all the material are the same in:

TALFA:temperature elongation coefficient(no unit),value:11.7E-6

TECOND:thermal conductivity(dummy),value:2.0(W/m°C)

HEATC:heat capacity(dummy),value:50(J/kg°C)

BETA:tension/torsion coupling parameter,value:800

EA:axial stiffness,value:0(N)

EIY:bending stiffness about y axis,value:0(Nmm^2)

EIZ:bending stiffness about z axis,value:0(Nmm^2)

GIT:torsion stiffness,value:0(Nmm^2)

Different in:

POISS:poisson's ratio(no unit)

EM:Young's modulus(MPa)

GM:shear modulus(MPa)

DENSITY:density(kg/mm^3)

RTRANS:transverse Young's modulus(MPa)

A.1.3 Establish Cross Section and Cross Geometry Command

More details of cross section and geometry can be referred to Appendix B.

A.1.4 Modelling Command

Establish Node Coordinate Command

For ITCODE0 and ITCODE1 models:

Core Layer: using the global coordinate system with node number from 1 to 21, just define the coordinate of X,Y,Z.

Tensile Layer 1: using the polar local coordinate system, we define the polar local coordinate system is coincided with the global coordinate in these cases, no translation, no rotation of the local system, radius $R = \frac{ID}{2} + 5 + 5.1 + 6.4 + 2 + \frac{2}{2}$, totally 16 tendons, the first tendon node number is from 1001 to 1021,X coordinate is from 0 to 1196(mm), θ is from 0 to -13.2919 The first layer is anti-clock direction, using Repeat command to apply the other tendons with theta increment $\delta\theta = (2\pi)/16$=0.392.

Tensile Layer 2: same as Tensile Layer 1.

For FullFE cases: in addition to the 3 layers mentioned as ITCODE0 and ITCODE1 models, contact layers are defined.

Establish Element Connectivity Command

For ITCODE0 and ITCODE1 models:

Core Layer: using PIPE52 element, two consecutive nodes of the core layer define an element, totally 20 elements.

Tensile Layer 1: usig HSHEAR352 element, two consecutive nodes of the core layer and two consecutive nodes of Tensile Layer 1 defines an element, unlike with the definition of the node number, the element number is numbered in transverse direction, then longitudinal

direction.
Tensile Layer 2: same as Tensile Layer 1.

For FullFE cases: in addition to the 3 layers mentioned above, connection with contact layers are also needed.

Establish Element Orientation Command

For all layers, the vector of the local y-plane is defined positive.

A.1.5 Establish Boundary Condition Command

For ITCODE0 and ITCODE1 models:
Core Layer Nodes: fix the left node number 1 in all 6 directions
fix the right node number 21 only in the second direction, which means no transverse displacement in the y-direction
Tensile Layer 1 Nodes: fix all tendons the first node at left and the last node at right in the first direction,
which means these nodes are restricted in the x-direction, due to the property of the HSHEAR352 element (reference to Figure 3.7), no transverse translate in the y-direction.
Tensile Layer 2 Nodes: same as Tensile Layer 1.

For Full FE case:
Core Layer Nodes: fix all the core layer nodes in the 2,4,6 directions
fix the left node number 1 in 1,3,5 directions
Carcass Layer Nodes: fix all the carcass layer nodes in 1,2,3 directions
Seal and Zeta Layer Nodes: fix all the nodes in 2,3 directions
Tape Layer Nodes: fix all the nodes in 2,3 directions
Outer Sheath Layer Nodes: fix all the nodes in 2,3 directions
Tensile Layer1 Nodes: fix all tendons the first node at left and the last node at right in 1, 2 directions, fix all tendon nodes in 4,5 directions
Tensile Layer2 Nodes: same as Tensile Layer 1 Nodes

A.1.6 Apply Fatigue Data Command

Among these 3 cases, one Fatigue Data Sheet is applied, the method is to add result type ***fatigue*** in the Visual presentation card VISRES, add Fatigue properties card FATPROP,while in this card, add the material name of the Tensile Layer and the file name at which the fatigue data are stored, in these three cases the material name is ***steel_190*** and the file name is ***FATIGUEDATA***.

After running FAPLOT in the prefix.2bpi file, the fatigue information of the tensile layers are stored in the prefix.2bpl file.

Interpretation of the Fatigue Parameters (based on the S-N curve):

- NUSMOD: The number of failure modes to be considered,in this thesis, because we mainly focus on the tensile layer, choose failure mode 1 (longitudinal failure (transverse cracks)) or failure mode 2 (both longitudinal(transverse cracks)and transverse (longitudinal cracks along pressure armour due to stresses in cross-section plane))makes no difference. Apply NUSMOD=2.
- NFDPO1: The number of points in the fatigue S-N diagram for longitudinal failure (which means can not use in transverse failure mode). Apply NFDPO1=2.
- R1:The R-ratio defined as $\sigma_{min}/\sigma_{max}$ for the S-N diagram except values 21 and 22 in the IGERB, which means the mean stress. Apply R1=0.1.
- IGERB1: Method for taking the mean stress into account for longitudinal failure mode, mainly apply Goodnan and Gerber interpolation, value 2 means Gerber interpolation mean stress calculated as $\sigma_{xx} + \sigma_{yy} + \sigma_{zz}$, where σ_{yy} and σ_{zz} only apply for the pressure armour, stress range calculated considering longitudinal stress range for tensile armour, von Mises for pressure armour. Apply IGERB1=2.
- INTCO1: Axis scale in the S-N diagram, 1 means both stress and N in log scale, 2 means stress in liner scale, N in log scale. Apply INTCO1=1.
- SCF1: Stress concentration factor for longitudinal failure mode. Apply SCF1=1.
- SIGUTS: Ultimate stress (MPa). Apply SIGUTS=1250.

- POINT: Number points. Apply POINT=1,2.
- SRANGE: Stress range(increasing order) (MPa). Apply SRANGE=10,400.
- NCYFAL: Corresponding number of cycles. Apply NCYFAL=1E10,3.5E3.

A.1.7 Apply Load Command

In this thesis, we only apply the constant internal pressure with different values by using the Internal pressure loads card PILOAD.

A.2 Post Processing Parameters

The command for post processing is written in the file with suffix (.2bpi), in this thesis, ELPLOT is applied for extracting the core layer curvature, while IPPLOT is for element stress components and the FAPLOT is for fatigue damage.

The ELPLOT parameter explanations are shown below:

RAFPRE: the Bflex2010.raf file name prefix, "4inch-fullfe"

MPFPRE: the Output.raf file name prefix, "4inch-fullfe-curvature"

XLEG: the legend name for the x-axis, "TIME(s)"

XRES: the x-axis result type, TIME

YLEG: the legend name for y-axis, "Curvature (1/m)"

YRES: the y-axis result type, ELCUR-Y

FELID: the first element ID number in numerical model, 3

LELID: the last element ID number in numerical model, 3

XSCL: the unit scaling factor for x-axis, 1

YSCL: the unit scaling factor for y-axis, 1E3

ELEND: the element end number, 1

The IPPLOT parameter explanations are shown below:

RAFPRE: the Bflex2010.raf file name prefix, "4inch-fullfe"

MPFPRE: the Output.raf file name prefix, "4inch-fullfe-sigmaxx"

XLEG: the legend name for the x-axis, "TIME(s)"

XRES: the x-axis result type, TIME

YLEG: the legend name for y-axis, "Sigma-xx(MPa)"

YRES: the y-axis result type, SIGMA-XX

FELID: the first element ID number in numerical model, 30033

LELID: the last element ID number in numerical model, 30048

LSECID: the integration section number along one element, 1

CSECID: the integration corner number in cross section along one element, 1

XSCL: the unit scaling factor for x-axis, 1

YSCL: the unit scaling factor for y-axis, 1

The FAPLOT parameter explanations are shown below:

RAFPRE: the Bflex2010.raf file name prefix, "4inch-fullfe"

MPFPRE: the Output.lof file name prefix, "4inch-fullfe-fatigue"

I3: the number of load cycles, 1

FTIME: the first load step for calculating stress range, 4

LTIME: the last load step point for calculating stress range, 200

OPTSTR: Option for stress range calculating stress range, option=1,where options are:

$\neq 1$:stress range is taken to be the difference between the stress ranges obtained at load steps FTIME and LTIME

1:stress range is taken to be the largest stress range between load steps FTIME and LTIME

UNTCONV: unit conversion factor to fit the fatigue data, 1.

Appendix B Pipe Cross Section Calculation

B.1 The 6 inch pipe

B.1.1 The 6 inch pipe original data

Inside Diameter:	152.4 mm		Service:	Sweet dynamic			
Design Pressure:	41.37 MPa		Conveyed Fluid:	oil/gas/water			
Max.Fluid Temp.:	125.0°C		Water Depth[m]:	990.6m			
No	Layer	Material	Strength [MPa]	I.D [mm]	Thick [mm]	O.D [mm]	Weight [kg/m]
1	Flexbody	Stainless 316L	689	152.40	7.00	166.40	15.664
2	Flexwear	PVDF Solef		166.40	3.00	172.40	2.826
3	Flexbarrier	PVDF Solef		172.40	6.00	184.40	5.952
4	Flexwear	PVDF Solef		184.40	3.00	190.40	3.126
5	Flexlok	Carbon Steel	758	190.40	6.35	203.10	25.774
6	Flextape	PA11 P20Tape		203.10	1.52	206.14	1.026
7	Flextens1	Carbon Steel	1310	206.14	3.99	214.12	18.800
8	Flextape	PA11 P20Tape		214.12	1.52	217.16	1.081
9	Flextens2	Carbon Steel	1310	217.16	3.99	225.13	19.907
10	Flextape	Polypropylene		225.13	0.30	225.72	0.189
11	Flextape	Glass Filament		225.72	0.81	227.35	0.732
12	Flextape	Polypropylene		227.35	0.30	227.94	0.196
13	Flexwear	HDPE(Natural)		227.94	5.00	237.94	3.425
14	Flexinsul	Syntactic Foam		237.94	5.00	247.94	2.347
15	Flextape	Fabric		247.94	0.45	248.84	0.235
16	Flexshield	PA11(Yellow)		248.84	7.00	262.84	5.908
Original–Carcass Layer / Pressure Armour Layer / Tensile Armour Layer details							
Layer	U.S.Customary $[in] \times [in]$	Metric $[mm] \times [mm]$	Mfg Pitch [mm]		Wires	Angle deg[°]	Filled %
Flexbody	2.165 × 0.055	55 × 1.4	—		—	—	—
Flexlok	0.565 × 0.250	14.4 × 6.4	—		—	—	—
Flextens1	0.394 × 0.157	10 × 4	637.5		41	-46.0	91.2
Flextens2	0.394 × 0.157	10 × 4	719.4		45	44.0	91.8
Flexinsul	2.000 × 0.197	50.8 × 5	—		—	—	84.2

Table B.1: The 6 inch pipe original data.

B.1.2 6 inch pipe model input data

Original No	Model No	Layer	Material	I.D [mm]	Thick [mm]	O.D [mm]	Weight [kg/m]
1	1	CARC	Steel_316	152.4	7.0	166.4	15.664
2-4	2	THER	Plast_PVDF	166.4	12.0	190.4	11.904
5	3	ZETA	Steel_110	190.4	6.35	203.1	25.774
6	4	THER	Plast_PA11	203.1	1.52	206.14	1.026
7	5	TENS	Steel_190	206.14	3.99	214.12	18.800
8	6	THER	Plast_PA11	214.12	1.52	217.16	1.081
9	7	TENS	Steel_190	217.16	3.99	225.13	19.907
10-16	8	THER	Rubber	225.13	18.86	262.85	13.032
Model–Carcass Layer / Pressure Armour Layer / Tensile Armour Layer details							
Layer	Mean $\bar{R}[mm]$	Metric $[mm]\times[mm]$	Mfg Pitch [mm]	Wires	Angle deg[°]	Area $[mm^2]$	Filled %
1-CARC	79.7	55 × 1.4	19.551	1	87.7462	77.0	90.24
3-ZETA	98.375	14.4 × 6.4	16.3	1	88.4894	84.93	92.15
5-TENS	105.065	10 × 4	637.5	41	-46.0	40	91.2
7-TENS	110.575	10 × 4	719.4	45	44.0	40	91.8

Table B.2: The 6 inch pipe model input data.

B.1.3 6 inch cross-section parameters calculation

Due to the missing parameters of this cross section original data, the area of the pressure layer is calculated through the equation:

$A = b \times h \times f_i$

In the next calculation, some parameters of the input data are different from the original data:

For pressure layer, the Bflex software can only accept 1 tendon,

For carcass and pressure layer:

When the area A is given, then the lay angle α can be calculated by the equation:

$\frac{\rho \times A}{cos(\alpha)} = m$, where m is the corresponding layer weight along the pipe.

When the pitch p is given, the lay angleθ can also be calculated by the equation: $\frac{2\times\pi\times\bar{R}}{tan(\alpha)} = p$, where $\bar{R}$ is the mean radius of the layer.
Which means that

1. **Carcass Layer**:
    - Mean Radius: $\bar{R}$=$\frac{I.D}{2} + \frac{h}{2} = \frac{152.4}{2} + \frac{7}{2} = 79.7mm$
    - Area: $A = b \times h = 55 \times 1.4 = 77.0mm^2$
    - Lay Angle: $\alpha = acos(\rho \times A/weight) = acos(8000 \times 77 \times 10^{-6}/15.664) = 87.7462°$
    - Pitch: $p = 2 \times \pi \times \bar{R}/tan(\alpha) = 2 \times \pi \times 79.7/tan(87.7642°) = 19.551mm$
2. **Pressure layer**:
    - Mean Radius:$\bar{R}$=$\frac{I.D}{2} + \frac{h}{2} = \frac{190.4}{2} + \frac{6.35}{2} = 98.375mm$
    - Area: $A = b \times h \times f_i = 14.4 \times 6.4 \times 92.15\% = 84.93mm^2$
    - Lay Angle: $\alpha = acos(\rho \times A/weight) = acos(8000 \times 84.93 \times 10^{-6}/25.774) = 88.4894°$
    - Pitch: $p = 2 \times \pi \times \bar{R}/tan(\alpha) = 2 \times \pi \times 98.375/tan(88.4894°) = 16.3mm$
3. **Tensile layer1**:
    - Mean Radius:$\bar{R}$=$\frac{I.D}{2} + \frac{h}{2} = \frac{206.14}{2} + \frac{3.99}{2} = 105.065mm$
    - Area: $A = b \times h = 10 \times 4 = 40mm^2$
    - Lay Angle: Given $\alpha = -46°$
    - Pitch:Given $p = 2 \times \pi \times \bar{R}/tan(\alpha) = 2 \times \pi \times 105.065/tan(|-46°|) = 637.5mm$
4. **Tensile layer2**:
    - Mean Radius:$\bar{R}$=$\frac{I.D}{2} + \frac{h}{2} = \frac{217.16}{2} + \frac{3.99}{2} = 110.575mm$
    - Area: $A = b \times h = 10 \times 4 = 40mm^2$
    - Lay Angle: Given $\alpha = 44°$
    - Pitch:$p = 2 \times \pi \times \bar{R}/tan(\alpha) = 2 \times \pi \times 110.575/tan(44°) = 719.4mm$

B.2 8 inch pipe

B.2.1 8 inch pipe original data

Layer No	Material	Profile $[mm] \times [mm]$	Dir	No	Gap [mm]	Pitch [mm]	O.D [mm]	T [mm]	Angle deg	Weight [kg/m]
–	Bore	–	–	–	–	–	203.2	–	–	–
1	Lean Duplex	2.0 × 100	Z	1	5.0	34.0	227.2	12.0	87.1210	30.66
2	Diolen 14K	0.2 × 100	S	2	–	90.0	228.1	0.4	-82.8274	0.26
3	Diolen 14K	0.2 × 100	S	2	–	50.0	229.7	0.8	-86.0226	0.46
4	PVDF	–	–	–	–	–	245.7	8.0	–	10.60
5	Basic grade	C6	Z	2	0.7	21.4			–	
5	Basic grade	C3	Z	2	0.7	21.4	263.7	9.0	–	50.61
6	Diolen 14K	0.2 × 100	S	2	9.0	110	264.5	0.4	-82.4535	0.24
7	PVDF	1.0 × 60	S	2	7.1	136	266.5	1.0	-80.7393	1.34
8	High s.grade	5 × 12.5	Z	54	1.2	1474	276.5	5.0	30.0562	30.65
9	Diolen 14K	0.2 × 100	S	2	57.4	160	277.3	0.4	-79.5855	0.18
10	Diolen 14K	0.2 × 100	Z	2	57.4	160	278.1	0.4	79.6149	0.18
11	PVDF	1.0 × 60	Z	2	7.2	136	280.1	1.0	81.1833	1.41
12	High s.grade	5 × 12.5	S	56	1.3	1525	290.1	5.0	-30.4267	31.90
13	Diolen 14K	0.2 × 100	Z	2	9.2	110	290.9	0.4	83.1319	0.27
14	cords	1.8 × 2.2	Z	8	0.9	25.0	294.5	1.8	88.4427	1.62
15	tape	0.075 × 100	S	1	–	45.0	294.8	0.2	-87.2170	0.15
16	Diolen 14K	0.2 × 100	S	1	–	45.0	295.7	0.4	-87.2228	0.33
17	PT7000	8.3 × 50	S	4	4.9	55.0	362.1	33.2	-87.1673	22.80
18	Diolen 14K	0.2 × 100	Z	2	9.5	110.0	362.9	0.4	84.4863	0.33
19	PT7000	6.3 × 50	Z	4	4.9	55.0	413.3	25.2	87.5371	20.41
20	Diolen 14K	0.2 × 100	S	2	9.6	110.0	414.1	0.4	-85.1648	0.38
21	Marix	0.2 × 80	S	4	–	72.0	415.9	0.9	-86.8392	0.35
22	PA11	–	–	–	–	–	435.9	10.0	–	14.05

Pressure Armour Details							
Grp./	Layer	Pro-	R to n	Angle	Area	Wf	Kw
Layer	Layout	file	mm	deg	mm^2	strand	group
1/5	[-][-]	C6	125.796	88.4491	57.96	0.8000	0.9327
5	[-][-]	C3	130.347	88.5032	28.16	0.8000	
Tensile Armour Details							
Layer	Layer	Gap	Spiral	Area	Wf	Kw	Max length
No	Layout	%		mm^2	strand	group	no welding
8	[54]	8.57	1.703m	62.50	0.7000	0.9815	1685.1
12	[56]	9.36	1.769m	62.50	0.7000	0.9821	1678.5

Table B.3: The 8 inch pipe original data.

The geometry of the C3,C6 profiles are shown as below:

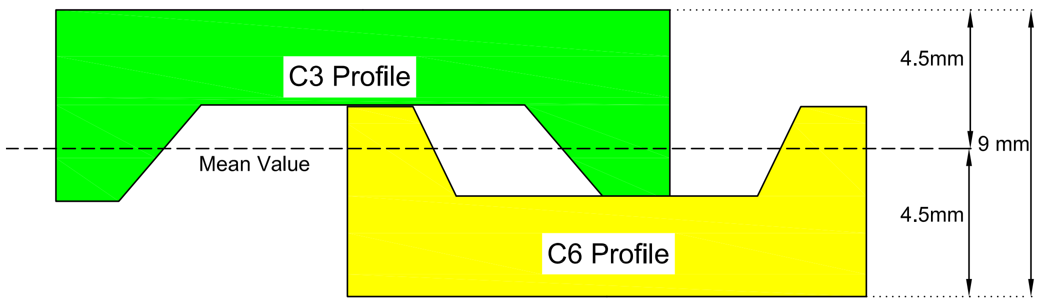

Figure B.1: The C3-C6 profile.

B.2.2 8 inch pipe model input data

Original No	Model No	Layer	Material	I.D [mm]	Thick [mm]	O.D [mm]	Weight [kg/m]
1	1	CARC	Steel_316	203.2	12.0	227.2	30.660
2-4	2	THER	Plast_PVDF	227.2	9.2	245.7	11.320
5	3	ZETA	Steel_110	245.7	9.0	263.7	50.610
6-7	4	THER	Plast_PA11	263.7	1.4	266.5	1.580
8	5	TENS	Steel_190	266.5	5.0	276.5	30.650
9-11	6	THER	Plast_PA11	276.5	1.8	280.1	1.770
12	7	TENS	Steel_190	280.1	5.0	290.1	31.900
13-22	8	THER	Rubber	290.1	72.9	435.9	60.69
Model–Carcass Layer / Pressure Armour Layer / Tensile Armour Layer details							
Layer	Mean $\bar{R}[mm]$	Metric $[mm] \times [mm]$	Mfg Pitch [mm]	Wires	Angle deg[°]	Area $[mm^2]$	
1-CARC	107.6	2.0×100	34.0	1	87.1210	200.0	
3-ZETA	127.35		10.7	1	89.2336	86.12	
5-TENS	135.75	12.5×5	1474.0	54	-30.0562	62.50	
7-TENS	142.55	12.5×5	1525.0	56	30.4267	62.50	

Table B.4: The 8 inch pipe model input data.

B.2.3 8 inch cross-section parameters calculation

In the next calculation, some parameters of the input data are different from the original data:

For pressure layer, the Bflex software can only accept 1 tendon.

For carcass and pressure layer:

When the area A is given, then the lay angle α can be calculated by the equation:

$\frac{\rho \times A}{cos(\alpha)} = m$, where m is the corresponding layer weight along the pipe.

When the pitch p is given, the lay angleα can also be calculated by the equation:

$\frac{2\times\pi\times\bar{R}}{tan(\alpha)} = p$, where $\bar{R}$ is the mean radius of the layer.

Which means that

1. **Carcass Layer**:

   - Mean Radius: $\bar{R}$=$\frac{I.D}{2}+\frac{h}{2}=\frac{203.2}{2}+\frac{12}{2}=107.6mm$
   - Area: $A=b\times h=2\times 100=200mm^2$
   - Lay Angle: $\alpha=atan(2\times\pi\times\bar{R}/p)=atan(2\times\pi\times 107.6/34)=87.1210°$
   - Pitch: Given $p=34.0mm$

2. **Pressure layer**:

   - Mean Radius:$\bar{R}$=$\frac{I.D}{2}+\frac{h}{2}=\frac{245.7}{2}+\frac{9}{2}=127.35mm$
   - Area: Given $A=57.96+28.16=86.12mm^2$
   - Lay Angle: $\alpha=atan(2\times\pi\times\bar{R}/p)=atan(2\times\pi\times 127.35/10.7)=89.2336°$
   - Pitch: $p=21.4/2=10.7mm$

3. **Tensile layer1**:

   - Mean Radius:$\bar{R}$=$\frac{I.D}{2}+\frac{h}{2}=\frac{266.5}{2}+\frac{5}{2}=135.75mm$
   - Area: $A=b\times h=12.5\times 5=62.5mm^2$
   - Lay Angle: Given $\alpha=-30.0562°$
   - Pitch:$p=2\times\pi\times\bar{R}/tan(\alpha)=2\times\pi\times 135.75/tan(|-30.0562°|)=1474.0mm$

4. **Tensile layer2**:

   - Mean Radius:$\bar{R}$=$\frac{I.D}{2}+\frac{h}{2}=\frac{280.1}{2}+\frac{5}{2}=142.55mm$
   - Area: $A=b\times h=12.5\times 5=62.5mm^2$
   - Lay Angle: Given $\alpha=30.4267°$
   - Pitch:$p=2\times\pi\times\bar{R}/tan(\alpha)=2\times\pi\times 142.55/tan(30.4267°)=1525.0mm$

B.3 16 inch pipe

B.3.1 16 inch pipe original data

Inside Diameter: 406.4 mm		Service: Sweet dynamic			Max.Fluid Temp.: 70°C		
Design Pressure: 13.793 MPa		Conveyed Fluid: oil/gas			Water Depth[m]: 300m		
No	Layer	Material	Strength [MPa]	I.D [mm]	Thick [mm]	O.D [mm]	Weight [kg/m]
1	Flexbody	Stainless 316L		406.40	10.35	427.10	61.360
2	Flexwear	PVDF Solef Copolymer		427.10	6.00	439.10	14.450
3	Flexbarrier	PVDF Solef Copolymer		439.10	9.00	457.10	22.425
4	Flexlok	Carbon Steel	758	457.10	11.99	481.08	120.003
5	Flextape	PA11 P20 Tape		481.08	1.52	484.12	2.420
6	Flextens1	Carbon Steel	1310	484.12	3.99	492.09	41.553
7	Flextape	PA11 P20 Tape		492.09	1.52	495.13	2.475
8	Flextens2	Carbon Steel	1310	495.13	3.99	503.11	42.664
9	Flextape	Polypropylene		503.11	0.30	503.70	0.434
10	Flextape	High Strength Glass Filament		503.70	1.63	506.95	3.355
11	Flextape	Polypropylene		506.95	0.30	507.54	0.437
12	Flextape	Fabric		507.54	0.41	508.36	0.433
13	Flexshield	PA12(Black)		508.36	15.00	538.36	25.156
Carcass Layer / Pressure Armour Layer / Tensile Armour Layer details							
Layer	Raw Material $[mm] \times [mm]$	Cross Dimensions $[in] \times [in]$	Pitch $[mm]$	Wires	Area $[mm^2]$	Angle deg[°]	Filled %
Flexbody	68.0×1.8	2.677×0.071	—	—	122.4	89.0	90.24
Flexlok (Profile G)	26.6×12.0	1.047×0.472	—	—	202	89.2	92.15
Flextens1	12.0×4	0.472×0.157	1827.5	89	—	-40.0	91.58
Flextens2	12.0×4	0.472×0.157	2007.0	94	—	38.0	91.94

Table B.5: The 16 inch pipe original data.

B.3.2 16 inch pipe model input data

Original No	Model No	Layer	Material	I.D [mm]	Thick [mm]	O.D [mm]	Weight [kg/m]
1	1	CARC	Steel_316	406.40	10.35	427.10	61.360
2-3	2	THER	Plast_PVDF	427.10	15.0	457.10	36.875
4	3	ZETA	Steel_110	457.10	11.99	481.08	120.003
5	4	THER	Plast_PA11	481.08	1.52	484.12	2.420
6	5	TENS	Steel_190	484.12	3.99	492.09	41.553
7	6	THER	Plast_PA11	492.09	1.52	495.13	2.475
8	7	TENS	Steel_190	495.13	3.99	503.11	42.664
9-13	8	THER	Rubber	503.11	17.64	538.36	29.815
Model–Carcass Layer / Pressure Armour Layer / Tensile Armour Layer details							
Layer	Mean $\bar{R}[mm]$	Metric $[mm]\times[mm]$	Mfg Pitch [mm]	Wires	Angle deg[°]	Area $[mm^2]$	Filled %
1-CARC	208.375	68.0 × 1.8	20.5035	1	89.1028	122.4	90.24
3-ZETA	234.545	26.6 × 12	19.4743	1	89.2429	202.0	92.15
5-TENS	244.055	12 × 4	1827.5	89	-40.0	48.0	91.58
7-TENS	249.56	12 × 4	2007.0	94	38.0	48.0	91.94

Table B.6: The 16 inch pipe model input data.

B.3.3 16 inch cross-section parameters calculation

In the next calculation, some parameters of the input data are different from the original data:

For carcass and pressure layer:

When the area A is given, then the lay angle α can be calculated by the equation:

$\frac{\rho\times A}{cos(\alpha)} = m$, where m is the corresponding layer weight along the pipe.

When the pitch p is given, the lay angleα can also be calculated by the equation:

$\frac{2\times\pi\times\bar{R}}{tan(\alpha)} = p$, where $\bar{R}$ is the mean radius of the layer.

Which means that

1. **Carcass Layer**:
   - Mean Radius: $\bar{R} = \frac{I.D}{2} + \frac{h}{2} = \frac{406.40}{2} + \frac{10.35}{2} = 208.375mm$
   - Area: $A = b \times h = 68 \times 1.8 = 122.4mm^2$
   - Lay Angle: $\alpha = acos(\rho \times A/weight) = acos(7850 \times 122.4 \times 10^{-6}/61.36) = 89.1028°$
   - Pitch: $p = 2 \times \pi \times \bar{R}/tan(\alpha) = 2 \times \pi \times 208.375/tan(89.1028°) = 20.5035mm$

2. **Pressure layer**:
   - Mean Radius: $\bar{R} = \frac{I.D}{2} + \frac{h}{2} = \frac{457.10}{2} + \frac{11.99}{2} = 234.545mm$
   - Area: Given $A = 202.0mm^2$
   - Lay Angle: $\alpha = acos(\rho \times A/weight) = acos(7850 \times 202 \times 10^{-6}/120.003) = 89.2429°$
   - Pitch: $p = 2 \times \pi \times \bar{R}/tan(\alpha) = 2 \times \pi \times 234.545/tan(89.2429°) = 19.4743mm$

3. **Tensile layer1**:
   - Mean Radius: $\bar{R} = \frac{I.D}{2} + \frac{h}{2} = \frac{484.12}{2} + \frac{3.99}{2} = 244.055mm$
   - Area: $A = b \times h = 12 \times 4 = 48mm^2$
   - Lay Angle: Given $\alpha = -40°$
   - Pitch: $p = 2 \times \pi \times \bar{R}/tan(\alpha) = 2 \times \pi \times 244.055/tan(|-40°|) = 1827.5mm$

4. **Tensile layer2**:
   - Mean Radius: $\bar{R} = \frac{I.D}{2} + \frac{h}{2} = \frac{495.13}{2} + \frac{3.99}{2} = 249.56mm$
   - Area: $A = b \times h = 12 \times 4 = 48mm^2$
   - Lay Angle: Given $\alpha = 38°$
   - Pitch: $p = 2 \times \pi \times \bar{R}/tan(\alpha) = 2 \times \pi \times 249.56/tan(38°) = 2007.0mm$

B.4 The 7.5 inch 2 tensile layers pipe

B.4.1 The 7.5 inch 2 tensile layers pipe original data

Inside Diameter: 190.50 mm			Service: Sour-Sweet service			
Design temperature: 65°C			Design Pressure: 10000psi,689bars			
Factory Test Pressure: 15000psi,1034bars.						
No	Layer	UTS [MPa]	SDP [MPa]	Thick [mm]	I.D [mm]	Mass [kg/m]
1	Tube			13.00	190.50	7.88
2	Zeta	850	359	12.00	216.50	57.17
3	Spiral	780	329	3.60	240.50	18.35
4	Antitape			6.70	247.70	5.04
5	First armour	1400	549	5.00	261.10	29.22
6	Antiweartape			1.50	271.10	1.22
7	Second armour	1400	528	5.00	274.10	30.80
8	External sheath			3.20	280.50	8.88

Table B.7: The 7.5 inch 2 tensile layers pipe original data.

B.4.2 The 7.5 inch 2 tensile layers pipe model input data

Original No	Model No	Layer	Material	I.D [mm]	Thick [mm]	O.D [mm]	Weight [kg/m]
1	1	THER	Plast_PVDF	190.50	13.0	216.50	7.88
2	2	ZETA	Steel_110	216.50	12.0	240.50	57.17
3-4	3	THER	Plast_PA11	240.50	10.3	261.10	23.39
5	4	TENS	Steel_190	261.10	5.00	271.10	29.22
6	5	THER	Plast_PA11	271.10	1.50	274.10	1.22
7	6	TENS	Steel_190	274.10	5.00	284.10	30.80
8	7	THER	Plast_PA11	284.10	3.20	290.50	8.88
Model–Carcass Layer / Pressure Armour Layer / Tensile Armour Layer details							
Layer	Mean $\bar{R}[mm]$	Metric $[mm/mm]$	Mfg Pitch [mm]	Wires	Angle deg[°]	Area $[mm^2]$	
2-ZETA	114.25		19	1	88.4839	192.5	
4-TENS	133.05	15×5	1109.38	42	-37.0	75	
6-TENS	139.55	15×5	1122.28	44	38.0	75	

Table B.8: The 7.5 inch 2 tensile layers pipe model input data.

B.4.3 7.5 inch 2 tens cross-section parameters calculation

1. **Pressure layer**:
   - Mean Radius:$\bar{R}=\frac{I.D}{2}+\frac{h}{2}=\frac{216.50}{2}+\frac{12.0}{2}=114.25mm$
   - Area: Given $A=192.5mm^2$
   - Lay Angle: $\alpha=atan(2\times\pi\times\bar{R}/p)=atan(2\times\pi\times114.25/19)=88.4839°$
   - Pitch: Given $p=19mm$
2. **Tensile layer1**:
   - Mean Radius:$\bar{R}=\frac{I.D}{2}+\frac{h}{2}=\frac{261.10}{2}+\frac{5.0}{2}=133.05mm$
   - Area: $A=b\times h=15\times5=75mm^2$
   - Lay Angle: Given $\alpha=-37°$
   - Pitch:$p=2\times\pi\times\bar{R}/tan(\alpha)=2\times\pi\times133.05/tan(|-37°|)=1109.38mm$
3. **Tensile layer2**:
   - Mean Radius:$\bar{R}=\frac{I.D}{2}+\frac{h}{2}=\frac{274.10}{2}+\frac{5.0}{2}=139.55mm$
   - Area: $A=b\times h=15\times5=75mm^2$
   - Lay Angle: Given $\alpha=38°$
   - Pitch:$p=2\times\pi\times\bar{R}/tan(\alpha)=2\times\pi\times139.55/tan(38°)=1122.28mm$

B.5 The 7.5 inch 4 tensile layers pipe

B.5.1 The 7.5 inch 4 tensile layers pipe original data

Inside Diameter: 190.50 mm			Service: Sweet service			
Design temperature: 60°C			Design Pressure: 10000psi, 689bars			
Factory Test Pressure: 15000psi,1034bars.						
No	Layer	UTS [MPa]	SDP [MPa]	Thick [mm]	I.D [mm]	Mass [kg/m]
1	Tube			13.00	190.50	7.88
2	Zeta	980	491	12.00	216.50	57.17
3	Spiral	1400	461	3.60	240.50	18.35
4	Antitape			6.70	247.70	5.04
5	First armour	1400	291	5.00	261.10	29.22
6	Antiweartape			1.50	271.10	1.22
7	Second armour	1400	235	5.00	274.10	30.80
8	Fabrictape			1.70	284.10	0.70
9	Antiweartape			1.50	287.50	1.30
10	Third armour	1400	262	5.00	290.50	32.70
11	Antiweartape			1.50	300.50	1.35
12	Fourth armour	1400	211	5.00	303.50	34.24
13	High strength tape			4.45	313.50	3.18
14	External sheath			8.50	322.40	8.88

Table B.9: The 7.5 inch 4 tensile layers pipe original data.

B.5.2 The 7.5 inch 4 tensile layers pipe model input data

Original No	Model No	Layer	Material	I.D [mm]	Thick [mm]	O.D [mm]	Weight [kg/m]
1	1	THER	Plast_PVDF	190.50	13.0	216.50	7.88
2	2	ZETA	Steel_110	216.50	12.0	240.50	57.17
3-4	3	THER	Plast_PA11	240.50	10.3	261.10	23.39
5	4	TENS	Steel_190	261.10	5.00	271.10	29.22
6	5	THER	Plast_PA11	271.10	1.50	274.10	1.22
7	6	TENS	Steel_190	274.10	5.00	284.10	30.80
8-9	7	THER	Plast_PA11	284.10	3.20	290.50	2.00
10	8	TENS	Steel_190	290.50	5.00	300.50	32.70
11	9	THER	Plast_PA11	300.50	1.50	303.50	1.35
12	10	TENS	Steel_190	303.50	5.00	313.50	34.24
13-14	11	THER	Rubber	313.50	12.95	339.40	12.06
Model–Carcass Layer / Pressure Armour Layer / Tensile Armour Layer details							
Layer	Mean $\bar{R}[mm]$	Metric $[mm/mm]$	Mfg Pitch [mm]	Wires	Angle deg[°]	Area $[mm^2]$	
2-ZETA	114.25		19	1	88.4839	192.5	
4-TENS	133.05	15 × 5	1109.38	42	-37.0	75	
6-TENS	139.55	15 × 5	1122.28	44	38.0	75	
8-TENS	147.75	15 × 5	1231.95	47	-37.0	75	
10-TENS	154.25	15 × 5	1286.15	49	37.0	75	

Table B.10: The 7.5 inch 4 tensile layers pipe model input data.

B.5.3 7.5 inch 4 tens cross-section parameters calculation

1. **Pressure layer**:
   - Mean Radius:$\bar{R}$=$\frac{I.D}{2}+\frac{h}{2}=\frac{216.50}{2}+\frac{12.0}{2}=114.25mm$
   - Area: Given $A=192.5mm^2$
   - Lay Angle: $\alpha=atan(2\times\pi\times\bar{R}/p)=atan(2\times\pi\times 114.25/19)=88.4839°$
   - Pitch: Given $p=19mm$
2. **Tensile layer1**:
   - Mean Radius:$\bar{R}$=$\frac{I.D}{2}+\frac{h}{2}=\frac{261.10}{2}+\frac{5.0}{2}=133.05mm$
   - Area: $A=b\times h=15\times 5=75mm^2$
   - Lay Angle: Given $\alpha=-37°$
   - Pitch:$p=2\times\pi\times\bar{R}/tan(\alpha)=2\times\pi\times 133.05/tan(|-37°|)=1109.38mm$
3. **Tensile layer2**:
   - Mean Radius:$\bar{R}$=$\frac{I.D}{2}+\frac{h}{2}=\frac{274.10}{2}+\frac{5.0}{2}=139.55mm$
   - Area: $A=b\times h=15\times 5=75mm^2$
   - Lay Angle: Given $\alpha=38°$
   - Pitch:$p=2\times\pi\times\bar{R}/tan(\alpha)=2\times\pi\times 139.55/tan(38°)=1122.28mm$
4. **Tensile layer3**:
   - Mean Radius:$\bar{R}$=$\frac{I.D}{2}+\frac{h}{2}=\frac{290.50}{2}+\frac{5.0}{2}=147.75mm$
   - Area: $A=b\times h=15\times 5=75mm^2$
   - Lay Angle: Given $\alpha=-37°$
   - Pitch:$p=2\times\pi\times\bar{R}/tan(\alpha)=2\times\pi\times 139.55/tan(|-37°|)=1231.95mm$
5. **Tensile layer4**:
   - Mean Radius:$\bar{R}$=$\frac{I.D}{2}+\frac{h}{2}=\frac{303.50}{2}+\frac{5.0}{2}=154.25mm$
   - Area: $A=b\times h=15\times 5=75mm^2$
   - Lay Angle: Given $\alpha=37°$
   - Pitch:$p=2\times\pi\times\bar{R}/tan(\alpha)=2\times\pi\times 154.25/tan(37°)=1286.15mm$

Appendix C The 6-8-16 inch pipe analysis

C.1 The 6 inch pipe analysis

The 6 inch pipe model friction data and friction plots

6 inch pipe model friction data								
Layer	tensile layer 1				tensile layer 2			
models	Point	Relative Disp (–)	Unit Force (–)	Applied fric-force per-length	Point	Relative Disp (–)	Unit Force (–)	Applied fric-force per-length
itcode0-loxodromic	1	0	0	11.044809	1	0	0	3.578660
	2	0.42696E-02	0.9		2	0.42696E-02	0.9	
	3	0.85393E-02	1		3	0.85393E-02	1	
	4	0.10000E+05	10		4	0.10000E+05	10	
itcode0-geodesic	1	0	0	11.044809	1	0	0	3.578660
	2	0.42696E-02	0.9		2	0.42696E-02	0.9	
	3	0.85393E-02	1		3	0.85393E-02	1	
	4	0.10000E+05	10		4	0.10000E+05	10	
itcode1-loxodromic	1	0	0	11.044809	1	0	0	3.578660
	2	0.42696E-02	0.9		2	0.16426E-02	0.9	
	3	0.85393E-02	1		3	0.32851E-02	1	
	4	0.10000E+05	10		4	0.10000E+05	10	
itcode1-geodesic	1	0	0	11.044809	1	0	0	3.578660
	2	0.42696E-02	0.9		2	0.16426E-02	0.9	
	3	0.85393E-02	1		3	0.32851E-02	1	
	4	0.10000E+05	10		4	0.10000E+05	10	
fullfe	1	0	0	10.422374	1	0	0	3.480392
	2	0.40290E-02	0.9		2	0.15975E-02	0.9	
	3	0.80581E-02	1		3	0.31949E-02	1	
	4	0.11057E+06	10		4	0.11057E+06	10	

Table C.1: The 6 inch pipe model friction data.

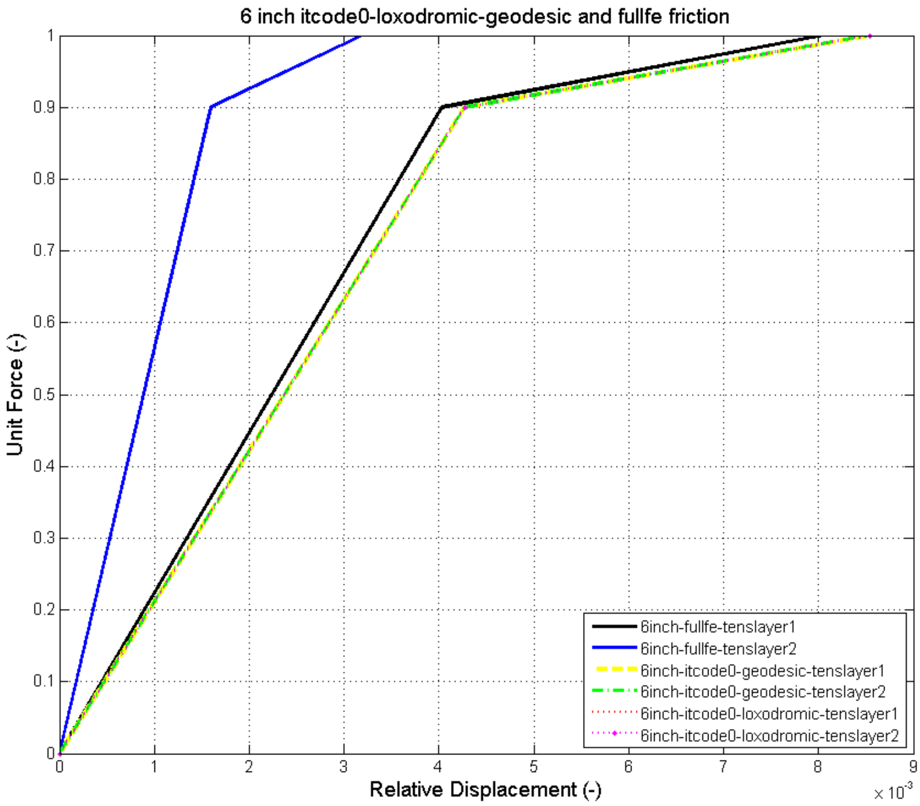

Figure C.1: The 6 inch lox-geo friction for itcode0 and fullfe.

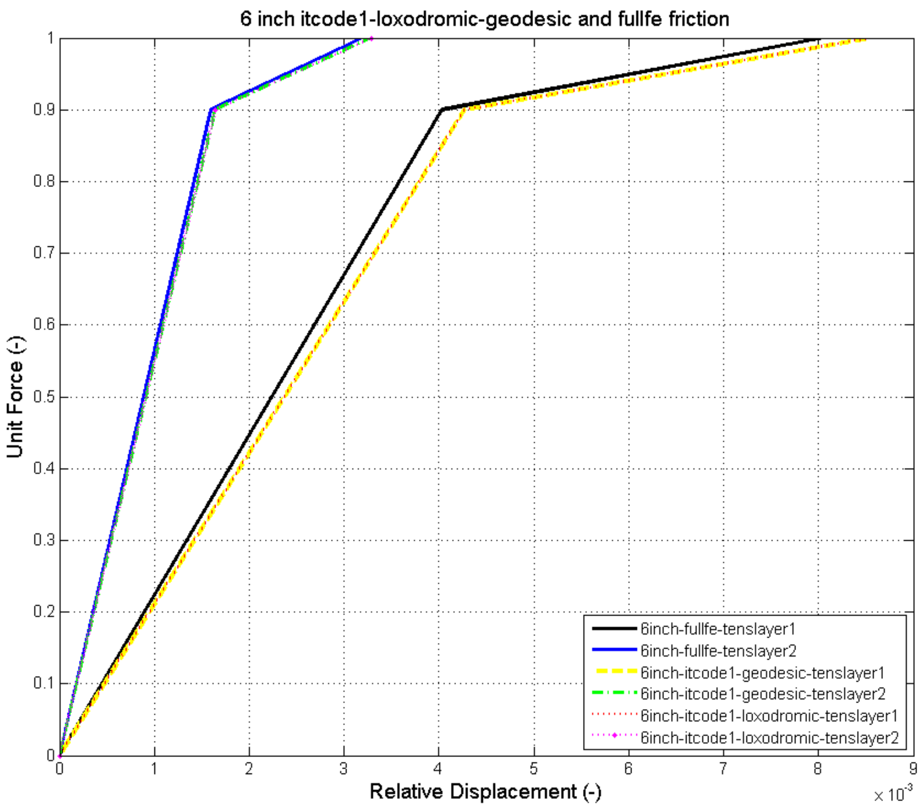

Figure C.2: The 6 inch lox-geo friction for itcode1 and fullfe.

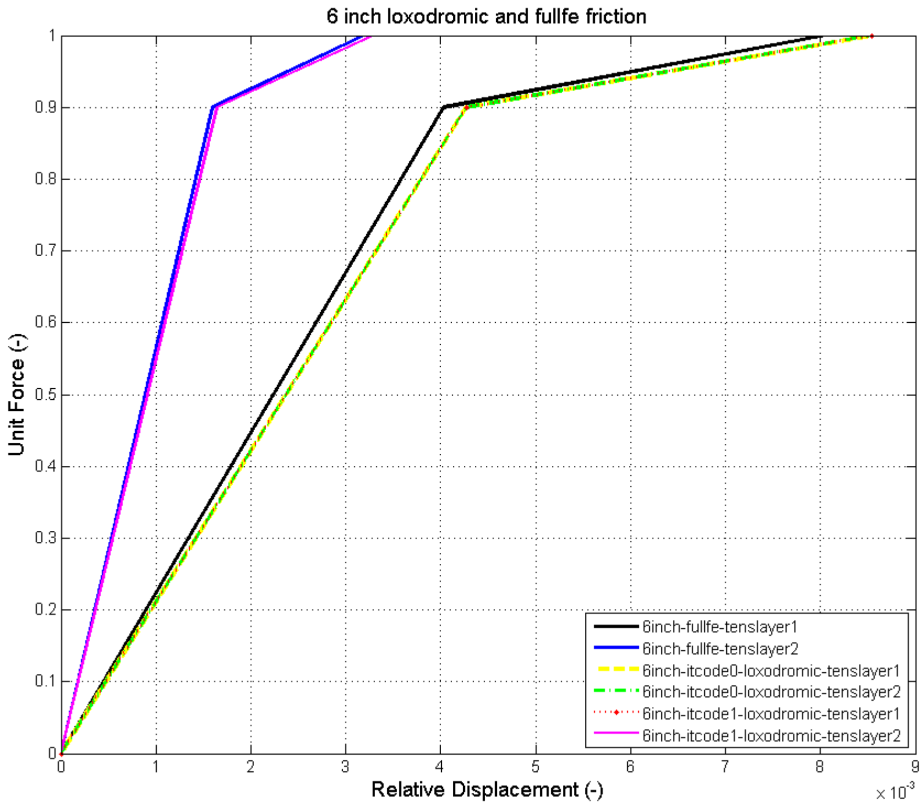

Figure C.3: The 6 inch lox friction for itcode0-itcode1 and fullfe.

C.1.1 Stress components plots

The 6 inch stress components under two assumptions

Figure C.4–Figure C.11 show the stress components comparisons of itcode0 and itcode1 models under both the loxodromic and geodesic assumptions and the fullfe model.

The 6 inch stress study for lox assumption and fullfe model

Figure C.12 – Figure C.19 show the stress components comparisons of itcode0 and itcode1 models under loxodromic assumption and fullfe model.

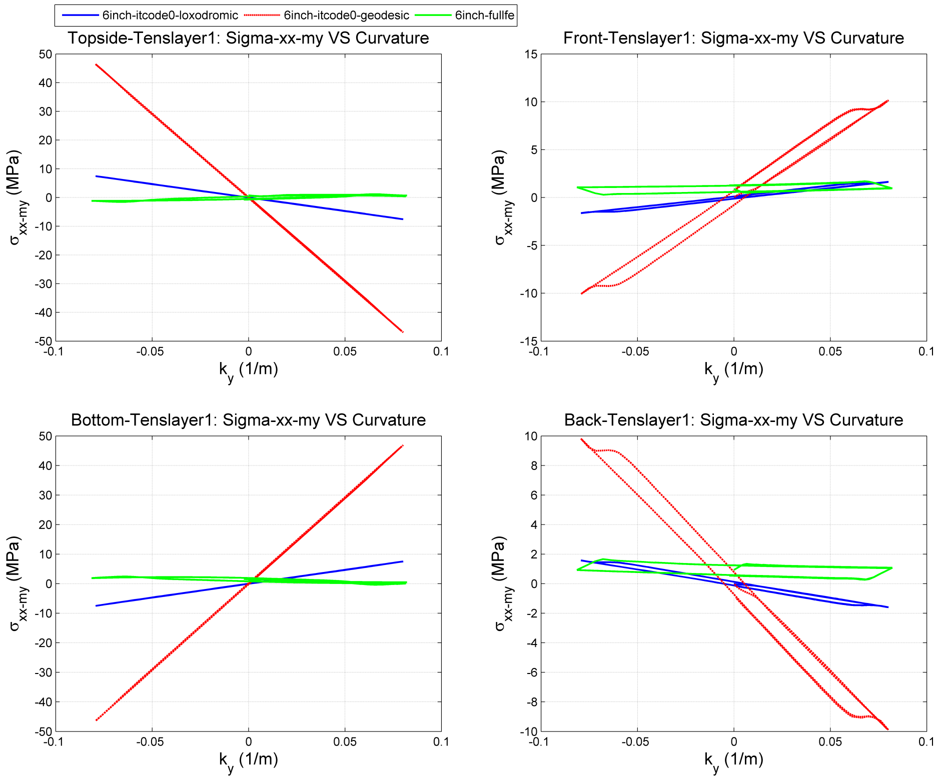

Figure C.4: The 6 inch tenslayer1 σ_{xx-my} lox-geo for itcode0 and fullfe.

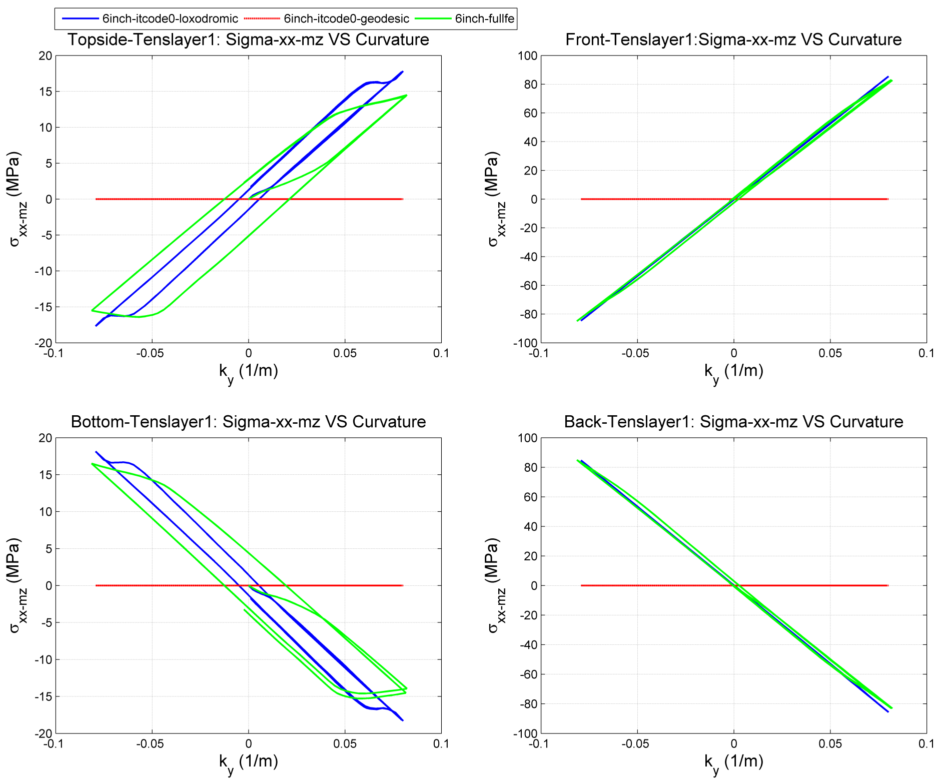

Figure C.5: The 6 inch tenslayer1 σ_{xx-mz} lox-geo for itcode0 and fullfe.

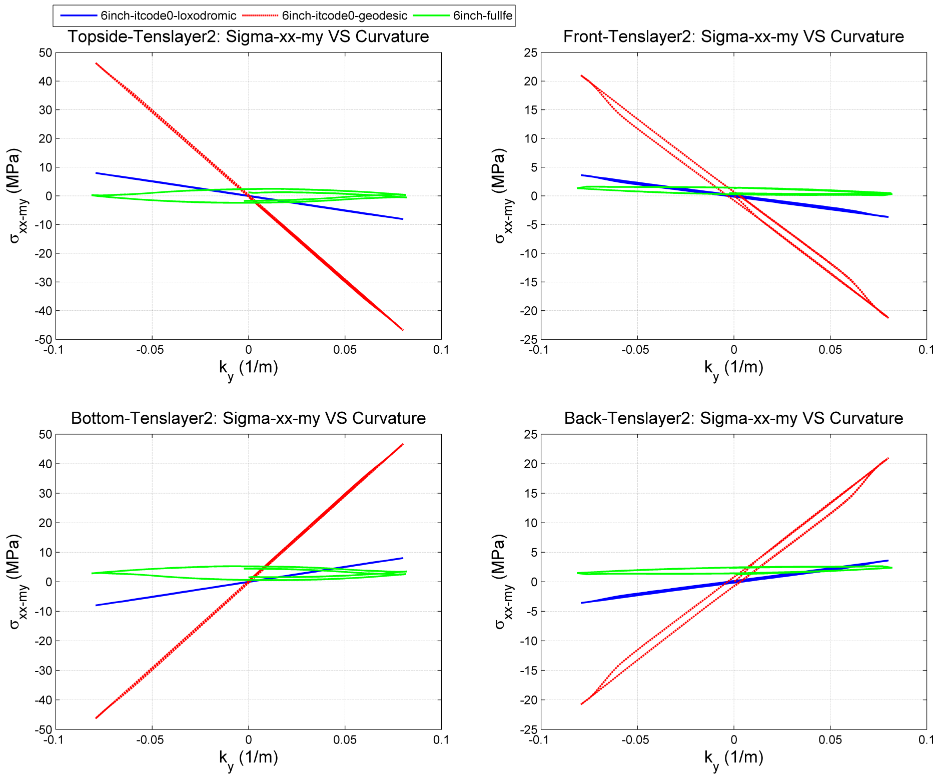

Figure C.6: The 6 inch tenslayer2 σ_{xx-my} lox-geo for itcode0 and fullfe.

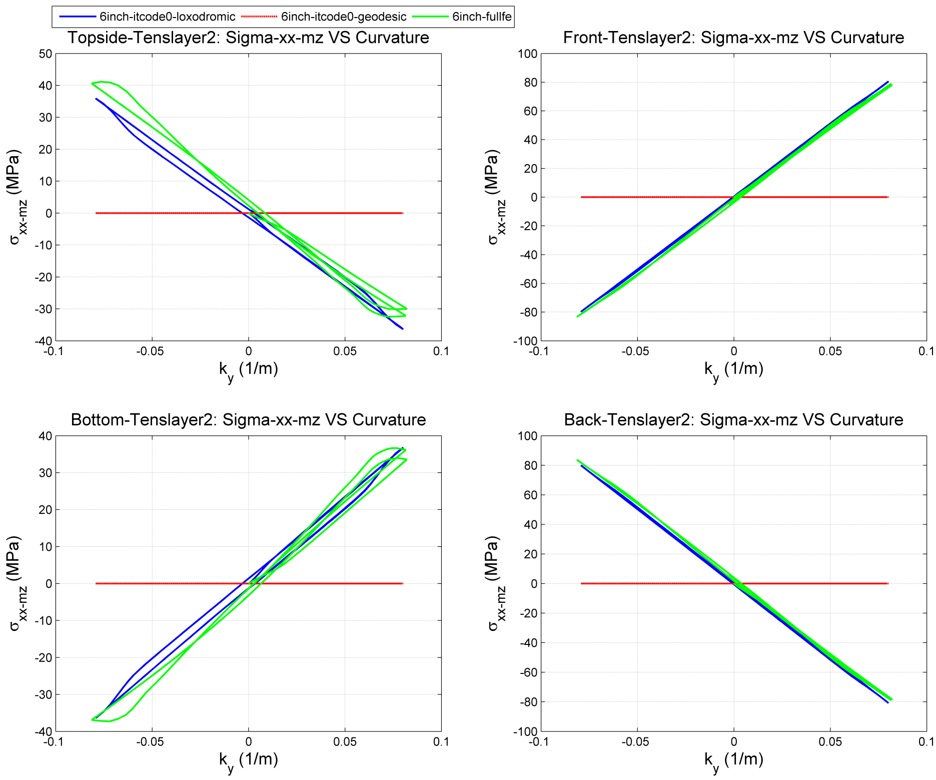

Figure C.7: The 6 inch tenslayer2 σ_{xx-mz} lox-geo for itcode0 and fullfe.

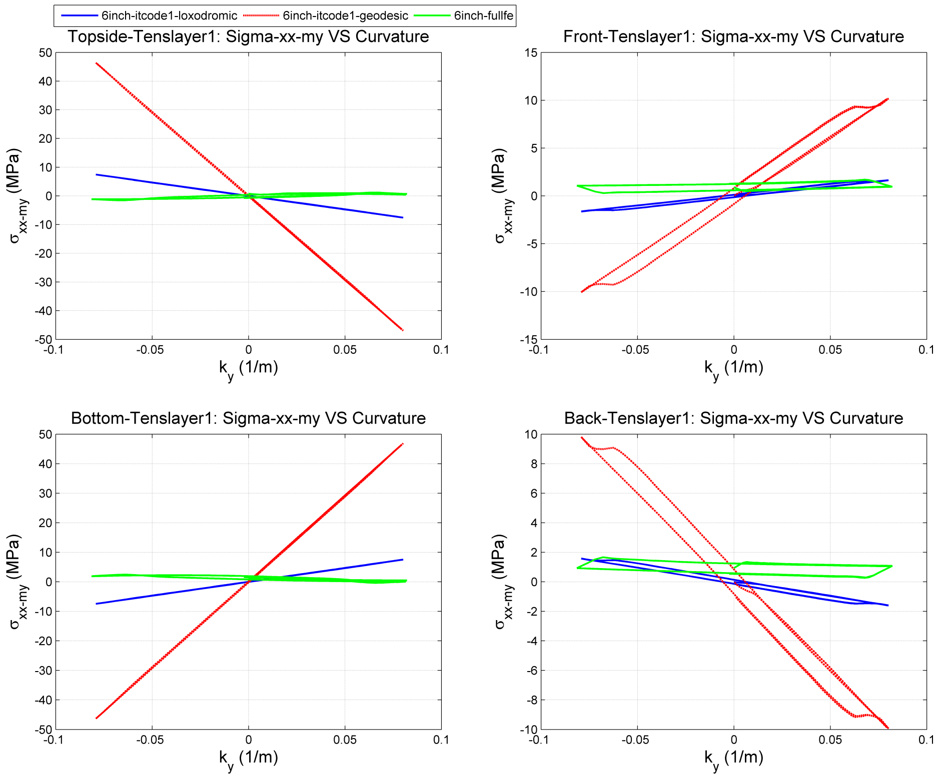

Figure C.8: The 6 inch tenslayer1 σ_{xx-my} lox-geo for itcode1 and fullfe.

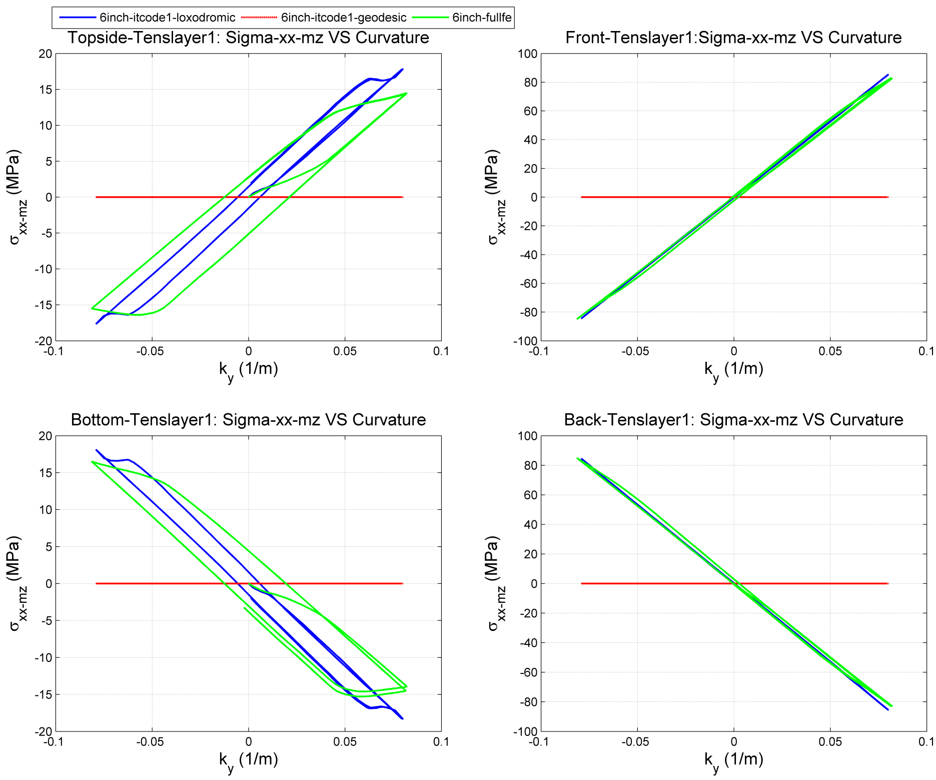

Figure C.9: The 6 inch tenslayer1 σ_{xx-mz} lox-geo for itcode1 and fullfe.

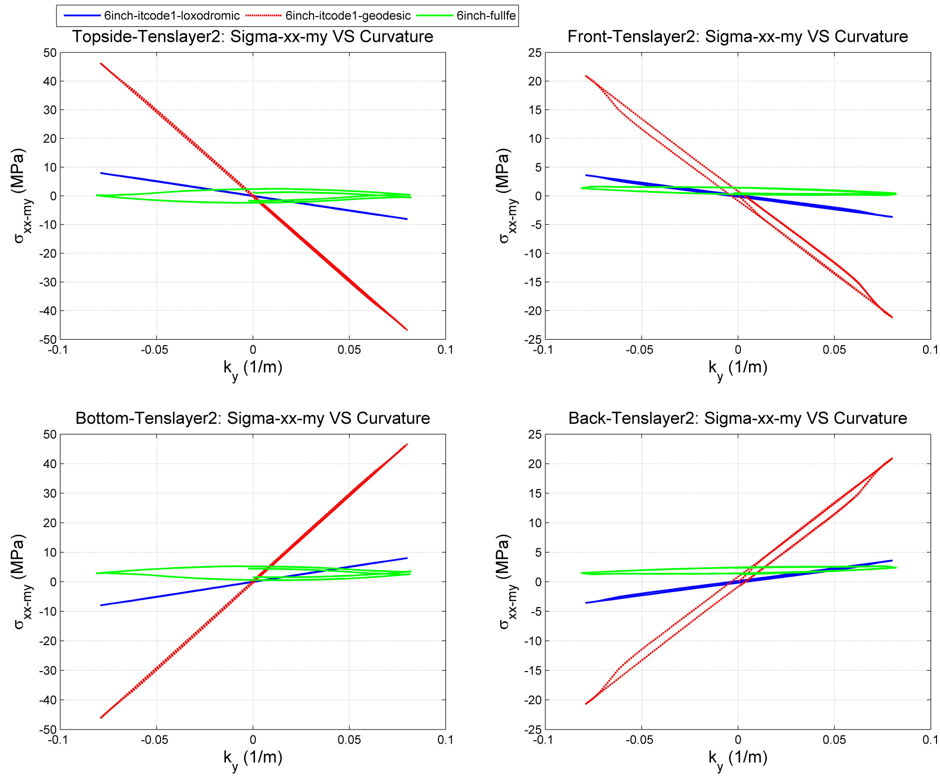

Figure C.10: The 6 inch tenslayer2 σ_{xx-my} lox-geo for itcode1 and fullfe.

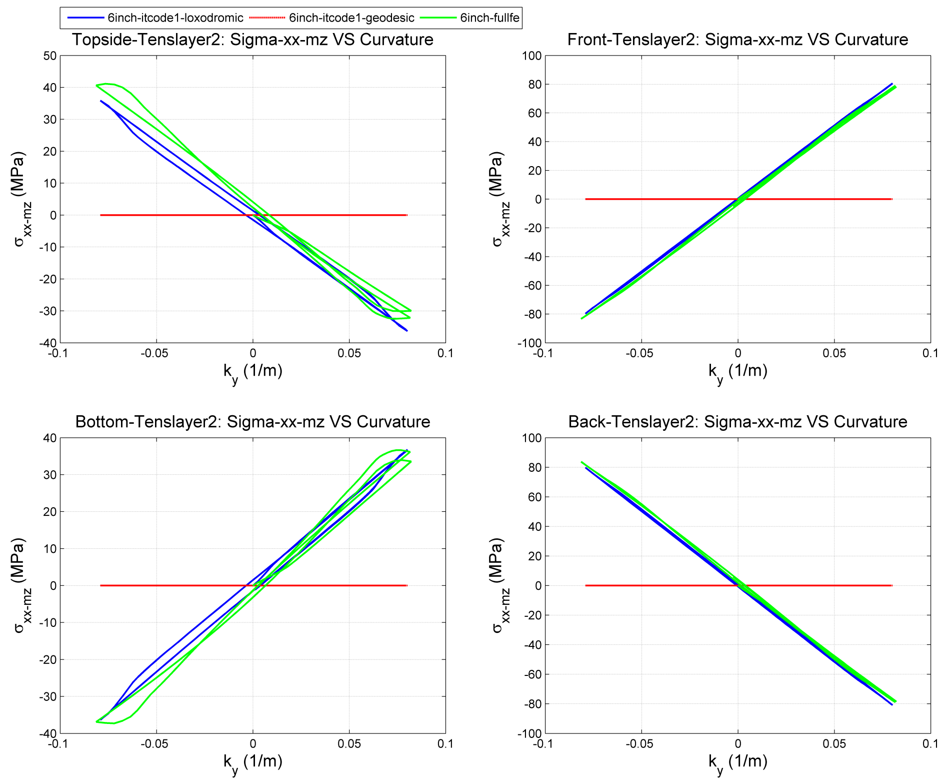

Figure C.11: The 6 inch tenslayer2 σ_{xx-mz} lox-geo for itcode1 and fullfe.

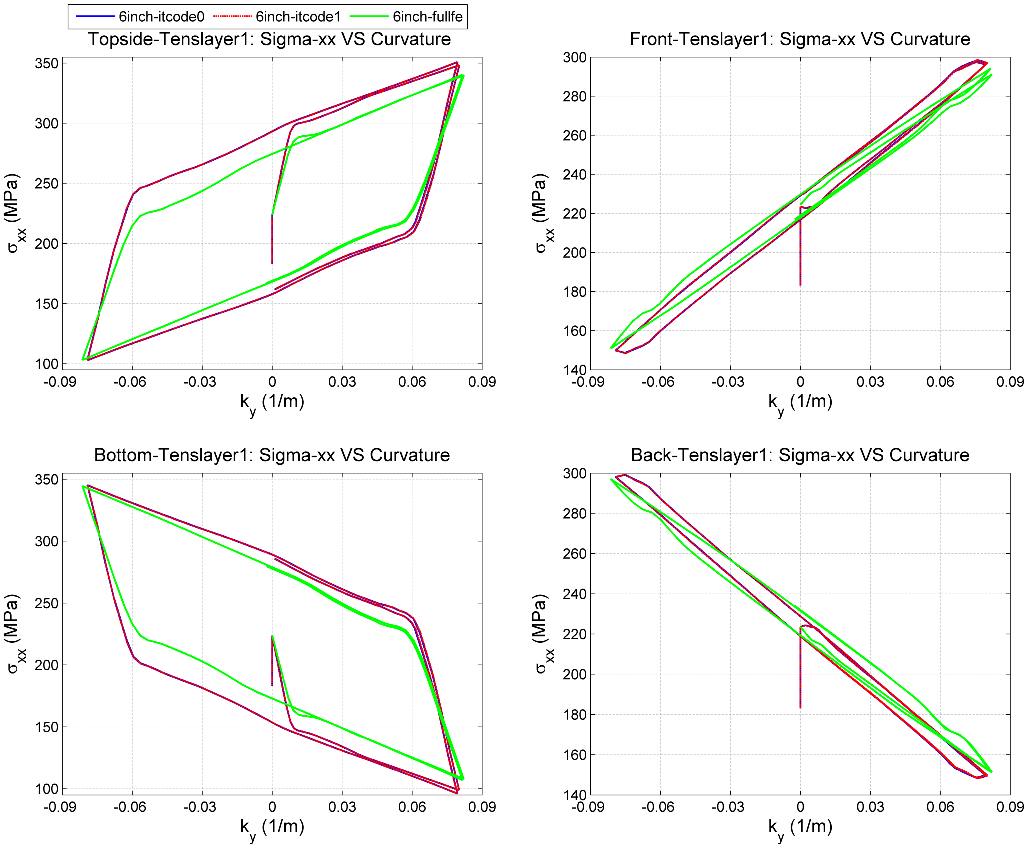

Figure C.12: The 6 inch tenslayer1 σ_{xx} for three models.

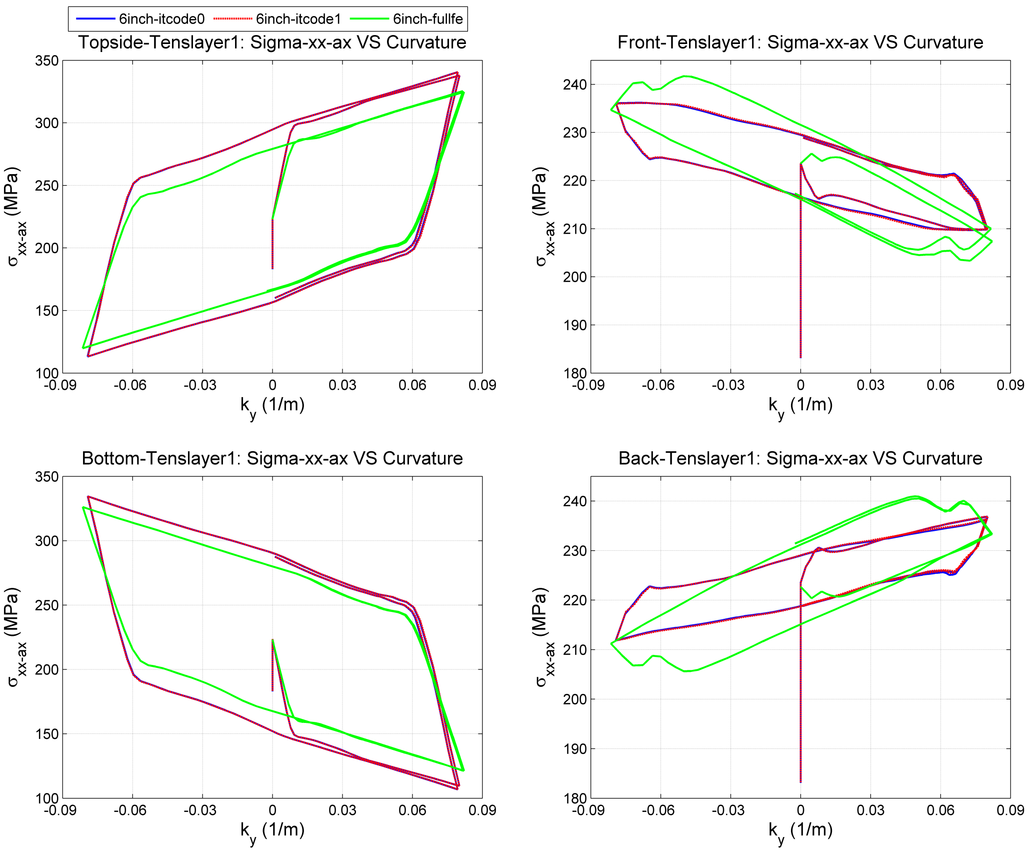

Figure C.13: The 6 inch tenslayer1 σ_{xx-ax} for three models.

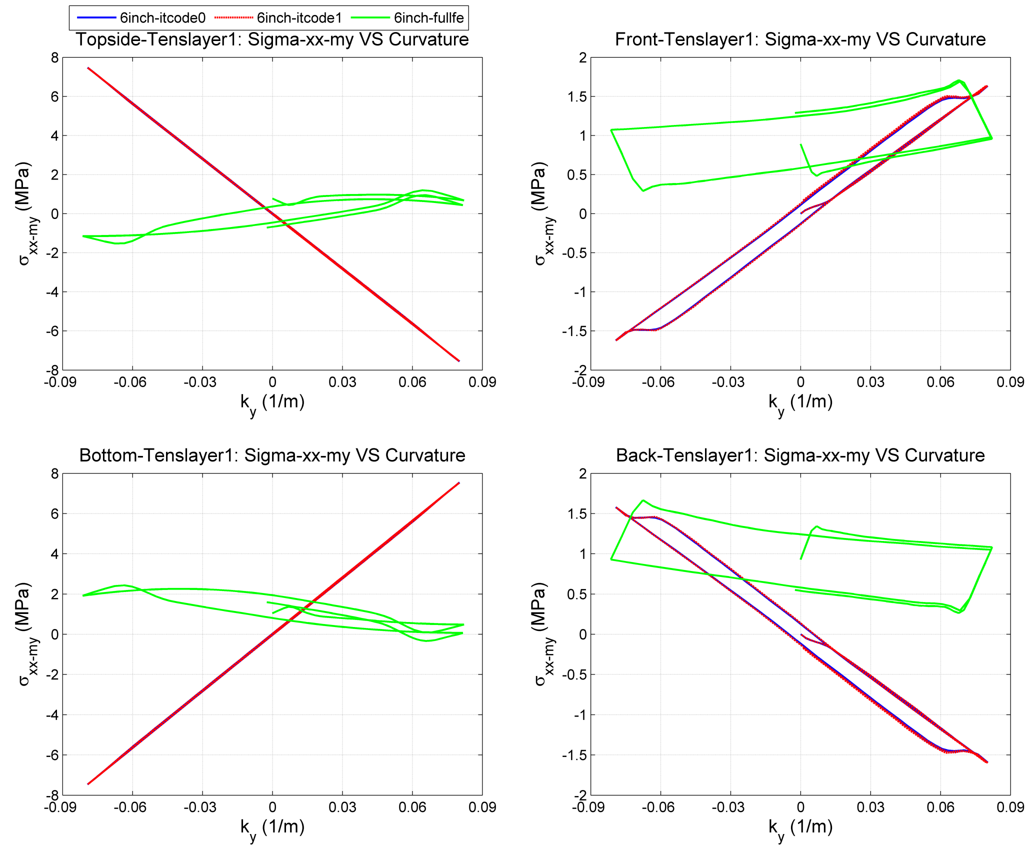

Figure C.14: The 6 inch tenslayer1 σ_{xx-my} for three models.

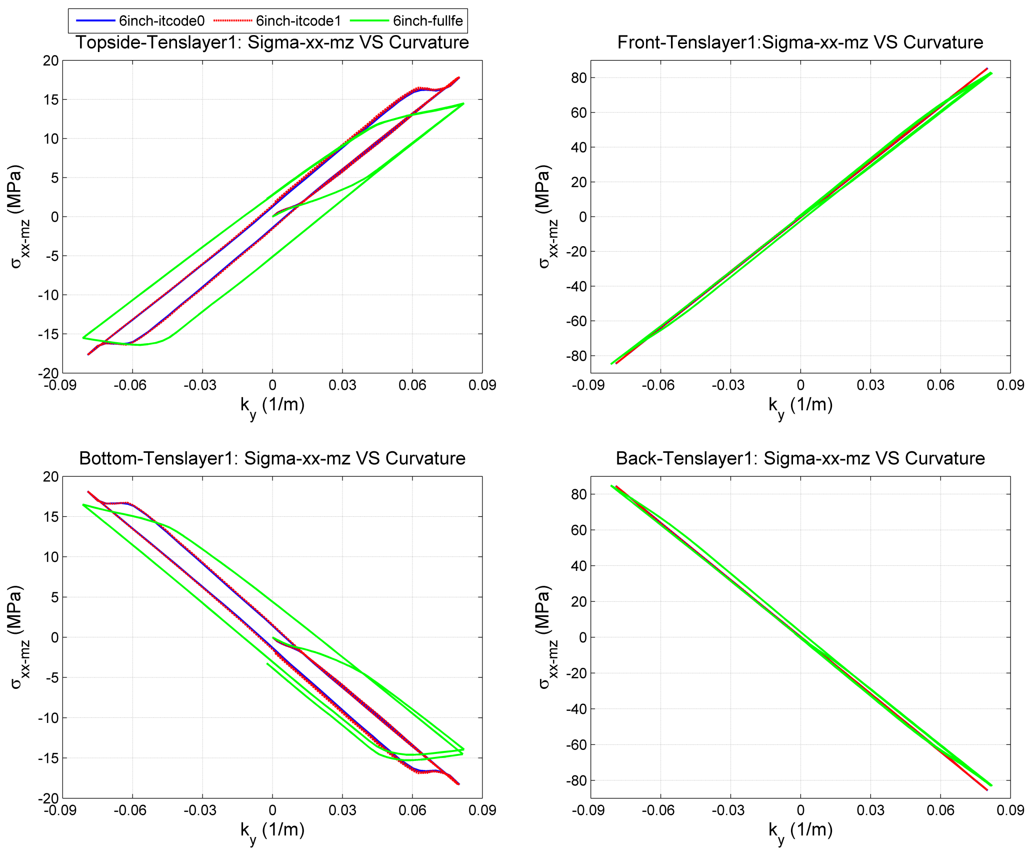

Figure C.15: The 6 inch tenslayer1 σ_{xx-mz} for three models.

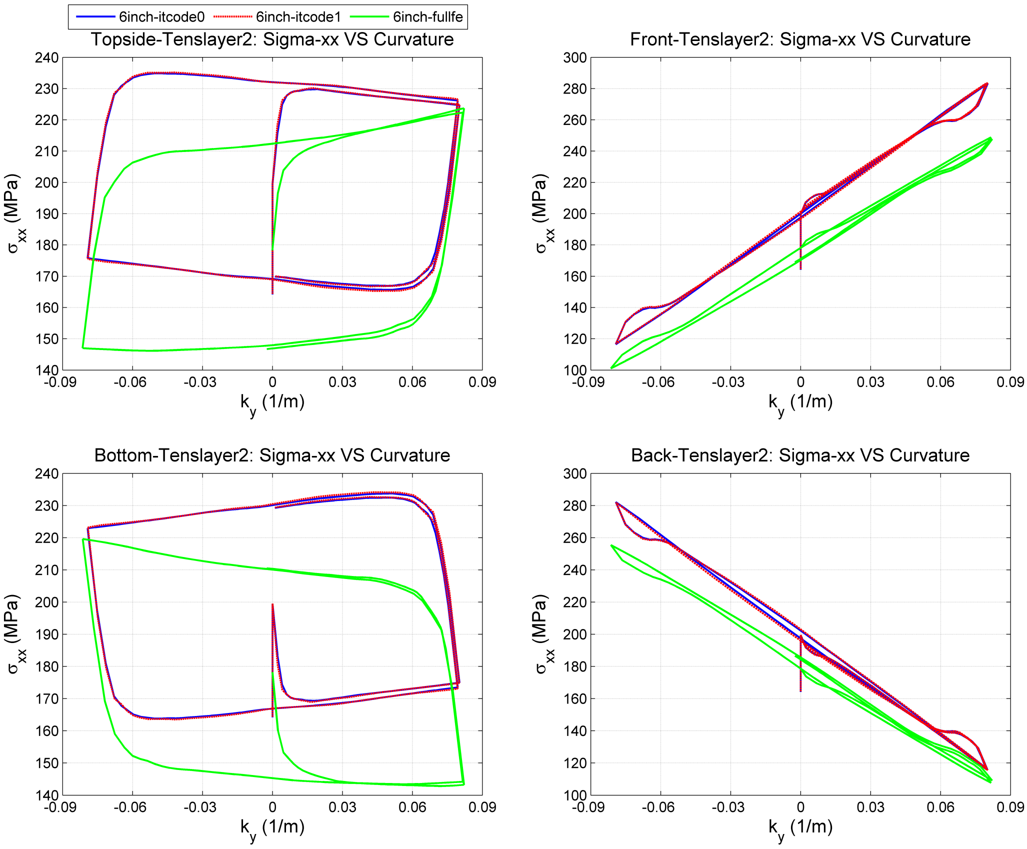

Figure C.16: The 6 inch tenslayer2 σ_{xx} for three models.

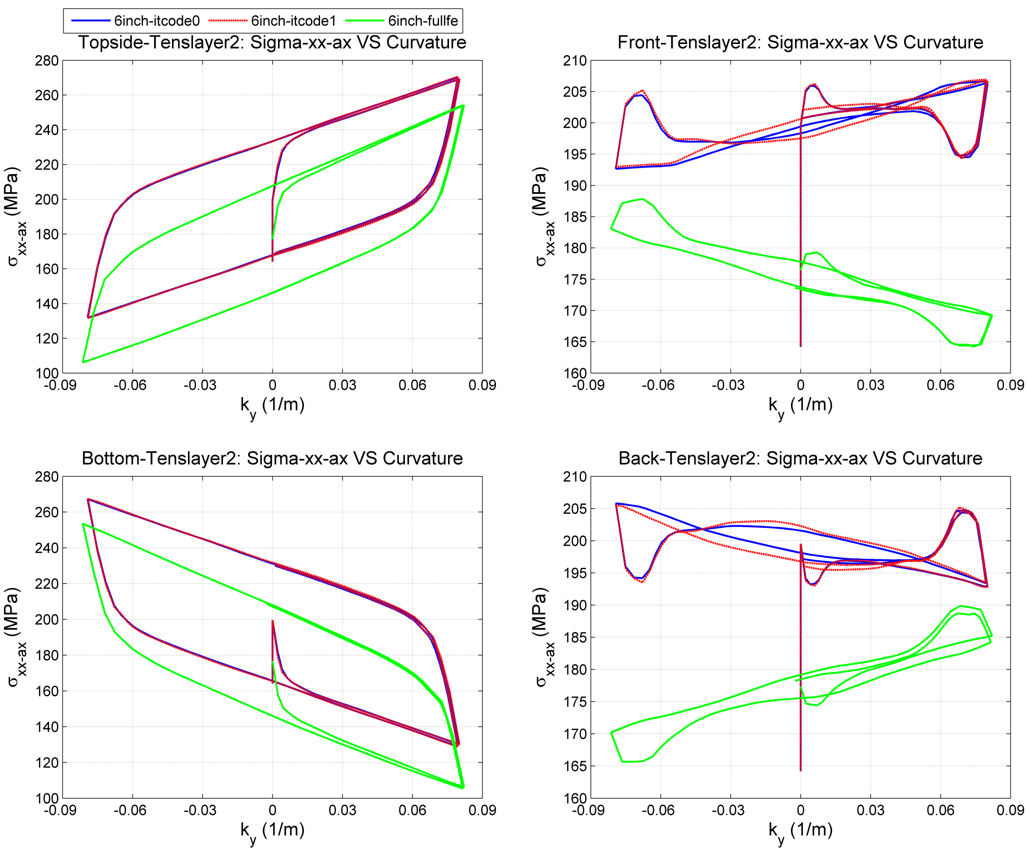

Figure C.17: The 6 inch tenslayer2 σ_{xx-ax} for three models.

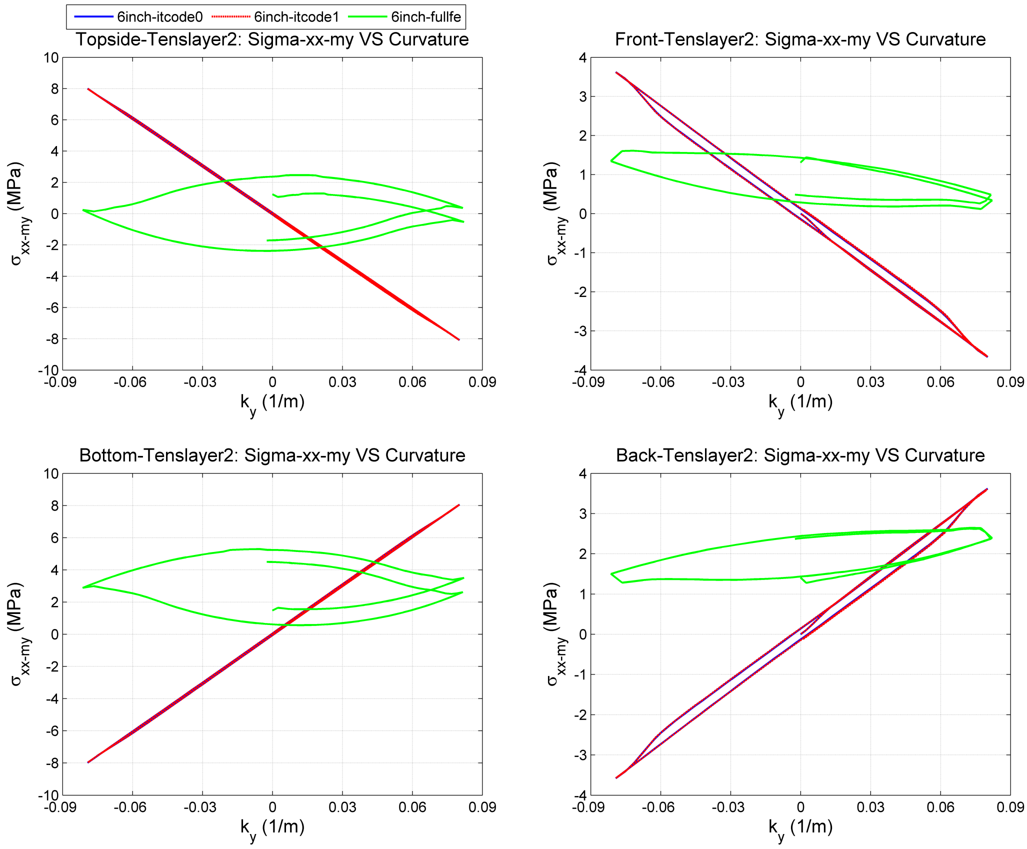

Figure C.18: The 6 inch tenslayer2 σ_{xx-my} for three models.

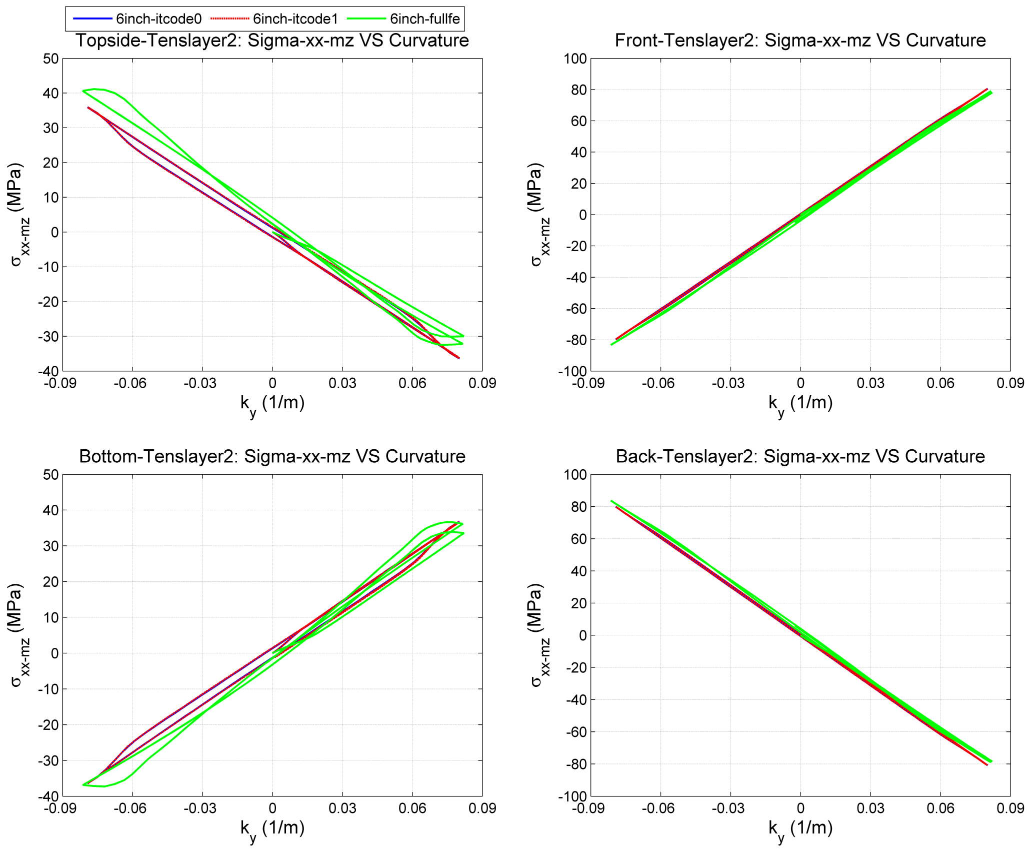

Figure C.19: The 6 inch tenslayer2 σ_{xx-mz} for three models.

C.2 The 8 inch pipe analysis

C.2.1 The 8 inch pipe model friction data and friction plots

8 inch pipe model friction data								
Layer	tensile layer 1				tensile layer 2			
models	Point	Relative Disp (–)	Unit Force (–)	Applied fric-force per-length	Point	Relative Disp (–)	Unit Force (–)	Applied fric-force per-length
itcode0-loxodromic	1	0	0	8.964317	1	0	0	4.207717
	2	0.76331E-02	0.9		2	0.76331E-02	0.9	
	3	0.15266E-01	1		3	0.15266E-01	1	
	4	0.10000E+05	10		4	0.10000E+05	10	
itcode0-geodesic	1	0	0	8.964317	1	0	0	4.207717
	2	0.76331E-02	0.9		2	0.76331E-02	0.9	
	3	0.15266E-01	1		3	0.15266E-01	1	
	4	0.10000E+05	10		4	0.10000E+05	10	
itcode1-loxodromic	1	0	0	8.964317	1	0	0	4.207717
	2	0.76331E-02	0.9		2	0.38645E-02	0.9	
	3	0.15266E-01	1		3	0.77291E-02	1	
	4	0.10000E+05	10		4	0.10000E+05	10	
itcode1-geodesic	1	0	0	8.964317	1	0	0	4.207717
	2	0.76331E-02	0.9		2	0.38645E-02	0.9	
	3	0.15266E-01	1		3	0.77291E-02	1	
	4	0.10000E+05	10		4	0.10000E+05	10	
fullfe	1	0	0	9.034268	1	0	0	4.242097
	2	0.76927E-02	0.9		2	0.38961E-02	0.9	
	3	0.15385E-01	1		3	0.77922E-02	1	
	4	0.14250E+06	10		4	0.14250E+05	10	

Table C.2: The 8 inch pipe model friction data.

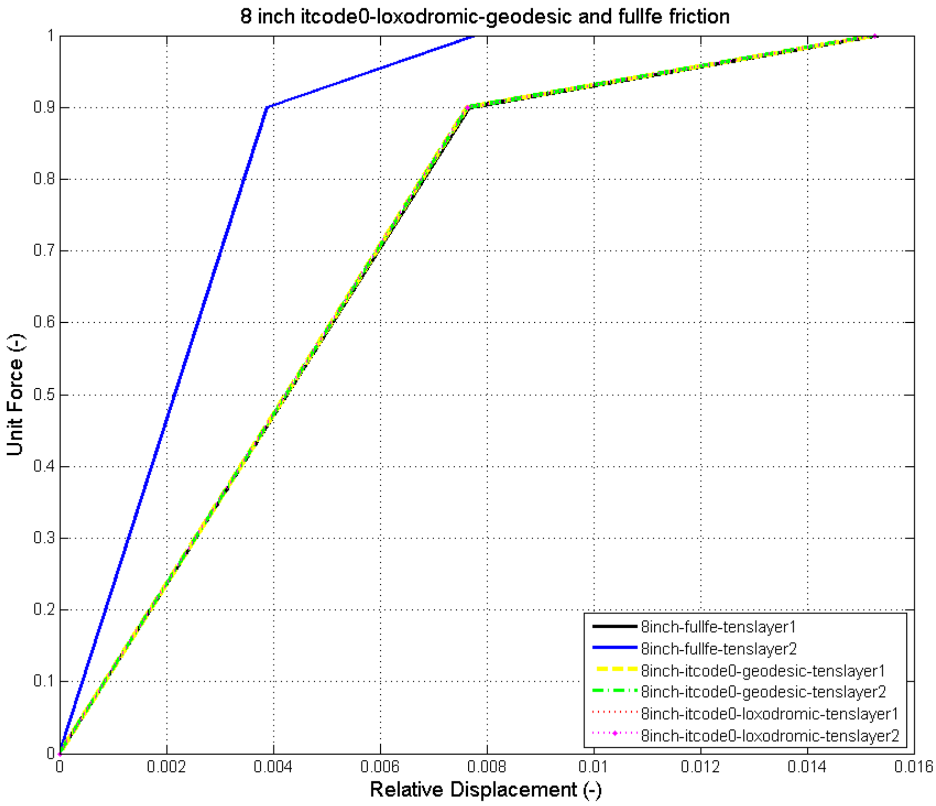

Figure C.20: The 8 inch lox-geo friction for itcode0 and fullfe.

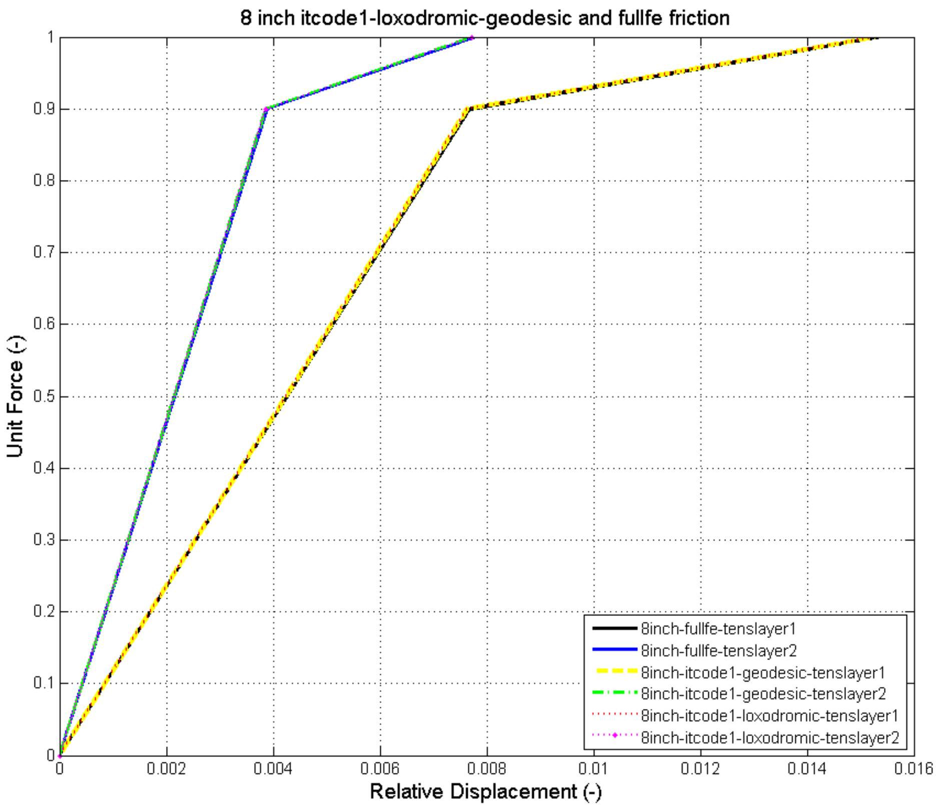

Figure C.21: The 8 inch lox-geo friction for itcode1 and fullfe.

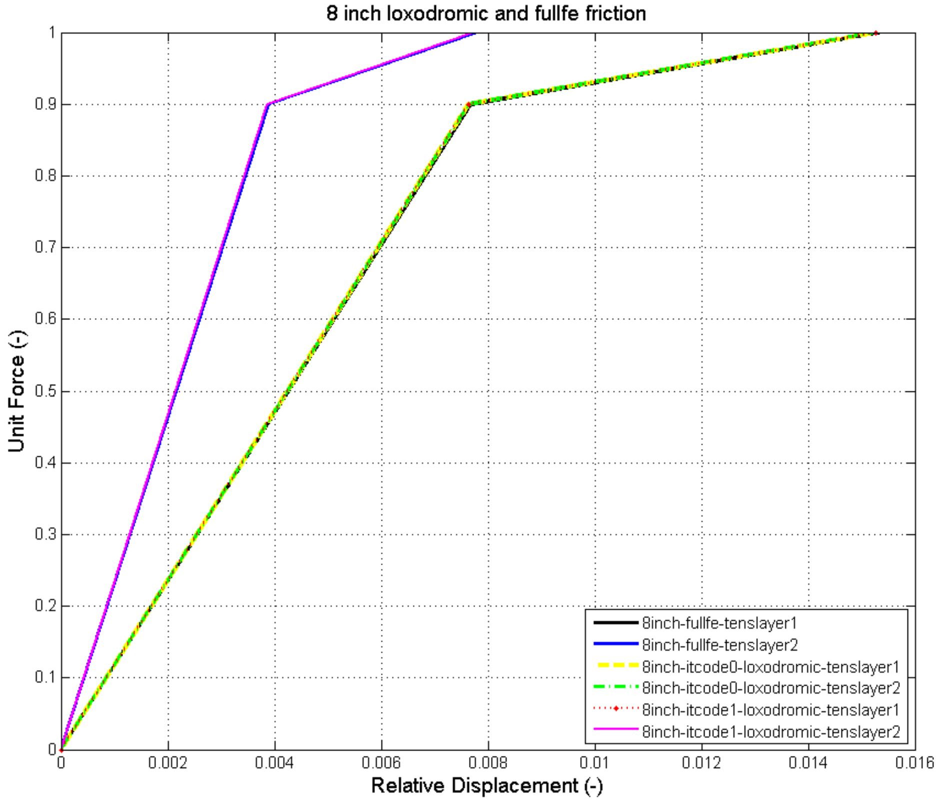

Figure C.22: The 8 inch lox friction for itcode0-itcode1 and fullfe.

C.2.2 Stress components plots

The 8 inch stress components under two assumptions

Figure C.23–Figure C.30 show the stress components comparisons of itcode0 and itcode1 models under both the loxodromic and geodesic assumptions and the fullfe model.

The 8 inch stress study for lox assumption and fullfe model

Figure C.31 – Figure C.38 show the stress components comparisons of itcode0 and itcode1 models under loxodromic assumption and fullfe model.

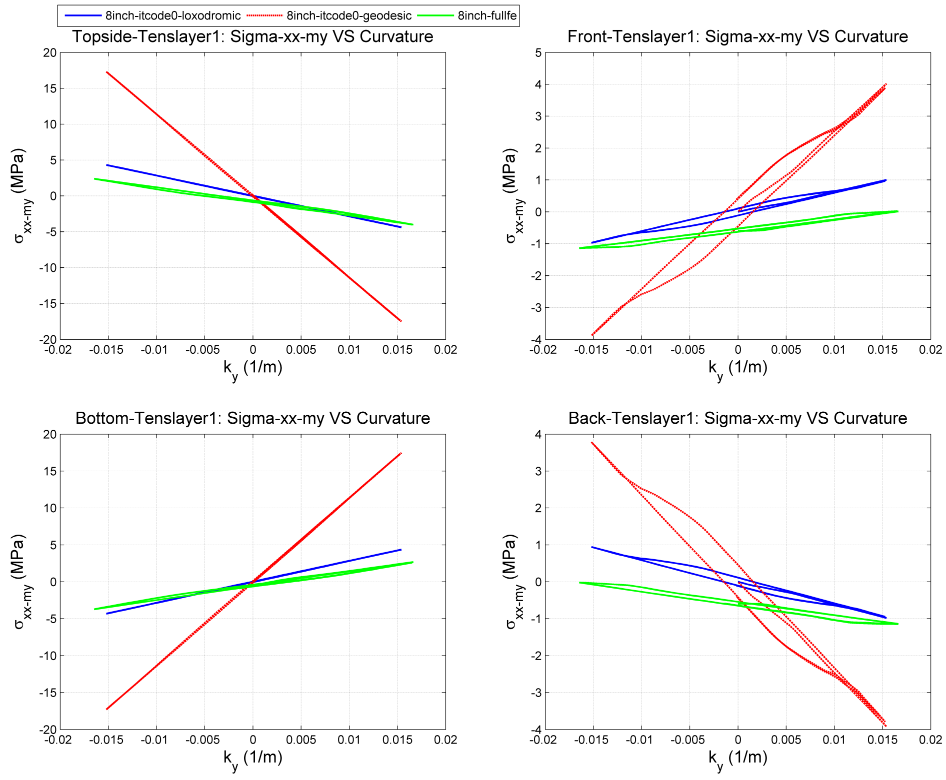

Figure C.23: The 8 inch tenslayer1 σ_{xx-my} lox-geo for itcode0 and fullfe.

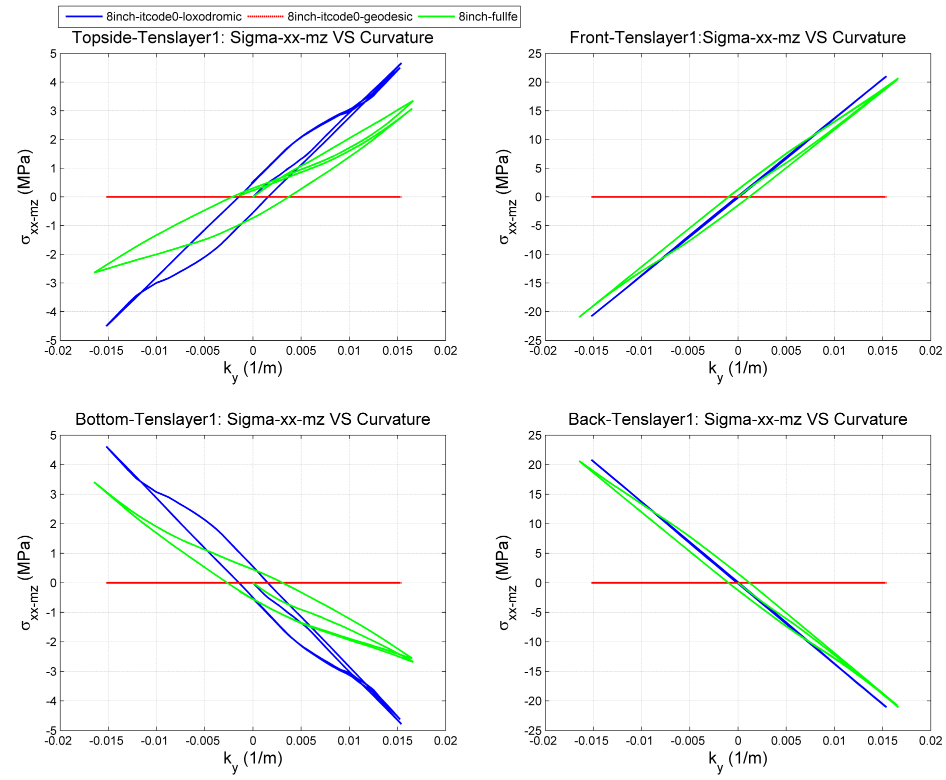

Figure C.24: The 8 inch tenslayer1 σ_{xx-mz} lox-geo for itcode0 and fullfe.

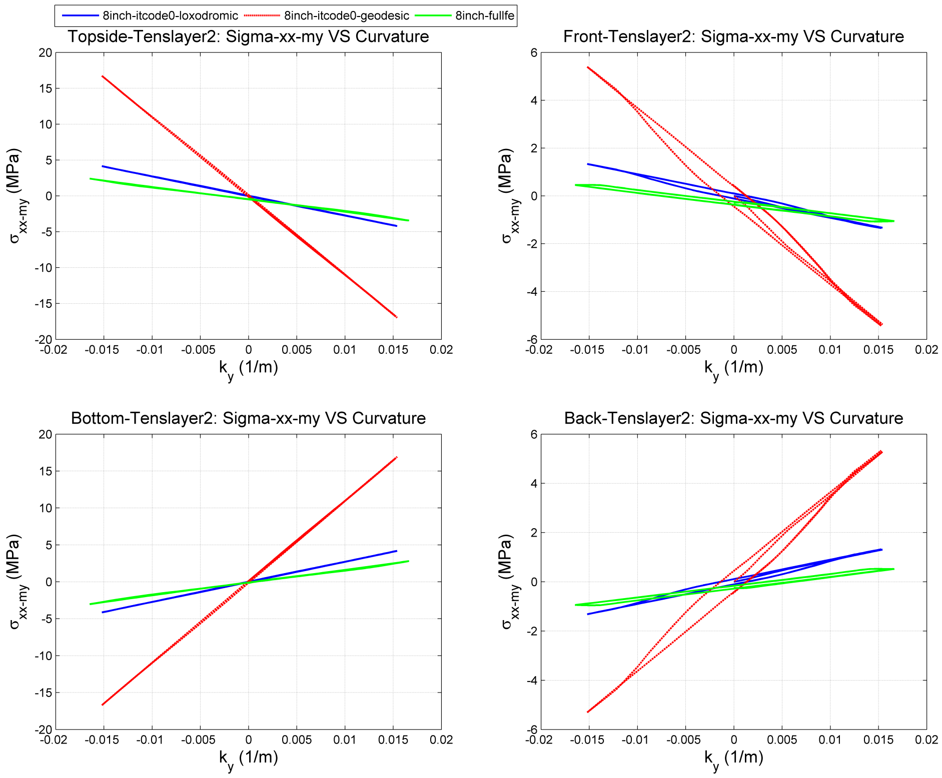

Figure C.25: The 8 inch tenslayer2 σ_{xx-my} lox-geo for itcode0 and fullfe.

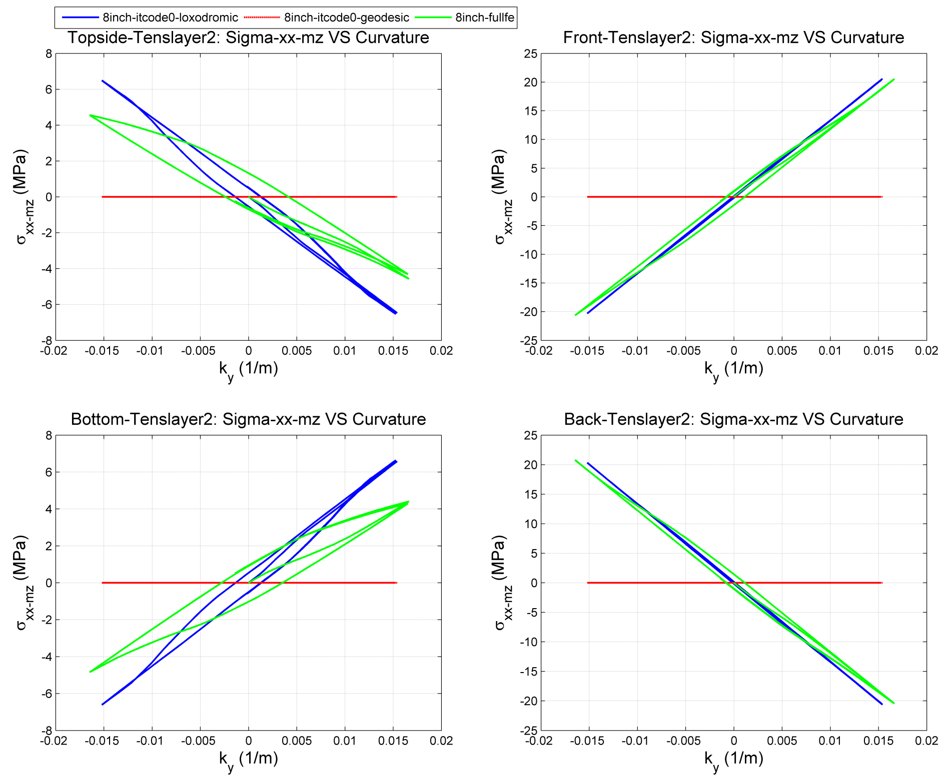

Figure C.26: The 8 inch tenslayer2 σ_{xx-mz} lox-geo for itcode0 and fullfe.

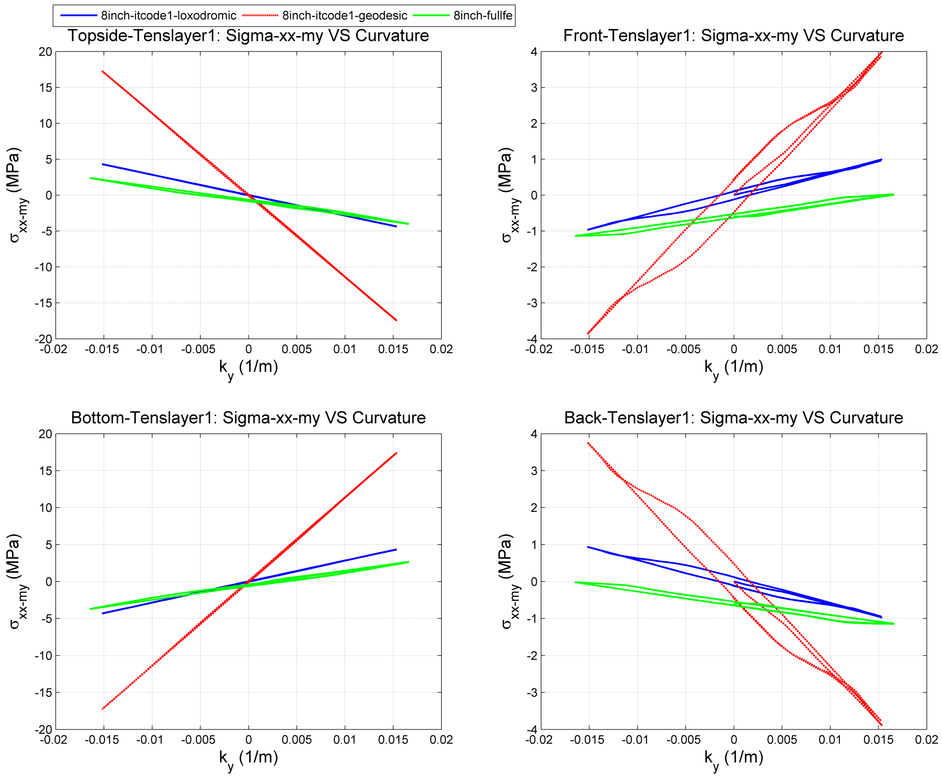

Figure C.27: The 8 inch tenslayer1 σ_{xx-my} lox-geo for itcode1 and fullfe.

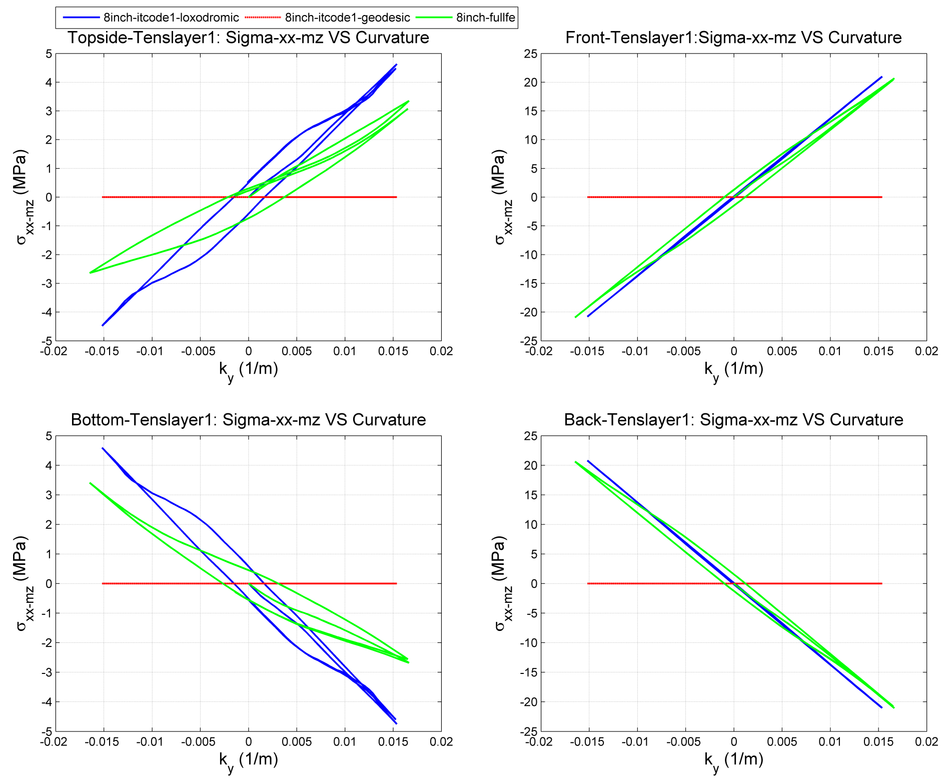

Figure C.28: The 8 inch tenslayer1 σ_{xx-mz} lox-geo for itcode1 and fullfe.

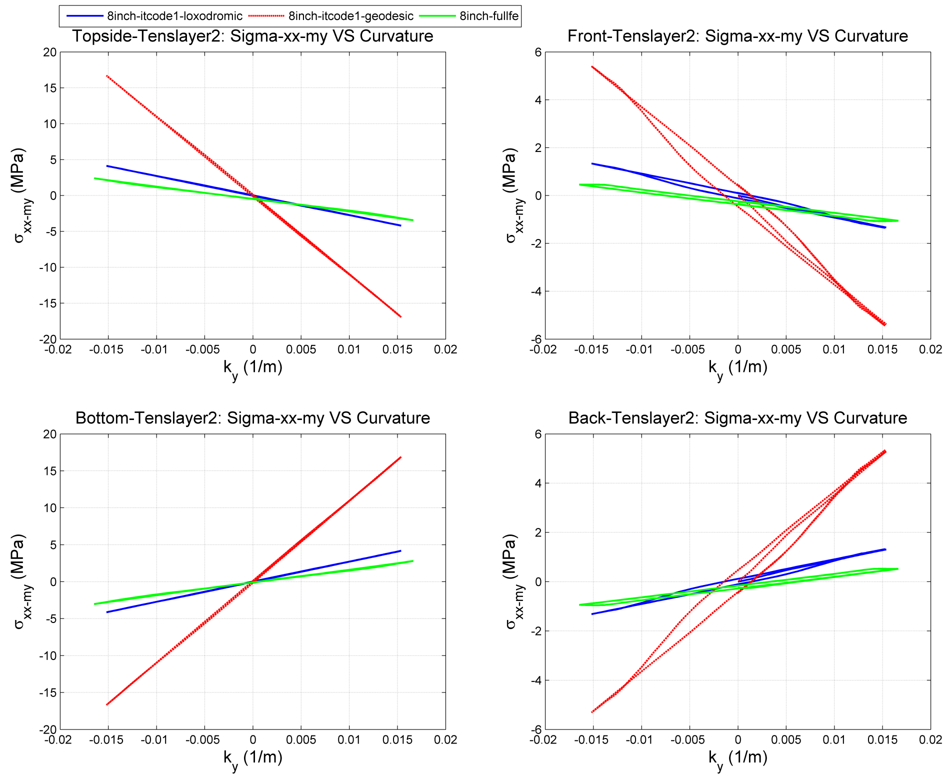

Figure C.29: The 8 inch tenslayer2 σ_{xx-my} lox-geo for itcode1 and fullfe.

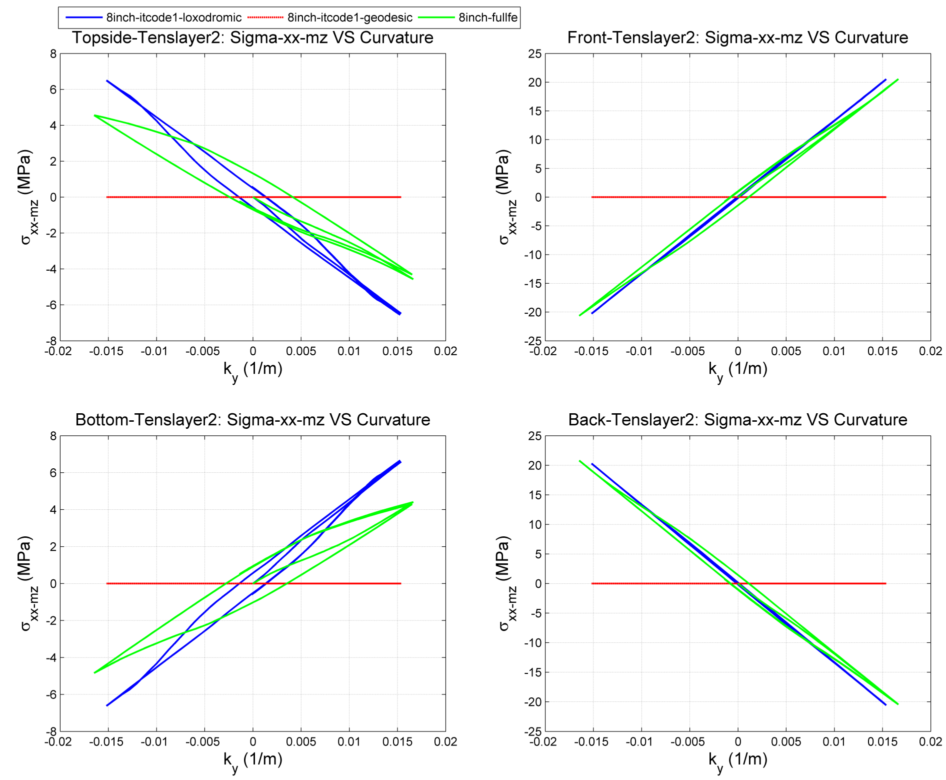

Figure C.30: The 8 inch tenslayer2 σ_{xx-mz} lox-geo for itcode1 and fullfe.

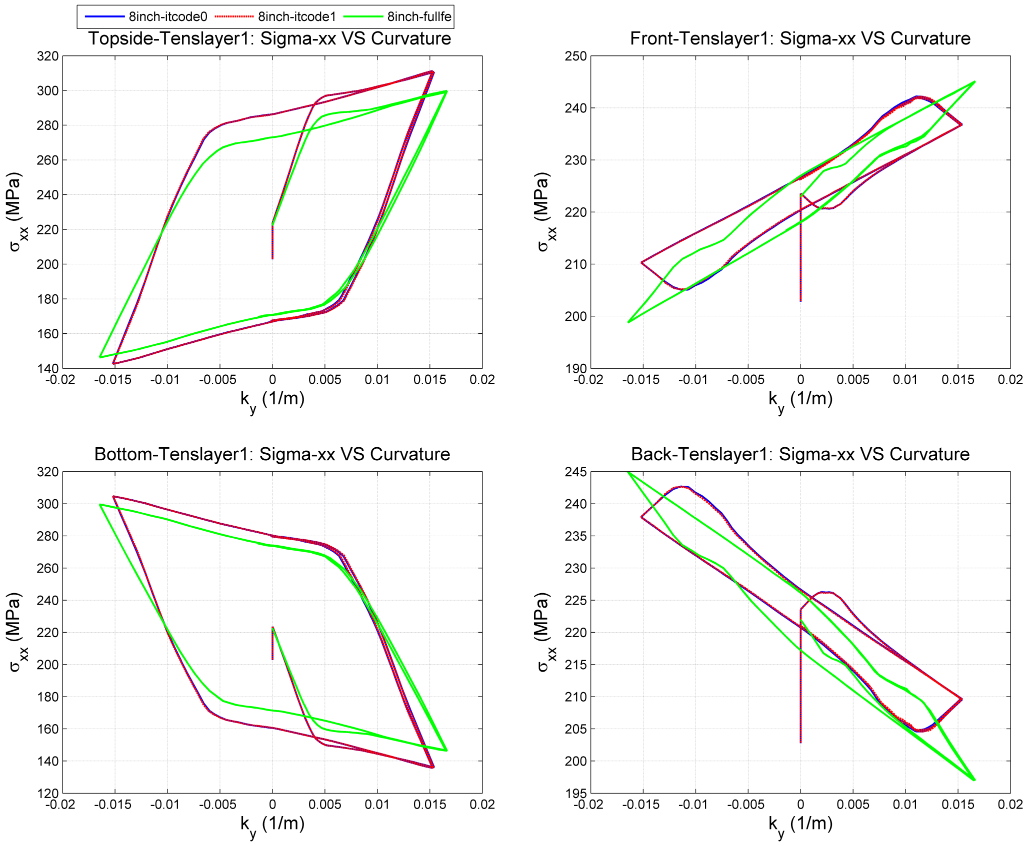

Figure C.31: The 8 inch tenslayer1 σ_{xx} for three models.

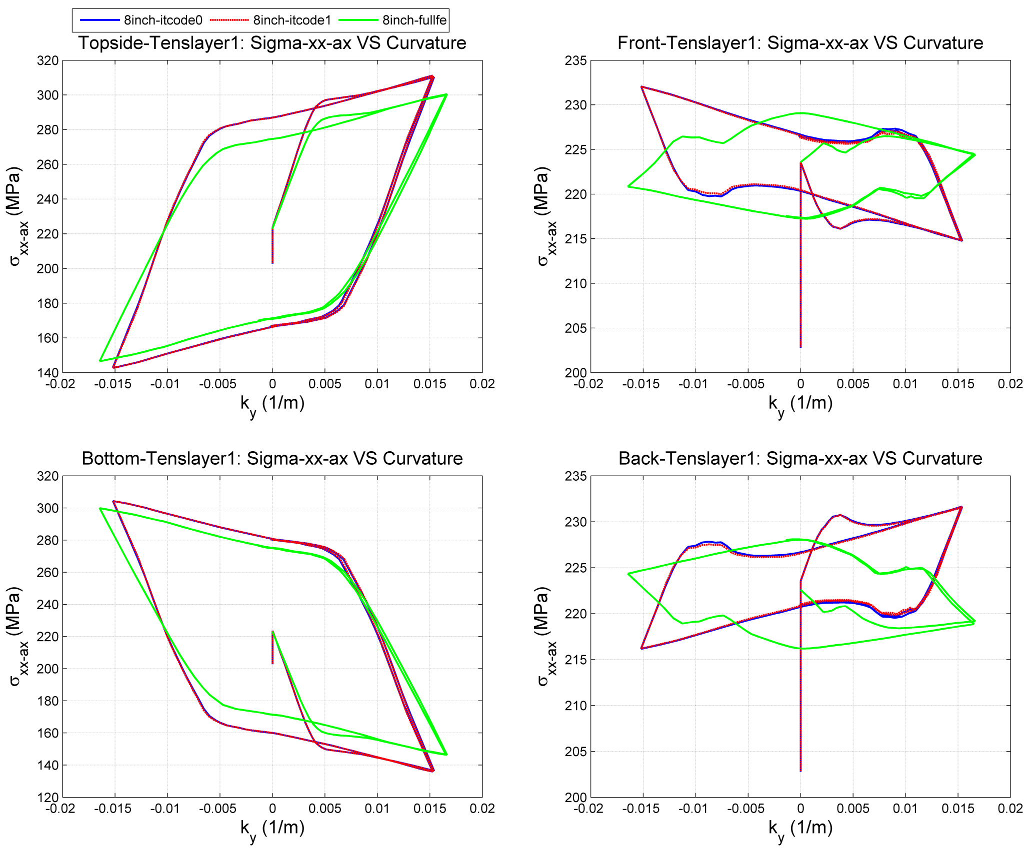

Figure C.32: The 8 inch tenslayer1 σ_{xx-ax} for three models.

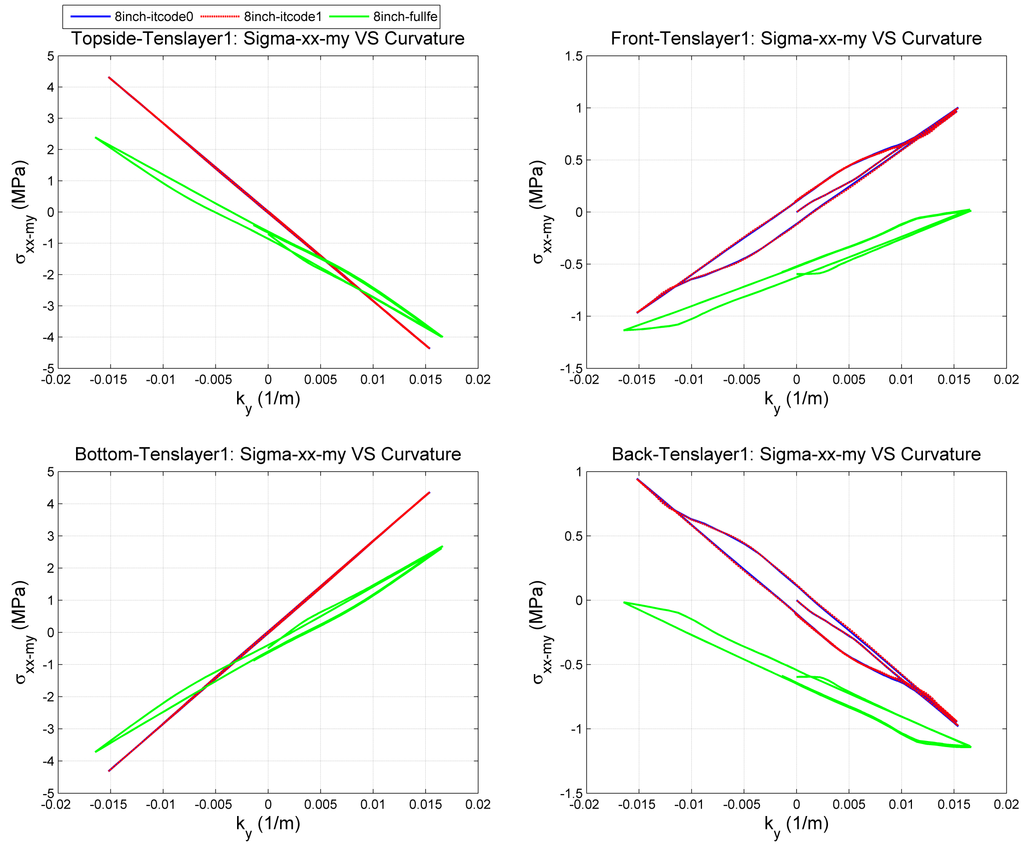

Figure C.33: The 8 inch tenslayer1 σ_{xx-my} for three models.

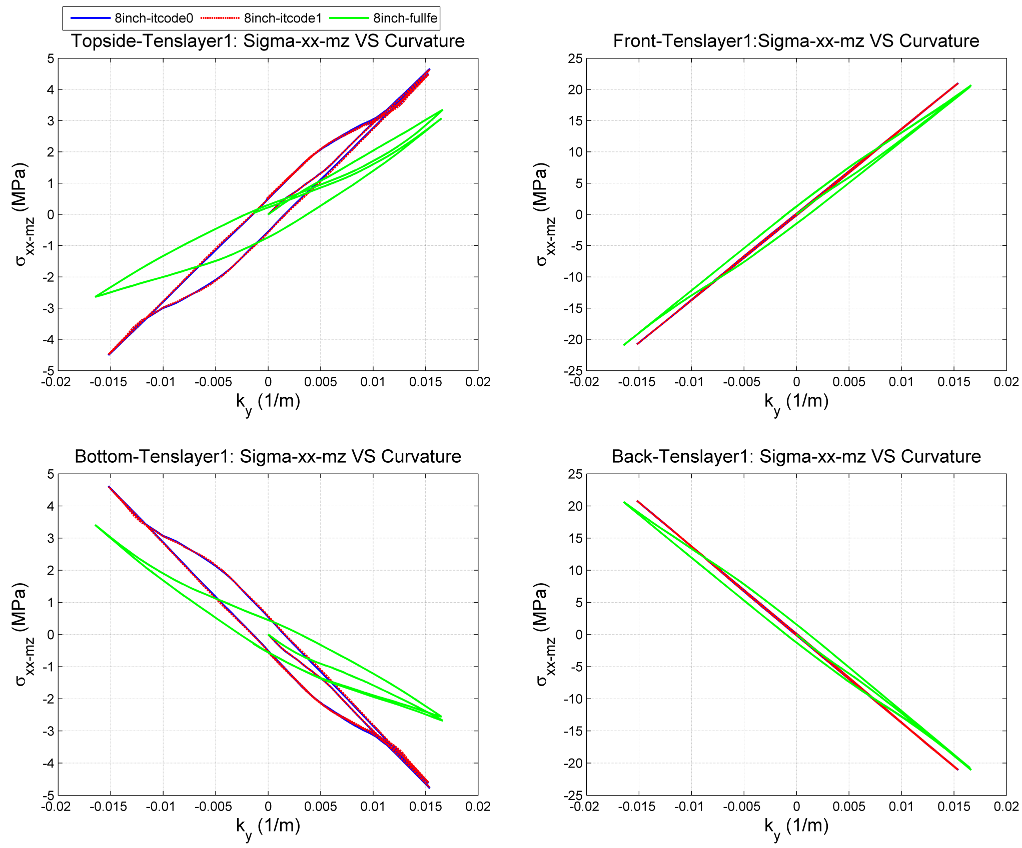

Figure C.34: The 8 inch tenslayer1 σ_{xx-mz} for three models.

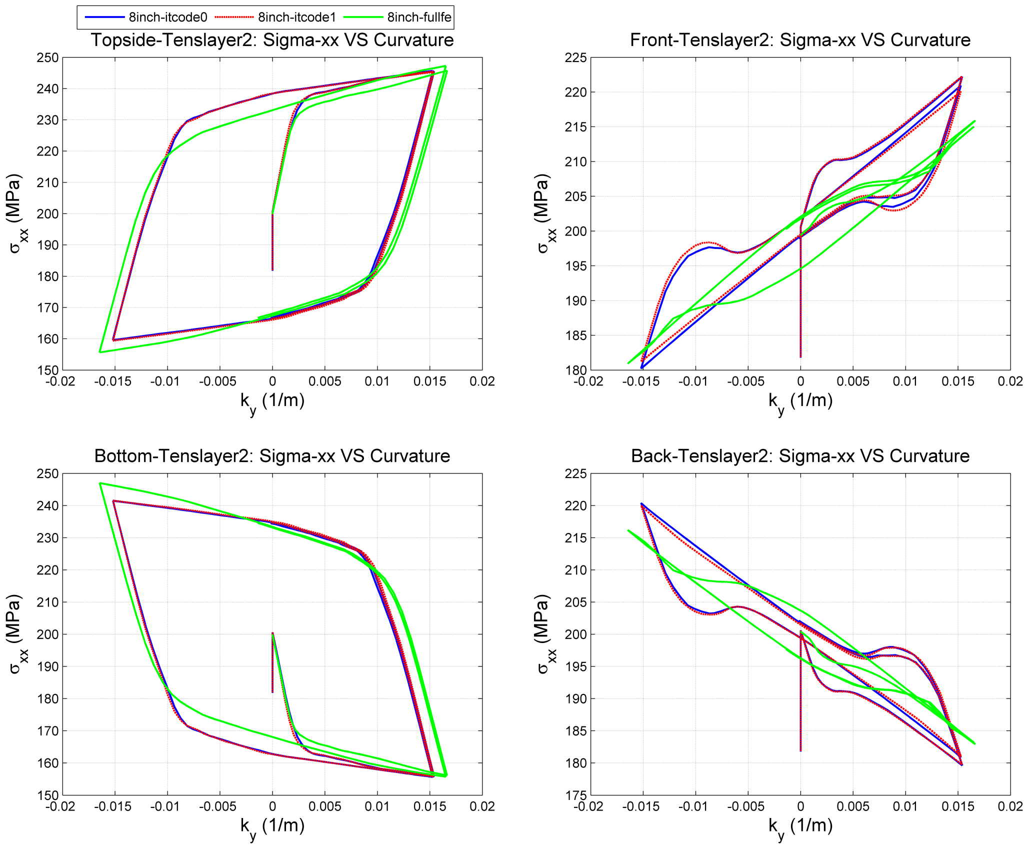

Figure C.35: The 8 inch tenslayer2 σ_{xx} for three models.

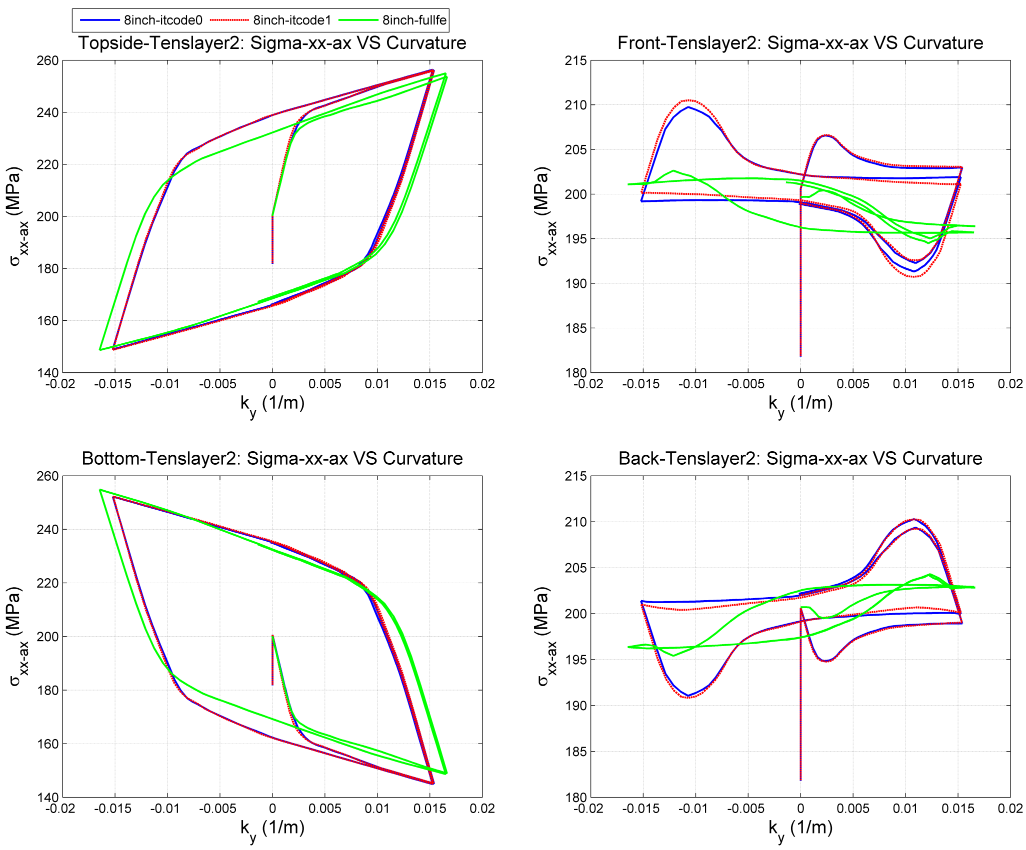

Figure C.36: The 8 inch tenslayer2 σ_{xx-ax} for three models.

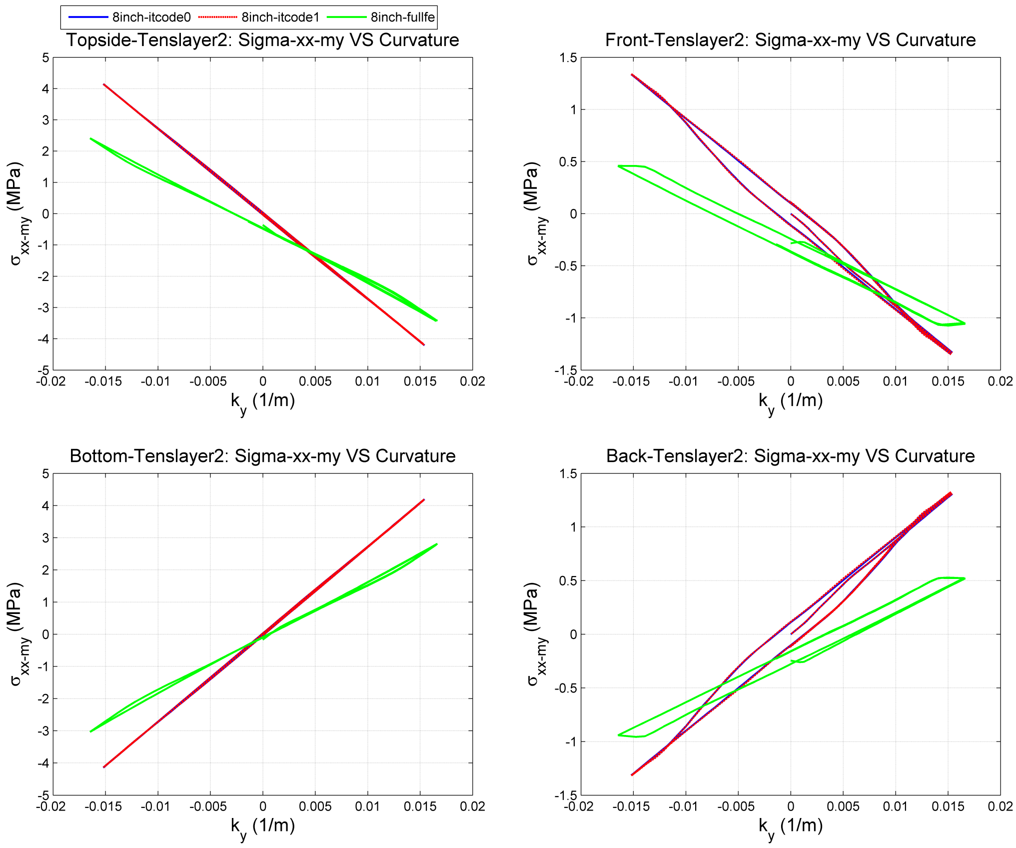

Figure C.37: The 8 inch tenslayer2 σ_{xx-my} for three models.

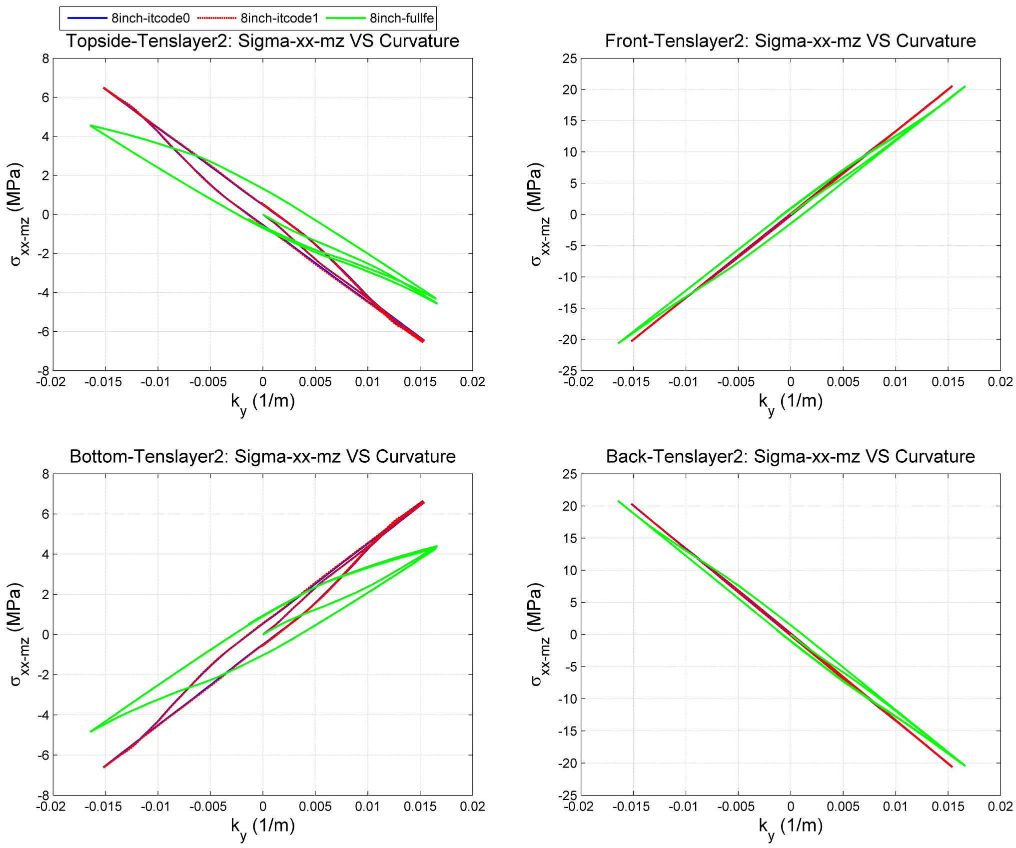

Figure C.38: The 8 inch tenslayer2 σ_{xx-mz} for three models.

C.3 The 16 inch pipe analysis

C.3.1 The 16 inch pipe model friction data and friction plots

16 inch pipe model friction data								
Layer	tensile layer 1				tensile layer 2			
models	Point	Relative Disp (–)	Unit Force (–)	Applied fric-force per-length	Point	Relative Disp (–)	Unit Force (–)	Applied fric-force per-length
itcode0-loxodromic	1	0	0	4.969271	1	0	0	1.746385
	2	0.10815E-01	0.9		2	0.10815E-01	0.9	
	3	0.21629E-01	1		3	0.21629E-01	1	
	4	0.10000E+05	10		4	0.10000E+05	10	
itcode0-geodesic	1	0	0	4.969271	1	0	0	1.746385
	2	0.10815E-01	0.9		2	0.10815E-01	0.9	
	3	0.21629E-01	1		3	0.21629E-01	1	
	4	0.10000E+05	10		4	0.10000E+05	10	
itcode1-loxodromic	1	0	0	4.969271	1	0	0	1.746385
	2	0.10815E-01	0.9		2	0.43321E-02	0.9	
	3	0.21629E-01	1		3	0.86642E-02	1	
	4	0.10000E+05	10		4	0.10000E+05	10	
itcode1-geodesic	1	0	0	4.969271	1	0	0	1.746385
	2	0.10815E-01	0.9		2	0.43321E-02	0.9	
	3	0.21629E-01	1		3	0.86642E-02	1	
	4	0.10000E+05	10		4	0.10000E+05	10	
fullfe	1	0	0	5.114196	1	0	0	1.879417
	2	0.11130E-01	0.9		2	0.46621E-02	0.9	
	3	0.22260E-01	1		3	0.93242E-02	1	
	4	0.24957E+06	10		4	0.24957E+06	10	

Table C.3: The 16 inch pipe model friction data.

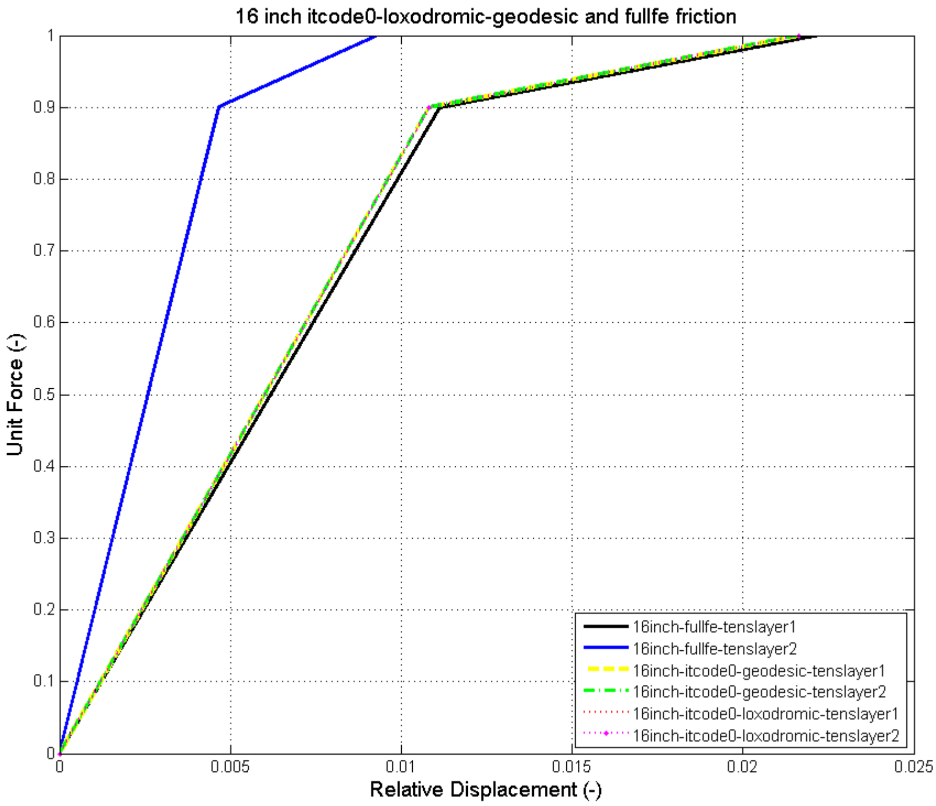

Figure C.39: The 16 inch lox-geo friction for itcode0 and fullfe.

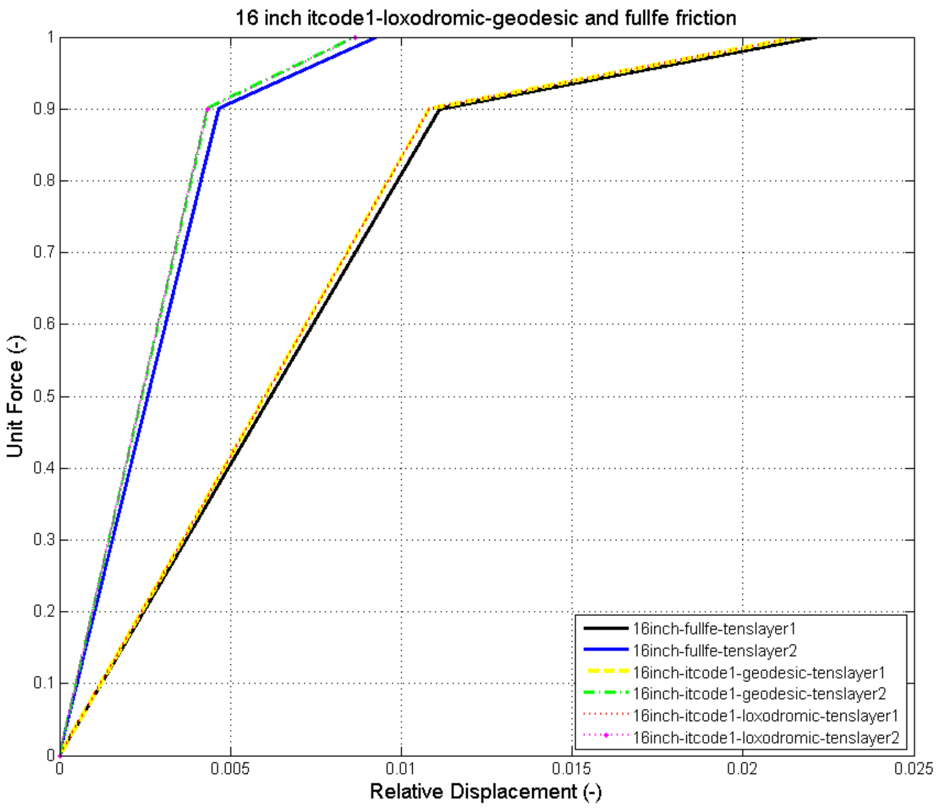

Figure C.40: The 16 inch lox-geo friction for itcode1 and fullfe.

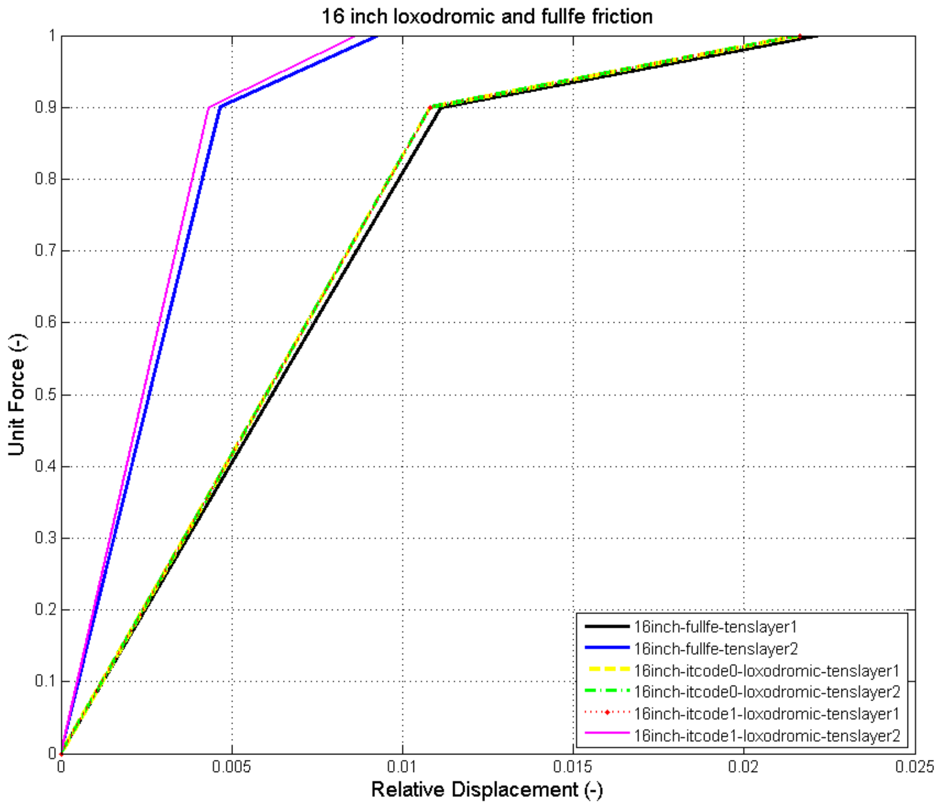

Figure C.41: The 16 inch lox friction for itcode0-itcode1 and fullfe.

C.3.2 Stress components plots

The 16 inch stress components under two assumptions

Figure C.42–Figure C.49 show the stress components comparisons of itcode0 and itcode1 models under both the loxodromic and geodesic assumptions and the fullfe model.

The 16 inch stress study for lox assumption and fullfe model

Figure C.50 – Figure C.57 show the stress components comparisons of itcode0 and itcode1 models under loxodromic assumption and fullfe model.

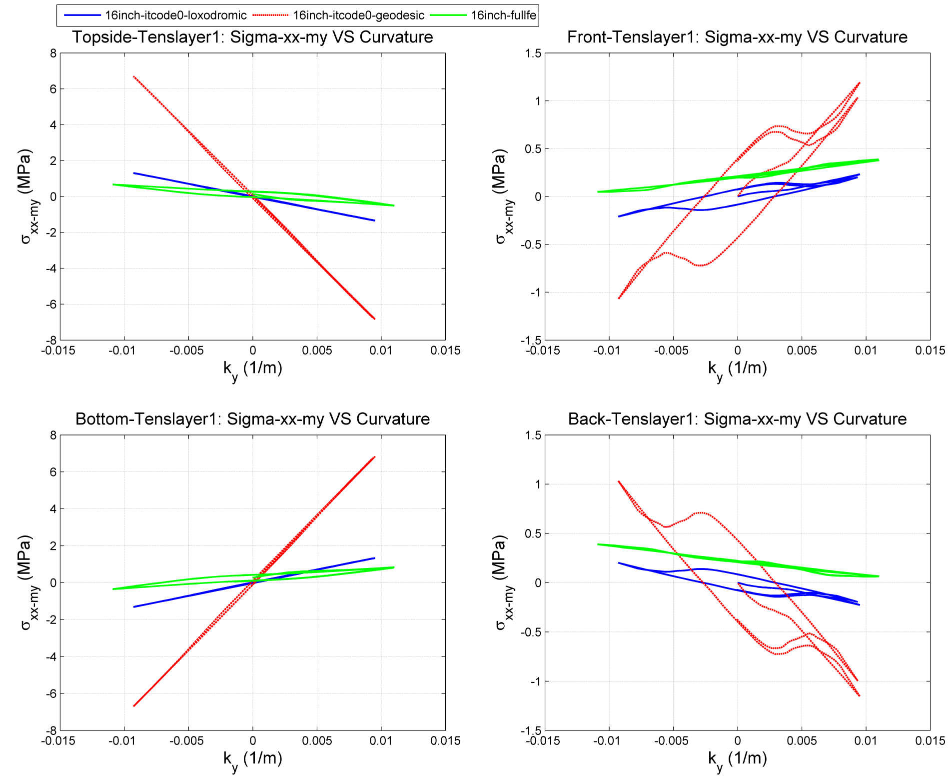

Figure C.42: The 16 inch tenslayer1 σ_{xx-my} lox-geo for itcode0 and fullfe.

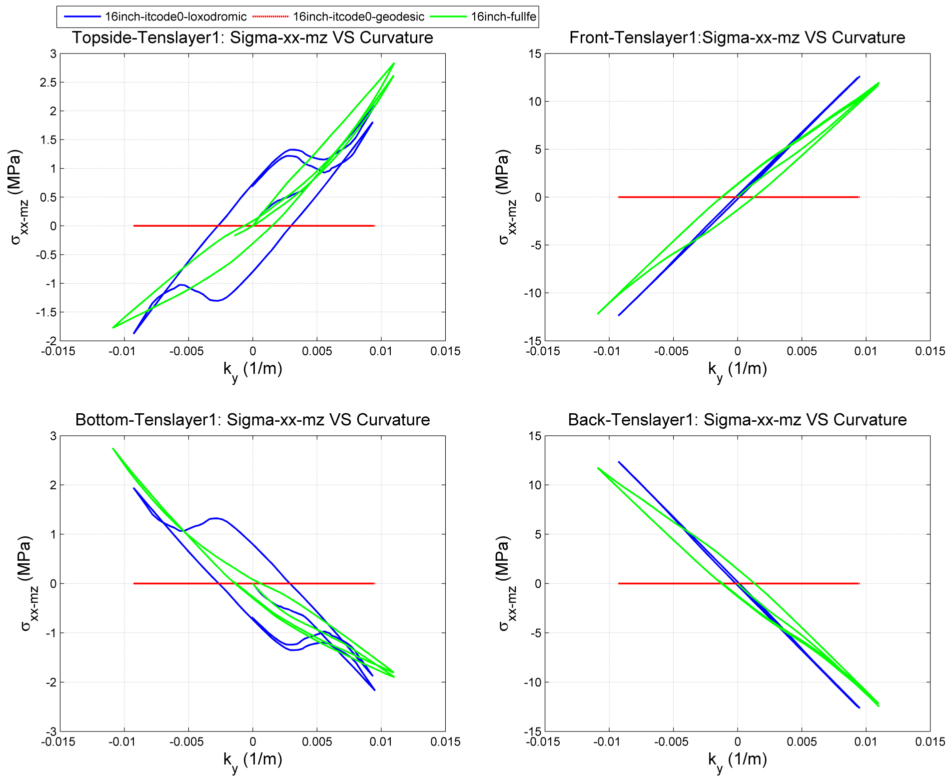

Figure C.43: The 16 inch tenslayer1 σ_{xx-mz} lox-geo for itcode0 and fullfe.

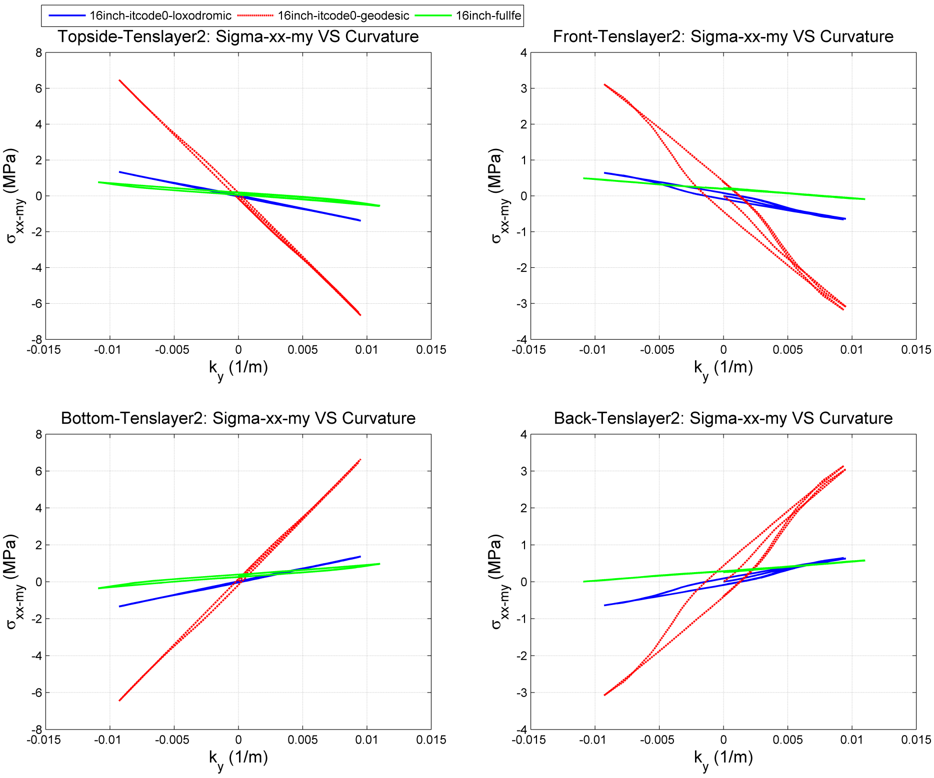

Figure C.44: The 16 inch tenslayer2 σ_{xx-my} lox-geo for itcode0 and fullfe.

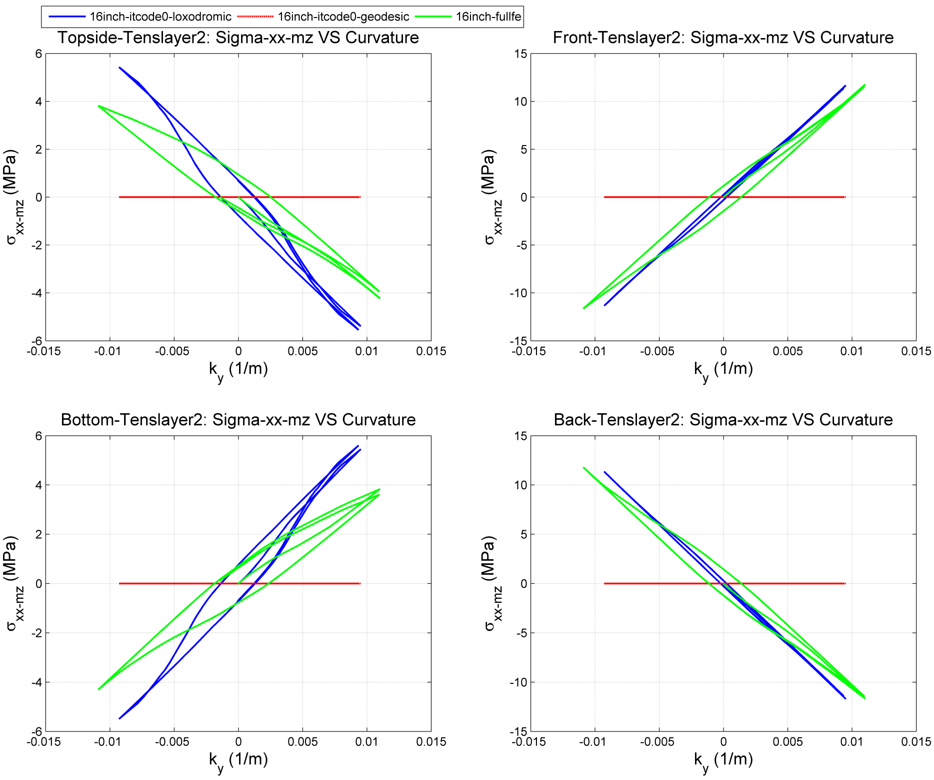

Figure C.45: The 16 inch tenslayer2 σ_{xx-mz} lox-geo for itcode0 and fullfe.

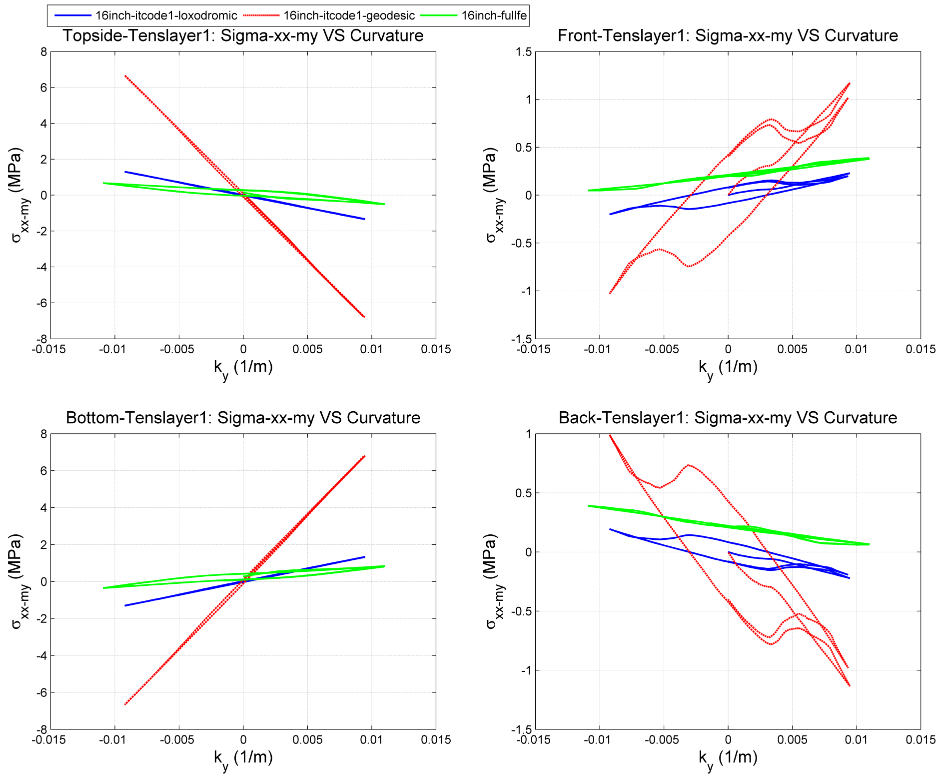

Figure C.46: The 16 inch tenslayer1 σ_{xx-my} lox-geo for itcode1 and fullfe.

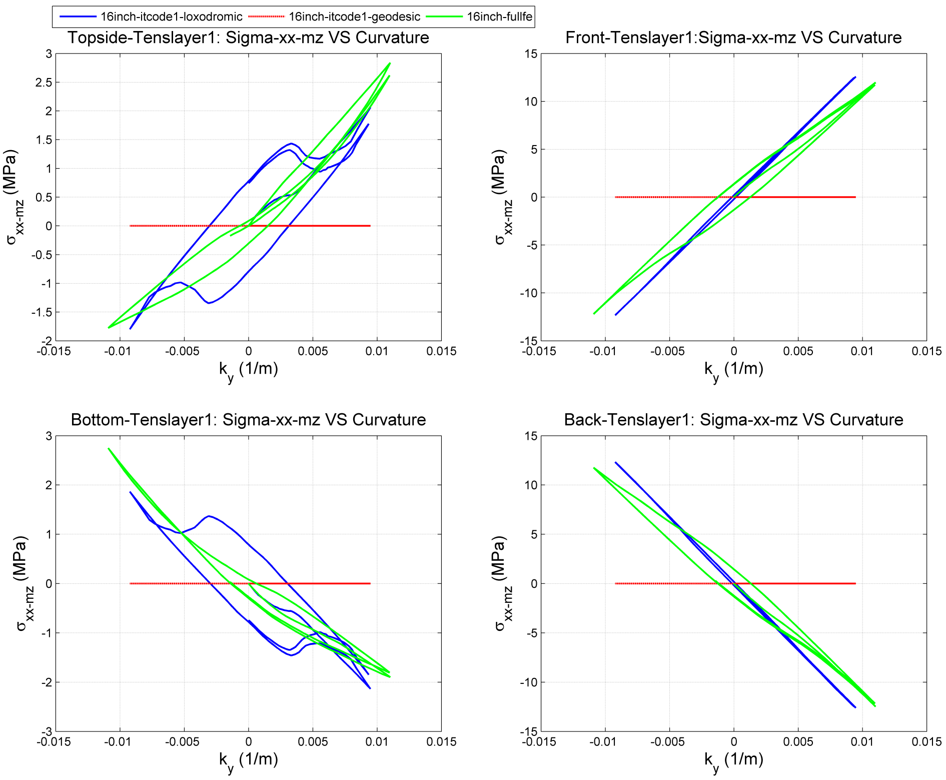

Figure C.47: The 16 inch tenslayer1 σ_{xx-mz} lox-geo for itcode1 and fullfe.

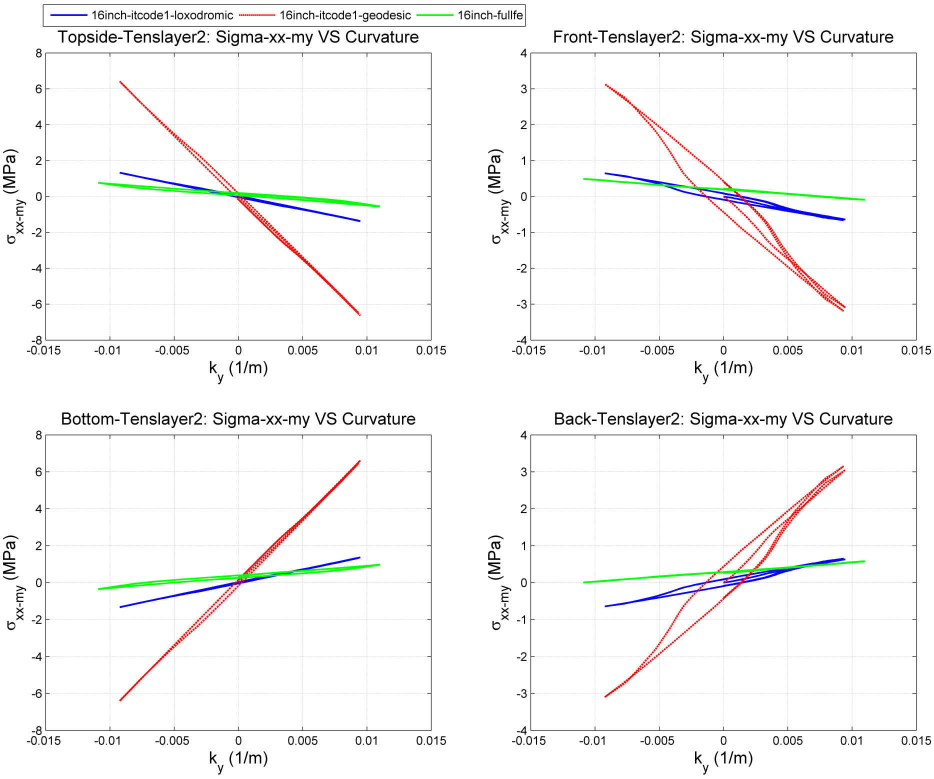

Figure C.48: The 16 inch tenslayer2 σ_{xx-my} lox-geo for itcode1 and fullfe.

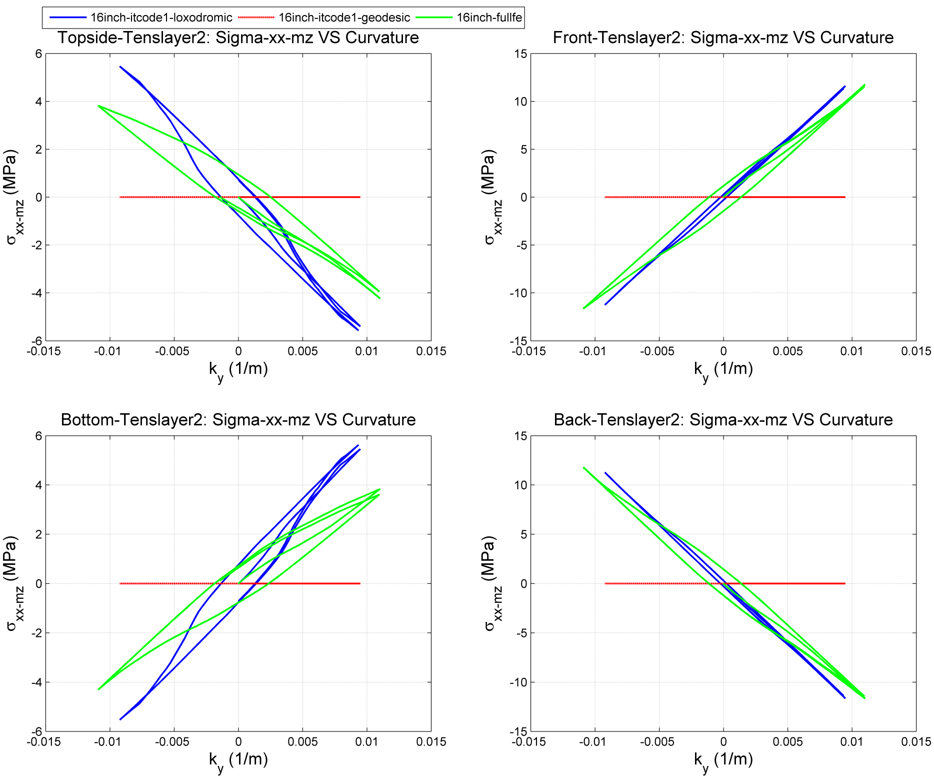

Figure C.49: The 16 inch tenslayer2 σ_{xx-mz} lox-geo for itcode1 and fullfe.

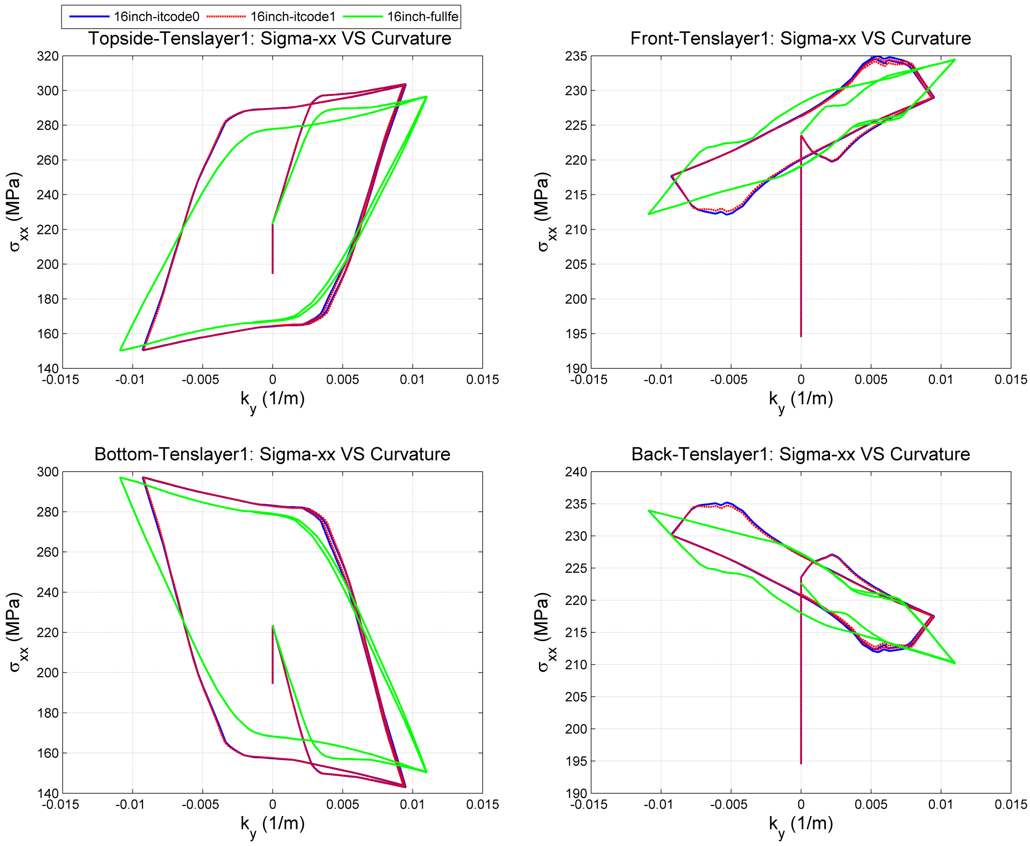

Figure C.50: The 16 inch tenslayer1 σ_{xx} for three models.

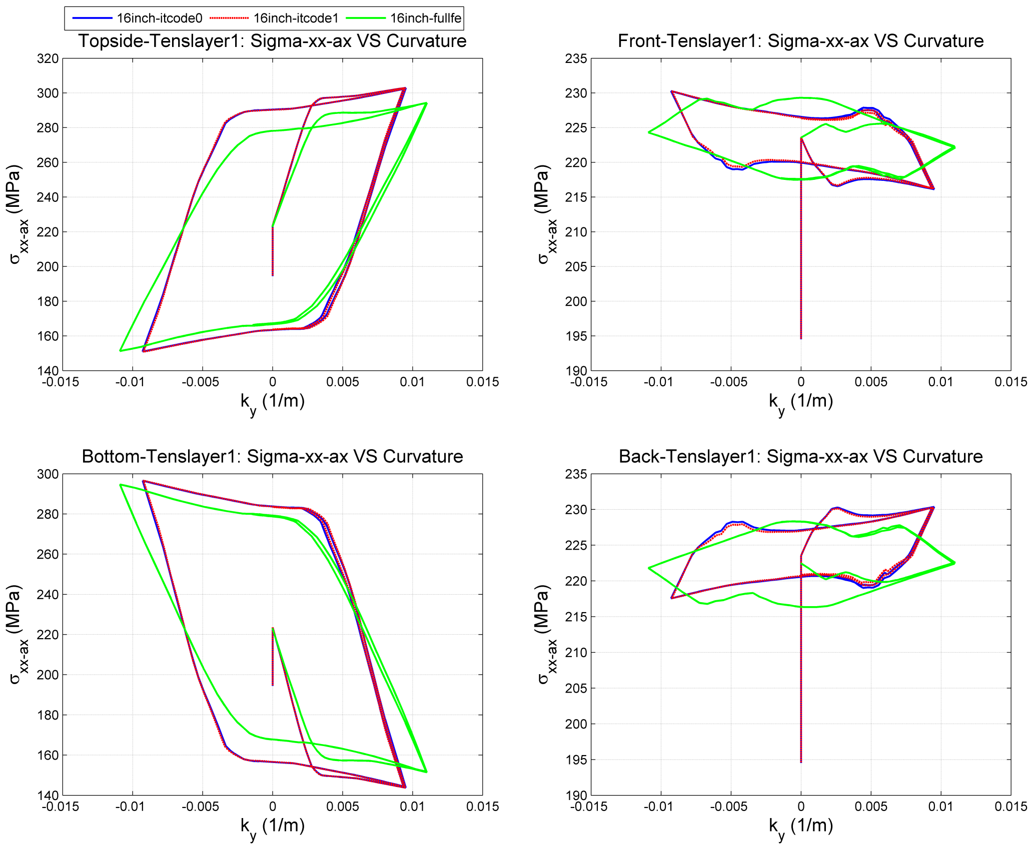

Figure C.51: The 16 inch tenslayer1 σ_{xx-ax} for three models.

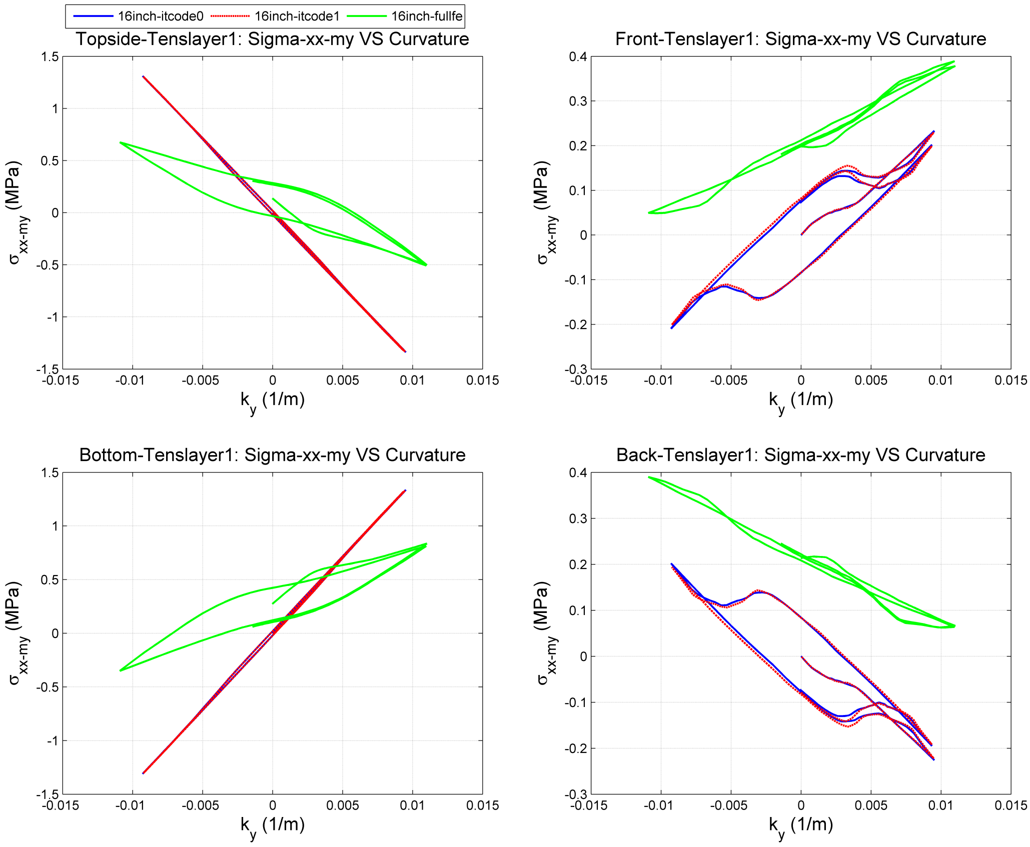

Figure C.52: The 16 inch tenslayer1 σ_{xx-my} for three models.

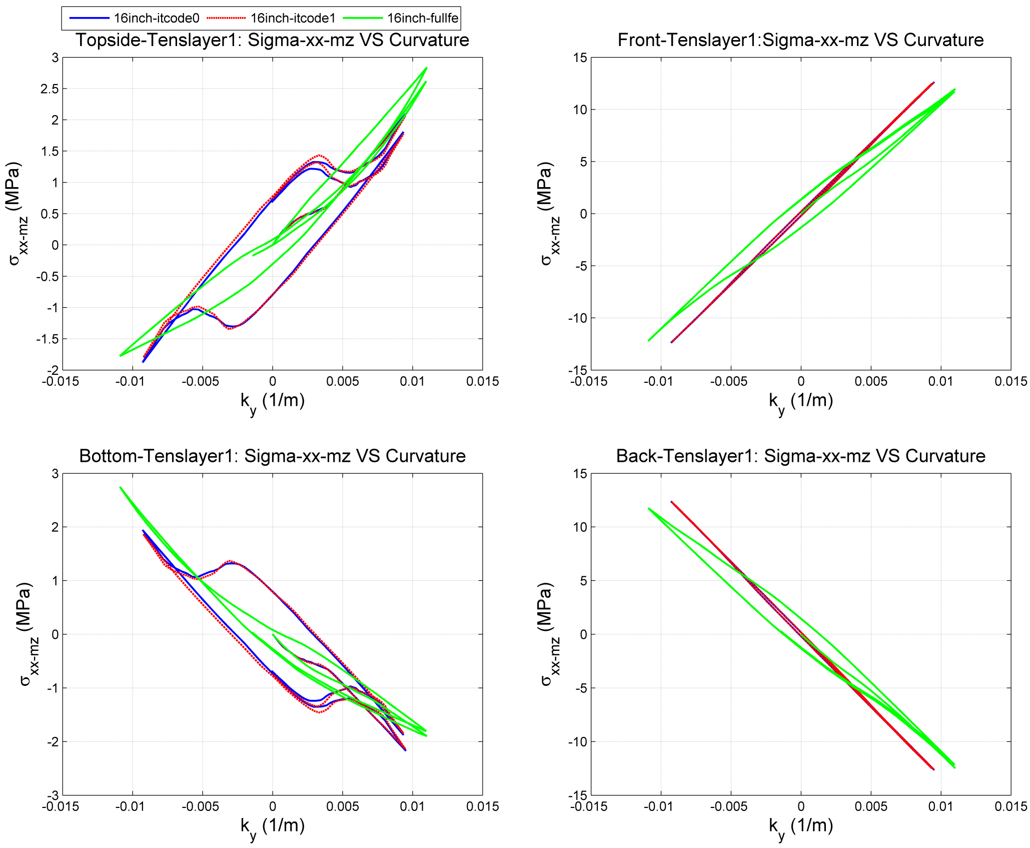

Figure C.53: The 16 inch tenslayer1 σ_{xx-mz} for three models.

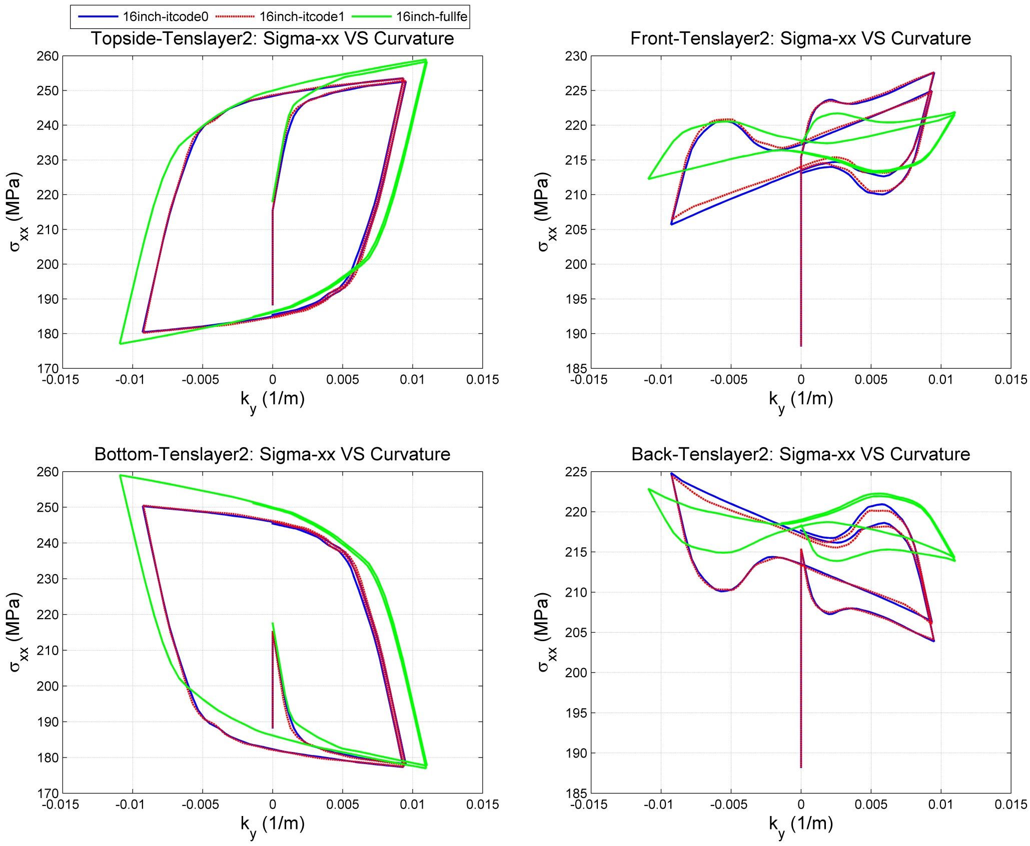

Figure C.54: The 16 inch tenslayer2 σ_{xx} for three models.

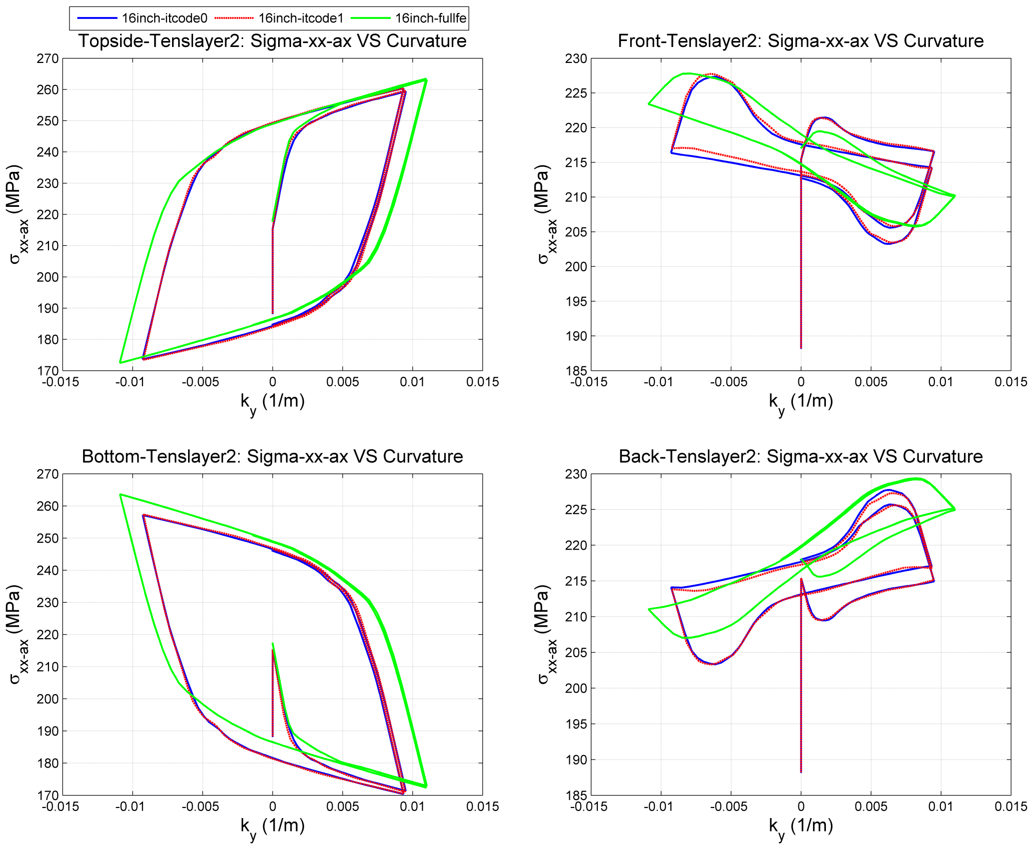

Figure C.55: The 16 inch tenslayer2 σ_{xx-ax} for three models.

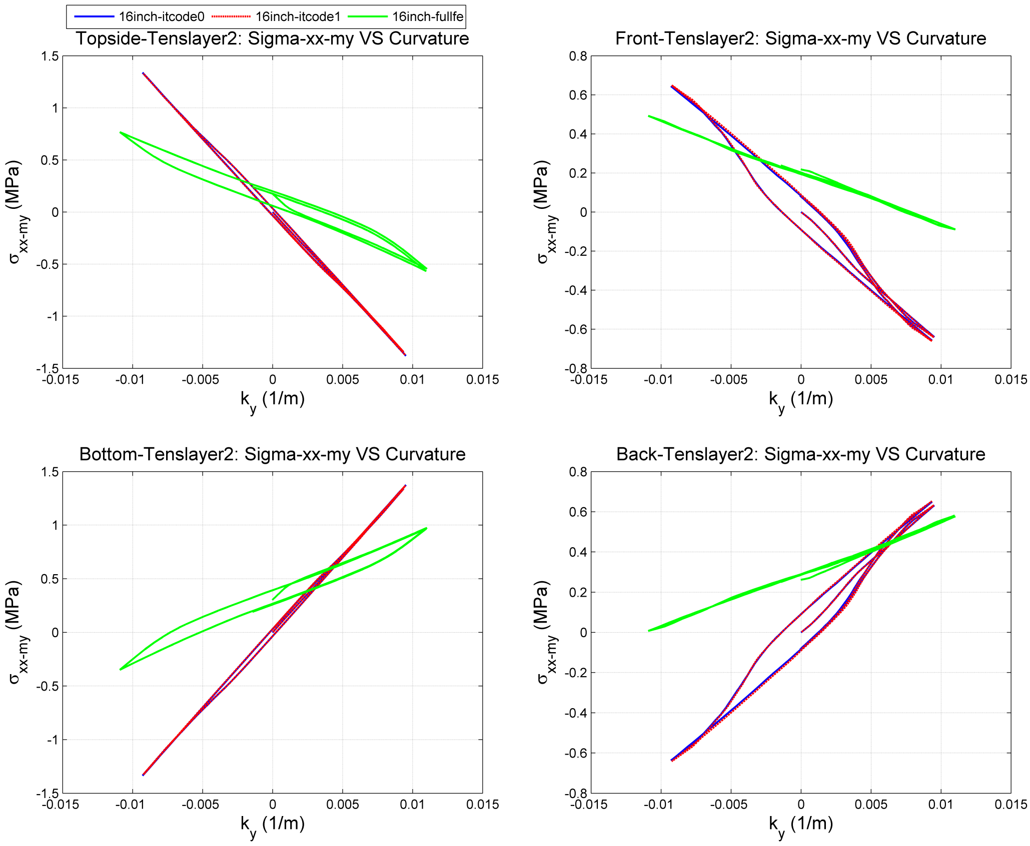

Figure C.56: The 16 inch tenslayer2 σ_{xx-my} for three models.

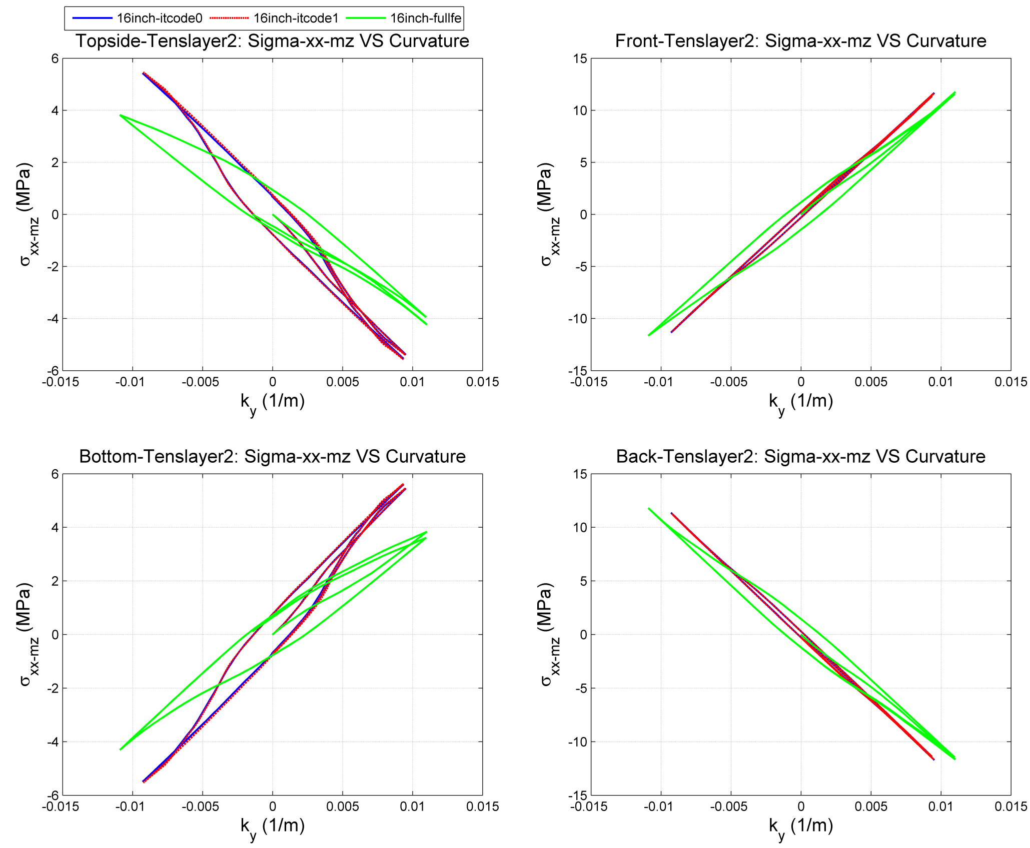

Figure C.57: The 16 inch tenslayer2 σ_{xx-mz} for three models.

Appendix D The 7.5 inch pipe analysis

D.1 The 2 tensile layer 7.5 inch pipe analysis

D.1.1 The 7.5 inch pipe two tenslayer model friction data and friction plots

7.5 inch pipe two tens model friction data								
Layer	tensile layer 1				tensile layer 2			
models	Point	Relative Disp (–)	Unit Force (–)	Applied fric-force per-length	Point	Relative Disp (–)	Unit Force (–)	Applied fric-force per-length
itcode0-loxodromic	1	0	0	12.448119	1	0	0	3.746252
	2	0.58789E-02	0.9		2	0.58789E-02	0.9	
	3	0.11758E-01	1		3	0.11758E-01	1	
	4	0.10000E+05	10		4	0.10000E+05	10	
itcode0-geodesic	1	0	0	12.448119	1	0	0	3.746252
	2	0.58789E-02	0.9		2	0.58789E-02	0.9	
	3	0.11758E-01	1		3	0.11758E-01	1	
	4	0.10000E+05	10		4	0.10000E+05	10	
itcode1-loxodromic	1	0	0	12.448119	1	0	0	3.746252
	2	0.58789E-02	0.9		2	0.18596E-02	0.9	
	3	0.11758E-01	1		3	0.37193E-02	1	
	4	0.10000E+05	10		4	0.10000E+05	10	
itcode1-geodesic	1	0	0	12.448119	1	0	0	3.746252
	2	0.58789E-02	0.9		2	0.18596E-02	0.9	
	3	0.11758E-01	1		3	0.37193E-02	1	
	4	0.10000E+05	10		4	0.10000E+05	10	
fullfe	1	0	0	12.245896	1	0	0	3.908039
	2	0.57834E-02	0.9		2	0.19400E-02	0.9	
	3	0.11567E-01	1		3	0.38799E-02	1	
	4	0.13955E+06	10		4	0.13955E+06	10	

Table D.1: The 7.5 inch pipe 2 tens model friction data.

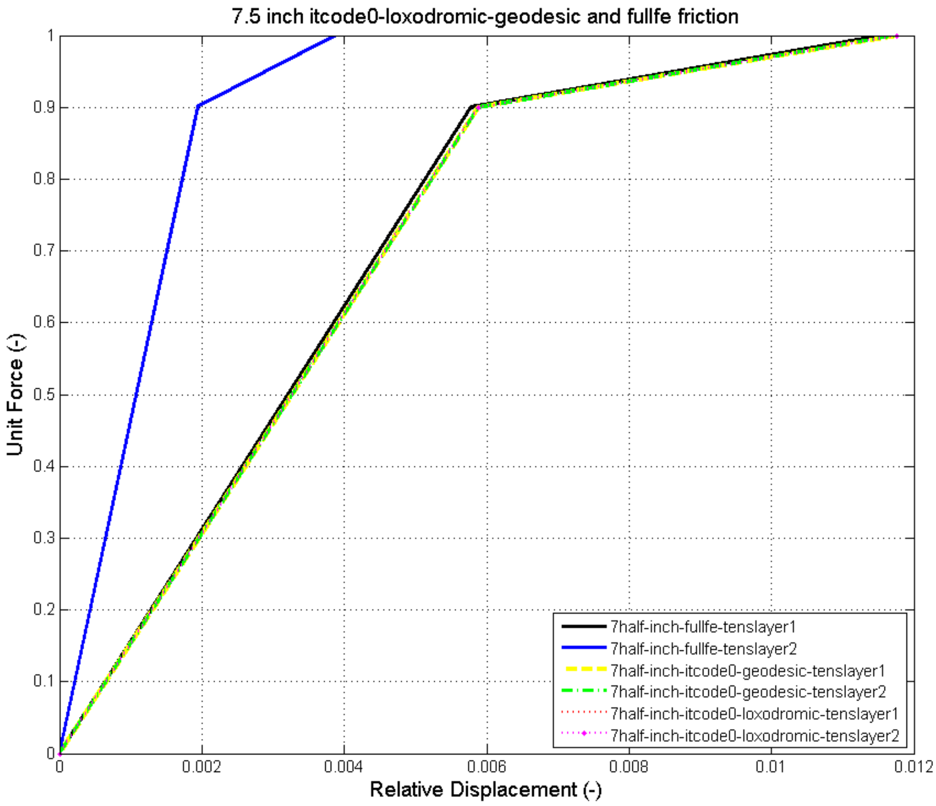

Figure D.1: The 7.5 inch 2 tens lox-geo friction for itcode0 and fullfe.

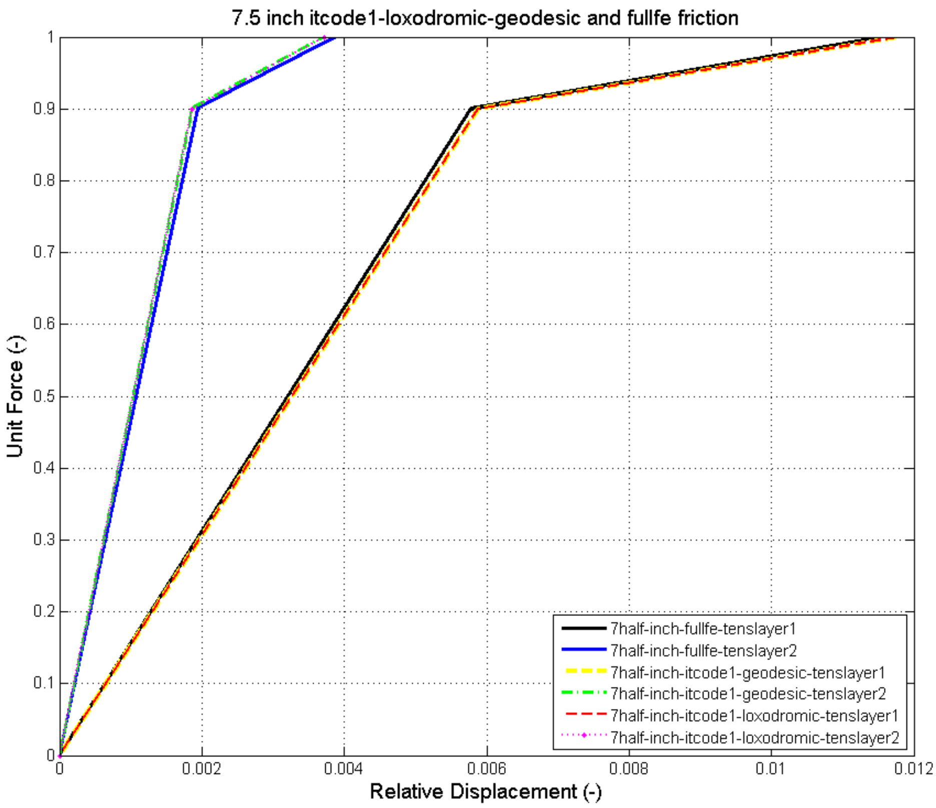

Figure D.2: The 7.5 inch 2 tens lox-geo friction for itcode1 and fullfe.

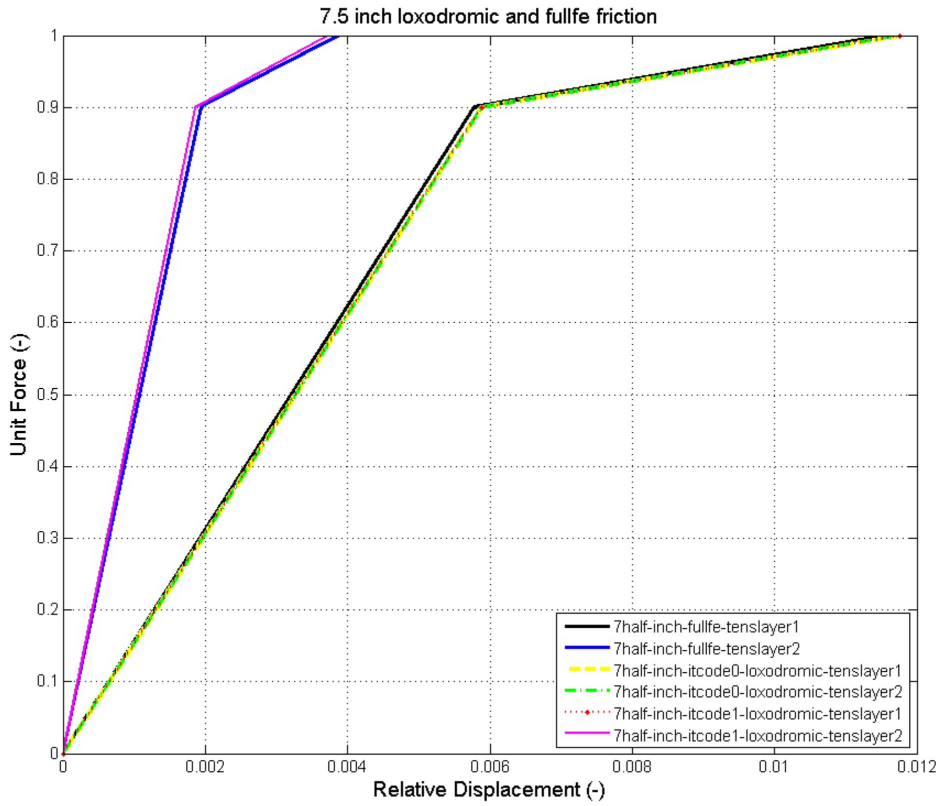

Figure D.3: The 7.5 inch 2 tens lox friction for itcode0-itcode1 and fullfe.

D.1.2 Stress components figure results for 7.5 inch two tensile layer pipe

Two tensile layer stress components under two assumptions

Figure D.4–Figure D.11 show the stress components comparison of itcode0 and itcode1 models under both the loxodromic and geodesic assumptions and the fullfe model.

Two tensile layer stress components for loxodromic assumption and fullfe model

Figure D.12 – Figure D.19 show the stress components comparison of itcode0 and itcode1 models under loxodromic assumption and fullfe model.

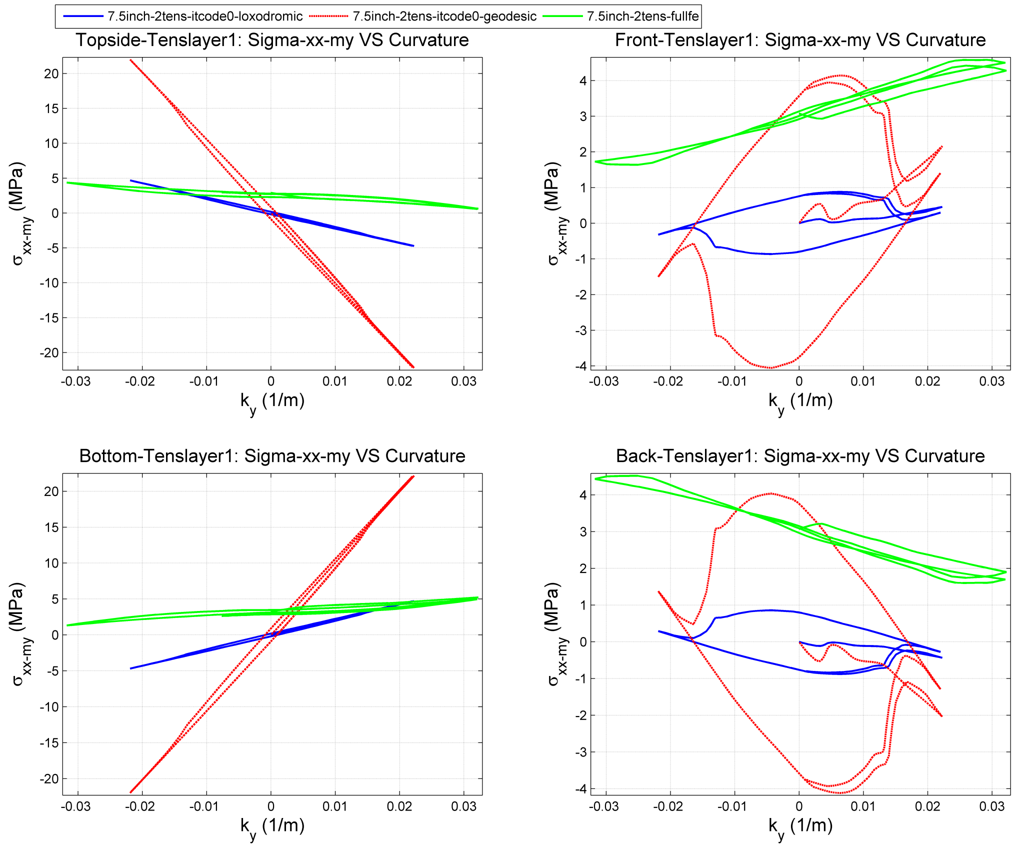

Figure D.4: The 7.5"-2tens tenslayer1 σ_{xx-my} lox-geo sensitivity for itcode0 and fullfe.

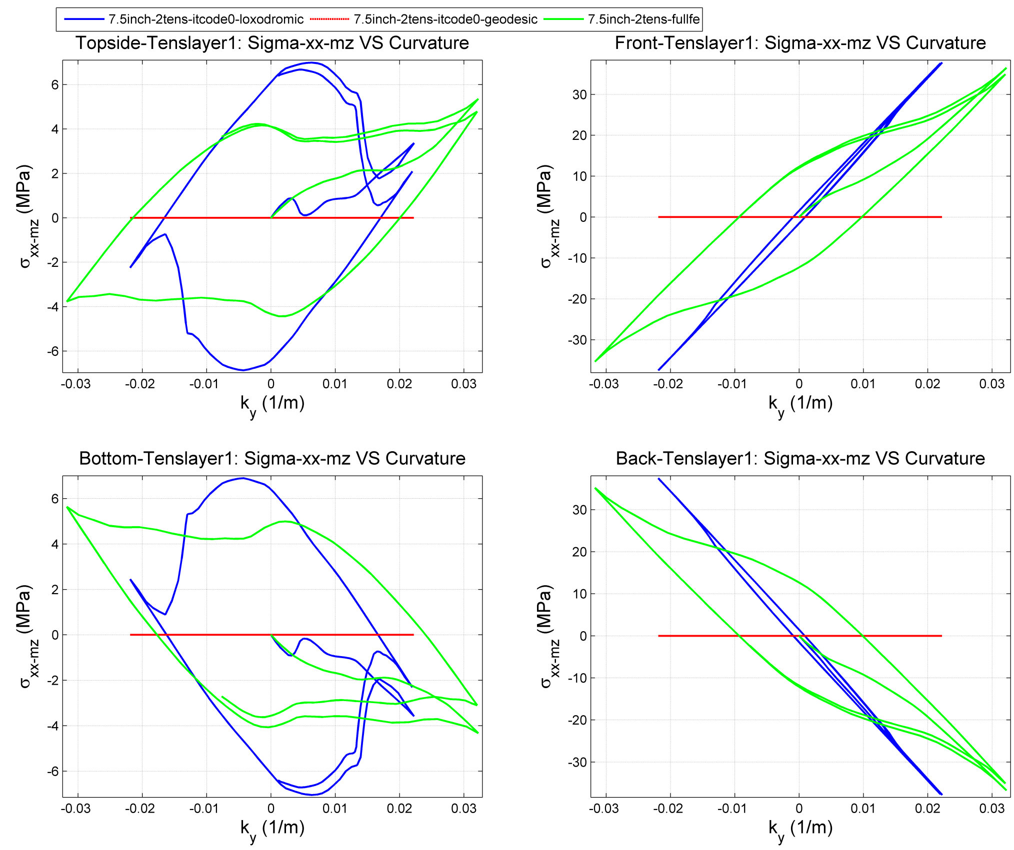

Figure D.5: The 7.5"-2tens tenslayer1 σ_{xx-mz} lox-geo sensitivity for itcode0 and fullfe.

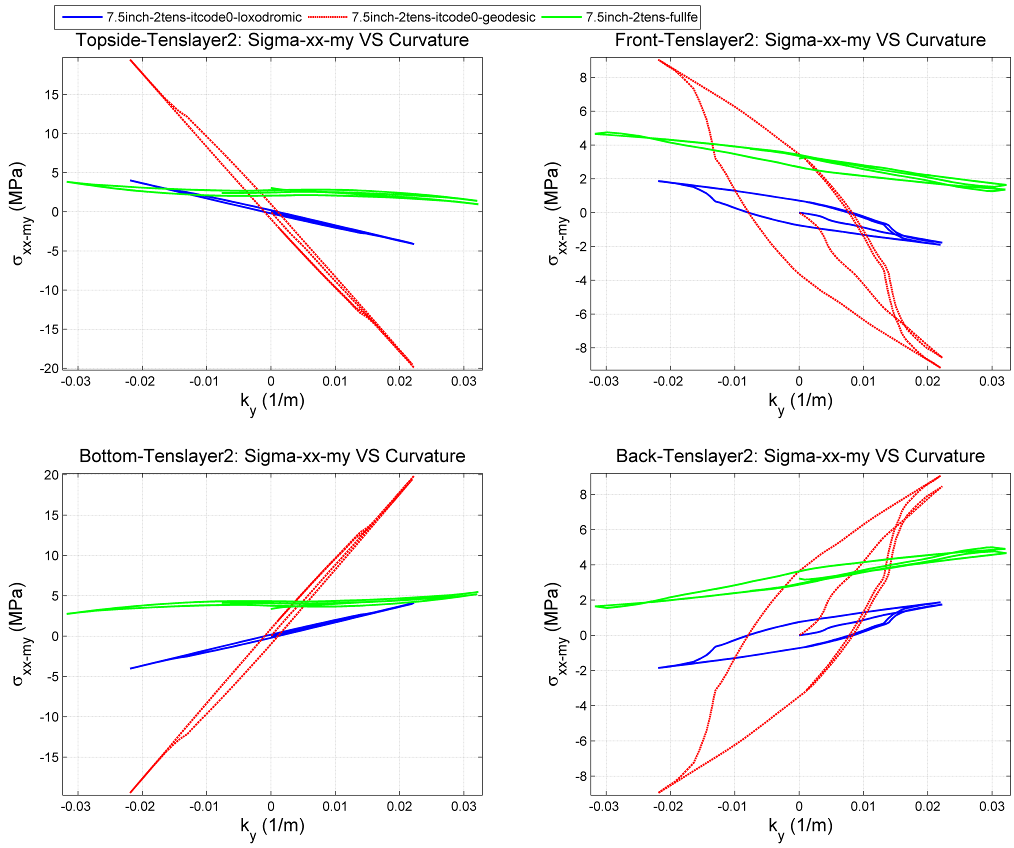

Figure D.6: The 7.5"-2tens tenslayer2 σ_{xx-my} lox-geo sensitivity for itcode0 and fullfe.

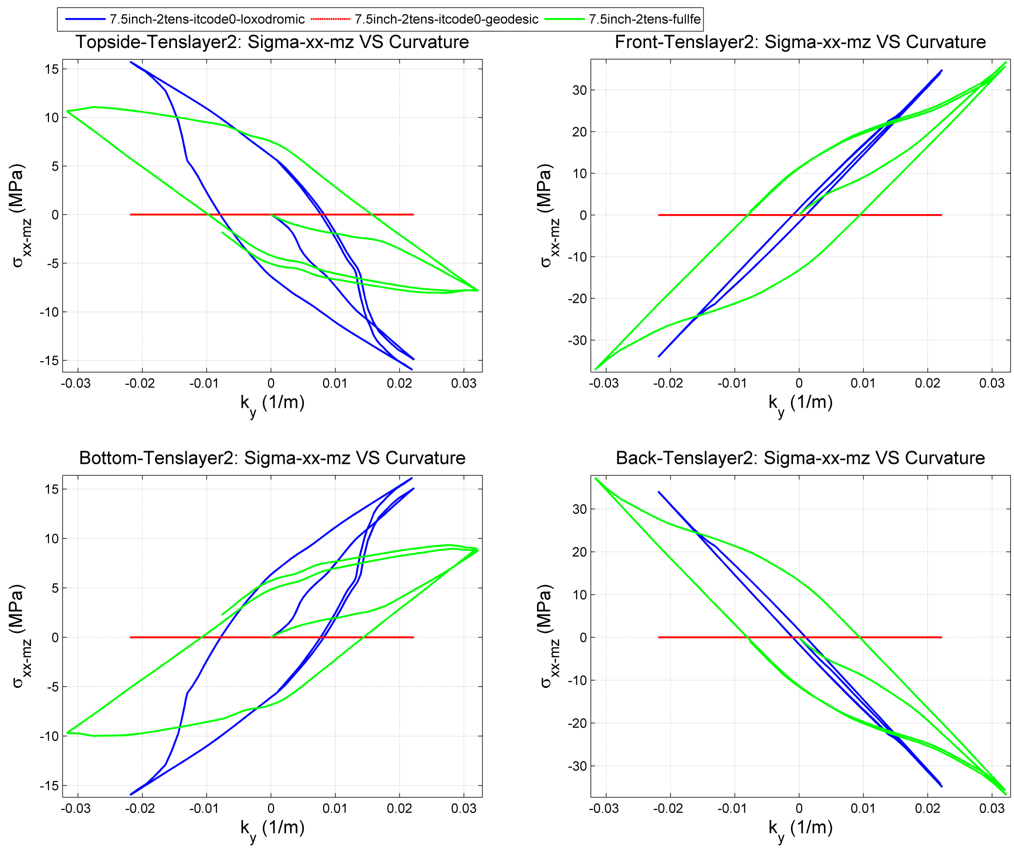

Figure D.7: The 7.5"-2tens tenslayer2 σ_{xx-mz} lox-geo sensitivity for itcode0 and fullfe.

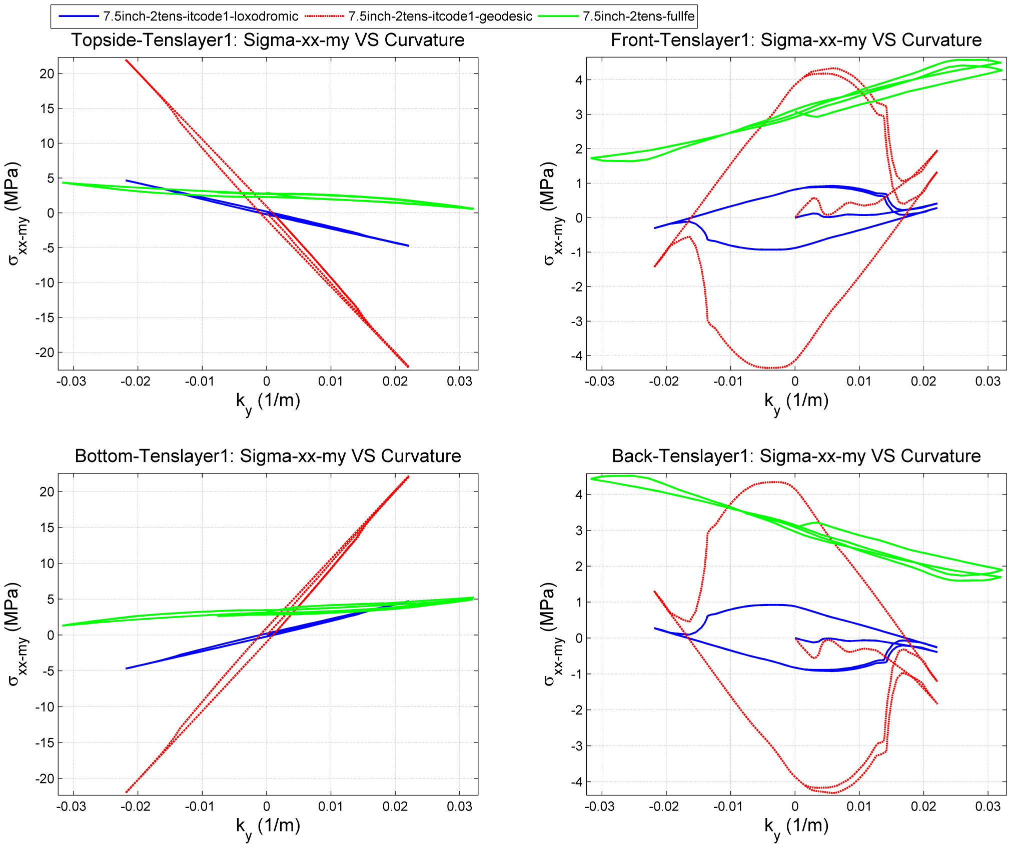

Figure D.8: The 7.5"-2tens tenslayer1 σ_{xx-my} lox-geo sensitivity for itcode1 and fullfe.

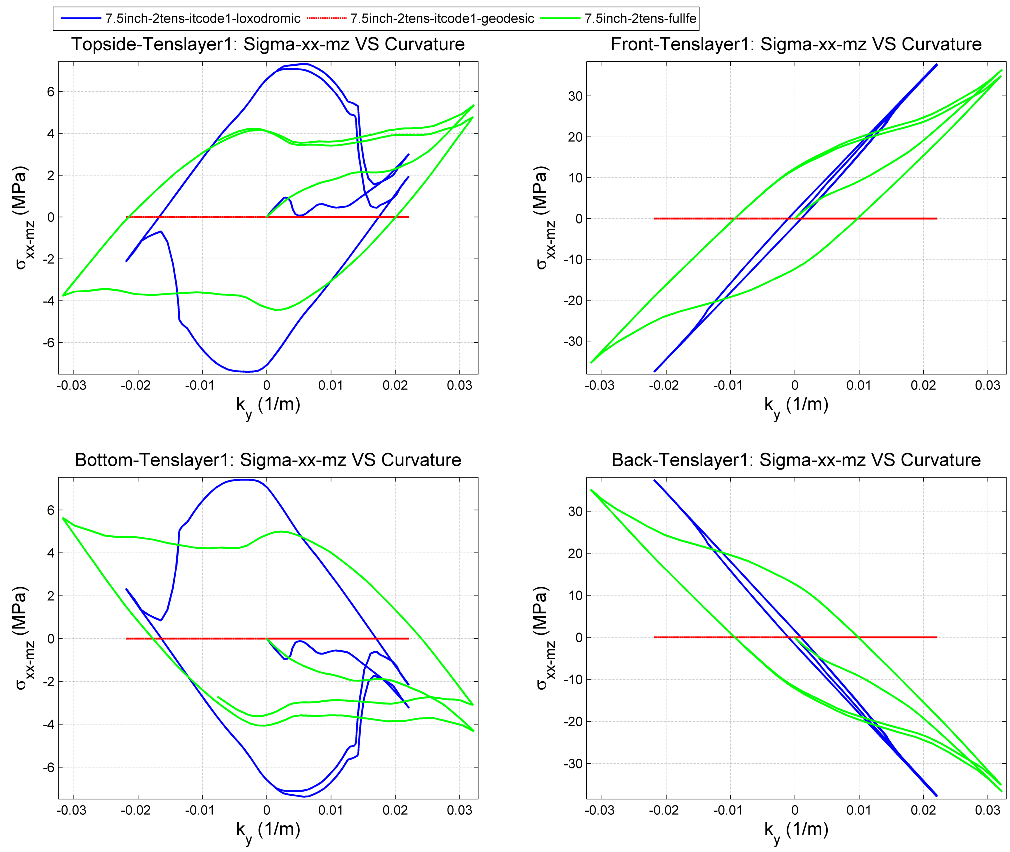

Figure D.9: The 7.5"-2tens tenslayer1 σ_{xx-mz} lox-geo sensitivity for itcode1 and fullfe.

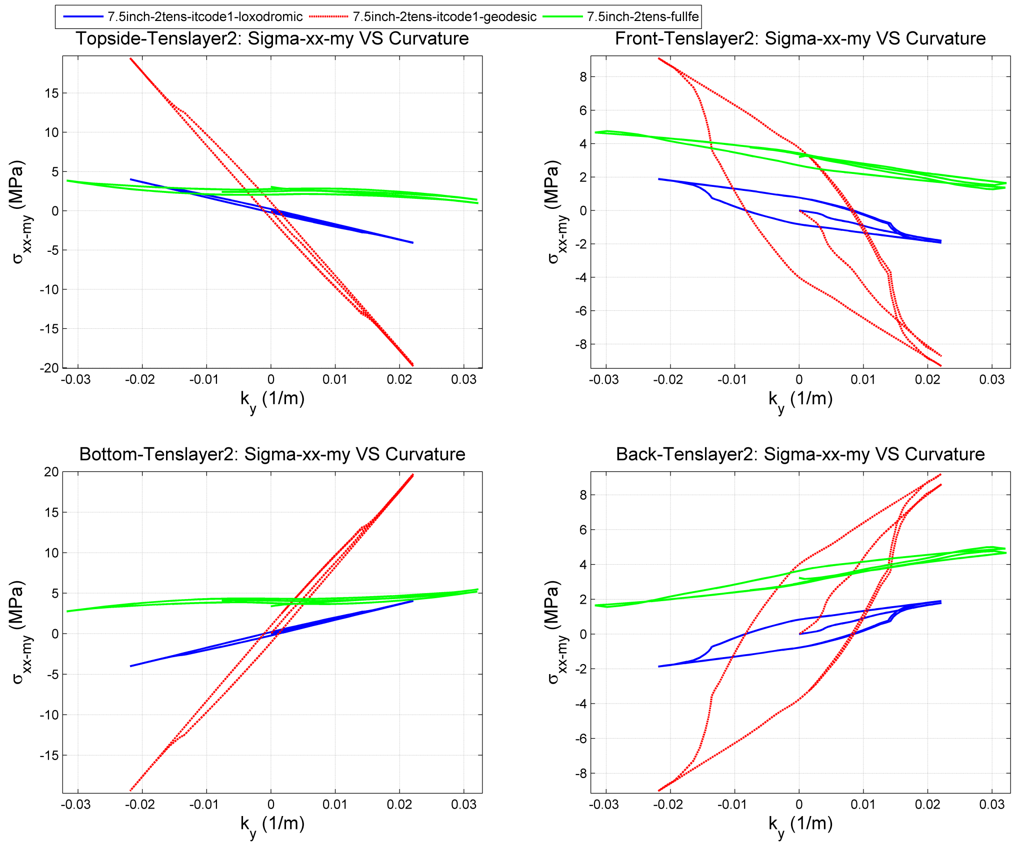

Figure D.10: The 7.5"-2tens tenslayer2 σ_{xx-my} lox-geo sensitivity for itcode1 and fullfe.

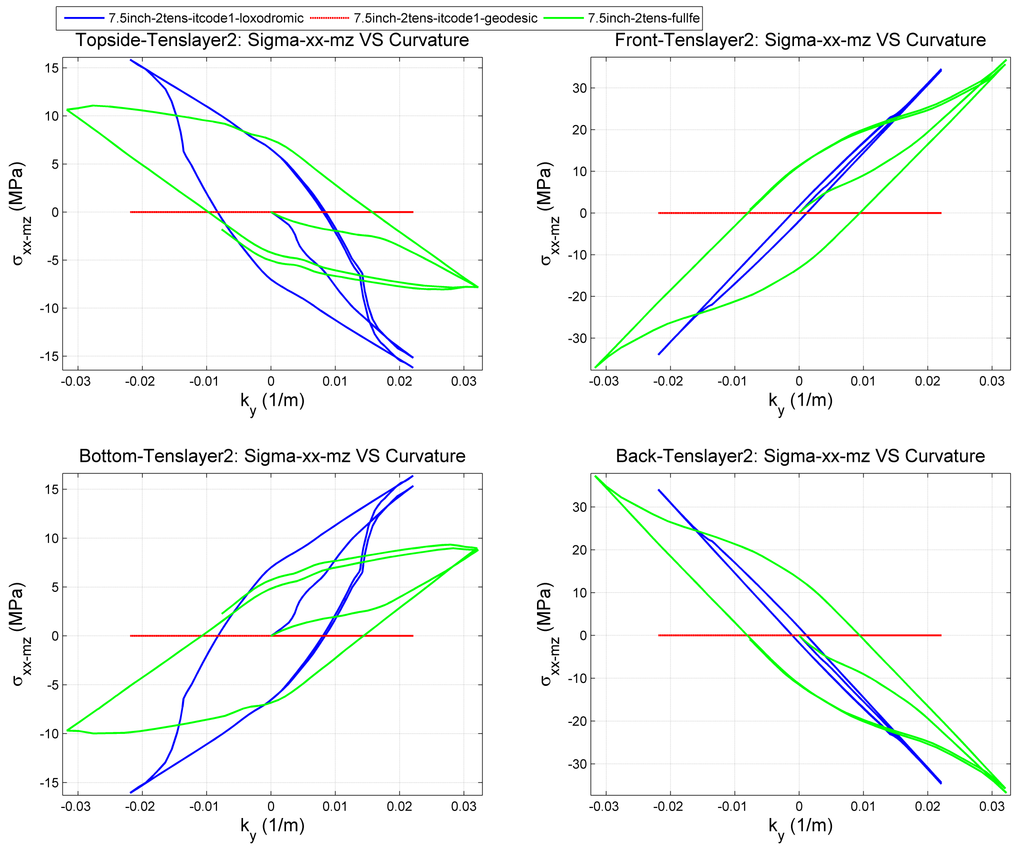

Figure D.11: The 7.5"-2tens tenslayer2 σ_{xx-mz} lox-geo sensitivity for itcode1 and fullfe.

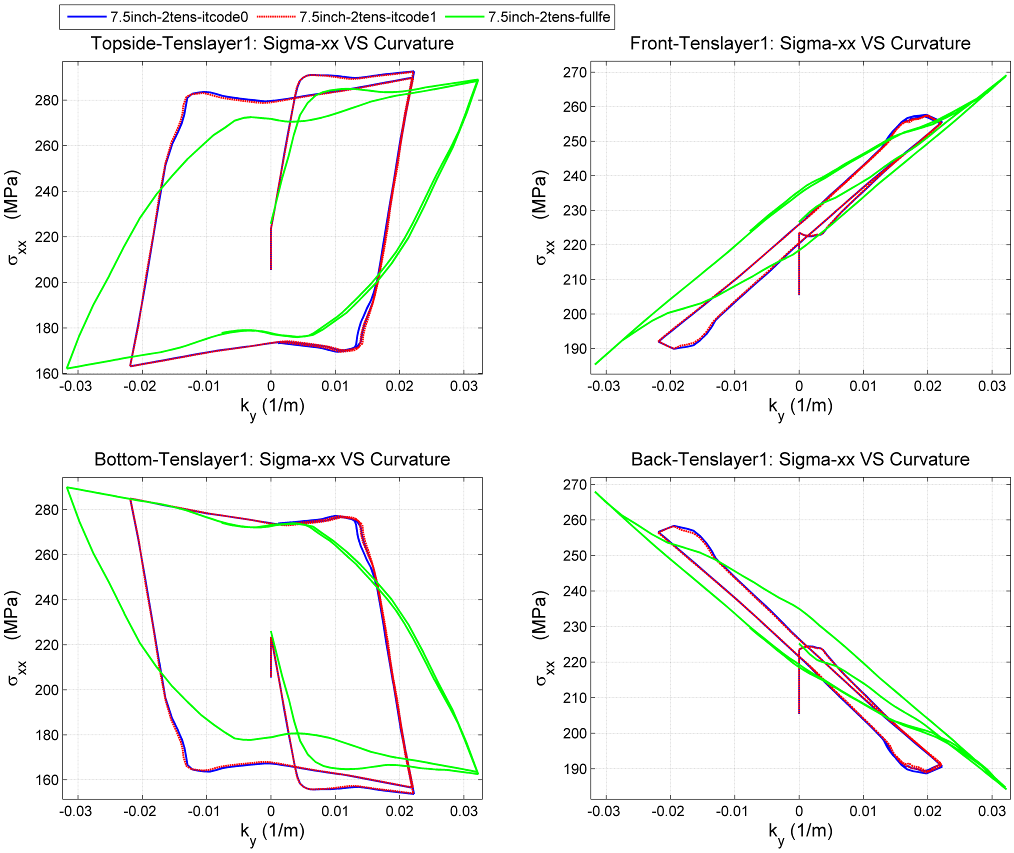

Figure D.12: The 7.5"-2tens tenslayer1 σ_{xx} for itcode0-itcode1-fullfe.

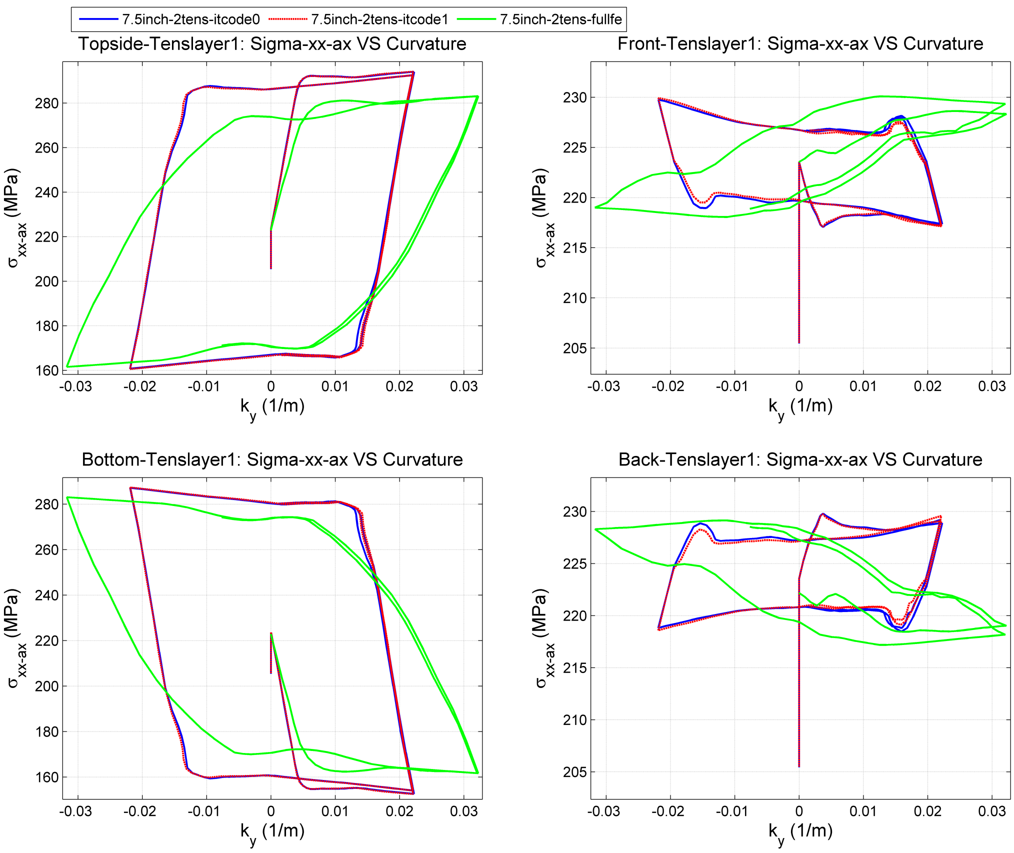

Figure D.13: The 7.5"-2tens tenslayer1 σ_{xx-ax} for itcode0-itcode1-fullfe.

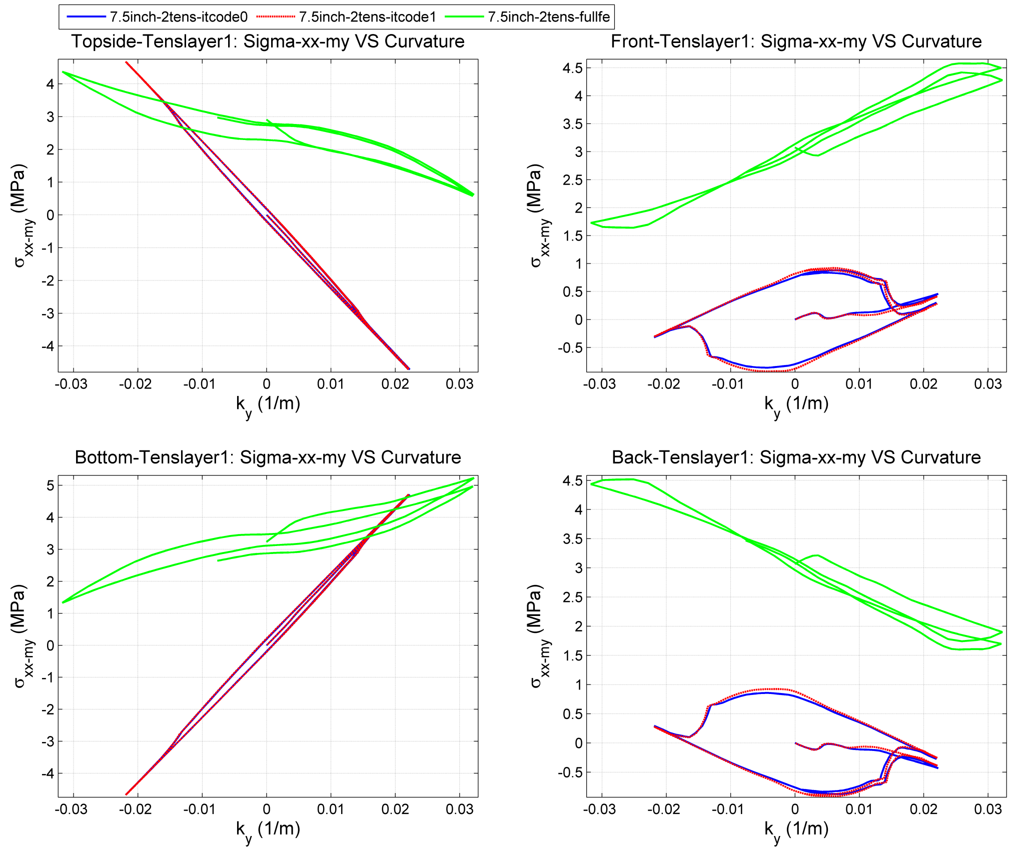

Figure D.14: The 7.5"-2tens tenslayer1 σ_{xx-my} for itcode0-itcode1-fullfe.

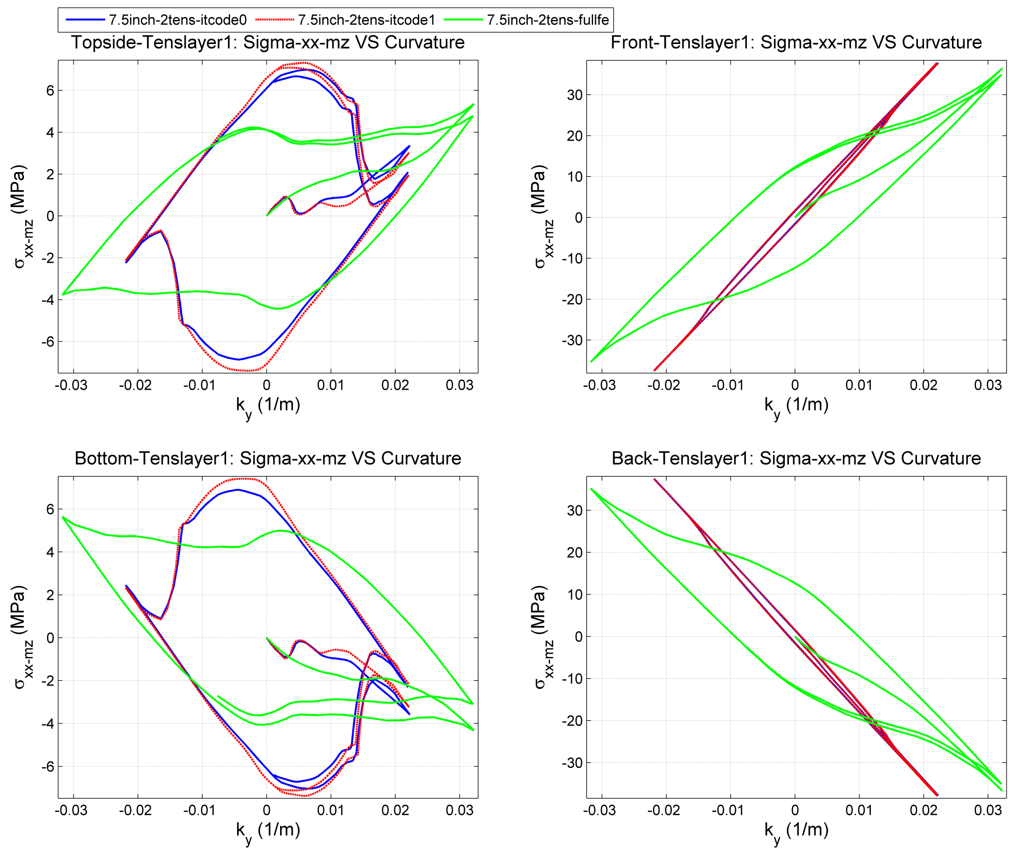

Figure D.15: The 7.5"-2tens tenslayer1 σ_{xx-mz} for itcode0-itcode1-fullfe.

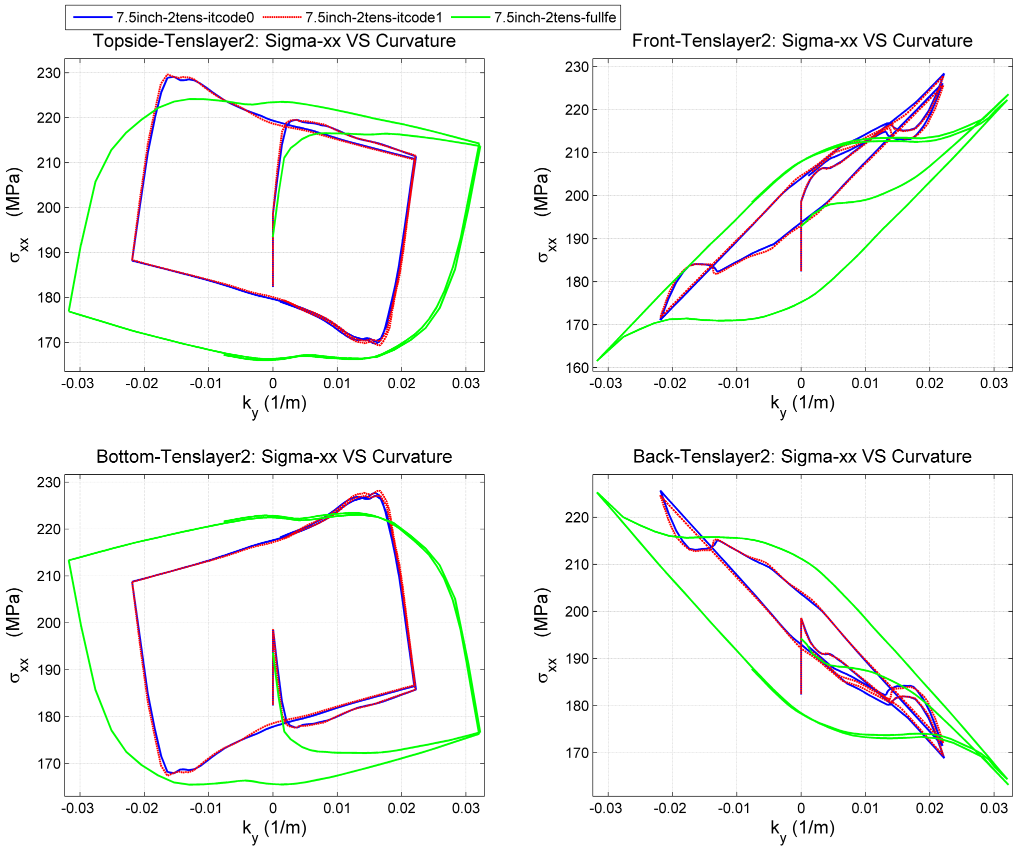

Figure D.16: The 7.5"-2tens tenslayer2 σ_{xx} for itcode0-itcode1-fullfe.

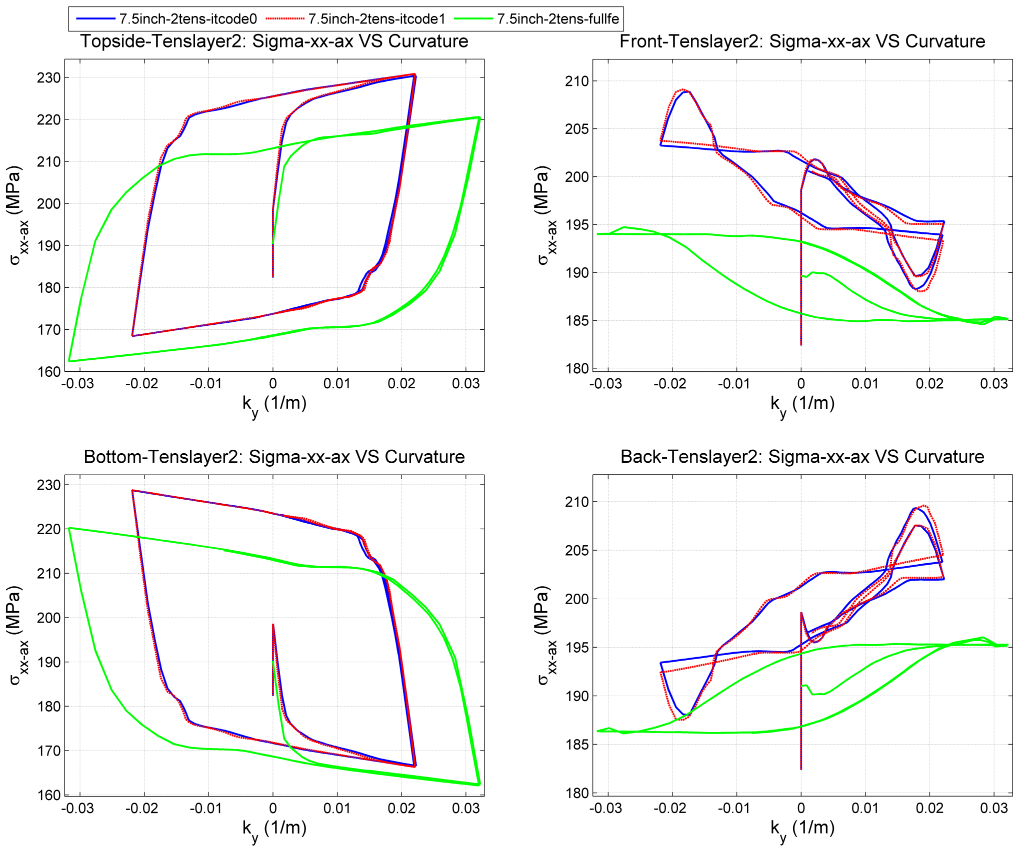

Figure D.17: The 7.5"-2tens tenslayer2 σ_{xx-ax} for three models.

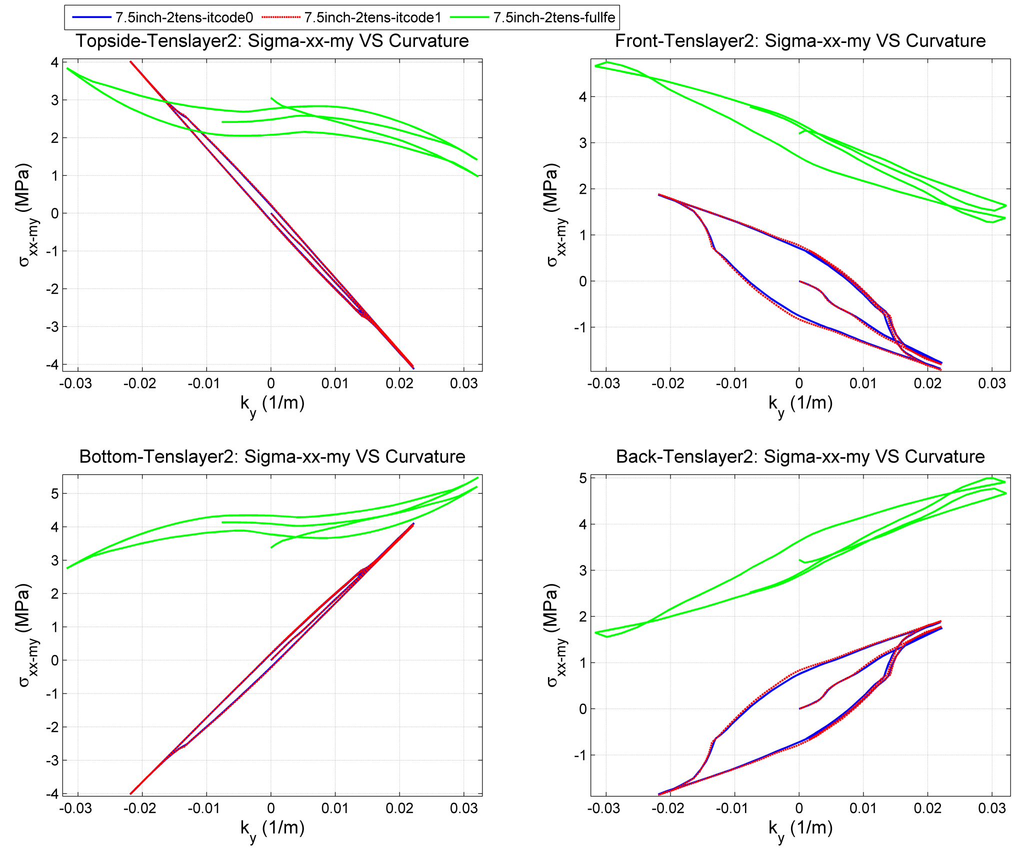

Figure D.18: The 7.5"-2tens tenslayer2 σ_{xx-my} for three models.

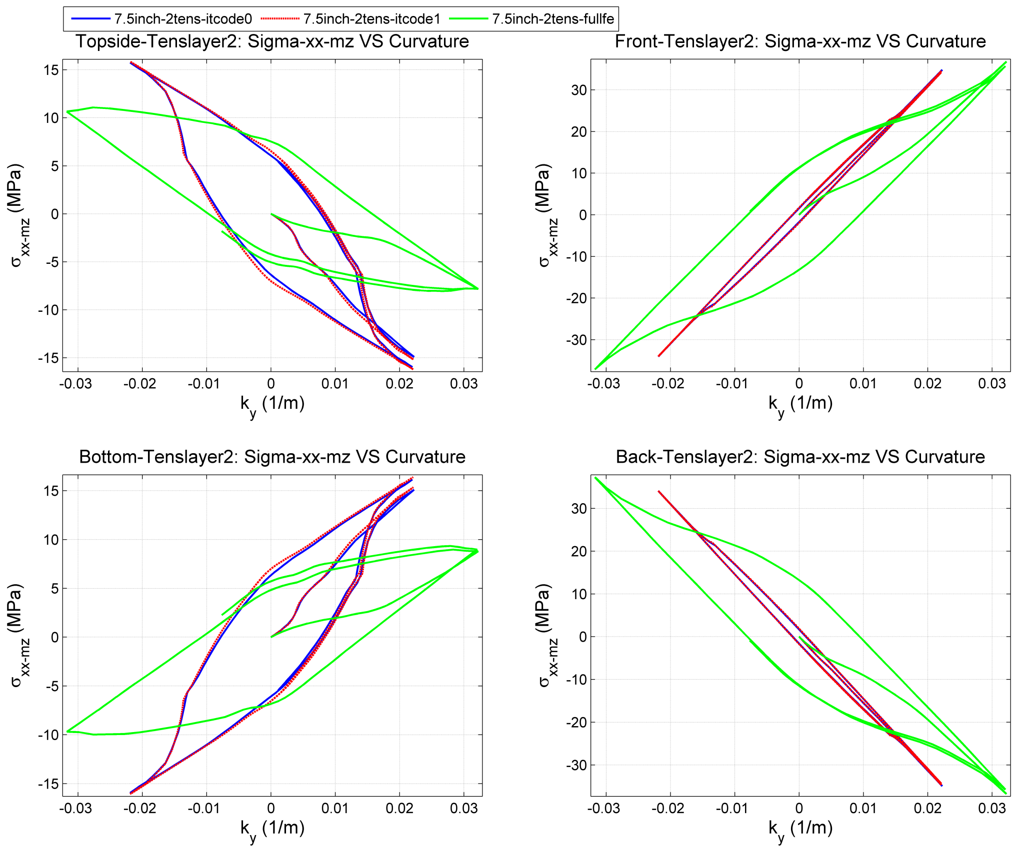

Figure D.19: The 7.5"-2tens tenslayer2 σ_{xx-mz} for three models.

D.1.3 The 4 tensile layer 7.5 inch pipe model friction data

4 tensile layer:7.5 inch pipe model friction data								
Tensile layer 1 and Tensile layer 2								
Layer	tensile layer 1				tensile layer 2			
models	Point	Relative Disp (–)	Unit Force (–)	Applied fric-force per-length	Point	Relative Disp (–)	Unit Force (–)	Applied fric-force per-length
itcode0-loxodromic	1	0	0	25.869646	1	0	0	16.67732
	2	0.12218E-01	0.9		2	0.12218E-01	0.9	
	3	0.24435E-01	1		3	0.24435E-01	1	
	4	0.10000E+05	10		4	0.10000E+05	10	
itcode0-geodesic	1	0	0	25.869646	1	0	0	16.677320
	2	0.12218E-01	0.9		2	0.12218E-01	0.9	
	3	0.24435E-01	1		3	0.24435E-01	1	
	4	0.10000E+05	10		4	0.10000E+05	10	
itcode1-loxodromic	1	0	0	25.869646	1	0	0	16.677320
	2	0.12218E-01	0.9		2	0.82786E-02	0.9	
	3	0.24435E-01	1		3	0.16557E-01	1	
	4	0.10000E+05	10		4	0.10000E+05	10	
itcode1-geodesic	1	0	0	25.869646	1	0	0	16.677320
	2	0.12218E-01	0.9		2	0.82786E-02	0.9	
	3	0.24435E-01	1		3	0.16557E-01	1	
	4	0.10000E+05	10		4	0.10000E+05	10	
fullfe	1	0	0	19.344191	1	0	0	12.172701
	2	0.91385E-02	0.9		2	0.60425E-02	0.9	
	3	0.18272E-01	1		3	0.12085E-01	1	
	4	0.15425E+06	10		4	0.15425E+06	10	

Tensile layer 3 and tensile layer 4								
Layer	tensile layer 3				tensile layer 4			
models	Point	Relative Disp (–)	Unit Force (–)	Applied fric-force per-length	Point	Relative Disp (–)	Unit Force (–)	Applied fric-force per-length
itcode0-loxodromic	1	0	0	9.216250	1	0	0	2.772635
	2	0.12218E-01	0.9		2	0.12218E-01	0.9	
	3	0.24435E-01	1		3	0.24435E-01	1	
	4	0.10000E+05	10		4	0.10000E+05	10	
itcode0-geodesic	1	0	0	9.216250	1	0	0	2.772635
	2	0.12218E-01	0.9		2	0.12218E-01	0.9	
	3	0.24435E-01	1		3	0.24435E-01	1	
	4	0.10000E+05	10		4	0.10000E+05	10	
itcode1-loxodromic	1	0	0	9.216250	1	0	0	2.772635
	2	0.53671E-02	0.9		2	0.17599E-02	0.9	
	3	0.10734E-01	1		3	0.35197E-02	1	
	4	0.10000E+05	10		4	0.10000E+05	10	
itcode1-geodesic	1	0	0	9.216250	1	0	0	2.772635
	2	0.53671E-02	0.9		2	0.17599E-02	0.9	
	3	0.10734E-01	1		3	0.35197E-02	1	
	4	0.10000E+05	10		4	0.10000E+05	10	
fullfe	1	0	0	6.876358	1	0	0	2.273987
	2	0.40045E-02	0.9		2	0.14448E-02	0.9	
	3	0.80089E-02	1		3	0.28896E-02	1	
	4	0.15425E+06	10		4	0.15425E+06	10	

Table D.2: The 7.5 inch pipe 4 tens model friction data.

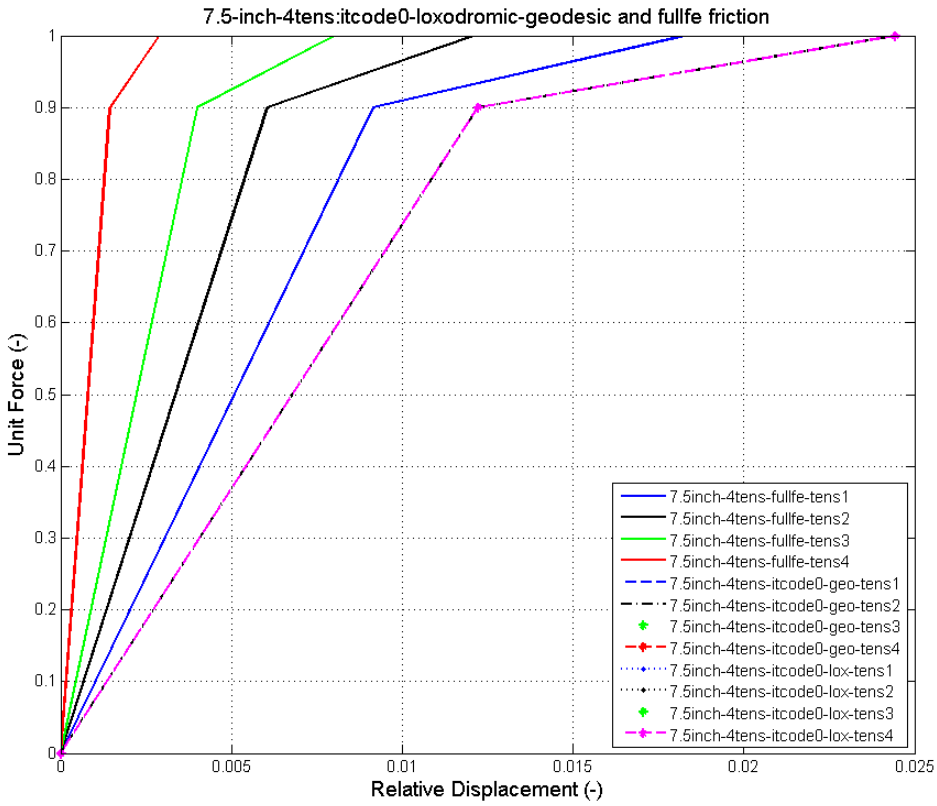

Figure D.20: The 4 tens 7.5 inch lox-geo friction sensitivity for itcode0 and fullfe.

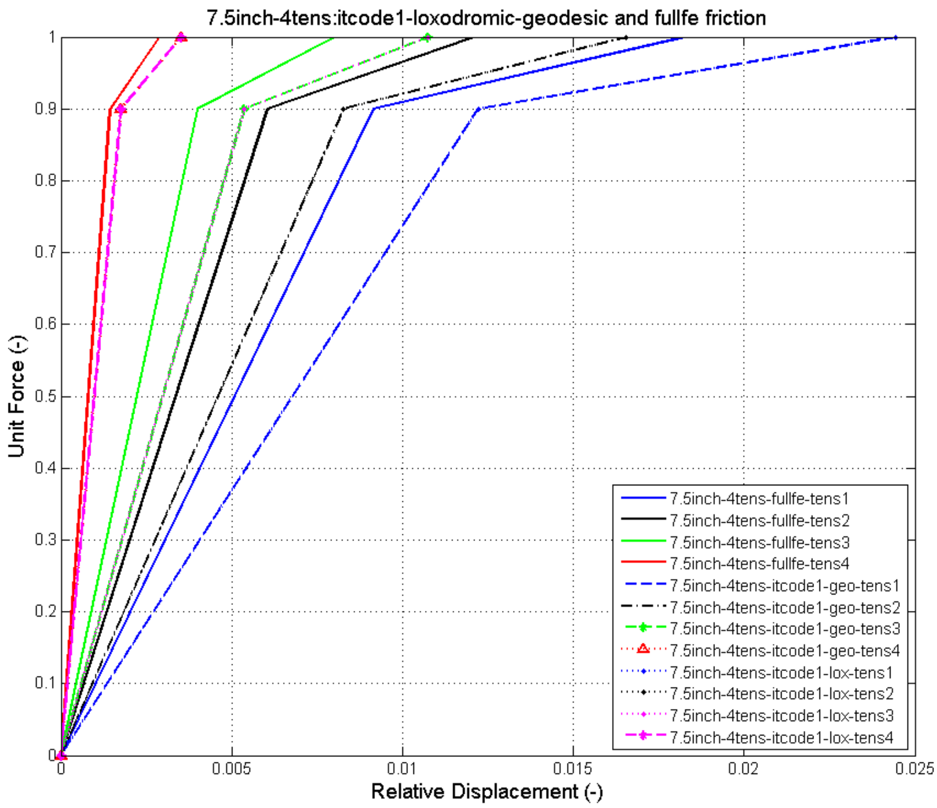

Figure D.21: The 4 tens 7.5 inch lox-geo friction sensitivity for itcode1 and fullfe.

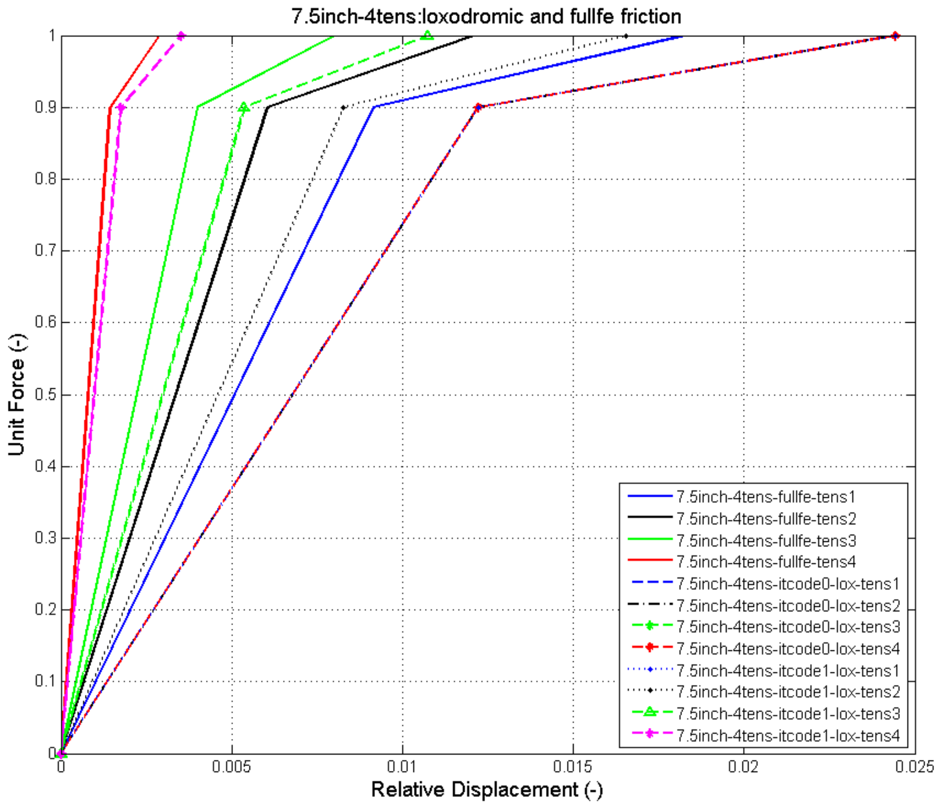

Figure D.22: The 4 tens 7.5 inch lox friction sensitivity for three models.

D.1.4 Stress components figure results for 7.5 inch four tensile layer pipe

The 7.5 inch pipe four tens stress components under two assumptions

Figure D.23–Figure D.38 show the stress components comparison of itcode0 and itcode1 models under both the loxodromic and geodesic assumptions and the fullfe model.

The 7.5 inch pipe four tens stress study for lox assumption and fullfe model

Figure D.39 – Figure D.54 show the stress components comparison of itcode0 and itcode1 models under loxodromic assumption and fullfe model.

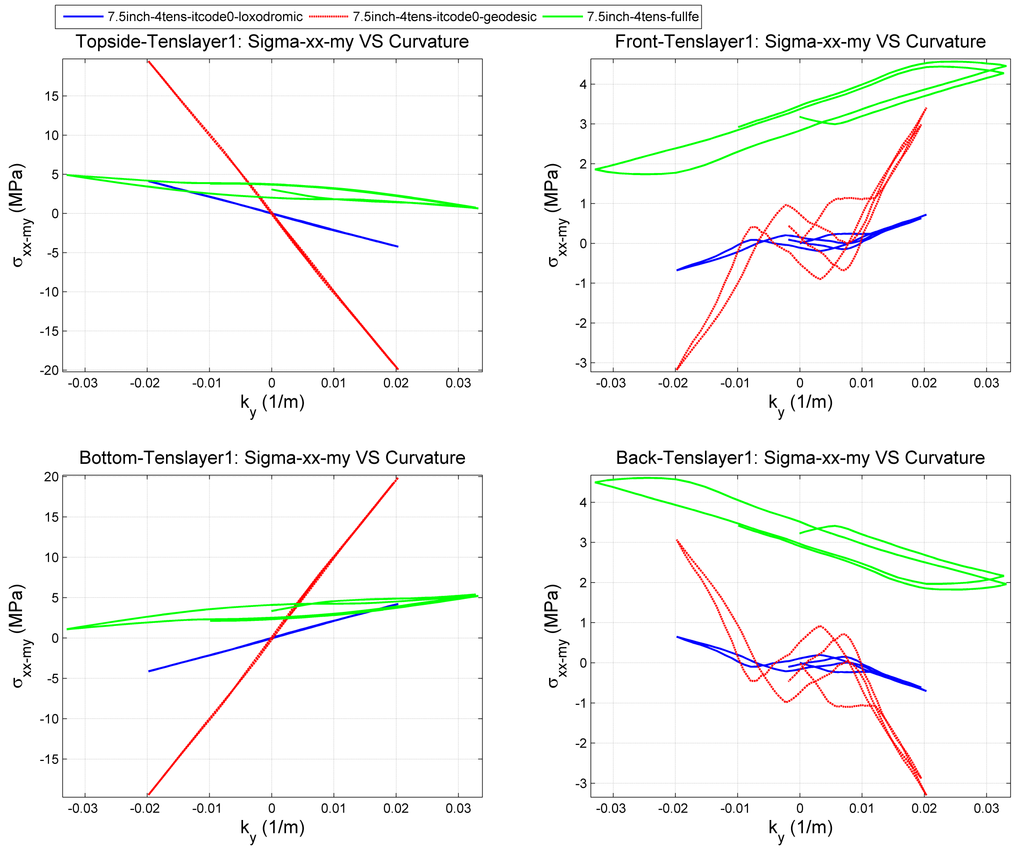

Figure D.23: The 7.5"-4tens tenslayer1 σ_{xx-my} lox-geo sensitivity for itcode0 and fullfe.

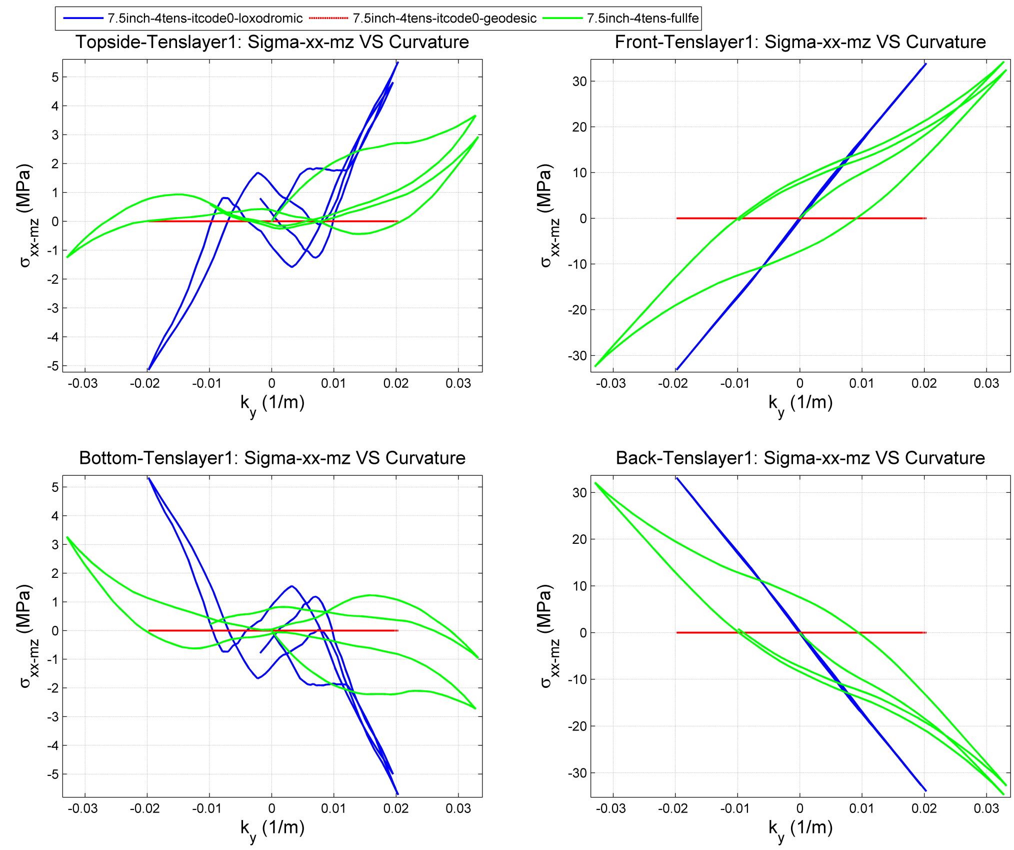

Figure D.24: The 7.5"-4tens tenslayer1 σ_{xx-mz} lox-geo sensitivity for itcode0 and fullfe.

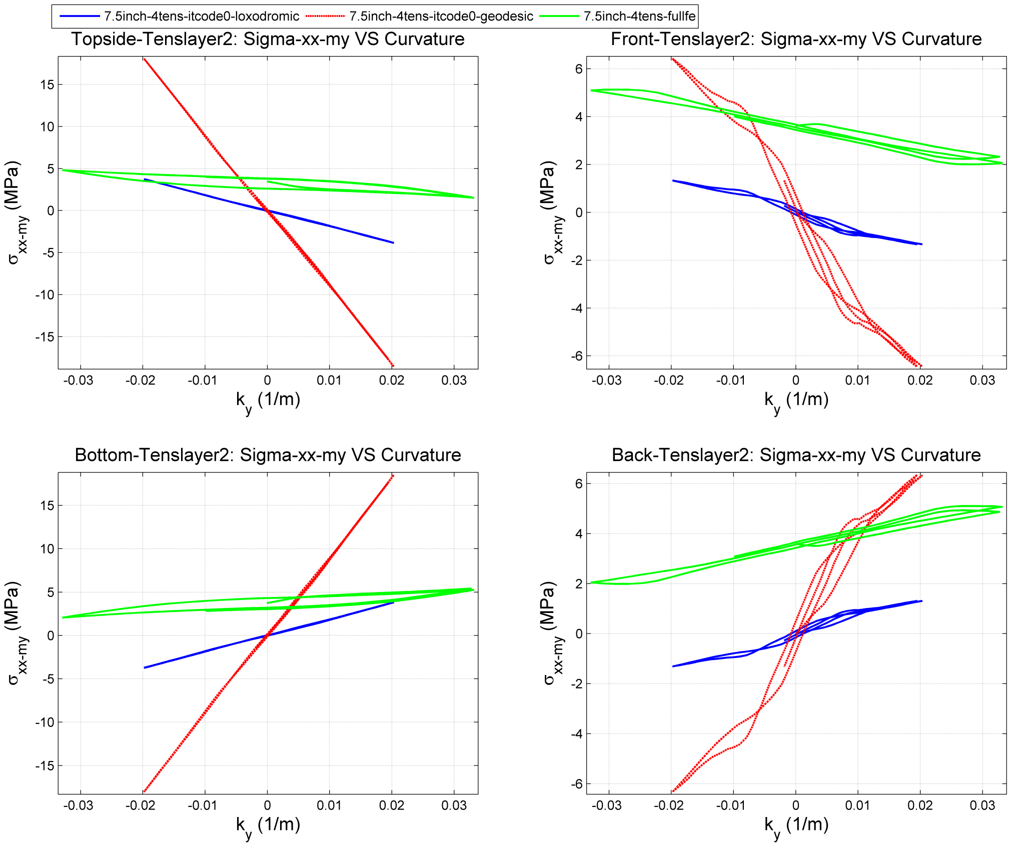

Figure D.25: The 7.5"-4tens tenslayer2 σ_{xx-my} lox-geo sensitivity for itcode0 and fullfe.

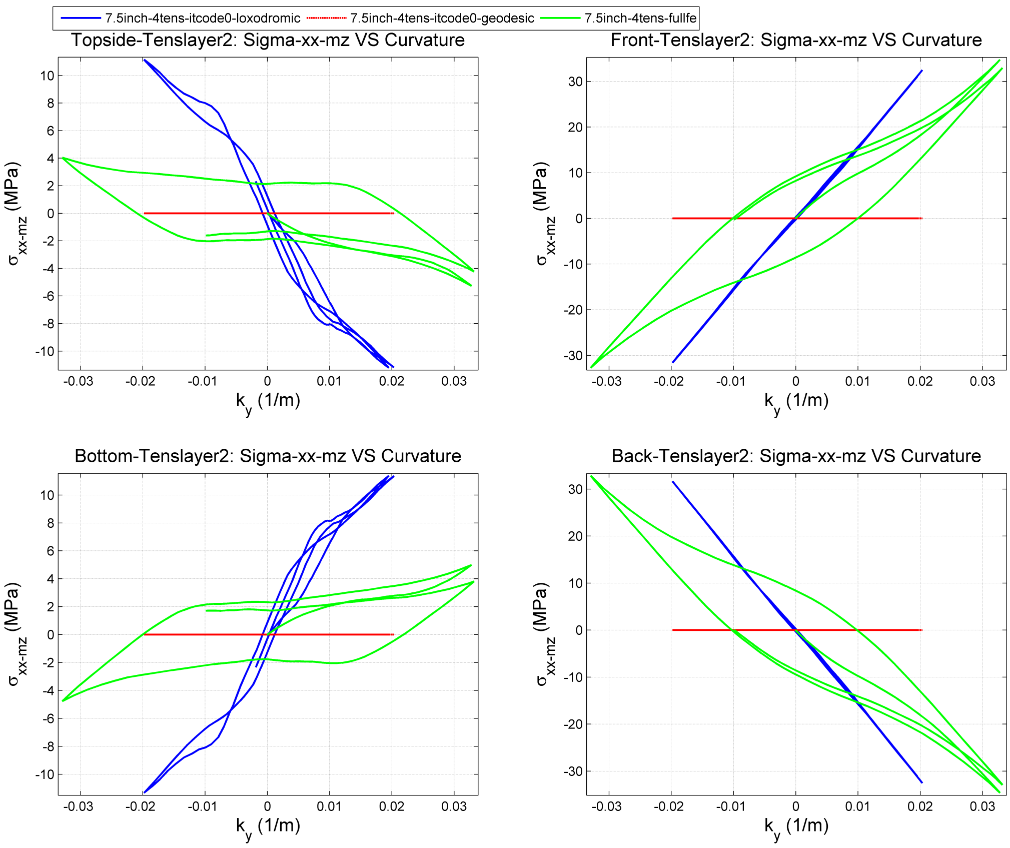

Figure D.26: The 7.5"-4tens tenslayer2 σ_{xx-mz} lox-geo sensitivity for itcode0 and fullfe.

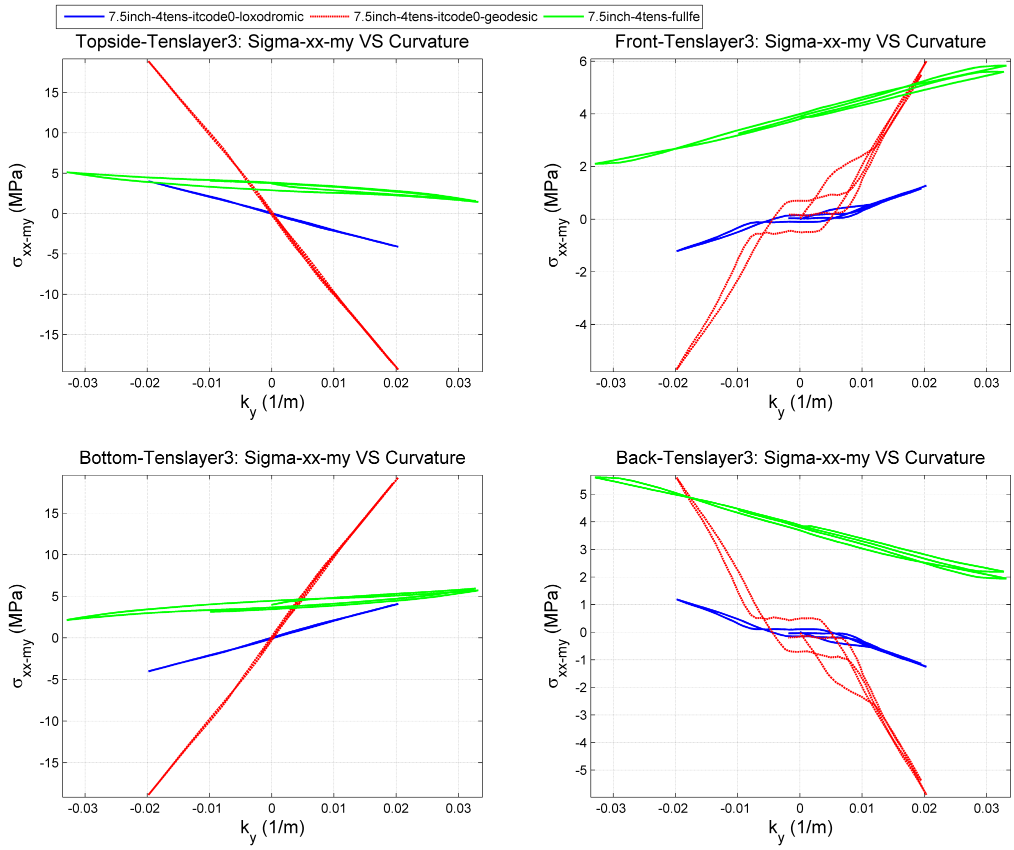

Figure D.27: The 7.5"-4tens tenslayer3 σ_{xx-my} lox-geo sensitivity for itcode0 and fullfe.

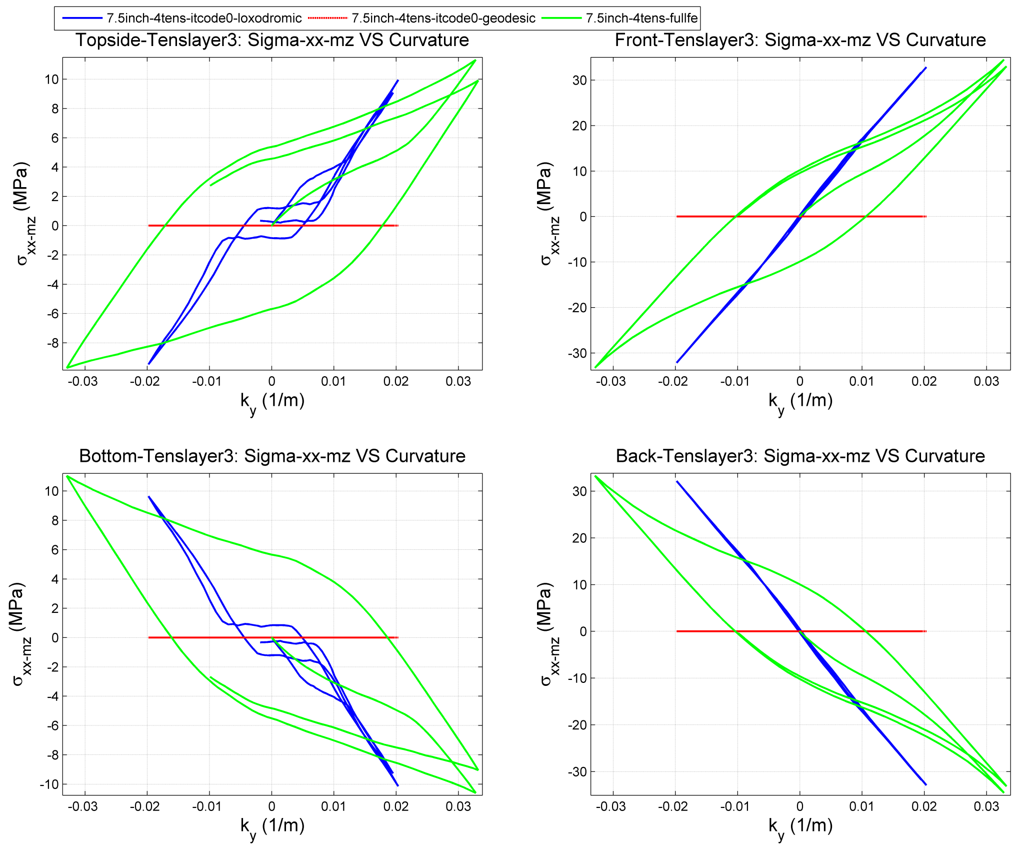

Figure D.28: The 7.5"-4tens tenslayer3 σ_{xx-mz} lox-geo sensitivity for itcode0 and fullfe.

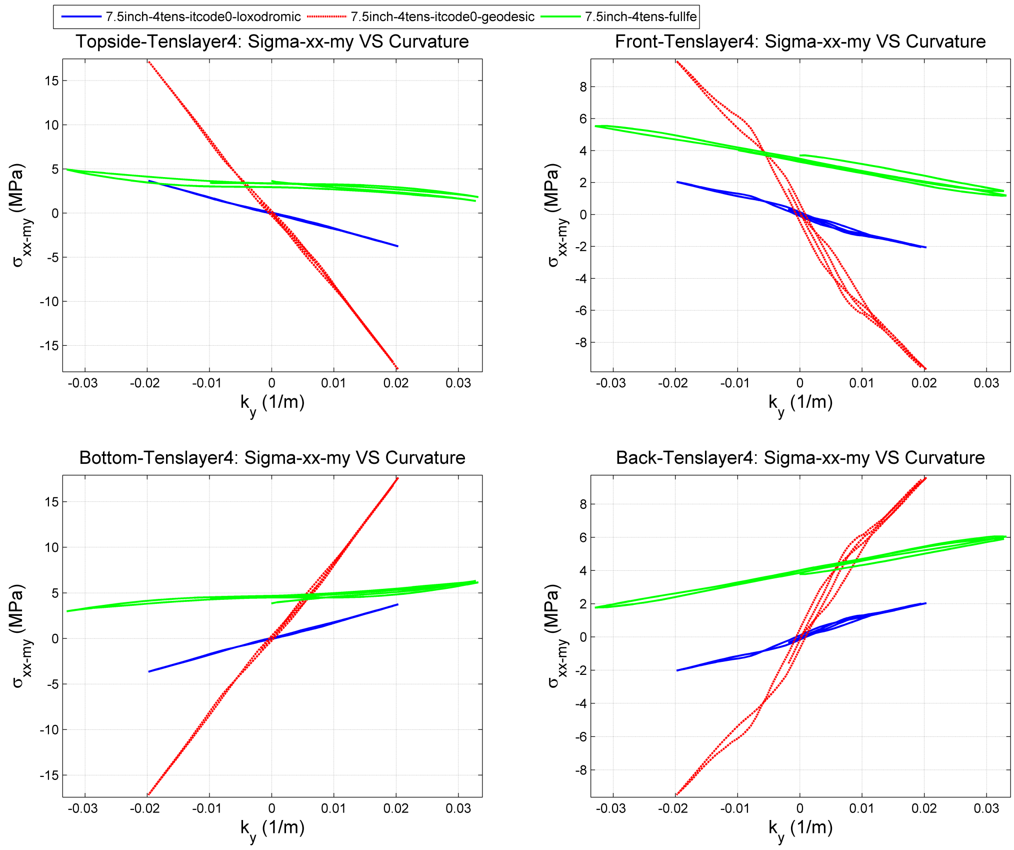

Figure D.29: The 7.5"-4tens tenslayer4 σ_{xx-my} lox-geo sensitivity for itcode0 and fullfe.

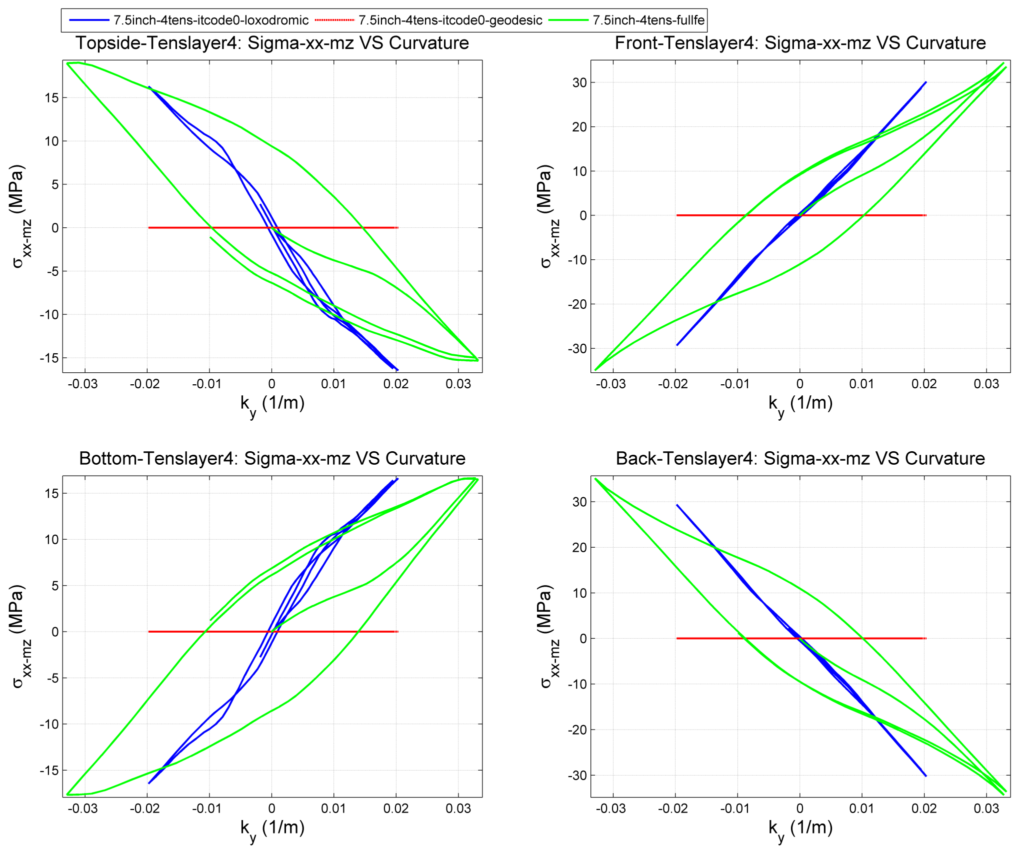

Figure D.30: The 7.5"-4tens tenslayer4 σ_{xx-mz} lox-geo sensitivity for itcode0 and fullfe.

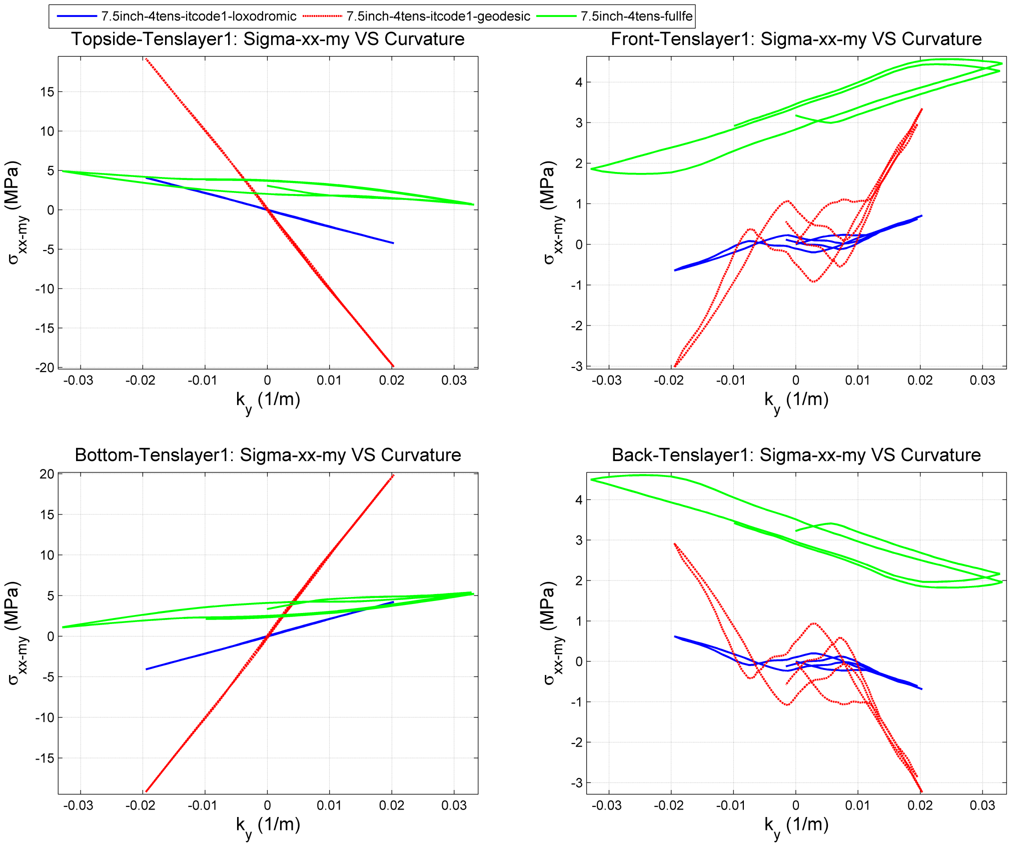

Figure D.31: The 7.5"-4tens tenslayer1 σ_{xx-my} lox-geo sensitivity for itcode1 and fullfe.

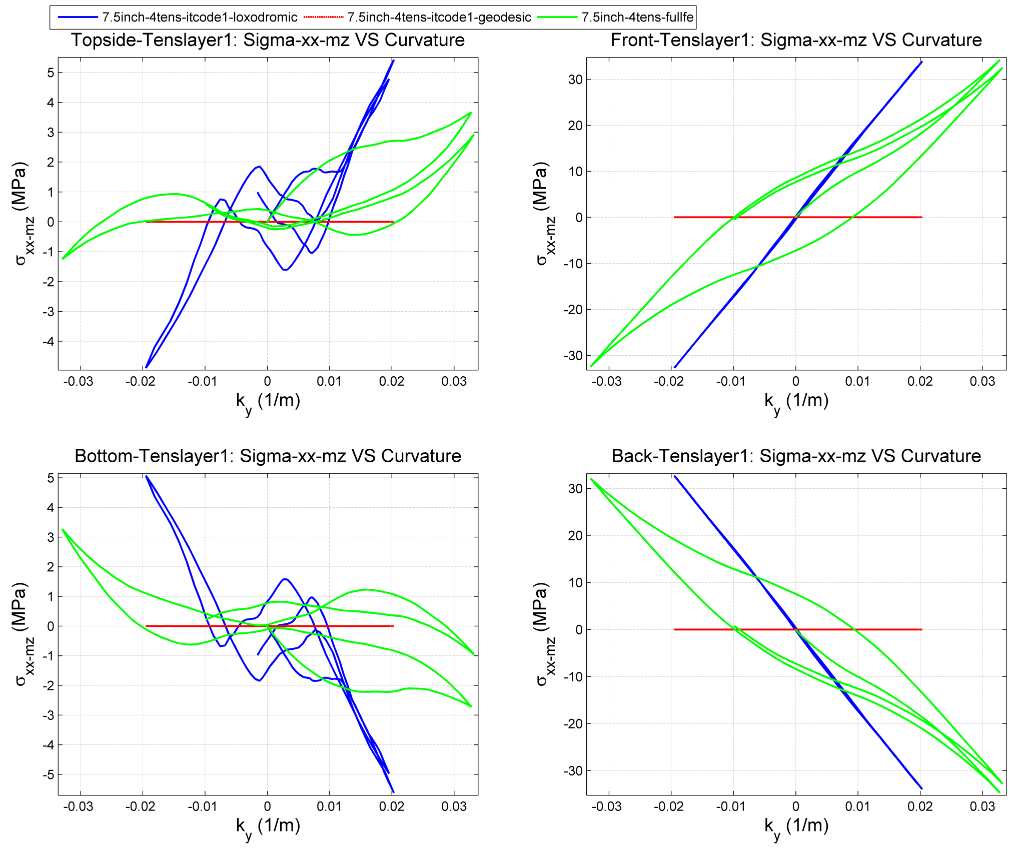

Figure D.32: The 7.5"-4tens tenslayer1 σ_{xx-mz} lox-geo sensitivity for itcode1 and fullfe.

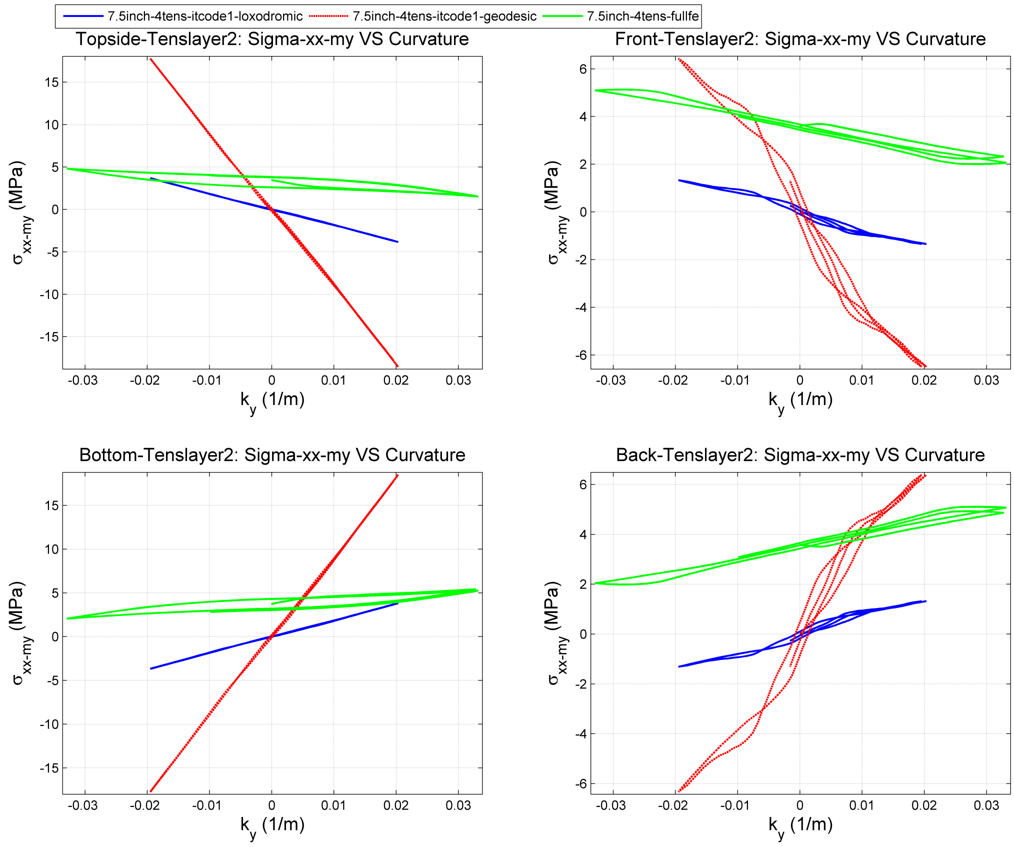

Figure D.33: The 7.5"-4tens tenslayer2 σ_{xx-my} lox-geo sensitivity for itcode1 and fullfe.

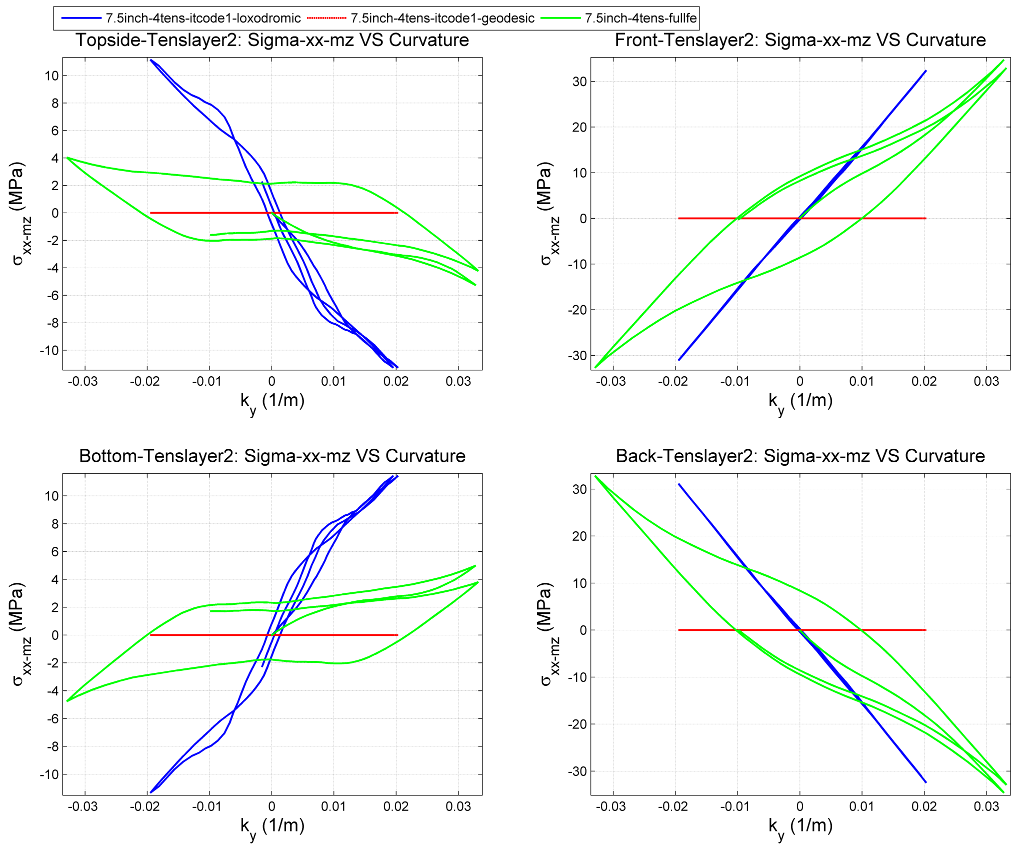

Figure D.34: The 7.5"-4tens tenslayer2 σ_{xx-mz} lox-geo sensitivity for itcode1 and fullfe.

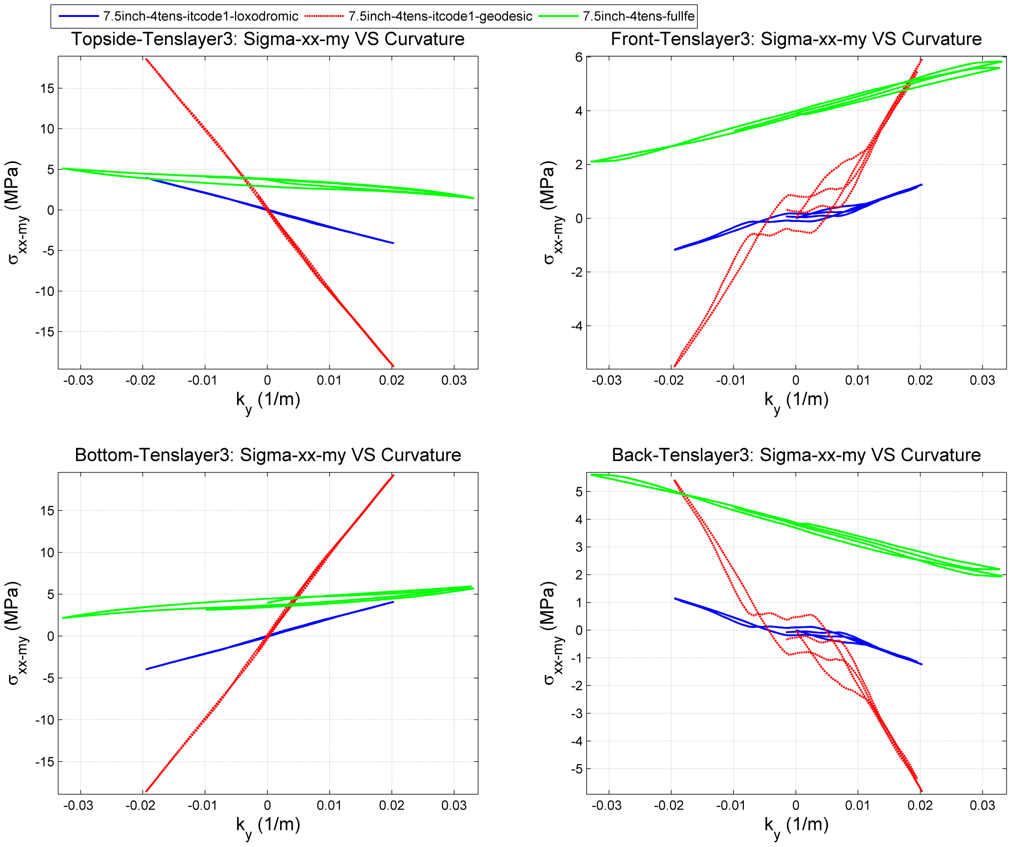

Figure D.35: The 7.5"-4tens tenslayer3 σ_{xx-my} lox-geo sensitivity for itcode1 and fullfe.

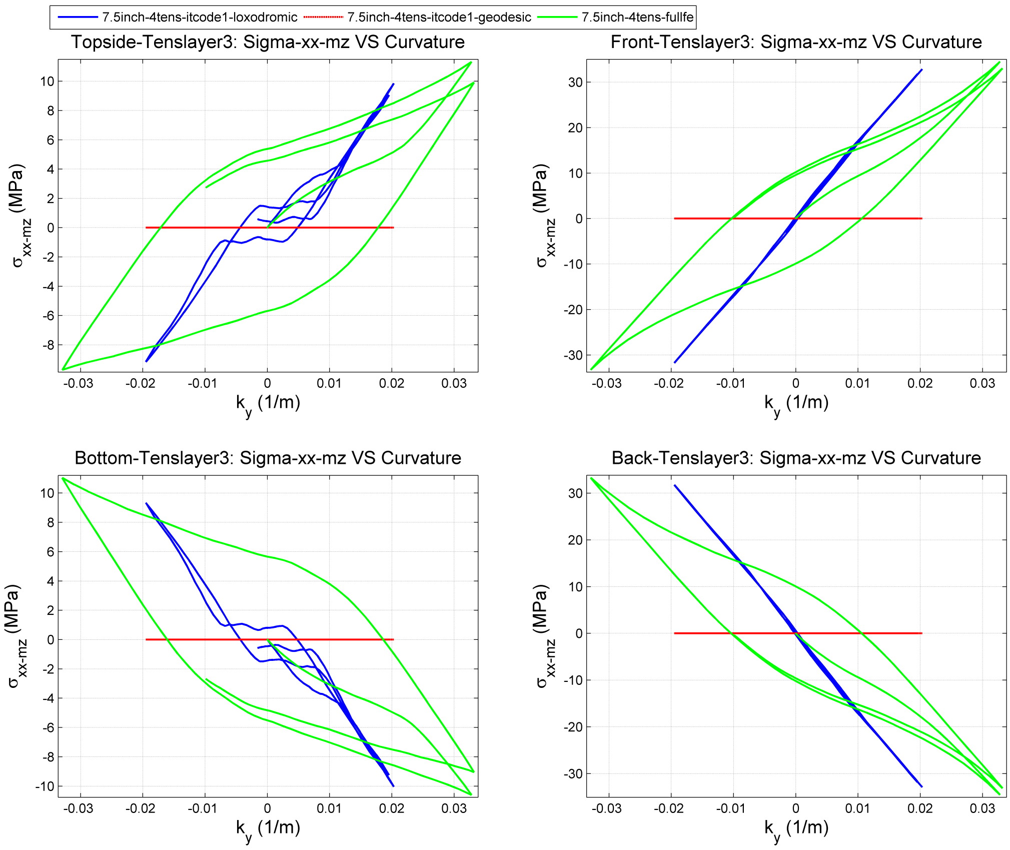

Figure D.36: The 7.5"-4tens tenslayer3 σ_{xx-mz} lox-geo sensitivity for itcode1 and fullfe.

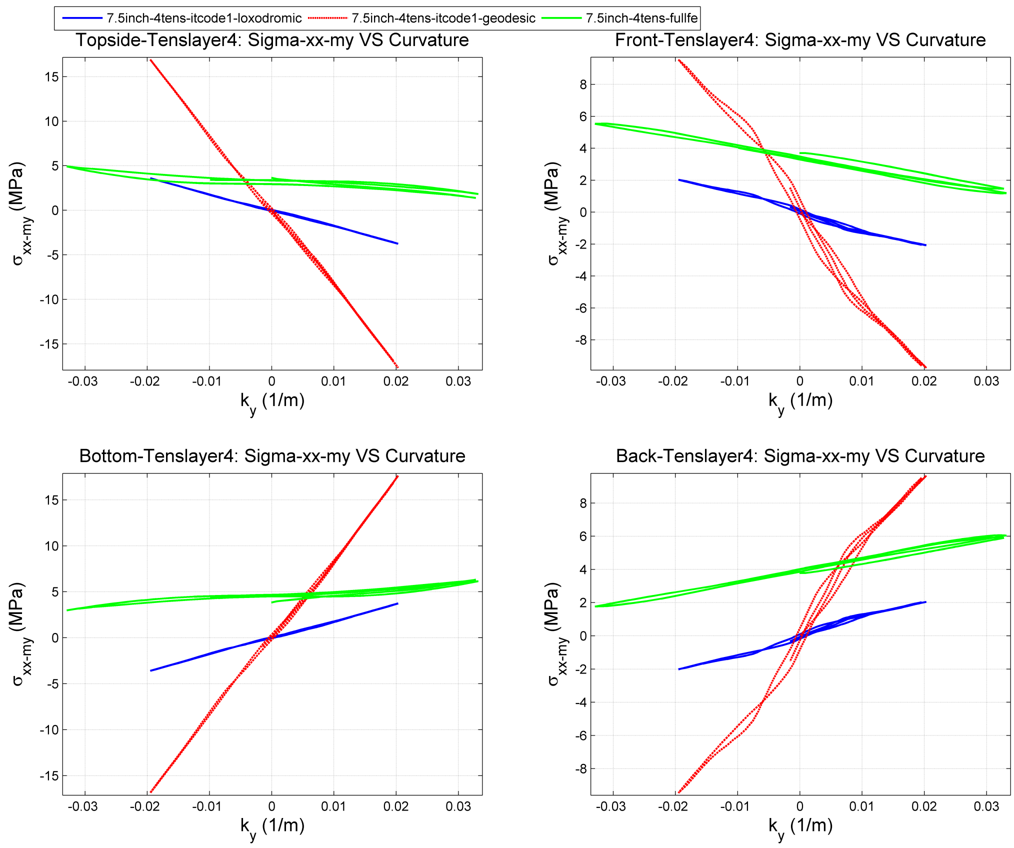

Figure D.37: The 7.5"-4tens tenslayer4 σ_{xx-my} lox-geo sensitivity for itcode1 and fullfe.

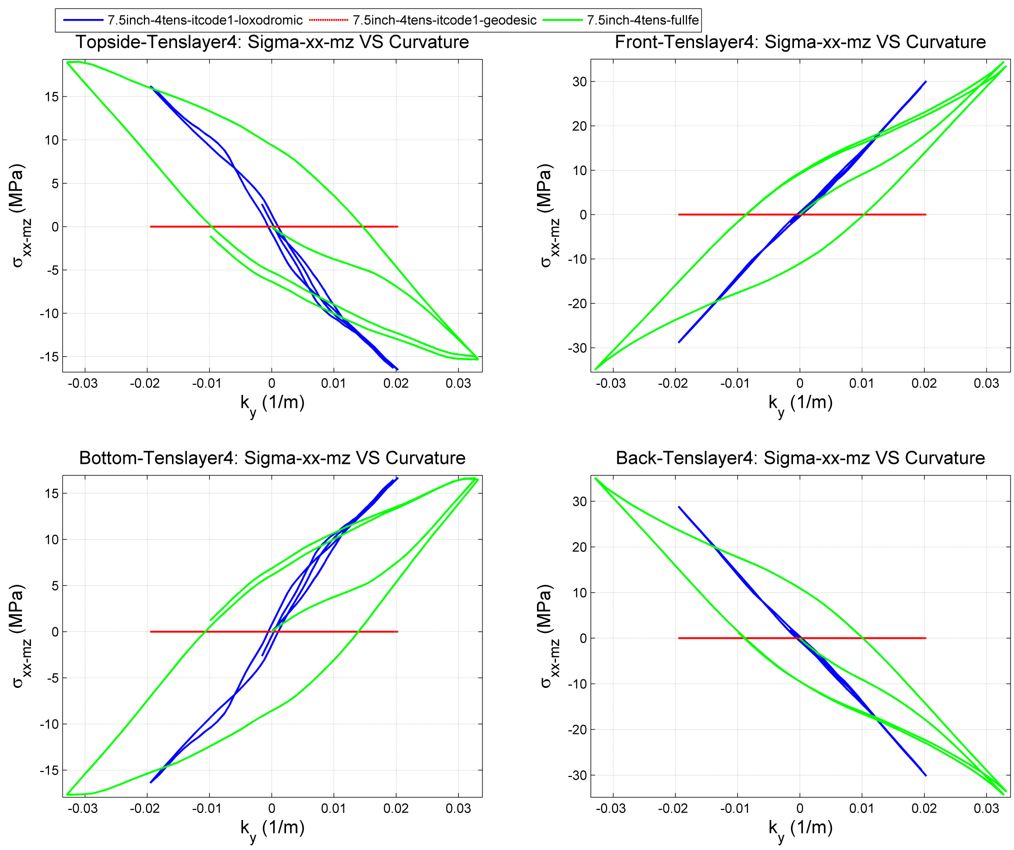

Figure D.38: The 7.5"-4tens tenslayer4 σ_{xx-mz} lox-geo sensitivity for itcode1 and fullfe.

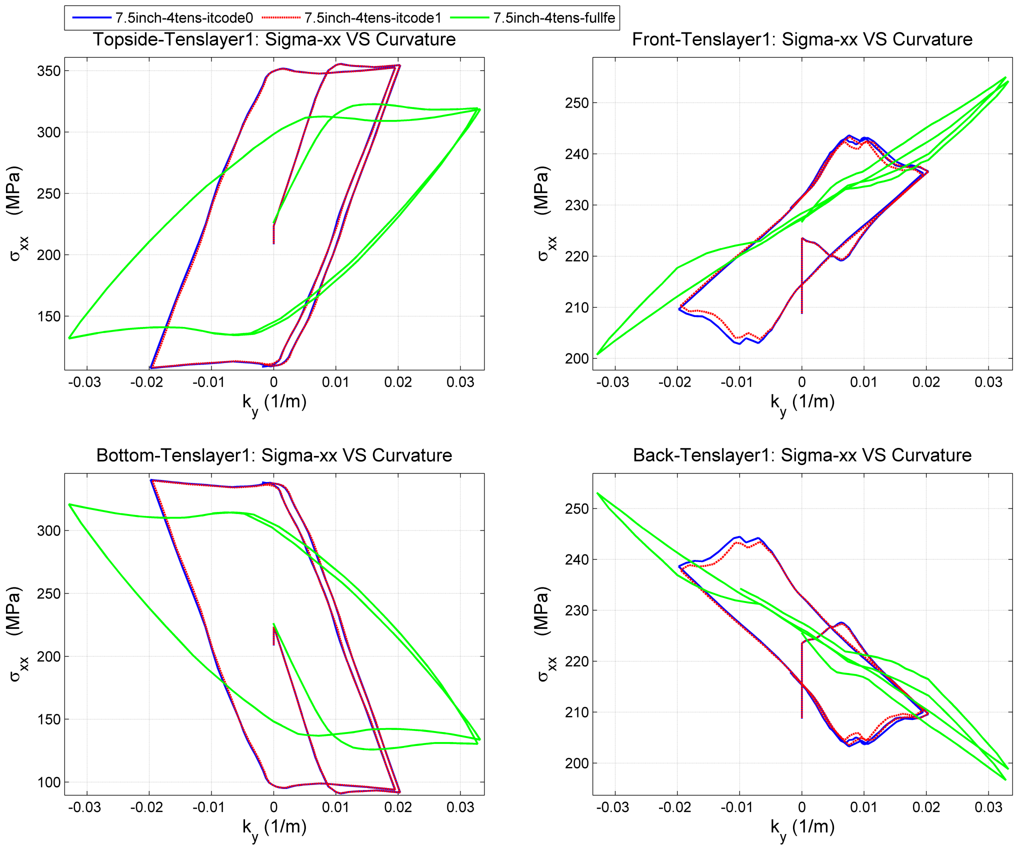

Figure D.39: The 7.5"-4tens tenslayer1 σ_{xx} for three models.

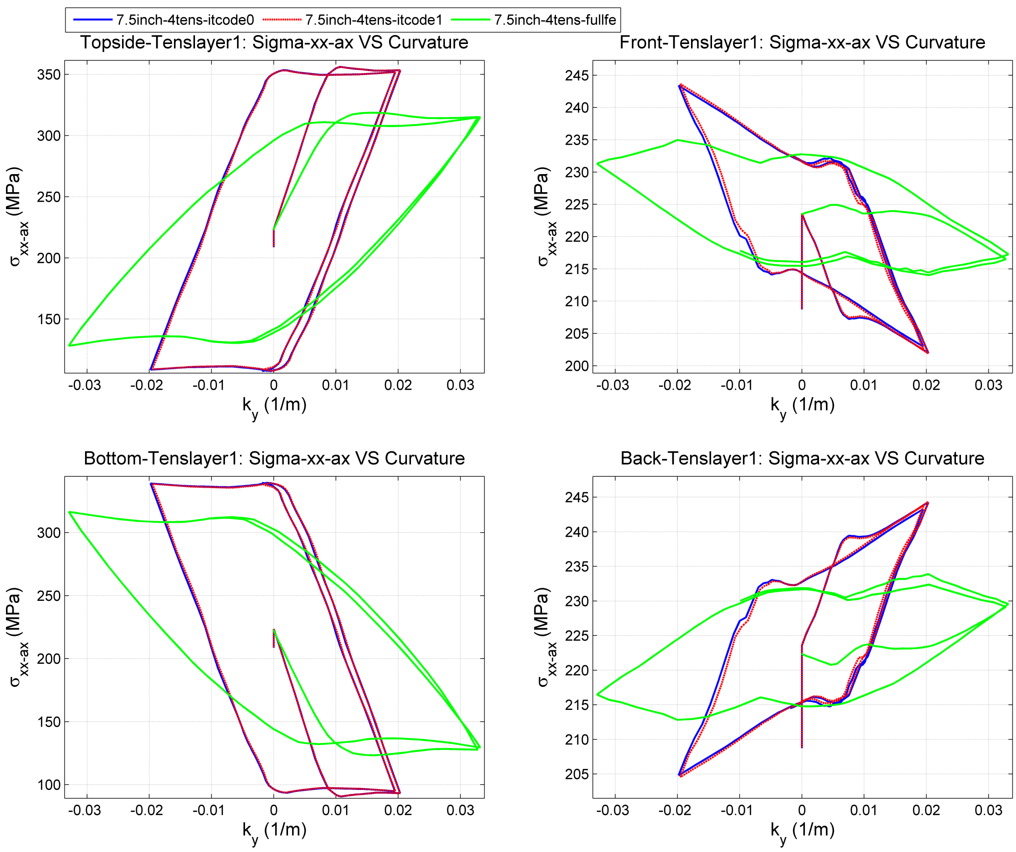

Figure D.40: The 7.5"-4tens tenslayer1 σ_{xx-ax} for three models.

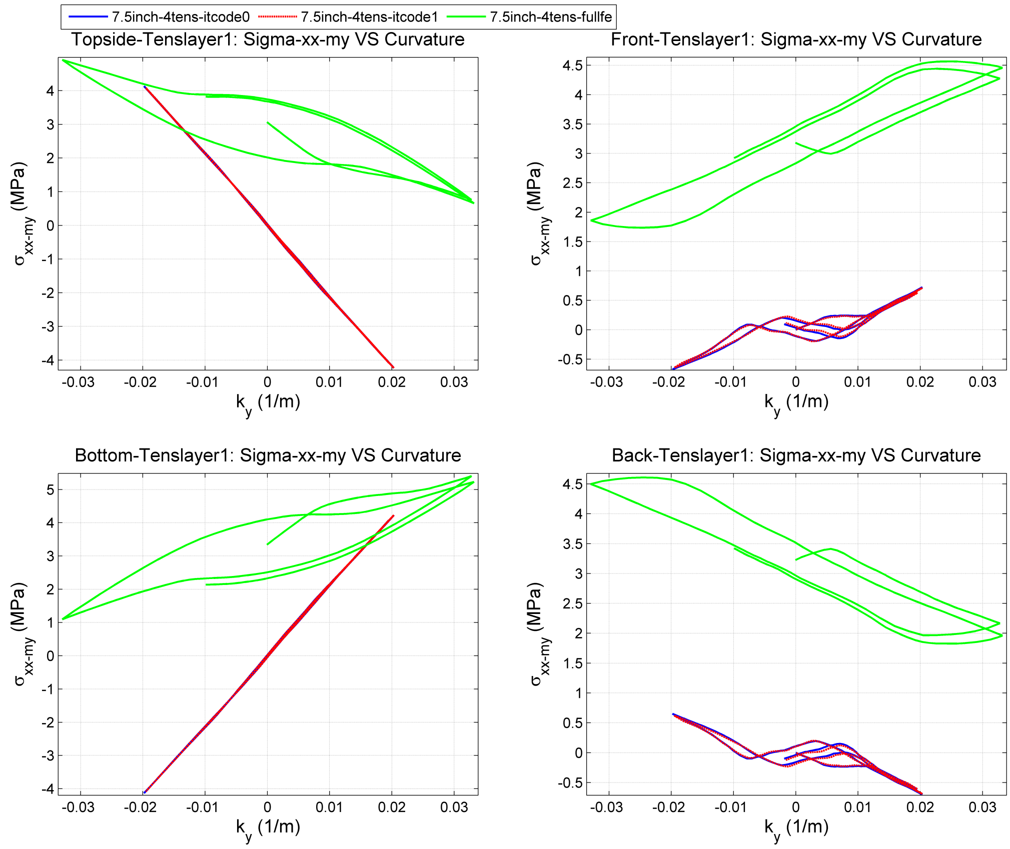

Figure D.41: The 7.5"-4tens tenslayer1 σ_{xx-my} for three models.

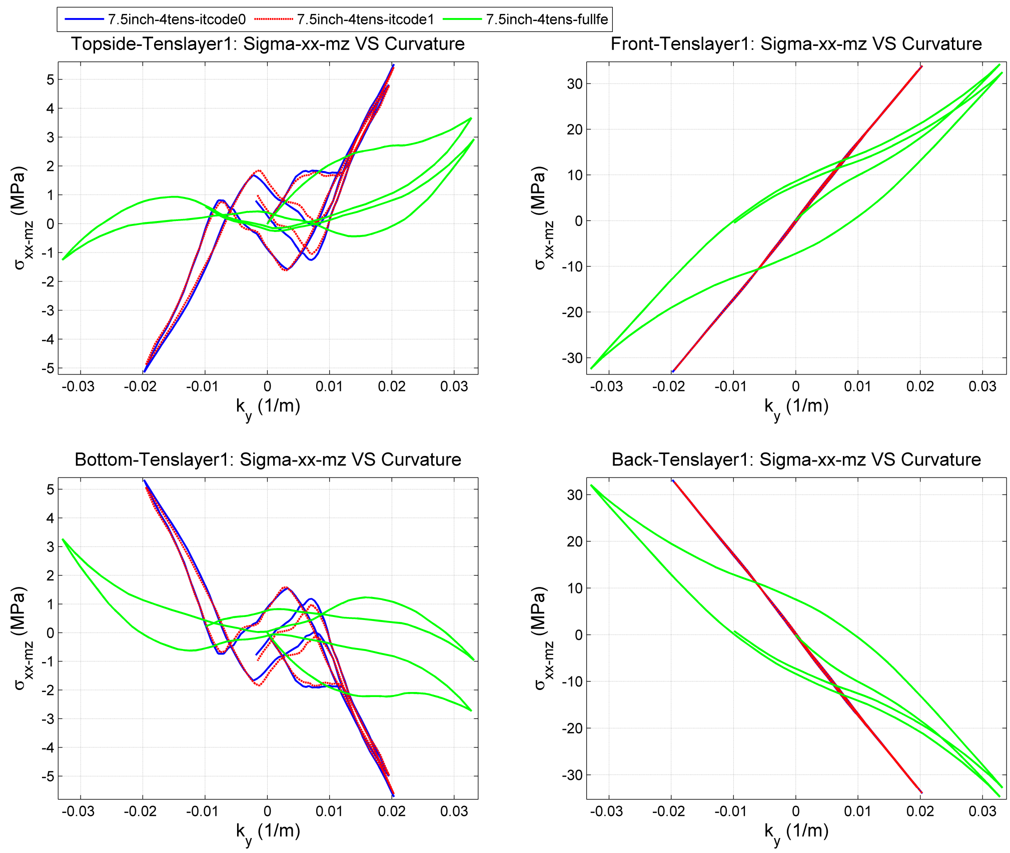

Figure D.42: The 7.5"-4tens tenslayer1 σ_{xx-mz} for three models.

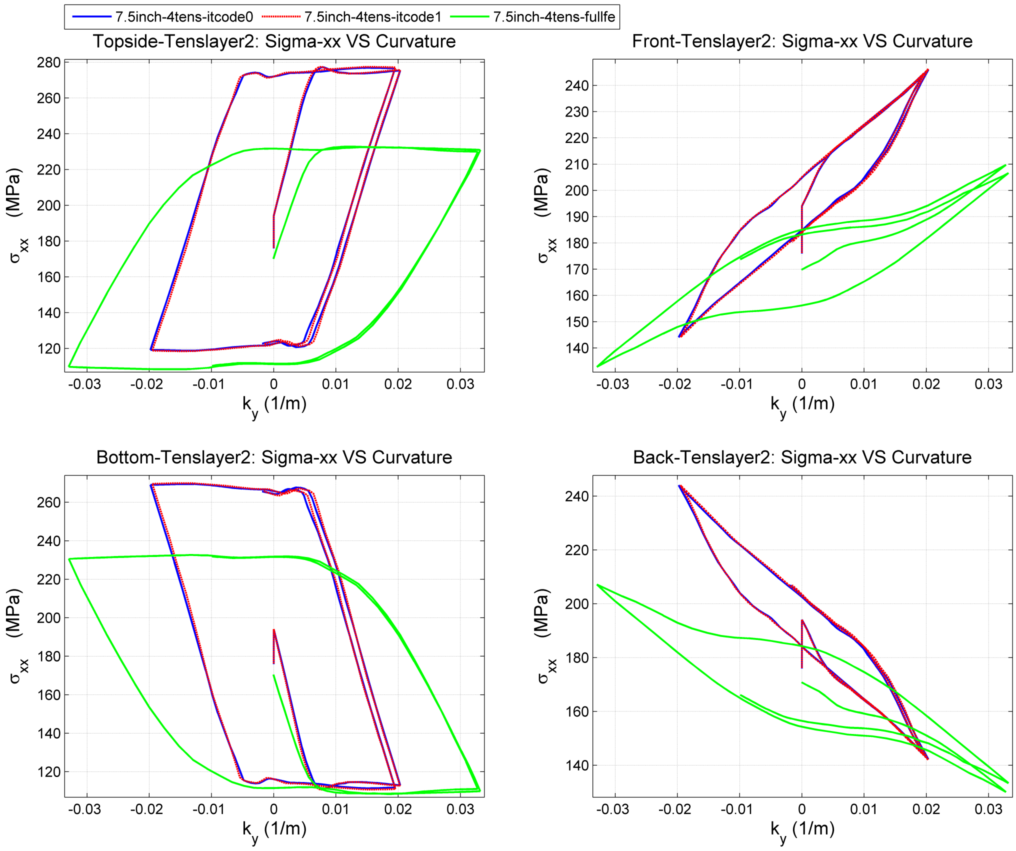

Figure D.43: The 7.5"-4tens tenslayer2 σ_{xx} for three models.

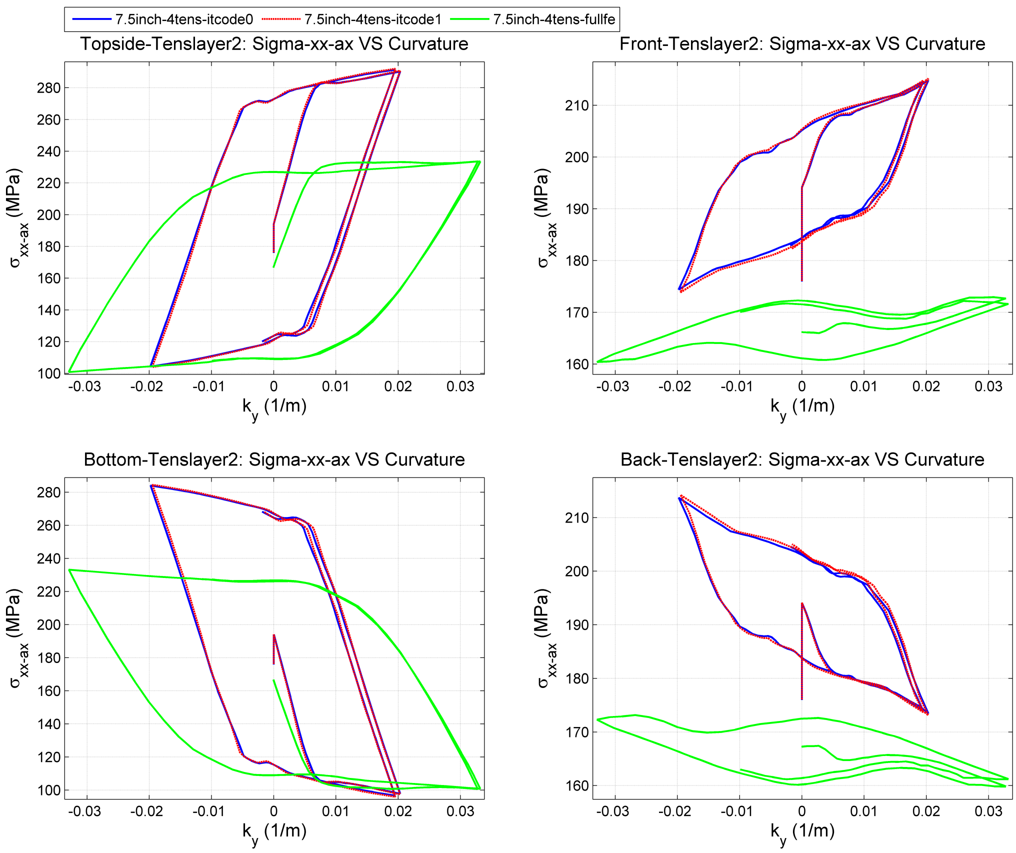

Figure D.44: The 7.5"-4tens tenslayer2 σ_{xx-ax} for three models.

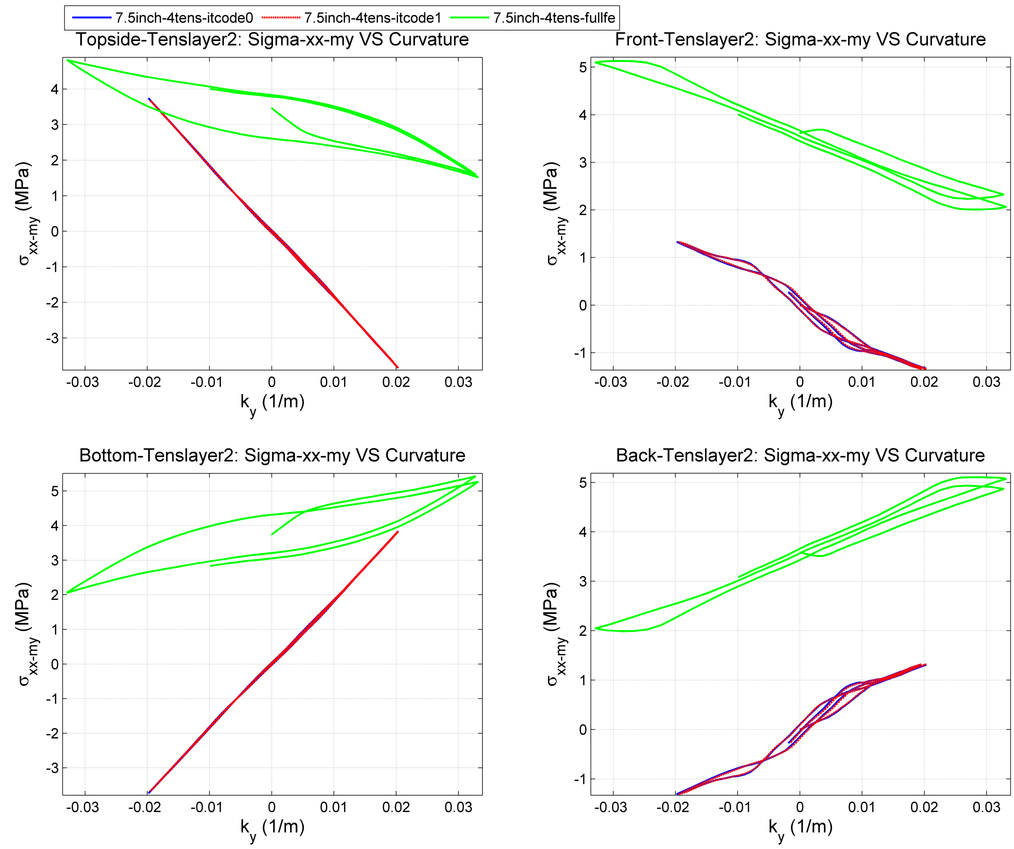

Figure D.45: The 7.5"-4tens tenslayer2 σ_{xx-my} for three models.

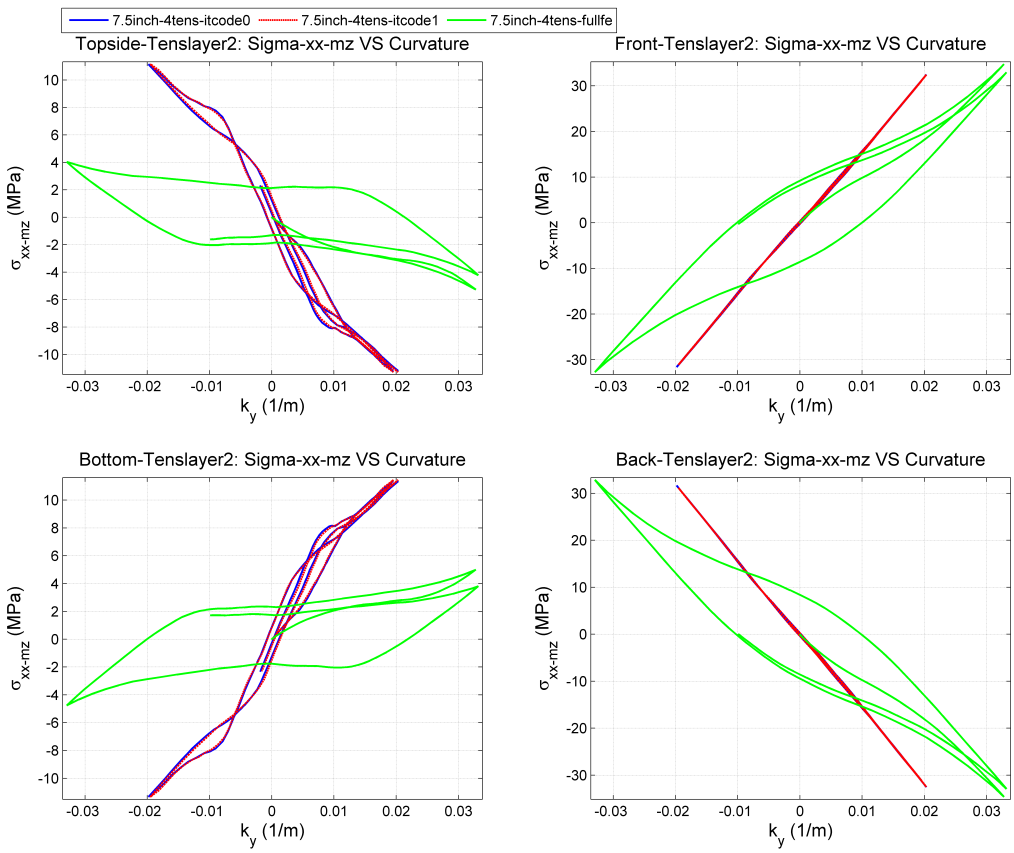

Figure D.46: The 7.5"-4tens tenslayer2 σ_{xx-mz} for three models.

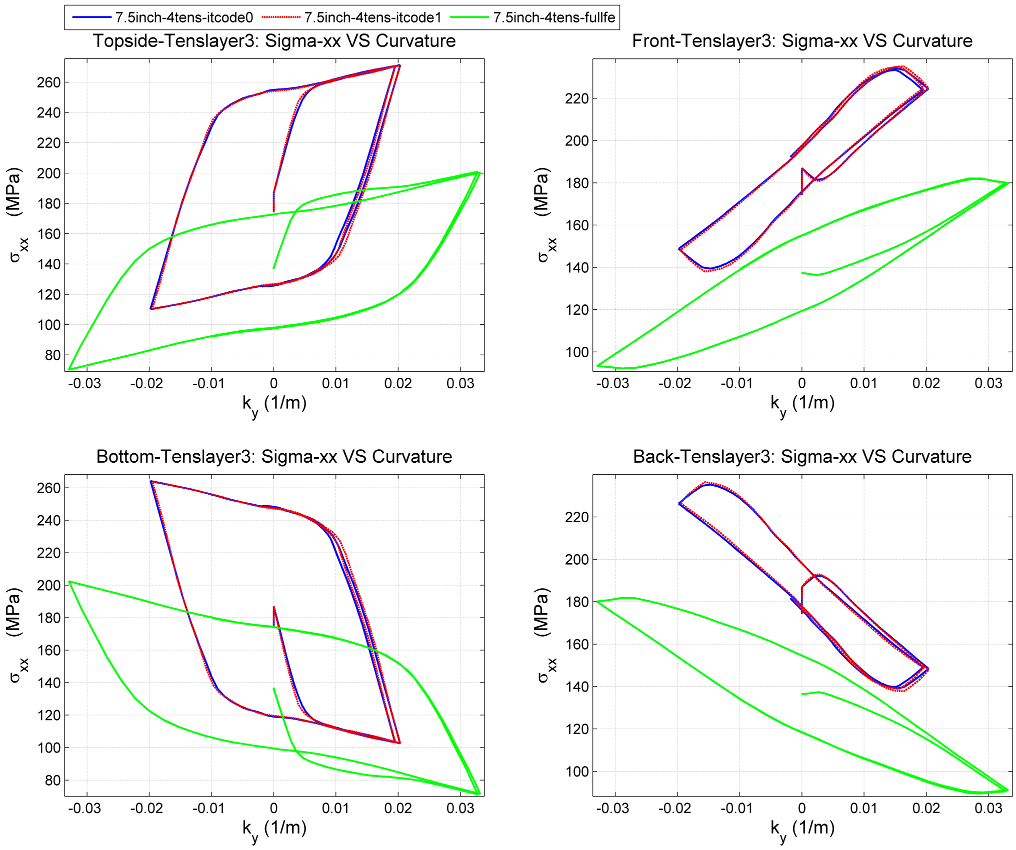

Figure D.47: The 7.5"-4tens tenslayer3 σ_{xx} for three models.

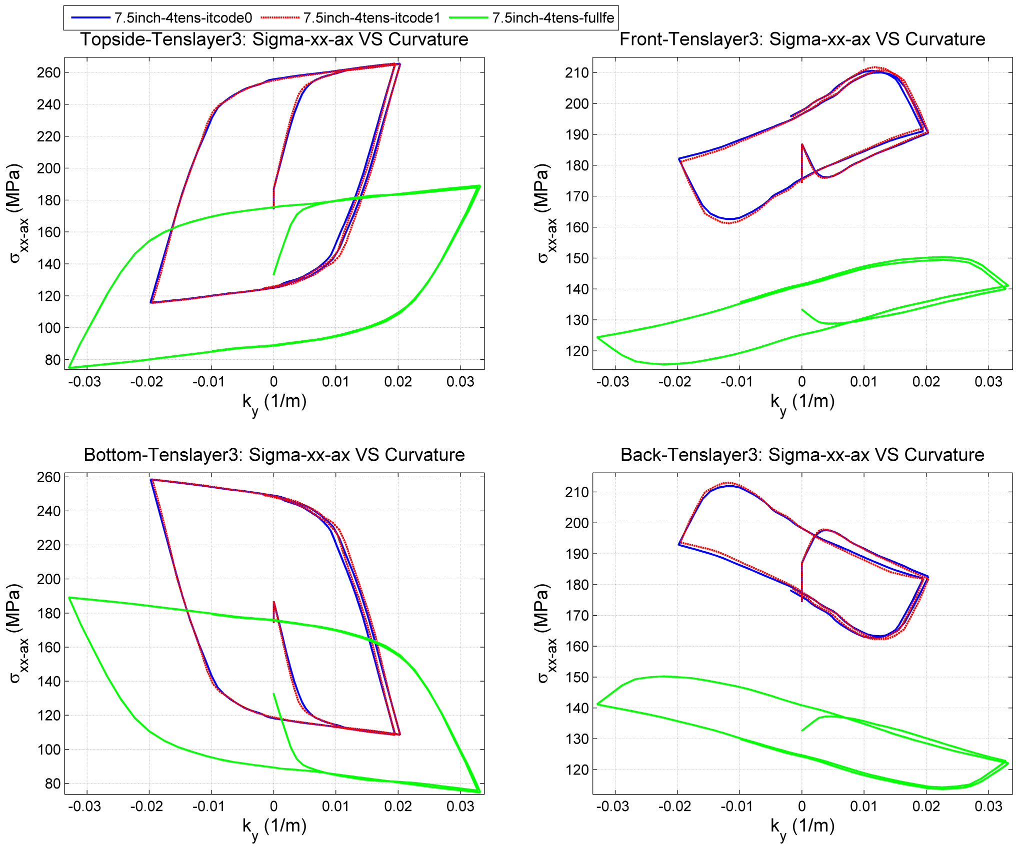

Figure D.48: The 7.5"-4tens tenslayer3 σ_{xx-ax} for three models.

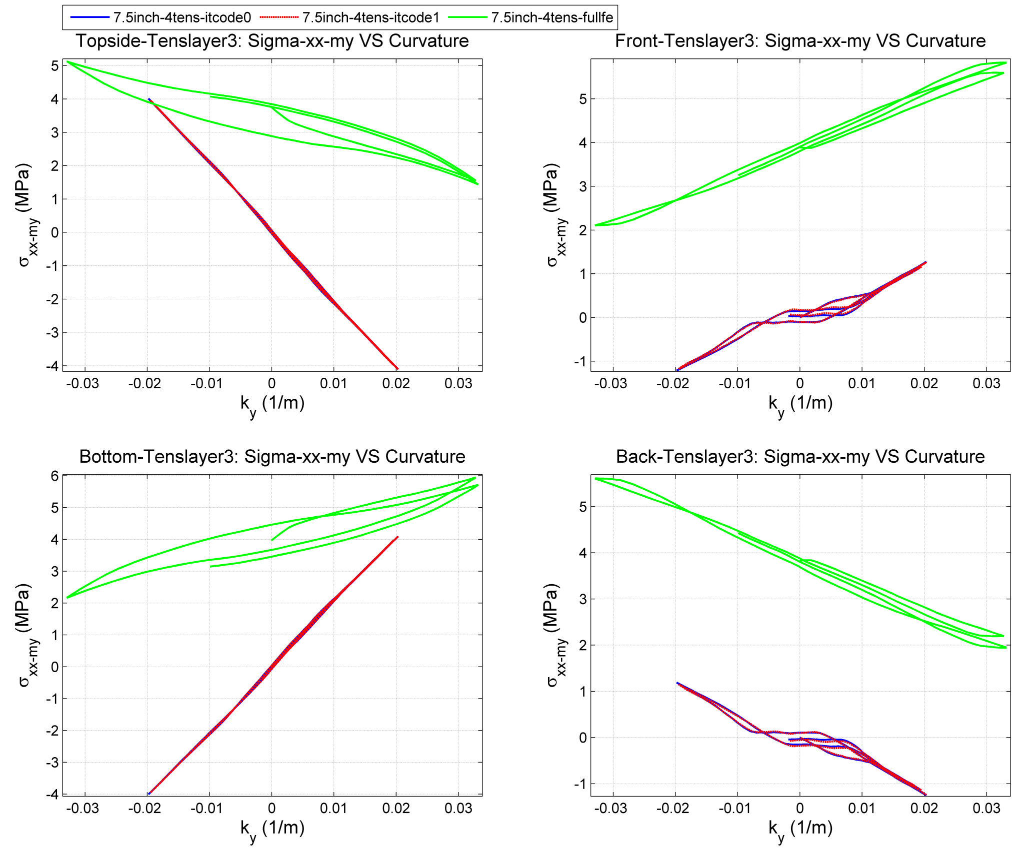

Figure D.49: The 7.5"-4tens tenslayer3 σ_{xx-my} for three models.

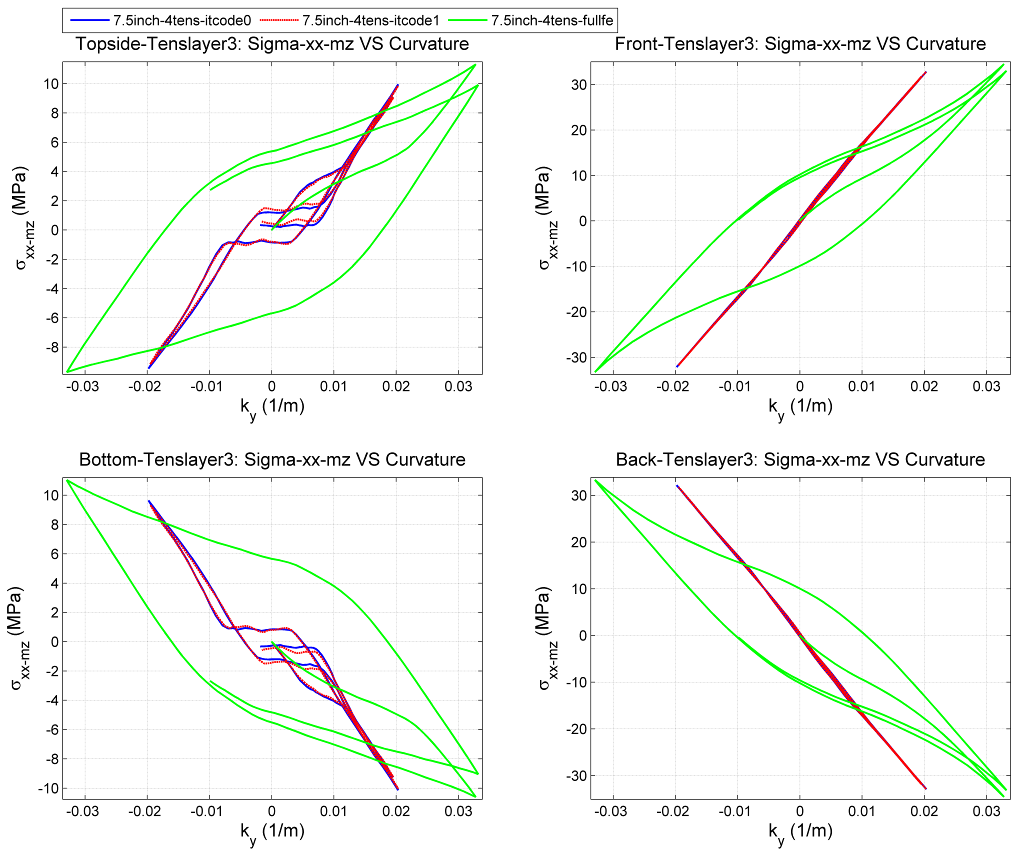

Figure D.50: The 7.5"-4tens tenslayer3 σ_{xx-mz} for three models.

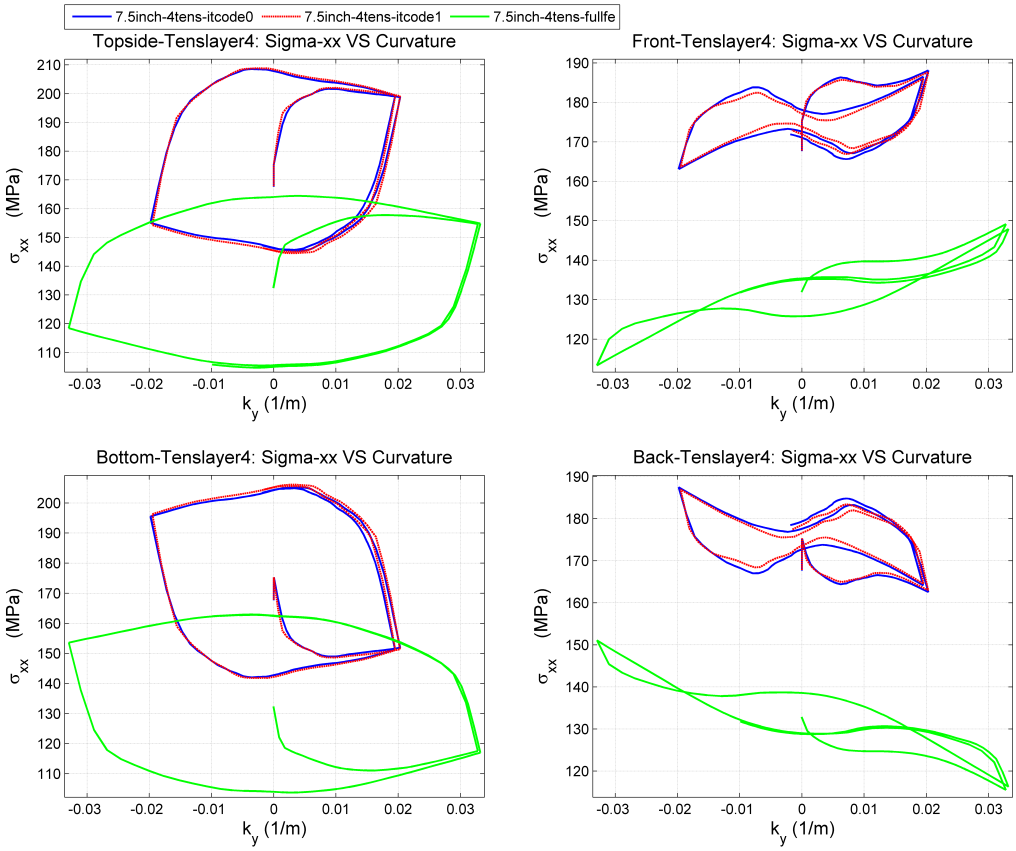

Figure D.51: The 7.5"-4tens tenslayer4 σ_{xx} for three models.

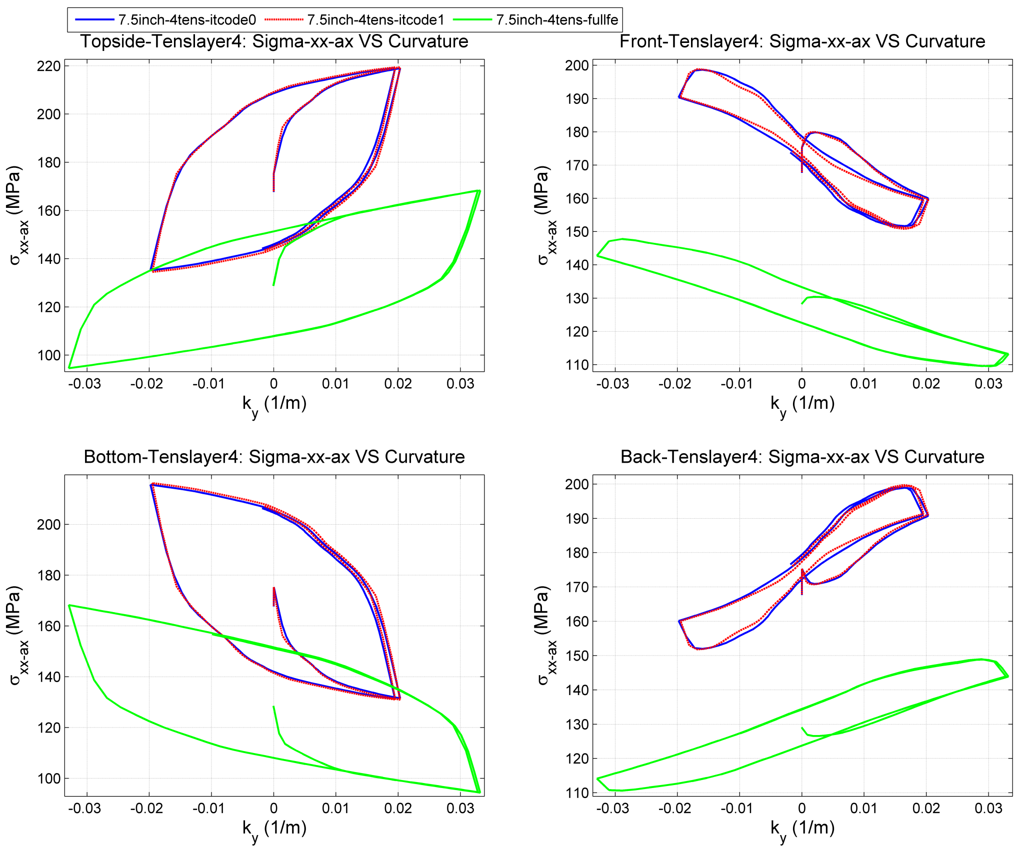

Figure D.52: The 7.5"-4tens tenslayer4 σ_{xx-ax} for three models.

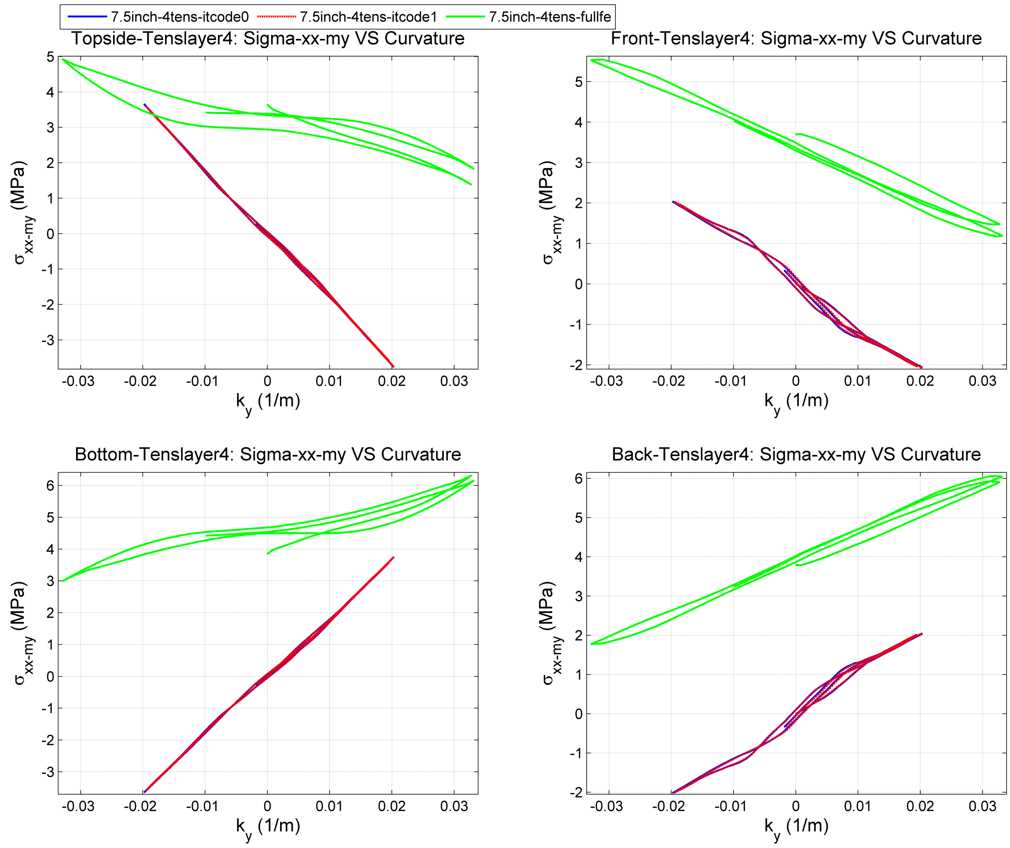

Figure D.53: The 7.5"-4tens tenslayer4 σ_{xx-my} for three models.

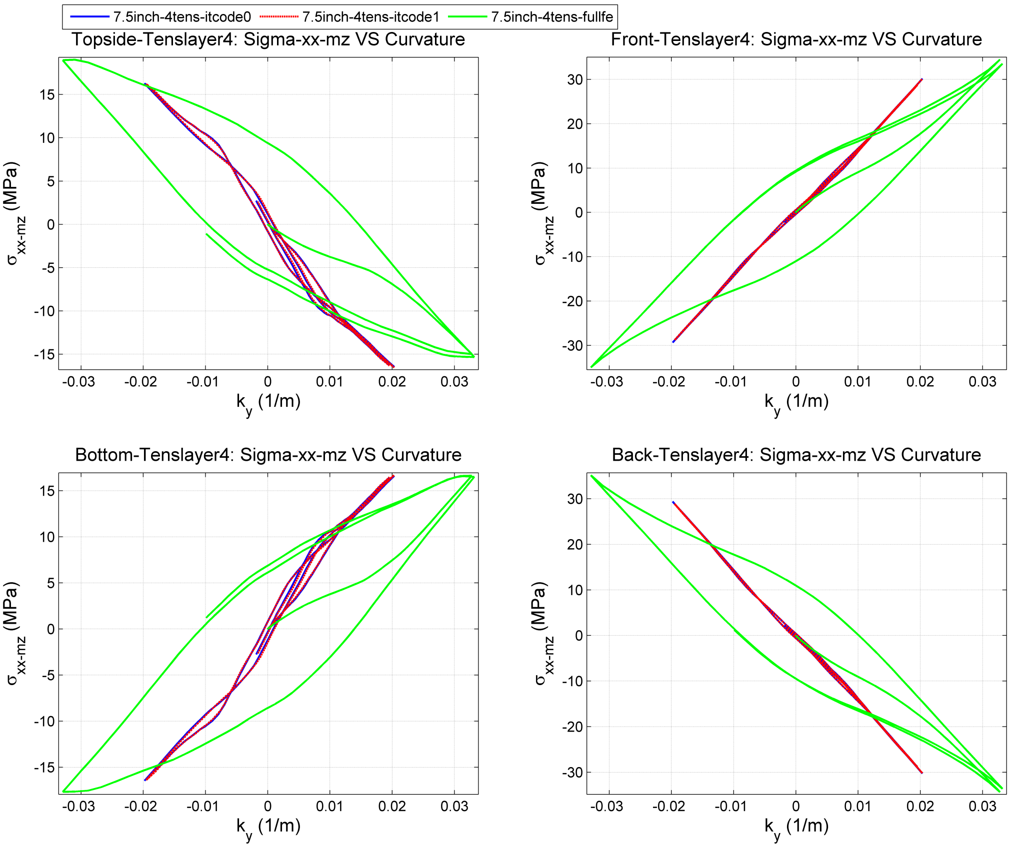

Figure D.54: The 7.5"-4tens tenslayer4 σ_{xx-mz} for three models.